The Role of Metabolism in Prostate Cancer Progression and Bone Metastases

Jessica Anna Sandhu Whitburn

Supervisors

Prof. Claire M. Edwards

Prof. Freddie C. Hamdy

Dr. Srinivasa Rao Rao



A thesis submitted for the degree Doctor of Philosophy

Balliol College & Nuffield Department of Surgical Sciences

University of Oxford

Trinity 2019

Acknowledgements

I would like to start by thanking Cancer Research UK Oxford Centre and the Japanese Society for the Promotion of Science for providing the funding to make this work possible.

Secondly I would like to thank my supervisors. Dr. Srinivasa Rao Rao for his endless patience explaining techniques and discussing ideas. He has taught me many of the techniques needed to complete this DPhil and has also been a great friend along the way. Professor Claire Edwards for her support in my research, encouraging me to apply for funding, present my work and become confident in my abilities as a scientist. Professor Hamdy for his support and interest in my work, and for the inspiration to pursue academia as a surgeon. I feel very lucky to have these supervisors who have given me a love of research and made these last few years so enjoyable.

Everyone within the Edwards research group has helped in some capacity over the years, and it has been great going to work with friend's everyday. Thank you to Dr Emma Morris for putting up with my constant questions on Western blots, always making time for my 'urgent' orders, and for keeping me entertained in tissue culture. Thank you to Dr. Sam Olechnowicz for his help with mouse work and trips to the pub. Thank you to Dr. Beatriz Gamez Molina for her great sense of humour and Professor James Edwards for his input at group meetings and his positivity. Thanks to Aneka Sowman, Quitterie Larrouture, Christina Turner and Laura Diment for sharing the highs and low of completing a DPhil

and for making it so enjoyable along the way. Thanks also to members of the group who have left over the years – Seint Lwin, Siobhan Webb, Ann Snaith and Gloria Cheng.

I am very grateful to everyone who made my fellowship in Japan so enjoyable and productive. Particularly Professor Soga for hosting me, Akiyoshi Hirayama and Sho Tabata for teaching me about Mass Spectrometry and Japanese cuisine, and Futaba Shoji for her friendship and for showing me around Tsuruoka. It was a highlight of my DPhil, and an experience I will never forget.

To my parents, Bhupinder Sandhu and Richard Whitburn. I will forever be indebted to you for the opportunities you have provided for me, and the inspiration you have given me. You brought me up knowing I could achieve anything, and I hope that I have made you proud.

I am grateful to my sister Tara, and her family, Ben and John, and to my family-in-law, Ilda, Amir, Morten, Anne, and particularly Shahla and Gholam for their love and support, and for helping with childcare to make this possible. Thank you also to my grandparents – Nain, Taid, Biji and Papaji for your love and support over the years.

Lastly, I would like to thank my husband Amin who has supported me throughout this DPhil in every way possible. Your encouragement has been endless and I am extremely lucky to have met you. And to Casper, who arrived in the world half way through this DPhil. Your endless laughter and kisses makes the world a better place.

Declaration of authorship

I affirm that all the work presented in this thesis is the result of my own work unless otherwise stated, and does not constitute part of any other thesis. The work herein described was carried out while I was a graduate student of the Nuffield Department of Surgical Sciences working at the Botnar Research Centre under the supervision of Dr. Srinivasa Rao Rao, Professor Claire Edwards and Professor Freddie Hamdy.

Jessica Whitburn

Date 18th June 2019.

Abstract

Prostate cancer (PCa) is the most common cancer in males in the Western world, and whilst treatment of localised disease is very effective, bone metastatic disease remains incurable and overall survival is only around 2-3 years. In view of this there is a need to identify novel therapeutics. Dysregulated cellular energetics is one of the new hallmarks of cancer, however the changes in cancer metabolism that occur when cancer metastasises remain relatively unexplored. The aim of this project was to identify the changes in PCa metabolism when it metastasises to the bone microenvironment, with the hope of identifying novel targets for advanced PCa therapeutics.

Using a combination of *in vitro* metabolomic profiling of PCa/bone cell co-cultures, an *in vivo* mouse model of PCa bone disease and *in silico* analyses of patient data sets it was established that the bone metastatic site causes alterations in several metabolic pathways in PCa cells, including up-regulation of oxidative phosphorylation, the tricarboxylic acid cycle, and the pentose phosphate pathway (PPP). The PPP alterations were of interest as this pathway provides nucleotide precursors necessary for cellular proliferation, and is the main cellular source of NADPH, which is vital in cellular detoxification of potentially harmful free radicals. PPP enzymes were found to be more highly expressed in bone metastatic PCa cell lines compared to benign or non-bone metastatic cell lines, and expression of its rate limiting enzyme glucose-6-phosphate-dehydrogenase (G6PD) could be up-regulated by bone marrow stromal cells (BMSCs), suggesting that the bone microenvironment is driving this effect. In multiple patient data sets G6PD mRNA expression was elevated in metastatic samples, particularly bone metastatic samples, and expression was higher in castration resistant prostate cancer samples compared to hormone dependent. BMSCs were found to secrete high levels of interleukin-6 (IL-6), and blocking IL-6 was able to in part abrogate the up-regulation of G6PD, whilst recombinant IL-6 could induce G6PD up-regulation.

BMSCs increased reactive oxygen species (ROS) in PCa cells and reduced the viability of non-bone metastatic cell lines. This was evident *in vitro* and in a xenograft mouse model. Pharmacological inhibition of G6PD further increased ROS levels, suggesting PCa up-regulates G6PD to counteract the high ROS induced by BMSCs.

Pharmacological or genetic blockade of G6PD in PCa cells reduced their proliferation, inhibited cell migration, reduced expression of mesenchymal markers, decreased antioxidant levels, increased ROS levels, and increased sensitivity to chemotherapy. Overexpression of G6PD promoted PCa cell proliferation and increased antioxidant levels. *In vivo*, knockdown of G6PD expression in PCa cells could reduce tumour burden within bone.

This work demonstrates for the first time that stromal cells of the metastatic environment drive changes in the metabolism of cancer cells that can promote their anti-oxidant abilities and increase their resistance to chemotherapy. Pharmacological targeting of the PPP pathway could be a novel approach to improve the efficacy of currently used treatments.

Table of Contents

List of Figures ..... **vii**

List of Tables ..... **x**

Acronyms ..... **xi**

1 Introduction **1**

1.1 The Prostate 1

1.1.1 Prostate Structure 2

1.2 Prostate Cancer 3

1.2.1 Epidemiology and Aetiology 3

1.2.2 Prostate tumourigenesis 4

1.2.3 Clinical Diagnosis 5

1.2.4 Tumour Grading 7

1.2.5 Tumour staging 8

1.2.6 Management of prostate cancer 10

1.3 Prostate Cancer Bone Metastases 14

1.3.1 The metastatic process 14

1.3.2 Bone metastases 15

1.3.3 Bone remodelling 16

1.3.4 The bone microenvironment 17

1.3.5 Vicious cycle 24

1.4 Metabolism 26

1.5 Cancer Metabolism 35

1.5.1 Warburg effect 35

1.5.2 Metabolic crosstalk in the tumour microenvironment and the "Reverse Warburg" effect 37

1.5.3 Prostate cancer metabolism 39

1.6 Bone cell metabolism 45

1.7 Prostate cancer mouse models 46

1.8 Hypothesis and aims 48

2 Materials and Methods 49
2.1 Cell Culture 49
2.1.1 Mycoplasma Testing 51
2.1.2 Transwell Co-culture 52
2.1.3 Conditioned media (CM) Treatment 52
2.1.4 Recombinant IL-6 and IL-6 neutralising antibody treatment 52
2.1.5 Drug treatments 53
2.1.6 Hypoxic conditions 53
2.1.7 Glucose free conditions 53
2.1.8 Androgen deprivation conditions 54
2.2 Cell proliferation 54
2.3 Cell viability 54
2.3.1 Alamar blue assay 54
2.3.2 Trypan blue 55
2.4 Colony formation assay 55
2.5 Cell cycle by propidium iodide staining 56
2.6 Migration Assay 56
2.6.1 IncuCyte WoundMaker Assay 56
2.6.2 Transwell migration assay 57
2.7 Oxygen consumption assays 58
2.8 Extracellular acidification assay 60
2.9 Capillary Electrophoresis Mass Spectrometry (CE-MS) analysis 60
2.10 Protein isolation and western blotting 62
2.11 Ribonucleic acid (RNA) isolation 65
2.12 cDNA synthesis 65
2.13 Quantitative real-time polymerase chain reaction (qPCR) 66
2.14 *In silico* analysis 68
2.15 Glucose-6-phosphate dehydrogenase (G6PD) activity quantification 68
2.16 Mitochondrial superoxide (MitoSox) quantification 69
2.17 Reactive oxygen species (ROS) quantification 70
2.18 Glutathione (GSH) quantification 70
2.19 Transfection 71
2.19.1 Short hairpin RNA (shRNA) and Open Reading Frame (ORF) Transfection 71
2.19.2 Lentiviral packaging and trasduction 73

2.20 RNA Sequencing (RNA Seq) ... 75
2.20.1 NEBNext Ultra II RNA library prep for Illumina ... 75
2.20.2 Illumina Sequencing ... 76
2.20.3 Bioinformatics ... 76
2.21 *In vivo* model ... 77
2.21.1 C4-2B Intra-tibial model ... 77
2.21.2 Human PSA (KLK3) enzyme-linked immunosorbent assay (ELISA) ... 78
2.21.3 PC3-EGFP Intra-tibial model ... 79
2.21.4 IVIS imaging ... 79
2.21.5 *Ex-vivo* µCT of bones ... 80
2.21.6 Extraction of *ex-vivo* tumour RNA ... 80
2.21.7 Histopathology ... 81
2.22 Statistical Analysis ... 82

3 Bone marrow stromal cells alter the metabolic profile of prostate cancer ... 83
3.1 Introduction ... 83
3.2 Aims ... 84
3.3 The bone microenvironment creates a permissive environment for prostate cancer cells to grow ... 85
3.4 The bone microenvironment alters the expression of metabolic genes ... 87
3.5 Oxidative phosphorylation is increased in bone metastatic prostate cancer cells ... 90
3.6 Bone marrow stromal cells alter the metabolite profile of prostate cancer cells ... 92
3.7 Metabolic pathways are significantly altered in prostate cancer cells isolated from metastases when compared to primary tumours ... 99
3.7.8 Hutchinson Data set (Kumar et al, 2016) ... 99
3.7.9 MSKCC 2010 Data set (Taylor et al, 2010) ... 104
3.8 Expression of pentose phosphate pathway enzymes, is increased in bone metastatic prostate cancer cells ... 106
3.9 Discussion ... 108
3.10 Future Direction ... 113

4 The bone microenvironment promotes up-regulation of G6PD ... 115
4.1 Introduction ... 115
4.2 Aims ... 116

4.3 G6PD is up-regulated in prostate cancer isolated from the bone of patients with bone metastases 117

4.4 Expression of G6PD can be induced in non-bone metastatic cell lines by co-culture with BMSCs 120

4.5 Expression of TCA and OXPHOS enzymes is not affected by bone stromal cells . 121

4.6 The increase in G6PD expression is not dependent on extracellular glucose or oxygen levels 122

4.7 The increase in G6PD expression is enhanced in androgen deprived conditions 124

4.8 The increase in G6PD is via a factor secreted by BMSCs 126

4.9 The increase in G6PD expression induced by BMSCs is specific to HS5 BMSCs .. 128

4.10 HS5 cells secrete high levels of IL-6 which activates STAT3 signalling in PCa cells 130

4.11 Neutralising IL-6 in HS5 CM inhibits the up-regulation of G6PD protein in LNCaP cells 132

4.12 Recombinant IL-6 causes up-regulation of G6PD in LNCaP cells 134

4.13 Mammalian target of rapamycin (mTOR) signalling is not stimulated by HS5 BMSCs 135

4.14 Discussion 136

4.15 Future Directions 142

5 Bone marrow stromal cells modulate the redox state and growth of prostate cancer 143

5.1 Introduction 143

5.2 Aims 145

5.3 Bone marrow stromal cell conditioned media increases reactive oxygen species 146

5.4 Bone metastatic PCa cells have increased GSH 148

5.5 BMSCs increase the anti-oxidant ability of prostate cancer cells 149

5.6 Antioxidants can inhibit the increase in G6PD protein induced by HS5 CM 150

5.7 HS5 CM causes cell cycle arrest and inhibits growth of non-bone metastatic prostate cancer cells 151

5.8 HS5 cells inhibit the growth of prostate cancer *in vivo* 155

5.9 Discussion 158

5.10 Future Directions 160

6 The effects of manipulating G6PD expression on prostate cancer 162

6.1 Introduction 162

6.2 Aims 163

6.3 Generation of stable G6PD knockdown cell lines 164

6.4 G6PD knockdown reduces the proliferation and colony forming ability of prostate cancer cells 166

6.5 G6PD knockdown alters the morphology of PCa cells 168

6.6 G6PD knockdown affects the expression of EMT markers 170

6.7 G6PD knockdown inhibits PCa cell migration 172

6.8 G6PD knockdown inhibits phosphorylation of STAT3 174

6.9 G6PD knockdown increases ROS levels and reduces levels of GSH 176

6.10 G6PD knockdown sensitises metastatic prostate cancer cell lines to chemotherapy 177

6.11 Knockdown of G6PD causes alterations in the expression of several cancer hallmark gene sets 179

6.12 G6PD knockdown inhibits the proliferation of prostate cancer *in vivo* 185

6.13 Pharmacological inhibition of G6PD with 6-aminonicotinamide reduces viability and increases ROS in PCa cells 187

6.14 Generation of G6PD overexpression cells 189

6.15 Overexpression of G6PD may increase the proliferation rate of PCa cells 190

6.16 Overexpression of G6PD down-regulates expression of an epithelial marker 191

6.17 G6PD overexpression promotes STAT3 signalling 192

6.18 Overexpression of G6PD in LNCaP cells decreases their baseline ROS level 193

6.19 Overexpression of G6PD in LNCaP cells did not increase resistance to chemotherapy 194

6.20 Discussion 195

6.21 Future Direction 199

7 Summary and Future Directions 201

7.1 Summary 201

7.2 Future Directions 208

7.2.10 Further exploration into the metabolic changes induced by the bone microenvironment 208

7.2.11 The effect of androgens on G6PD expression 209

7.2.12 The correlation between G6PD expression and treatment resistance in PCa 209

7.2.13 Does long term conditioning of PCa cells with BMSCs select a drug resistant population? 210
7.2.14 Does manipulating G6PD in PCa cells impact on bone remodelling? 211
7.2.15 The identification of novel G6PD targeted therapies 211
7.3 Summary statement 212

Appendix A 213

Appendix B 215

Bibliography 217

List of Figures

Figure 1.1: Structure of the prostate. 3
Figure 1.2 Prostate cancer initiation, progression and advancement. 5
Figure 1.3 Bone metastasis in prostate cancer 6
Figure 1.4 Gleason grading of prostate cancer 7
Figure 1.5 Treatment options in advanced prostate cancer 12
Figure 1.6 The metastatic process. 14
Figure 1.7 Bone cell differentiation 23
Figure 1.8 Cytokines and growth factors secreted by CAFs 23
Figure 1.9 The vicious cycle. 25
Figure 1.10 The glycolytic pathway. 27
Figure 1.11 The tricarboxylic acid cycle. 29
Figure 1.12 Oxidative phosphorylation and the electron transport chain. 30
Figure 1.13 The pentose phosphate pathway. 32
Figure 1.14: The Warburg effect 37
Figure 1.15 The Reverse Warburg effect between CAFs and cancer cells. 39
Figure 1.16: Alteration in prostate cell metabolism during malignant transformation. 40
Figure 2.1 Prostate cancer cell lines used 51
Figure 2.2 Cell seeding density optimisation MitoXpress kit. 59
Figure 2.3 Z-depth on TRF Optic head optimisation. 59
Figure 2.4 TRC2 Puromycin shKD Vector map and features. 72
Figure 2.5 TRC3 Puromycin ORF Vector map and features. 72
Figure 2.6 Puromycin kill curve. 74
Figure 3.1 In vivo growth of C4-2B PCa cells. 86
Figure 3.2 Gene expression changes in C4-2B intra-tibial tumours compared to C4-2B cells maintained in vitro. 89
Figure 3.3 Metabolic profile of prostate cell lines. 91
Figure 3.4 Heat map showing changes in intracellular metabolite levels 94

Figure 3.5 Pathway map demonstrating changes in intracellular metabolite levels in PC3 cells after co-culture with HS5 cells.. 95
Figure 3.6 Changes in levels of intracellular metabolites of the glycolysis pathway 96
Figure 3.7 Changes in levels of intracellular metabolites of the TCA cycle 97
Figure 3.8 Changes in levels of intracellular metabolites of the PPP 98
Figure 3.9 Changes in levels of intracellular metabolites of the gluatmine pathway 98
Figure 3.10 In-silico analysis of metabolic changes in the different metastatic sites compared to primary prostate tumours from the Hutchinson Data Set. 103
Figure 3.11 Baseline expression of metabolic proteins in a range of prostate caner cell lines.. 107
Figure 4.1 In Silico analysis of G6PD expression in publicly available advanced PCa patient sample data sets..... 119
Figure 4.2 G6PD expression is induced by BMSCs. 120
Figure 4.3 Expression of OXPHOS and TCA proteins after co-culture with HS5 BMSCs. 121
Figure 4.4 Glucose levels do not affect G6PD up-regulation. 122
Figure 4.5 Hypoxic conditions lower G6PD expression but do not affect G6PD up-regulation. 123
Figure 4.6 G6PD up-regulation is enhanced in androgen-deprived conditions.. 125
Figure 4.7 HS5 BMSCs CM promote expression of G6PD.. 127
Figure 4.8 The increase in G6PD protein expression is specific to HS5 BMSCs. 129
Figure 4.9 HS5 cells secrete IL-6 and cause phosphorylation of STAT3. 131
Figure 4.10 Neutralising IL-6 inhibits the up-regulation of G6PD protein..... 133
Figure 4.11 Recombinant Il-6 causes increased G6PD mRNA expression. 134
Figure 4.12 HS5 BMSC do not activate the mTOR pathway in prostate cancer cells.. 135
Figure 4.13 IL-6 signalling via STAT3 and its pro-tumourigenic effects. 141
Figure 5.1 BMSC CM and G6PD inhibition increases cellular ROS. 147
Figure 5.2 Metastatic PCa cells have higher GSH levels. 148
Figure 5.3 BMSCs increase the antioxidant level in PCa cells. 149
Figure 5.4 NAC inhibits the up-regulation of G6PD protein 150
Figure 5.5 HS5 CM causes cell cycle arrest in G1 in non-bone metastatic PCa cell lines. .. 152

Figure 5.6 HS-5 CM reduces the viability of non-bone metastatic cell lines.. 154
Figure 5.7 HS5 cells inhibit the growth of PCa cells in vivo. 157
Figure 6.1 shKD of G6PD.. 165
Figure 6.2 G6PD KD inhibits PC3-EGFP proliferation and colony formation but not cell cycle. 167
Figure 6.3 Morphology of G6PD shKD cells.. 169
Figure 6.4 mRNA expression of EMT markers..... 171
Figure 6.5 G6PD KD inhibits cancer cell migration. 173
Figure 6.6 STAT3 inhibition by shG6PD KD.. 175
Figure 6.7 G6PD KD increases ROS levels and reduces GSH levels in prostate cancer cell lines..... 176
Figure 6.8 Chemotherapy increases mitochondrial ROS..... 178
Figure 6.9 G6PD KD sensitises metastatic PCa cell lines to chemotherapy. 178
Figure 6.10 PCA plot from RNA Seq of PC3-EGFP SCR and shG6PD cells. 181
Figure 6.11 RNA Seq showing differentially expressed genes between PC3-EGFP SCR and shG6PD cells..... 183
Figure 6.12 In vivo growth of PC3-EGFP SCR and shG6PD cells. 186
Figure 6.13 Pharmacological inhibition of G6PD with 6AN..... 188
Figure 6.14 G6PD Overexpression in LNCaP cells..... 189
Figure 6.15 G6PD overexpression promotes proliferation and colony formation. 190
Figure 6.16 G6PD OE effect on EMT markers. 191
Figure 6.17 G6PD OE increases STAT3 phosphorylation. 192
Figure 6.18 Total ROS in G6PD OE cells. 193
Figure 6.19 G6PD OE did not increase resistance to chemotherapy. 194
Figure 7.1 Summary of the main findings of this thesis 205
Figure 7.2 Summary of the effects of inhibiting G6PD in prostate cancer cells. 207
Figure A.2 Autofluorescence of mice in the intra-tibial PC3-EGFP model. 214

List of Tables

Table 1.1: Gleason grading of prostate histology..... 8

Table 1.2: International Society of Urological Pathology 2014 Grades. 8

Table 1.3: Tumour Node Metastasis (TNM) classification of PCa..... 9

Table 1.4 Staging of PCa based on TNM classification..... 9

Table 2.1 Antibodies used 64

Table 2.2 Taqman primer list..... 67

Table 2.3 Qiagen Primer list. 67

Table 2.4 SYBR primer list.. 67

Table 2.5 Genes included on custom metabolism TLDA gene card. 81

Table 3.1 In silico gene set enrichment analysis of metabolic changes in metastatic sites compared to primary tumours from the Hutchinson Data Set using GSEA cancer hallmark gene set.. 102

Table 3.2 In silico gene set enrichment analysis of metabolic changes in metastatic sites compared to primary tumours from the Hutchinson Data Set using a metabolic specific gene set.. 102

Table 3.3 In-Silico analysis of metabolic changes in metastatic sites compared to primary tumours from the MSKCC Data Set. 105

Table 6.1 GSEA Cancer Hallmark gene sets analysis of PC3-EGFP shG6PD compared to SCR.. 184

List of Acronyms

1,3BPG - 1,3-bisphosphglycerate
2PG – 2-phosphoglycerate
3PG - 3-phosphoglycerate
6AN - 6-aminonicotinamide
6PG - 6-phosphogluconate
6PGluco(1,5)L - 6-phosphoglucono-δ- lactone
ACACA - acetyl-CoA Carboxylase
ACADS - acyl-CoA dehydrogenase short chain
Acetyl CoA - acetyl coenzyme A
ACLY - ATP citrate lyase
ADP - adenosine diphosphate
ADT - androgen deprivation therapy
AKT - protein kinase B
AMACR - alpha-methylacyl-CoA racemase
ANOVA - analysis of variance
Anti-IL-6- IL-6 neutralising antibody
AR - androgen receptor
ATCC - American Type Culture collection
ATP - adenosine triphosphate
BCA - bicinchoninic acid
BMD - bone mineral density
BMPs - bone morphogenetic proteins
BMSCs - bone marrow stromal cells
BPH - benign prostatic hyperplasia
BS- 99mTc-Bone scan
BSA - bovine serum albumin
CAFs - cancer-associated fibroblasts
CDH1- E-cadherin
cDNA - complementary DNA
CE-MS - capillary Electrophoresis Mass Spectrometry
CM - conditioned media
CO_2 - carbon dioxide
Complex I - NADH-Q oxidoreductase
Complex II - succinate-Q-reductase
Complex III - Q-cytochrome c oxidoreductase
Complex IV - cytochrome c oxidase
CPTI - carnitine palmitoyl transferase I
CRPC - castration-resistant prostate cancer
CS - citrate synthase
CSF-1 - colony stimulating factor 1

CT - computed tomography
CXCL12 - C-X-C motif chemokine 12
CXCR4 - C-X-C chemokine receptor 4
DBP - D-bifunctional protein
DHAP - dihydroxyacetone phosphate
DHEA - dehydroepiandrosterone
DHT - dihydrotestosterone
DKK1 - Dickkopf WNT Signalling Pathway Inhibitor-1
DNA - deoxyribonucleic acid
DRE - digital rectal examination of the prostate
DTX – docetaxel
E4P - erythrose 4-phosphate
ECAR - extracellular acidification rate
ECM - extracellular matrix
ELISA - enzyme-linked immunosorbent assay
EMT - epithelial-to-mesenchymal-transition
ET-1 - endothelin-1
ETC - electron transport chain
F1,6BP - fructose 1,6-bisphosphate
F6P - fructose 6-phosphate
FA - fatty acid
$FADH_2$ - flavin adenine dinucleotide
FASN - fatty acid synthase
FBS - fetal bovine serum
FDG - fluorine-18-fluorodeoxyglucose
FDR - false discover rate
FGF - fibroblast growth factor
G-CSF - granulocyte-colony stimulating factor
G6P - glucose 6-phosphate
G6PD – glucose-6-phosphate dehydrogenase
GAP - glyceraldehyde 3-phosphate
GAPDH - glyceraldehyde 3-phosphate dehydrogenase
GAS - interferon-gamma activated sequence
GC-MS - gas-chromatography mass spectrometry
GEM - genetically engineered mice
GFP - green fluorescent protein
GLS-1 - glutaminase-1
GSH – reduced glutathione
GSH-Px - glutathione peroxidase
GSR - glutathione reductase
GSSG - oxidised glutathione
GTP - guanosine tri-phosphate
H&E - haematoxylin and eosin
H_2O - water

H_2O_2 - hydrogen peroxide
H6PD - hexose-6-phosphate dehydrogenase
HIF1α - hypoxia-inducible factor 1-alpha
HMG-CoA - 3-hydroxy-3-methylglutaryl –Co enzyme A
IGFs - insulin-like growth factors
IgG – immunoglobulin G
IL-6 - interleukin-6
ISUP - International Society of Urological Pathology
JAK - janus tyrosine family kinase
LC-MS - liquid chromatography mass spectrometry
LHRH - luteinising hormone-releasing hormone
MAPK - mitogen-activated protein kinase
mCRPC - metastatic castrate resistant PCa
MCT - monocarboxylate transporter
MET - mesenchymal epithelial transition
miRNA - microRNA
Mp-MRI - multiparametric magnetic resonance imaging
MSCs - mesenchymal stem cells
mTOR - mammalian target of rapamycin
NAC - N-acetylcysteine
NADH - nicotinamide adenine dinucleotide
$NADP^+$ - nicotinamide adenine dinucleotide phosphate
NADPH - nicotinamide adenine dinucleotide phosphate hydrogen
NCPs - non-collagen proteins
Nkx3.1- homeobox protein NKx3.1
NOX - NADPH oxidases
O_2 - oxygen
OCR - oxygen consumption rate
OPG - osteoprotegerin
OPN - osteopontin
ORF - open reading frame
OS - overall survival
OXPHOS - oxidative phosphorylation
PBS - phosphate buffered saline
PCa – prostate cancer
PCA- principal component analysis
PDGF - platelet derived growth factor
PEP - phosphoenolpyruvate
PET - positron emission tomography
PFK - phosphofructokinase
PI - propidium iodide
PI3K - phosphatidylinositol-3-kinase
PIN - prostate intraepithelial neoplasia
Polr2a - RNA polymerase II subunit A

PPP - pentose phosphate pathway
PSA - prostate specific antigen
PTEN - phosphatase and tensin homolog
PTH - parathyroid hormone
PTHrP - parathyroid hormone related protein
PVDF - polyvinylidene difluoride membrane
qPCR - quantitative real-time polymerase chain reaction
R5P - ribose 5-phosphate
RNA - ribonucleic acid
RNA Seq - RNA-Sequencing
ROS - reactive oxygen species
RU5P – ribulose-5-phsophate
RUNX2 - runt-related transcription factor
S7P – sedoheptulose-7-phosphate
SCID - severe combined immune deficient
SDS-PAGE - sodium dodecyl sulphate-polyacrylamide
shRNA - short hairpin RNA
siRNAs - small interfering RNAs
SOC3 - cytokine signalling 3
SRE - skeletal related events
SREBP1c - sterol regulatory element binding protein-1c
STAT3- signal transducer and activator of transcription 3
TBS - tris-buffered saline
TCA cycle -tricarboxylic acid cycle
TGF-β - transforming growth factor-beta
TKT - transketolase
TNFR – tumour necrosis factor receptor
TPI - triose phosphate isomerase
TRAMP - transgenic adenocarcinoma mouse prostate
TRAP - tartrate resistant acid phosphatase
TUNEL - terminal deoxynucleotidyl transferase dUTP nick end labelling
uPA - urokinase-type plasminogen activator
VEGF-A - vascular endothelial growth factor-A
Xu5P - xylulose 5-phosphate
ZA - zoledronic acid
ZEB2- zinc finger E-box binding homeobox 2

1

Introduction

1.1 The Prostate

The human prostate is a small walnut-sized male exocrine gland located in the pelvis at the base of the bladder and surrounding the proximal urethra (Figure 1.1). It is separated from the surrounding organs and tissue by a band of fibrous connective tissue called the prostatic capsule. The primary function of the prostate gland is to produce and store part of the seminal fluid, and to assist in its expulsion during ejaculation. The fluid produced by the prostate makes up 25% of seminal fluid and aids sperm motility and viability, protecting the spermatozoa from the acidic environment of the female reproductive tract. The major constituents of prostatic secretions include prostate specific antigen (PSA), prostatic acid

phosphatase, citrate, zinc, spermine and cholesterol[1,2]. The prostate gland is made up of glandular epithelial cells (comprising of luminal and basal cells), which are surrounded by variable amounts of stroma (comprising of myoepithelial cells and stromal cells)[3]. The glandular epithelial cells are highly organised into a contiguous basal layer (composed of stem, transit amplifying and committed basal cells), and a layer of columnar secretory luminal cells that make up around 60% of the epithelial cells[4]. Prostate cancer typically develops from the glandular epithelial cells.

1.1.1 Prostate Structure

The structure of the prostate can be classified by two different systems. The zonal classification is more frequently used in pathology identifying three main morphological zones[5]: the peripheral zone (nearly 70% of the gland) surrounding the urethra, the central zone (constituting 25%) surrounding the ejaculatory ducts, and the transition zone that consists of fibromuscular tissue (Figure 1.1). Benign prostatic hyperplasia (BPH), a non-malignant overgrowth of the prostate, occurs mainly in the transition zone, whilst prostate carcinoma typically arises in the peripheral zone[6].

The lobe classification system is typically used when describing the anatomy of the prostate, and divides the prostate into four regions: the anterior lobe, the posterior lobe, lateral lobes, and the median or middle lobe.

Interestingly the prostate gland is highly susceptible to oncogenic transformation at a frequency significantly greater than that of other male secondary sexual tissues such as the seminal vesicles.

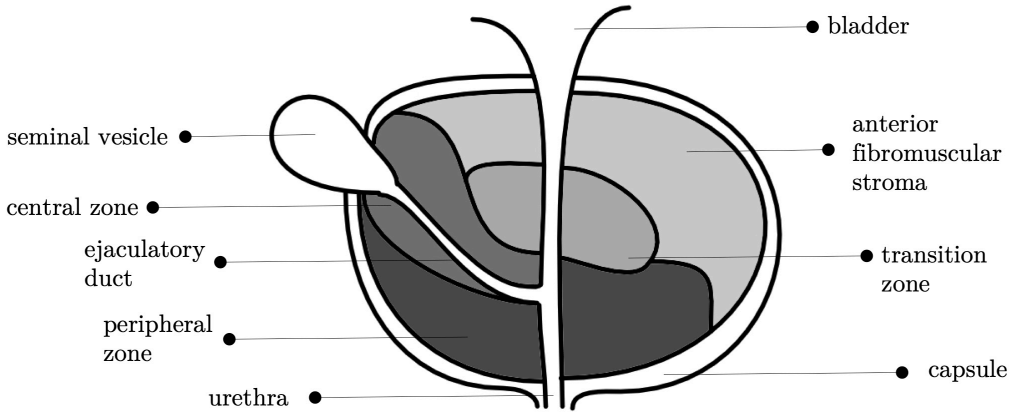


Figure 1.1: ***Structure of the prostate.*** Coronal cross-section of the prostate demonstrating zones and related structures.

1.2 Prostate Cancer

1.2.1 Epidemiology and Aetiology

Prostate cancer is the most common malignancy in men in the Western World, and the second leading cause of cancer associated death. In the UK almost 48,000 men are diagnosed, and 11,500 men die each year from the disease[7]. Whilst the incidence of PCa diagnosis varies widely between different geographical areas, the frequency of autopsy detected PCa is roughly the same worldwide[8], suggesting differences in incidence are largely due to differences in the use of PSA testing. The incidence of prostate cancer is known to increase with age[9], and therefore the disease burden is likely to increase in the future in developed countries, such as the UK, as the population ages. Other well established risk factors include family history and African ethnic origin, suggesting there is a genetic predisposition[10]. Men with African ethnic origin were found to have a 3-fold higher risk of developing prostate cancer compared to white males[11], whilst having a first degree relative with prostate cancer increases the risk of prostate cancer diagnosis 2 fold, with the risk increasing further if more

than one first degree relative is affected[12]. However, environmental factors are also thought to play an important role in the risk of progression of prostate cancer. This is supported by a study that showed that when Japanese men move from Japan to California, their risk of PCa increases, approaching that of American men[13]. Other factors that have been proposed to play a role in development of prostate cancer include the presence of metabolic syndrome[14], obesity[15,16] and dietary factors. However, currently there are no effective preventative dietary or pharmacological interventions.

1.2.2 Prostate tumourigenesis

Prostate intraepithelial neoplasia (PIN) is the major pre-cancerous lesion of the prostate. It is characterised by enhanced glandular epithelial cell hyperplasia, and is biochemically, genetically and phenotypically similar to prostate cancer, yet lacks any disruption of the basement membrane[4]. Prostate cancer develops as tumour cells invade through the basement membrane forming larger tumours in the prostate mesenchyme (Figure 1.2). As prostate cancer typically develops in the peripheral zone of the prostate, away from the urethra, early stages of carcinoma that are confined to the prostate are often asymptomatic. Later as the tumour expands patients may present with difficulty voiding urine, hesitancy, frequency and nocturia due to obstruction of the prostatic urethra / bladder. Tumour cells can go on to invade through the prostate capsule into surrounding tissues, and spread to lymph nodes and distant organs including bone through lymphatic drainage and blood vessels. Advanced or metastatic prostate cancer may present with bone pain, impotence, or weight loss. Nearly all PCa associated mortality is caused by distant metastases typically to the bone[17]. The 5

year survival rate for men diagnosed with localised disease is nearly 100%, while only 30% of men diagnosed with metastatic PCa survive beyond 5 years[7]. Bone is the most common metastatic site of prostate cancer with around 90% of patients with advanced prostate cancer having skeletal metastasis[18].

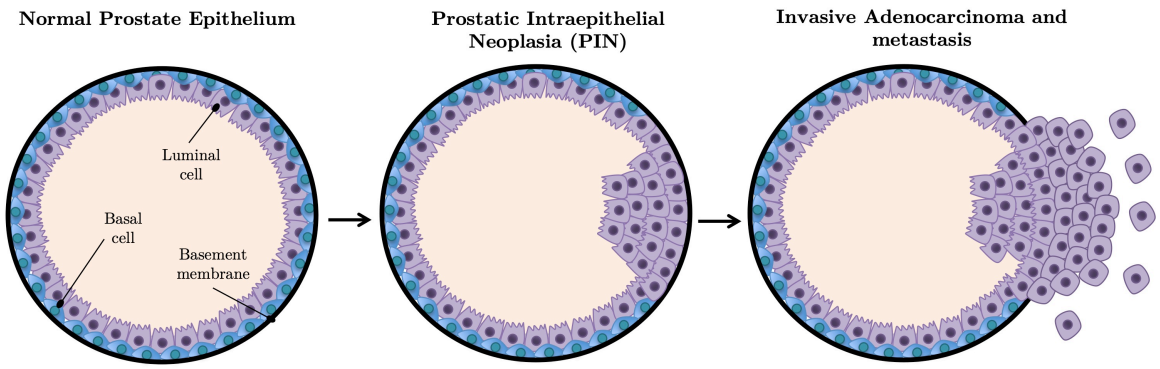


Figure 1.2 ***Prostate cancer initiation, progression and advancement.*** *PIN is characterised by glandular epithelial cell hyperplasia with no disruption of the basement membrane. Prostate cancer develops as the tumour cells invade through the basement membrane.*

1.2.3 Clinical Diagnosis

Most men with early prostate cancer are asymptomatic and therefore diagnoses are often based on a digital rectal examination of the prostate (DRE) and/or PSA levels. If palpation of the prostate (DRE) reveals hardness or an abnormal mass the patient is typically referred for biopsy. PSA is a serine protease secreted by the glandular epithelial cells of the prostate. Its serum level is typically elevated in prostate cancer, but whilst it is organ specific it is not cancer-specific, and therefore may be elevated in other prostatic conditions (e.g. prostatitis, benign prostatic hypertrophy). Despite this, it has been the mainstay of prostate cancer screening and monitoring since its development in 1980[19]. However, its routine use as a

screening tool remains controversial with concerns that it leads to over-investigation and over-diagnosis causing harm to men with no overall survival benefit[20]. Therefore, at present there is no routine screening programme for prostate cancer in the UK.

Definitive diagnosis depends on histological verification obtained via prostate biopsy. This may be supplemented with bone scanning and computed tomography (CT) (Figure 1.3) or multiparametric magnetic resonance imaging (mp-MRI) to give accurate staging, or enable targeted biopsy. ^{99m}Tc-Bone scan (BS) is the most widely used method to evaluate the presence of bone metastases in prostate cancer, although whole body MRI is gaining popularity. BS involves the administration of radioactive technetium, which has a tendency to localise to bones, particularly in areas of high bone turnover. Metastatic sites appear as dark spots on the bone scan due to increased radioactivity, as does the bladder from where the technetium is stored before excretion.

A **B**



Figure 1.3 ***Bone metastasis in prostate cancer*** *(A) CT scan of the thoracic spine showing multiple lesions due to prostate cancer metastases (By James Heilman, Open Access under CC BY-SA 4.0). (B) Radionuclide scintigraphy of a patient with prostate cancer bone metastases (RadsWiki, Open Access under CC BY-SA 3.0)*

1.2.4 Tumour Grading

The vast majority (95%) of malignant prostate tumours are adenocarcinomas that originate in the epithelial cells covering the prostatic acini and glandular ducts. Cancers are graded histologically using the Gleason grading system, which was first introduced in 1974[21] (Figure 1.4; Table 1.1). Two grade scores (1-5) are assigned for the two most dominant (in terms of volume) tumour patterns. These scores are added together to given an overall Gleason score (2-10). Histological grading of the apparent degree of malignancy of the tumour is the strongest prognostic factor for clinical behaviour and treatment response. An American study found men with Gleason 6 PCa have between 18-30% PCa mortality within 15 years of diagnosis, whilst men with Gleason 8-10 PCa have a 60-87% mortality[22]. The Gleason grade then determines the International Society of Urological Pathology 2014 (ISUP) grade, which correlates with disease risk (Table 1.2).

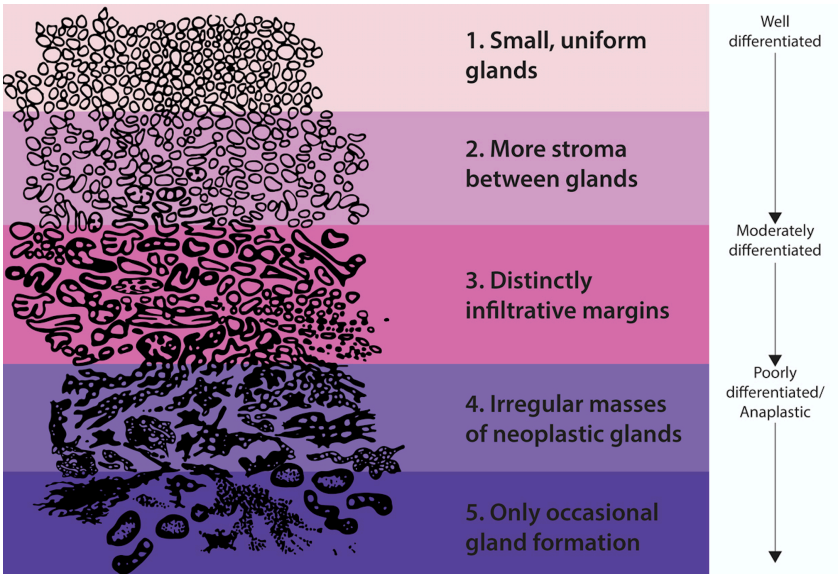


Figure 1.4 ***Gleason grading of prostate cancer.*** *Image in public domain from the National Institutes of Health.*

Grade	Histological features
1	Cells closely resemble normal prostate cells. Glands are small, well formed and closely packed
2	Glands are larger with more tissue between
3	The cells are darker with some invading surrounding tissue
4	Few recognizable glands. Many invading cells
5	The tissue does not have recognizable glands, often just sheets of cells throughout the surrounding tissue

Table 1.1: ***Gleason grading of prostate histology.***

Gleason score	ISUP grade
2 - 6	1
7 (3 + 4)	2
7 (4 + 3)	3
8	4
9 - 10	5

Table 1.2: ***International Society of Urological Pathology 2014 Grades.*** *Adapted from EAU-ESTRO-ESUR-SIOG Guidelines on Prostate cancer 2017* [23].

1.2.5 Tumour staging

Once a tumour has been diagnosed and graded the cancer is staged to determine treatment options (Table 1.4). The TNM staging is used to evaluate the extent of the primary tumour (T), the involvement of regional lymph nodes (N) and the presence of metastases (M) (Table 1.3).

Primary Tumour (T)		
TX		Primary tumour cannot be assessed
T0		No evidence of primary tumour
T1		Clinically inapparent tumour that is not palpable
	T1a	Tumour incidental histological finding in 5% of less of tissue resected
	T1b	Tumour incidental histological finding more than 5% of tissue resected
	T1c	Tumour identified by needle biopsy (e.g. because of elevated PSA level)
T2		Tumour that is palpable and confined within the prostate
	T2a	Tumour involves one half of one lobe or less
	T2b	Tumour involves more than half of one lobe, but not both lobes
	T2c	Tumour involves both lobes
T3		Tumour extends through the prostatic capsule
	T3a	Extra-capsular extension including microscopic bladder neck involvement
	T3b	Tumour invades seminal vesicle(s)
T4		Tumour is fixed or invades adjacent structures other than seminal vesicles
Regional Lymph Nodes (N)		
NX		Regional lymph nodes cannot be assessed
N0		No regional lymph node metastasis
N1		Regional lymph nodes metastasis
Distant Metastasis (M)		
M0		No distant metastasis
M1		Distant metastasis
	M1a	Non-regional lymph node(s)
	M1b	Bone(s)
	M1c	Other site(s)

Table 1.3: ***Tumour Node Metastasis (TNM) classification of PCa***[24]*.*

Stage			
Stage I	T1, T2a	N0	M0
Stage II	T2b-2c	N0	M0
Stage III	T3,T4	N0	M0
Stage IV	Any T	N1	M0
	Any T	Any N	M1

Table 1.4 ***Staging of PCa*** *based on TNM classification.*

1.2.6 Management of prostate cancer

In its initial stages, when confined to the prostatic capsule, prostate carcinoma is essentially curable by surgical excision and / or external-beam radiotherapy (Stages I-II). Surgical excision is done by radical prostatectomy where the entire gland is removed, and may also involve removal of regional lymph nodes and seminal vesicles depending on tumour involvement (Stage III-IV). In some patients adjuvant external-beam radiation therapy following surgery may be offered to reduce the risk of recurrence. However, many cases of prostate carcinoma are relatively indolent; many men diagnosed with prostate cancer will die with prostate cancer rather than of prostate cancer. In view of this low risk patients with a long life expectancy may be put on active surveillance, with treatment being initiated upon signs of tumour progression. Low risk patients with a short life expectancy may opt for watchful waiting where treatment is commenced when symptoms of metastasis develop. This is to avoid unnecessary treatments and their associated side-effects and complications.

Advanced prostate cancer (Stage IV), or relapse following surgery / radiation therapy is characterized by local invasion outside the capsule, followed by metastasis primarily to bone. In the setting of advanced metastatic prostate cancer, current treatments are not curative but purely palliative. The mainstay of treatment is androgen deprivation therapy (ADT), also known as hormone therapy, either by chemical (administration of luteinising hormone-releasing hormone (LHRH) agonists and non-steroidal anti-androgens) or surgical castration. Prostate cancer that has become resistant to hormonal therapy and progressed despite castrate levels of androgens (<50ng/ml) is termed castration-resistant prostate cancer

(CRPC) and effective treatments are limited[25]. Progression to CRPC typically occurs within 1-2 years of initial response[26], and overall survival only is 2-3 years[27]. Secondary hormonal therapy with abiraterone acetate or enzalutamide is an option in some patients, although responses are transient with currently available agents. Abiraterone acetate is a selective cytochrome p450 17A1 inhibitor that blocks steroid conversion and therefore androgen production within the prostate, testis and adrenal gland. Enzalutamide is a novel anti-androgen that antagonises the full-length androgen receptor (AR) and prevents its nuclear translocation, AR binding to DNA, and co-activator recruitment by the AR[28]. Both have been shown to improve overall survival (OS) in the post-chemotherapy setting. However, the use of ADT results in loss of bone mineral density (BMD) with a subsequent increased risk of osteoporotic fragility factures, and there is evidence that castration may even promote the growth of prostate cancer in bone metastases[29]. The bone metastases seen in prostate cancer are typically described as sclerotic or osteoblastic, although it is increasingly being recognised that lytic areas are also seen. In osteoblastic lesions the balance between bone resorption and bone formation is tipped in favour of the latter. Despite increased bone being formed the quality is poor leading to patients suffering from skeletal related events (SRE) that encompass a range of complications of bone metastasis including pathological fractures, spinal cord compression and severe bone pain necessitating surgery or radiotherapy[30].

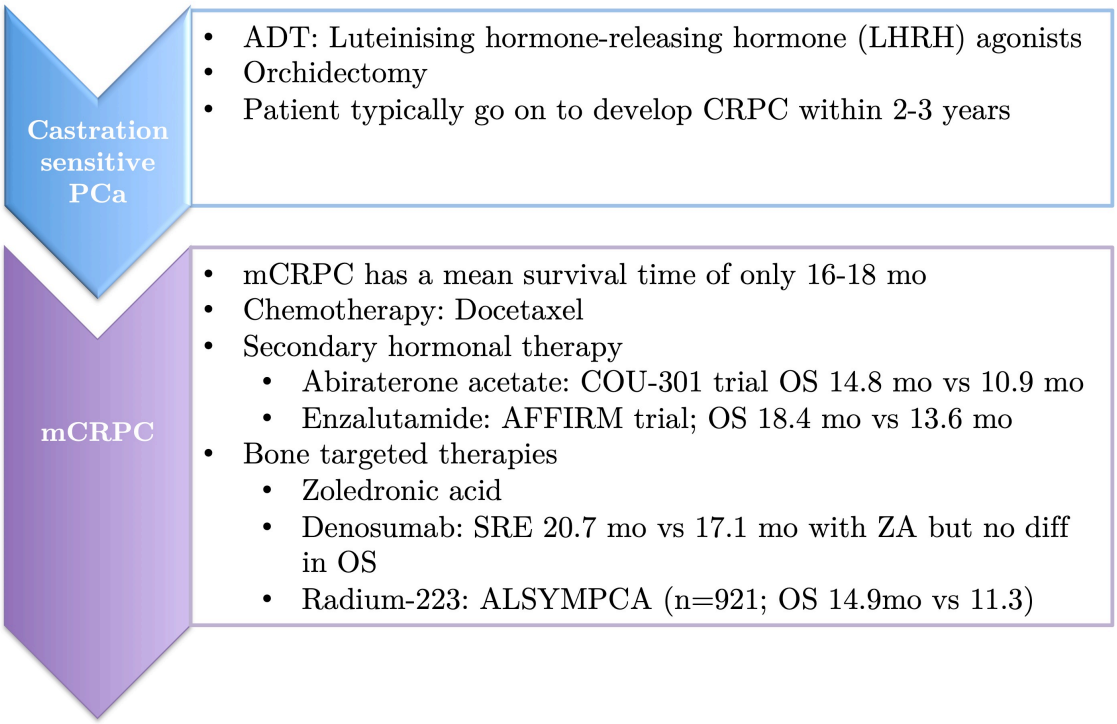


Figure 1.5 ***Treatment options in advanced prostate cancer*** *and associated trials. Mo: months; OS: overall survival, SRE: skeletal related event; ZA: zoledronic acid.*

Currently Docetaxel (DTX) is the standard chemotherapeutic drug for CRPC, and it has been shown to significantly prolong survival. Recent studies have even suggested a role for DTX earlier in the treatment pathway at the start of ADT[31]. DTX is a taxane that binds β-tubulin, stabilizing microtubules assembly and preventing depolymerisation in the absence of guanosine tri-phosphate (GTP)[32]. Furthermore, DTX leads to Bcl-2 phosphorylation, which causes apoptosis in cells that have previous blocked this apoptosis inducing pathway[33]. However, only approximately 50% of patients respond to docetaxel and most of them eventually develop resistance to this therapy[34]. As well as not always being effective, taxanes also lead to a range of toxic side-effects including neutropaenia, nausea and vomiting and cardiovascular events (deep vein thrombosis and pulmonary embolism)[35]. Therefore there is a

need to improve the efficacy and/or enable clinicians to use DTX at a lower, less toxic dose while maintaining efficacy.

Bone targeted therapies can be used in PCa to prevent bone disease and consequent pathological fractures. Zoledronic acid (ZA) is a pyrophosphate analogue that binds to hydroxyapatite, accumulating in bone and inhibiting osteoclastic action. Despite prostate cancer generally causing osteoblastic metastases ZA has been shown to reduce bone pain and SRE in men with CRPC[36]. Denosumab is an antibody against receptor activator of NF-κB ligand that has been shown to delay the time to first and subsequent SRE when compared to ZA[37]. Radium-223 dichloride (radium-223) is a targeted alpha emitter that selectively binds to areas of increased bone turnover in bone metastases and emits high-energy alpha particles of short range (<100 μm) which induce mainly double-stranded DNA breaks that result in a potent and localised cytotoxic effect. It has been shown to prolong time to first symptomatic SRE, as well as prolonging time to increase in serum alkaline phosphatase and PSA levels compared to placebo[38]. Whilst these therapies play a role in improving bone symptoms, only radium-223 has been shown to have any effect on OS, and this was by less than 4 months. In view of this there is an urgent need to identify novel targets to improve the outcomes for men with advanced bone metastatic prostate cancer.

1.3 Prostate Cancer Bone Metastases

1.3.1 The metastatic process

Metastasis is the process by which cancer cells spread from the primary tumour to distant sites to establish secondary tumours. The pathophysiology of the development of bone metastases is similar to those at any other site. It has traditionally been thought of as a linear complex multi-step process by which primary tumour cells (1) invade through their basement membrane by producing proteolytic enzymes, (2) enter into blood or lymphatic vessels (intravasation), (3) travel through and survive in the circulation, (4) adhere to the vessel at a distant organ site, (5) exit the circulation (extravasation) into the parenchyma of the distant site, and (6) survive and colonise the secondary site, reinitiating their proliferative program[39](Figure 1.6).

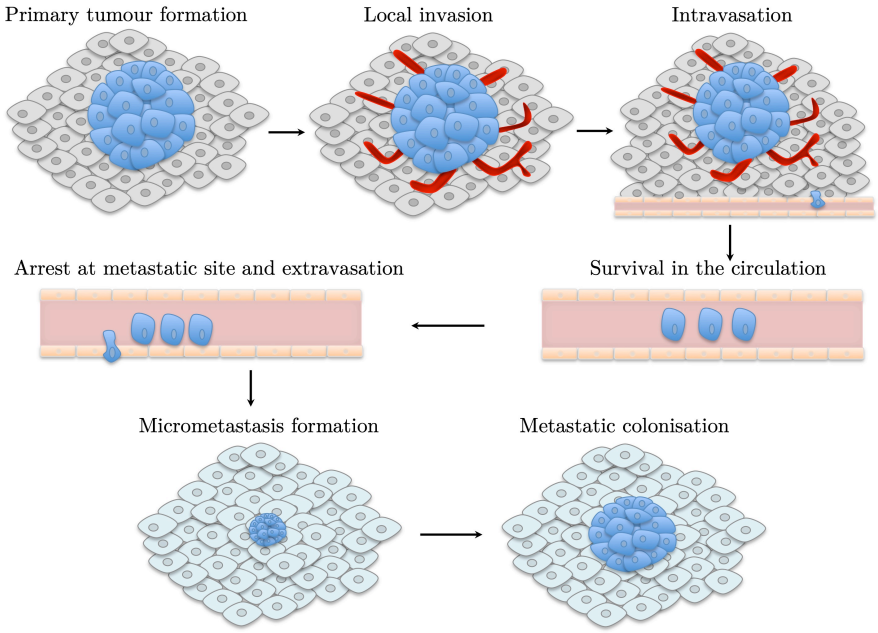


Figure 1.6 ***The metastatic process****. Steps involved in metastasis of cancer cells to distant sites.*

However, a recent study[40] has shown that metastatic spread might be more complicated. Multiple competing subclones were proposed to develop within a single primary tumour, each of which may have metastatic potential allowing multiple metastatic clones to develop. Rather than following a linear timeline of spread from primary tumour to metastasis to another metastasis, tumour cells may in fact spread from one metastatic site to another. However more work needs to be done to further support this study and to better elucidate the metastatic mechanisms in prostate cancer.

The process of metastatic spread relies on epithelial cells losing their cell-to-cell adhesion within their primary site, and assuming a mesenchymal phenotype; a process known as epithelial-to-mesenchymal-transition (EMT). This it thought to be critical in enabling tumour cells to migrate away from their primary site, and invade into blood / lymphatic vessels. Once circulating tumour cells have exited the circulation they revert to their epithelial phenotype, termed mesenchymal epithelial transition (MET) to allow the formation of metastasis at the secondary site[41–43]. This oscillation between epithelial and mesenchymal states is a dynamic and complex set of events that are thought to be vital to successful metastatic dissemination and colonisation.

1.3.2 Bone metastases

Bone comprises the largest proportion of the body's connective tissue mass and represents the fourth commonest site of solid tumour metastasis, behind lymph nodes, lung and liver[44]. Prostate cancer has a particular tropism to bone, with skeletal involvement present in approximately 90% of patients with metastatic disease, and skeletal complications are

frequently seen. Paget first proposed the 'seed' (tumour cell) and 'soil' (metastatic site) hypothesis in 1889 to explain the predisposition of breast cancer cells to metastasise to certain sites[45], but the mechanisms underlying prostate cancer's predilection to metastasise to bone still remain poorly understood. The 'seed and soil' hypothesis likens tumour cells to seeds that only survive and grow if they fall on favourable soil, with bone being a particularly favourable "soil" for prostate cancer.

Initial homing of prostate tumour cells to bone is largely regulated by numerous chemokines and integrins produced by bone marrow stromal cells. The most well known of these interactions is the C-X-C chemokine receptor 4 (CXCR4) expressed by tumour cells, and its ligand, C-X-C motif chemokine 12 (CXCL12), expressed by stromal cells and osteoblasts[46]. Osteoblasts are also known to express other anchorage molecules such as angiopoietin and osteopontin (OPN) that further contribute to tumour homing to the bone microenvironment.

1.3.3 Bone remodelling

Once prostate cancer has metastasised to the bone remodelling occurs. Physiological bone remodelling involves the destruction of existing bone matrix by osteoclasts, and formation of new bone by osteoblasts, and it is tightly regulated by cross-talk ('coupling') between osteoclasts and osteoblasts to repair damaged bone, preserve structural integrity and to maintain mineral homeostasis[47]. Bone metastases interact with osteoclasts and osteoblasts to upset the critical balance, resulting in bone destruction and/or the formation of bone in a disorganised manner. Bone metastases are typically classified as osteolytic, osteoblastic or mixed, according to the primary mechanism of bone remodelling[48]. Osteolytic lesions are

characterised by a shift in the balance towards increased osteoclast activity accompanied by a relative decrease in osteoblast number/ activity leading to a net bone loss (resorption). Multiple myeloma and breast cancer typically give rise to purely osteolytic lesions. Prostate cancer typically causes osteoblastic lesions, characterized by a shift in the balance of bone remodelling towards increased bone formation with abnormal bone forming around tumour foci. The increased osteoblast activity seen in prostate blastic metastases typically co-exists with increased osteoclast activity, with osteoblastic metastases forming on trabecular bone at sites of previous osteoblastic resoprtion[49]. Mature healthy bone is typically formed of lamellar bone, which consists of collagen bundles organised in a tightly packed linear fashion resulting in optimal bone strength. However, bone metastases induce the production of woven bone, which is composed of loosely packed randomly orientated collagen bundles that produce bone with suboptimal strength[50]. The combination of inferior bone production and underlying osteolysis leads to an increased risk of fracture. The disruption of normally well-coordinated osteoclast and osteoblast coupling not only results in accelerated bone remodelling, but also offers a fertile soil for further tumour expansion.

1.3.4 The bone microenvironment

Healthy bone is a dynamic structure that constantly undergoes renewal and turnover through the interaction of osteoclasts and osteoblasts. It serves a variety of functions including structural support, allowing movement, maintaining mineral and acid-base homeostasis, and providing a suitable environment of growth factors and cytokines for haematopoiesis. The majority of the bone matrix is inorganic and composed of the mineral

hydroxyapatite, while structural proteins (mainly type I collagen) constitute the organic matrix[51]. The term 'bone microenvironment' attempts to encompass a complex system consisting of haematopoietic and mesenchymal cells of multiple lineages, a sinusoidal blood supply, the bone marrow stroma and the bone extracellular matrix. The bone matrix can serve as a rich source of growth factors for cancer metastases, while the cells within the bone, or recruited to the bone, can orchestrate a myriad of bone-tumour interactions, making the bone a favourable site for prostate cancer metastasis. Resident bone cells (osteoclasts, osteoblasts, osteocytes, adipocytes), myeloid and immune cells, bone marrow endothelial and haematopoietic cells, platelets and bone marrow derived mesenchymal stem cells (MSCs) can all play a role in the metastatic process to some degree[52].

Osteoblasts

Osteoblasts are derived from MSCs (Figure 1.7) lining the endosteal surface of bone, and constitute approximately 4-6% of all bone cells. They differentiate under the direction of the regulatory transcription factors RUNX2 (runt-related transcription factor 2) and osterix. Osteoblasts are specialised in producing non-calcified organic bone matrix (osteoid) and subsequently deposit inorganic components (e.g. calcium and phosphate), to form mineralized bone. They also play a role in expression of osteoclastogenic factors (M-CSF and RANKL) and express parathyroid hormone (PTH) receptors. After mineralisation is complete most osteoblasts undergo apoptosis, but a proportion become entrapped within the mineralised bone where they differentiate into osteocytes[53]. These terminally differentiated cells form a network extending projections connecting them to other osteocytes, osteoblasts, blood vessels, nerves and bone lining cells. The long life span of osteocytes (estimated to be

10 – 20 yr) accounts for their accumulation in bone in numbers that far exceed those of any other bone cells[54]. However, their exact function has not yet been established, although most evidence supports a role as a sensory cells transducing mechanical queues into anabolic signals[55].

Prostate cancer cells have been shown to secrete various factors that can regulate osteoblast proliferation and/or differentiation including multiple Wnt ligands, Dickkopf WNT Signalling Pathway Inhibitor-1 (DKK1), Bone morphogenetic proteins (BMPs), Transforming growth factor-beta (TGF-β), Insulin-like growth factors (IGFs), Platelet derived growth factor (PDGF), Fibroblast growth factor (FGF) vascular endothelial growth factor-A (VEGF-A) endothelin-1 (ET-1), urokinase-type plasminogen activator (uPA) and PSA [56]. DKK1 has been linked to the lytic/blastic switch in prostate cancer. Inhibition of WNT signalling by DKK1 produced early in the development of skeletal metastases can suppress osteoblast function and result in osteolysis. As metastasis progresses, DKK1 expression is decreased, allowing WNT signalling to promote osteoblastic activity leading to osteosclerosis at the metastatic site[57]. Secretion of these various factors by prostate cancer cells can activate osteoblasts and stimulate abnormal bone formation through a process similar to that involved in normal bone repair.

Osteoclasts

Osteoclasts differentiate from haematopoietic cells of the monocyte/macrophage lineage (Figure 1.7). Mature osteoclasts are multi-nucleated giant cells formed by fusion of monocyte-macrophage precursors. They are uniquely adapted to resorb bone through the

secretion of acids and lytic enzymes into resorption pits on the bone surface. Colony stimulating factor 1 (CSF-1) and RANKL, Parathyroid hormone related protein (PTHrP) and interleukin-6 (IL-6) all play a role in the survival, expansion and differentiation of osteoclasts. Osteoprotegerin (OPG) is a member of the TNF receptor (TNFR) family expressed by osteoblasts, and is a secreted protein soluble decoy receptor for RANKL, thereby inhibiting RANK-RANKL signalling and decreasing osteoclast formation and function. Under normal physiological conditions osteoblasts regulate osteoclast activity through maintaining the balance between RANKL and OPG, determining the degree of osteoblast differentiation and function. The drug denosumab acts by targeting free RANKL and inhibiting binding to RANK, thereby inhibiting osteoclast differentiation and activation[58].

Whilst PCa is predominantly osteoblastic, it is increasingly being realised that bone resorption also plays a role, and that the disease has an underlying osteolytic component. In prostate cancer patients with osteoblastic lesions, urinary and blood levels of bone resorption markers are often elevated[59]. It has been suggested that osteoclast activation may be a key early mediator preparing the metastatic niche and nurturing early PCa metastasis. Prostate cancer can promote bone resorption through the induction of RANKL[58], and can inhibit resorption by releasing PSA, which can cleave PTHrP[60].

Osteolysis begins when a mature osteoclast is activated by RANKL, leading to up-regulation of MMP-9 and osteoclast polarization. This leads to ruffled membrane formation and the formation of a tight junction sealing the osteoclast to the bone surface. This resorption pit (Howships' lacunae) is then acidified by the export of hydrogen ions and the secretion of

lytic enzymes, tartrate resistant acid phosphatase (TRAP), cathepsins, and MMPs, leading to the breakdown of inorganic and organic ECM and the resorption of bone proteins[61]. Degradation produces (collagen fragments, calcium and phosphate) are processed within the osteoclast and released into the circulation. The survival of the mature osteoclast, and its utilisation in successive rounds of bone resorption is regulated in part by hormone and cytokines including RANKL and interleukin-1[62]. Bisphosphonates such as ZA bind preferentially to bone minerals at sites of active bone resorption where they are taken up by resorbing osteoclasts[52]. Within the cells they block the enzyme farnesyl diphosphate synthase, and inhibit protein prenylation. This leads to improper membrane integration and lack of protein function within the osteoclast inhibiting their activity. It can also inhibit the Rho family of proteins, leading to inhibition of osteolysis through improper fusion of the osteoclast to bone[58].

Mesenchymal stem cells (MSCs)

MSCs are multipotent stromal precursors that possess an innate ability for self-renewal, and differentiate into a variety of cell types including osteoblasts, adipocytes, chondrocytes and fibroblasts (Figure 1.7). They are also recruited to wounds during repair where they produce extracellular matrix (ECM) proteins and secrete cytokines that promote the recruitment of immune cells. Studies have shown that they modulate many aspects of tumourigeneis including tumour proliferation, angiogenesis, migration and metastasis, and can exert immunomodulatory properties that protect tumour cells from the immune system[63].

Bone marrow stromal cells (BMSCs)

The bone marrow stroma consists of a heterogeneous population of cells that provide the structural and physiological support cells of the bone microenvironment. They include MSCs, pericytes, fibroblasts and osteoblasts. Bone marrow derived fibroblasts are increasingly being associated with metastasis and poor prognosis. In normal conditions fibroblasts are considered inactive cells, however during inflammatory responses they are activated becoming myofibroblasts, and mediate the remodelling of the ECM by secreting MMPs to degrade the existing ECM as well as depositing new components such as collagens, fibronectin and laminins. Cancer-associated fibroblasts (CAFs) are defined as fibroblasts that are altered by tumour cells and reside in the tumour mass promoting tumour growth; they may be resident CAFs from the local tumour environment, or bone marrow derived MSCs that have been recruited to the primary tumour and differentiated into a distinct subpopulation of CAF. In healthy tissues, deactivation and removal of myofibroblasts is coordinated with the resolution of the wound; however CAFs remain in a permanently activated state and continue to secrete factors involved in tumourigenesis, including ECM factors and cytokines. CAFs are increasingly being recognised as key players in the metastatic process, secreting cytokines and growth factors that influence a range of tumorigenic pathways and impairing drug sensitivity (Figure 1.8)[64–66].

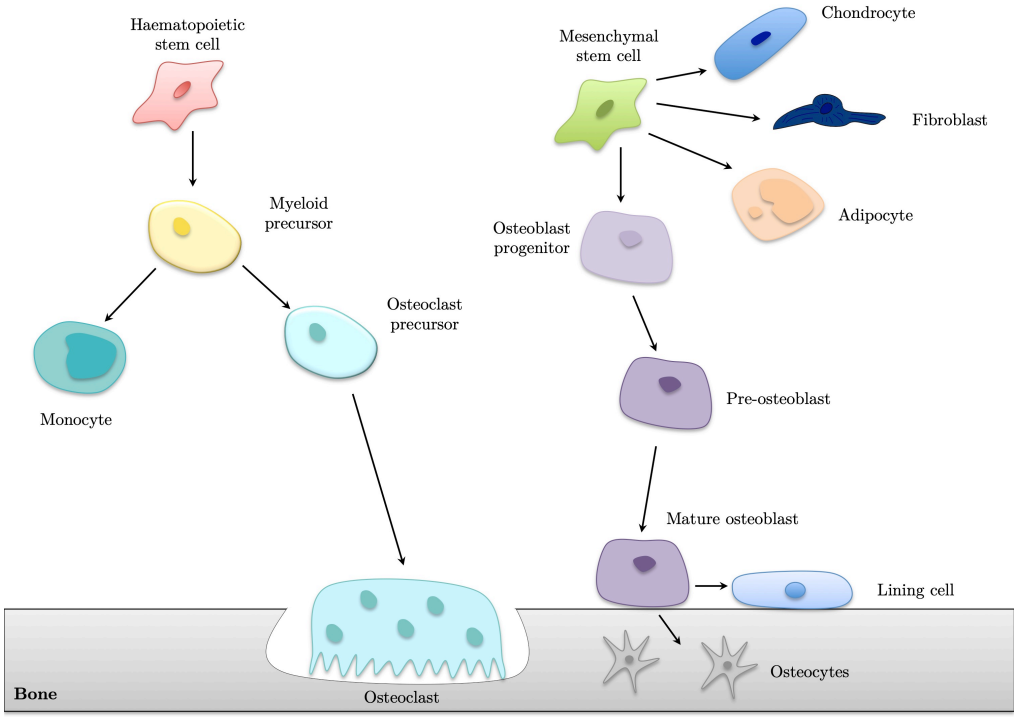


Figure 1.7 ***Bone cell differentiation.*** *Haematopoietic stem cells can differentiate into myeloid precursor cells, which can further differentiate into monocytes and osteoclasts. Mesenchymal stem cells can differentiate into chondrocytes, fibroblasts, adipocytes or osteoblasts. Mature osteoblasts can further differentiate into bone lining cells, which line the bone surface, or osteocytes, which are present inside the bone.*

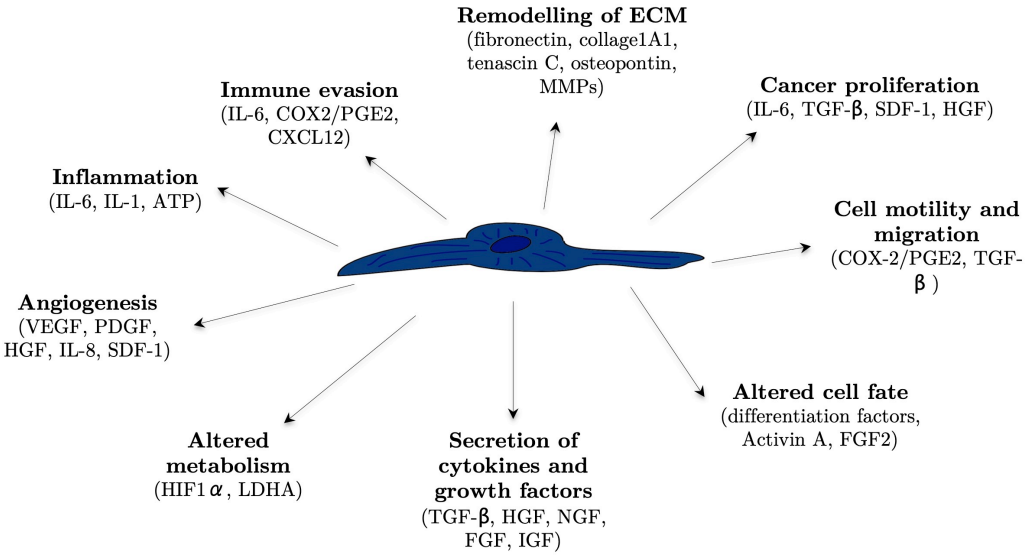


Figure 1.8 ***Cytokines and growth factors secreted by CAFs*** *leading to pro-tumorigenic phenotypes.*

1.3.5 Vicious cycle

The concept of a 'vicious cycle' developing between metastatic tumour and bone describes how interactions among tumour cells, bone cells and bone matrix promote enhanced tumour growth and accelerated bone remodelling (

Figure 1.9). Bone remodelling triggers the release of growth factors from the degraded bone matrix that can promote further tumour growth, resulting in the production of more pro-resorptive signals from the cancer leading to further bone remodelling. Early in the metastatic process PCa cells produce osteogenic factors such as ET-1, BMPs, and PDGF that promote differentiation and activation of osteoblasts. These osteoblasts deposit new matrix for bone formation; however, this unmineralised new matrix provides a fertile 'soil' enriched with growth factors and non-collagen proteins (NCPs) that help prostate cancer cells survive and proliferate in the bone microenvironment. Prostate cancer derived factors (PTHrP, DKK1, interleukins), and RANKL expressed by these new activated osteoblasts can activate osteoclasts leading to some bone resorption generating space for dominant osteoblastic lesions and releasing cytokines and NCPs from the bone matrix facilitating further proliferation of both prostate cancer cells and osteoblasts[30]. In view of this disrupting this vicious cycle has the potential to not only inhibit bone remodelling, but to also inhibit tumour growth in the bone microenvironment.

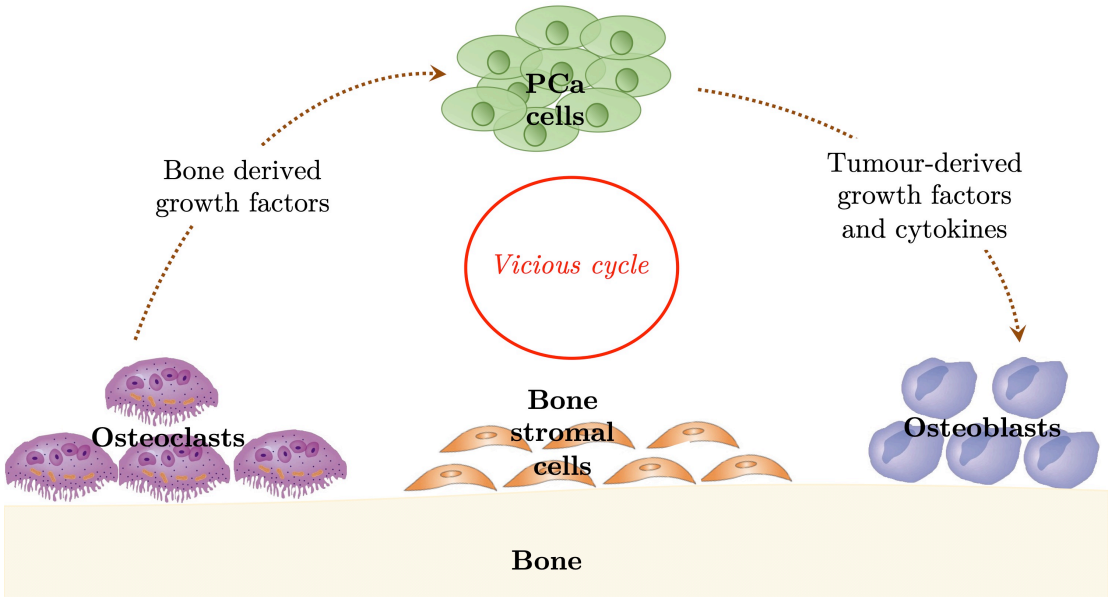


Figure 1.9 ***The vicious cycle*** *between the bone microenvironment and PCa cells.*

1.4 Metabolism

Metabolism encompasses all the biochemical reactions needed to allow cells and organisms to survive and propagate. It is a highly integrated network of reactions that sustain life by (1) converting food from the environment into energy for mechanical work and active transport of molecules and ions, (2) synthesising macromolecules and other biomolecules from simple precursors, and (3) the elimination of waste. It is made up of a complex network of interconnected biochemical pathways.

Glycolysis

Glycolysis is a sequence of reactions that metabolises one molecule of glucose to two molecules of pyruvate with the net production of two molecules of adenosine triphosphate (ATP), but also plays a role in providing building blocks for synthetic reactions. It is an anaerobic process, but the pyruvate produced can be further processed anaerobically to lactate, or under aerobic conditions it can be completely oxidised to carbon dioxide (CO_2), generating much more ATP[67]. The pathway takes place in the cytoplasm and is common to virtually all cells, both prokaryotic and eukaryotic. Glucose enters cells through specific transport proteins (GLUT1-5) and is phosphorylated by ATP to form glucose 6-phosphate (G6P), which cannot pass through the membrane. This reaction is catalysed by hexokinase, an important regulator of glycolytic flux. G6P is then isomerized to fructose 6-phosphate (F6P), which in turn is phosphorylated by ATP to fructose 1,6-bisphosphate (F1,6BP). This reaction is catalysed by phosphofructokinase (PFK), which sets the pace of glycolysis. F1,6BP is then split into glyceraldehyde 3-phosphate (GAP) and dihydroxyacetone

phosphate (DHAP). Triose phosphate isomerase (TPI) catalyses the rapid and reversible conversion of DHAP to GAP. GAP is then converted into 1,3-bisphosphglycerate (1,3BPG), an energy rich molecule which allows the synthesis of ATP from adenosine diphosphate (ADP) resulting in 3-phosphoglycerate (3PG), which is converted into 2-phosphoglycerate (2PG) followed by phosphoenolpyruvate (PEP) and finally pyruvate, forming a second molecule of ATP from ADP (Figure 1.10)[68].

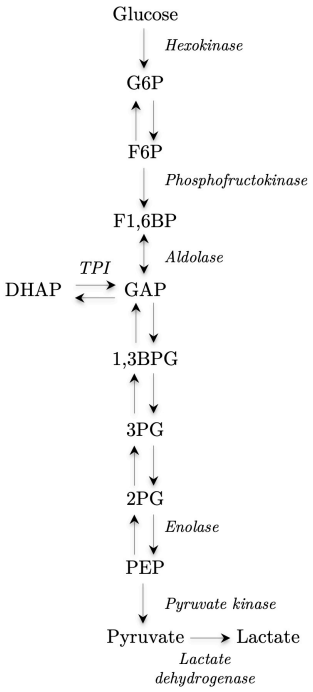


Figure 1.10 ***The glycolytic pathway.*** *Key enzymes shown in italics. Abbreviations defined in text.*

The Tricarboxylic acid cycle (TCA cycle)

Most of the ATP generated in metabolism is provided by the aerobic processing of glucose, which starts with the complete oxidation of glucose derivatives to CO_2 in a series of reactions called the Krebs cycle, or the TCA cycle. It is the final common pathway for the oxidation of fuel molecules (fatty acids, carbohydrates and amino acids), most of which enter

the cycle as acetyl coenzyme A (acetyl CoA), but also is an important source of building blocks for many other molecules including amino acids, nucleotide bases and porphyrin. Under aerobic conditions the pyruvate generated from glycolysis is transported into the mitochondria and is oxidatively decarboxylated to form acetyl CoA. Oxaloacetate then reacts with acetyl CoA and water (H_2O) to yield citrate and CoA, catalysed by citrate synthase (CS). Citrate is then isomerized into isocitrate catalysed by aconitase. The oxidative decarboxylation of isocitrate catalysed by isocitrate dehydrogenase forms α-ketoglutarate and generates the first high-transfer-potential electron carrier, nicotinamide adenine dinucleotide (NADH). α-ketoglutarate is converted to succinly-CoA by oxidative decarboxylation, which is then cleaved to form succinate. The final stages of the TCA cycle involve the regeneration of oxaloacetate, also producing energy in the form of flavin adenine dinucleotide ($FADH_2$) and NADH. Succinate is oxidised to fumarate by succinate dehydrogenase. Fumarate undergoes hydration to form malate catalysed by fumarase; and finally, malate is oxidised to regenerate oxaloacetate Figure (1.11)[68].

The net reactions of the TCA cycle:

$$Acteyl\ CoA\ + 3\ NAD^+\ + FAD\ + GDP\ + Pi\ + 2\ H_2O$$
$$\rightarrow\ 2CO_2\ + 3\ NADH\ +\ FADH_2\ + GTP\ + 2\ H^+\ + CoA$$

The electron-transport chain oxidises the NADH and $FADH_2$ formed, and it is the transfer of electrons from these carriers to oxygen (O_2) that leads to the generation of a proton gradient across the inner mitochondrial membrane, which drives the generation of ATP.

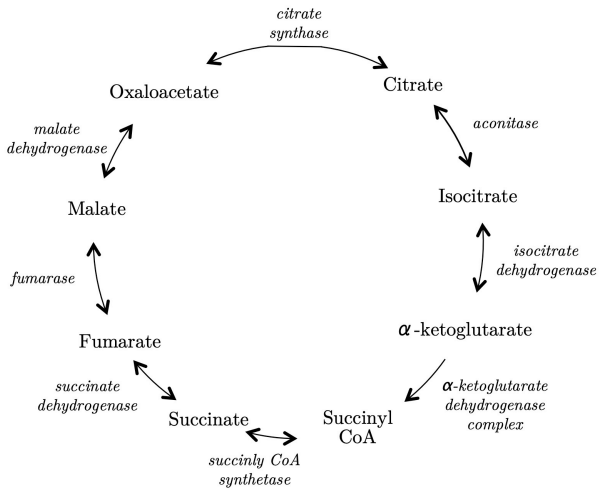


Figure 1.11 ***The tricarboxylic acid cycle.*** *Key enzymes shown in italics.*

Oxidative phosphorylation (OXPHOS)

OXPHOS is the process in which ATP is formed as a result of the transfer of electrons from NADH or $FADH_2$ to O_2 by a series of electron carriers. It takes place in the mitochondria and is the major source of ATP in aerobic organisms, generating 26 of the 30 molecules of ATP that are formed when glucose is completely oxidised to CO_2 and H_2O.

During OXPHOS the flow of electrons from NADH or $FADH_2$ to O_2 through protein complexes located in the mitochondrial inner membrane leads to the pumping of protons out of the mitochondrial matrix. The resulting unequal distribution of protons generates a pH gradient and a transmembrane electrical potential. ATP is synthesised when protons flow back into the mitochondrial matrix through an enzyme complex. The conversion of electron-motive force into proton-motive force is carried out by a respiratory chain consisting of three electron-driven proton pumps – NADH-Q oxidoreductase (complex I), Q-cytochrome c oxidoreductase (complex III) and cytochrome c oxidase (complex IV). Electron flow within

these complexes leads to the transport of protons across the inner mitochondrial membrane (Figure 1.12). A fourth complex, succinate-Q-reductase (complex II), contains the succinate dehydrogenase that generates $FADH_2$ in the TCA cycle; electrons from this $FADH_2$ enter the electron transport chain (ETC) at complex III. The final phase of OXPHOS is carried out by ATP synthase, driven by the flow of protons back into the mitochondrial matrix[68,69].

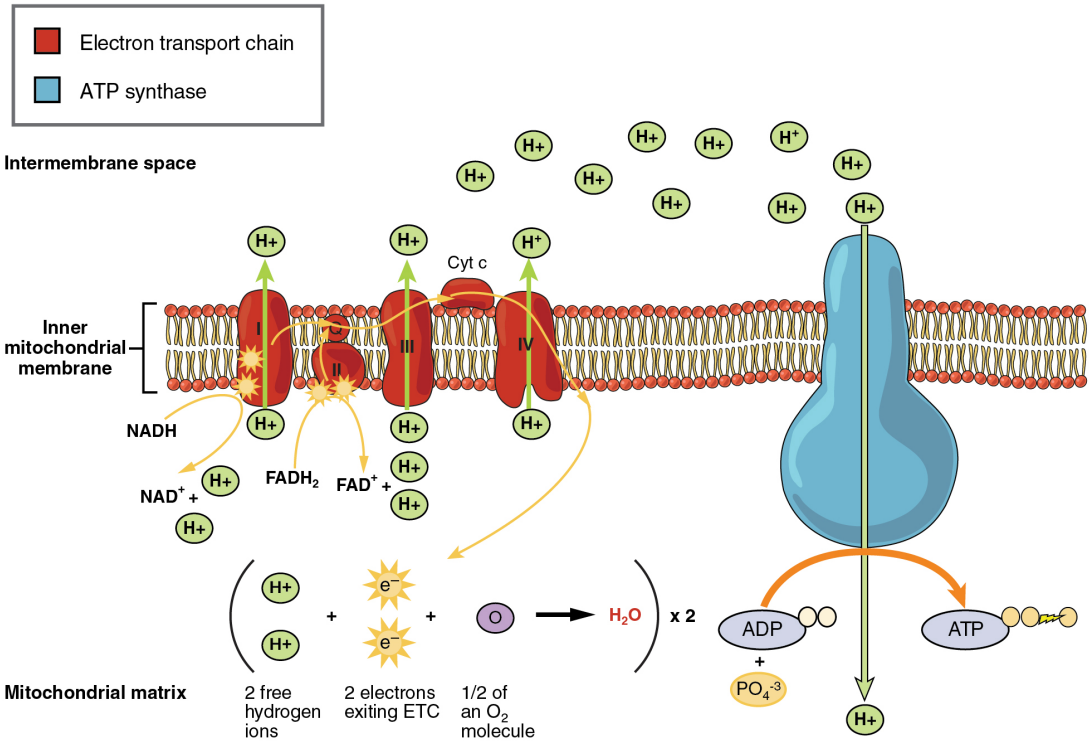


Figure 1.12 ***Oxidative phosphorylation and the electron transport chain.*** *Illustration from Anatomy & Physiology, Connexions Website (Open Access under CC-BY-3.0)*

Oxygen is the terminal electron acceptor in the ETC. Whilst the transfer of four electrons to oxygen leads to safe products (two molecules of H_2O), the partial reduction of oxygen can generate hazardous compounds, in particular the transfer of a single electron to O_2 forms a superoxide anion ($O_2^{\cdot-}$), while the transfer of two electrons yields peroxide (O_2^{2-}).

$$O_2 \xrightarrow{e^-} O_2^{\cdot-} \xrightarrow{e^-} O_2^{2-}$$

Both compounds are potentially harmful; to avoid this, cytochrome c oxidase and the other proteins that reduce O_2 do not release partly reduced intermediates by strongly binding to O_2. Despite this, small amounts of superoxide and hydrogen peroxide are formed inevitably. Superoxide, hydrogen peroxide and the species that can be generated from them are collectively referred to as reactive oxygen species (ROS), and these can lead to oxidative damage within the cell[68]. There are several cellular defence strategies against oxidative damage including the enzyme superoxide dismutase that catalyses the conversion of two superoxide radicals into hydrogen peroxide and molecular oxygen. The hydrogen peroxide formed is then scavenged by catalase and converted into water and molecular oxygen. Glutathione peroxidase is another important enzyme in the cells defence against ROS, catalysing the conversion of reduced glutathione (GSH) to its oxidised form (GSSG) and reducing hydrogen peroxide to water in the process. GSSG is then reduced back to GSH using nicotinamide adenine dinucleotide phosphate (NADPH) as an electron donor.

The pentose phosphate pathway (PPP)

The pentose phosphate pathway, also known as the hexose monophosphate pathway or the pentose shunt, provides an alternative pathway for glucose breakdown to generate NADPH, the main reducing power within cells for their biosynthetic processes[70]. The PPP is also important for the catabolism of pentose sugars from the diet for the synthesis of pentose sugars for nucleotide biosynthesis necessary for cell division, providing about 85% of pentoses incorporated into deoxyribonucleic acid (DNA)[71]. It consists of two phases: (1) the oxidative generation of NADPH, and (2) the non-oxidative inter-conversion of sugars[72]

(Figure 1.13) with activity of the oxidative branch generally being higher than that of the non-oxidative branch[73].

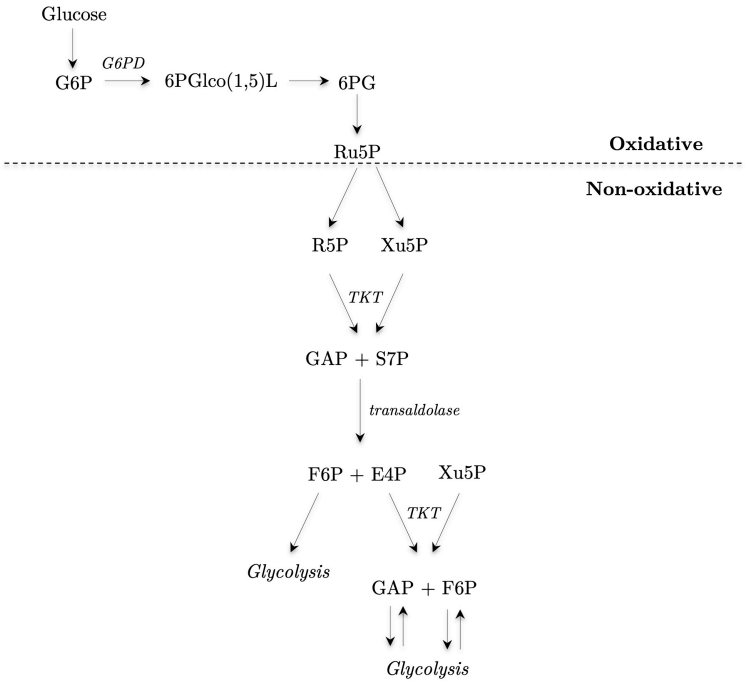


Figure 1.13 ***The pentose phosphate pathway.*** *Key enzymes shown in italics. Abbreviations of metabolites are expanded in the text.*

The first and rate-limiting step of the oxidative phase is the dehydrogenation of G6P, catalysed by the rate limiting enzyme glucose 6-phsohpate dehydrogenase (G6PD), producing 6-phosphoglucono-δ- lactone (6PGluco(1,5)L)[74]. This is then hydrolysed to give 6-phosphogluconate (6PG), which is oxidatively decarboxylated to yield ribulose 5-phosphate (RU5P), which is isomerised to ribose 5-phosphate (R5P). These reactions yield two molecules of NADPH and one molecule of R5P for each molecule of G6P oxidised. When cells need more NADPH than R5P the non-oxidative interconversion of sugars occurs. R5P is converted into GAP and F6P by transketolase (TKT) and transaldolase, creating a reversible link between the PPP and gluconeogenesis, as G6P is resynthesized from F6P and

GAP by the gluconeogenic pathway. Xylulose 5-phosphate (Xu5P), sedoheptulose-7-phosphate (S7P), and erythrose 4-phosphate (E4P) are intermediates in this pathway. In this way 12 molecules of NADPH can be generated for each molecule of G6P that is completely oxidised to CO_2. When more R5P than NADPH is needed, F6P and GAP are converted into R5P without the formation of NADPH. Alternatively if both NADPH and ATP are required R5P can be converted into pyruvate generating ATP and NADPH. The interplay of glycolysis and the PPP enables the levels of ATP, NADPH, and building blocks such as ribose and pyruvate to be continuously adjusted to meet the needs of the cell[68].

The PPP is the main cellular source of NADPH, which maintains the appropriate level of GSH to combat oxidative stress and maintain the reducing environment in the cell. Cells with diminished G6PD are especially sensitive to oxidative stress[75].

Fatty acid metabolism

Fatty acids have four major physiological roles: (1) as fuel, stored as triacylglycerols in adipose tissue (2) as building blocks of phospholipids and glycolipids, important components of cell membranes, (3) hydrophobic modifiers of protein to target them to membrane locations, and (4) as hormone and intracellular messengers.

Triacylglycerols are degraded to fatty acids and glycerol by lipase, which are then released from the adipose tissue and transported to energy requiring tissues carried by serum albumin. On the outer mitochondrial membrane fatty acids are activated by acyl CoA synthetase, and then conjugated to carnitine catalysed by carnitine palmitoyl transferse I (CPTI) to enable them to cross the inner mitochondrial membrane. Within the mitochondria

the acyl CoA undergoes β-oxidation. The resultant acetyl CoA is then processed in the TCA cycle to produce energy. The complete oxidation of a molecule of palmitate can yield 106 molecules of ATP.

Fatty acids are synthesised in the cytoplasm. Acetyl CoA is carboxylated to malonyl CoA, a reversible reaction that is the committed step in fatty acid synthesis. Fatty acid synthase (FASN) is a complex of distinct enzymes that catalyse the synthesis of saturated long-chain fatty acids from acetyl CoA, malonyl CoA, and NADPH. The NADPH needed is generated from the transfer of reducing equivalents from mitochondria by the malate-pyruvate shuttle, and by the PPP. The major product of fatty acid synthase is palmitate. The synthesis of palmitate requires 8 molecules of acetyl CoA, 14 molecules of NADPH and 7 molecules of ATP. Longer fatty acids are formed by elongation reactions in the endoplasmic reticulum[68].

Glutamine metabolism

Glutamine is involved in numerous energetic pathways within cells. It is converted into glutamate by glutaminase, which can then go on to be converted into α-ketoglutarate which can be fed into the TCA cycle[76,77]. It also plays a role in regulating GSH synthesis, nucleic acid synthesis via purine and pyrimidine nucleotide production, and serves as a metabolic intermediate in the synthesis of amino acids[78].

1.5 Cancer Metabolism

It is now widely accepted that metabolic changes occur during malignant transformation to satisfy cancer cells' increased need for energy and biosynthetic precursors. Deregulated cellular energetics is one of the emerging hallmarks of cancer identified by Hanahan and Weinberg in 2011[79], and indeed some argue that deregulated cellular energetics may underpin all the hallmarks of cancer[80,81]. The metabolic changes to accommodate altered energy requirements are achieved through modification of the activity and expression of key metabolic enzymes. These changes are often downstream of various oncogenes or tumour suppressor genes such as c-Myc, hypoxia-inducible factor 1-alpha (HIF1α), phosphatase and tensin homolog (PTEN) and runt-related transcription factor 2 (RUNX2). These metabolic shifts are not only an adaptive response of cancer cells, but can be a driver of tumourigenicity[82]. As the metabolic changes that underpin tumour progression become better understood, specific metabolic targeted therapies may be possible.

1.5.1 Warburg effect

The Nobel prize winner, Otto Warburg, first reported tumour-specific metabolic alterations in the 1920s, identifying that cancer cells preferentially rely on glycolysis as a major energy source even in the presence of oxygen[83,84]. During glycolysis glucose is converted to pyruvate with the generation of 2 molecules of ATP per molecule of glucose (Figure 1.10). Most normal tissues oxidise the pyruvate formed to CO_2 and water in the mitochondrion with the production of 38 molecules of ATP per molecule of glucose. Only in low oxygen conditions do normal tissues convert glucose to lactate. In contrast, tumours have been found to

preferentially convert glucose into lactate even in the presence of oxygen, a process described as aerobic glycolysis or the "Warburg effect" (Figure 1.14).

There are several reasons why enhanced glucose uptake for glycolytic ATP generation is advantageous for tumour growth; (1) it allows cells to live in conditions of fluctuating oxygen tension that would normally be lethal to cells that rely on OXPHOS to generate ATP, (2) the acid conditions produced from lactic acid generation favour tumour invasion and suppress anticancer immune effectors, (3) it allows glucose generation through the PPP to generate NADPH to ensure the cell's antioxidant defences in a hostile environment, (4) the intermediates of the glycolytic pathway can be used for anabolic reactions (e.g. glucose 6-phosphate for ribose synthesis, dihydroxyacetone phosphate for triacylglyceride and phospholipid synthesis, and pyruvate for alanine and malate synthesis).

The phenomenon of increased uptake of glucose by malignant cells is exploited in the clinic by the use of a glucose analogue fluorine-18-fluorodeoxyglucose (FDG) in positron emission tomography (PET) scan. FDG-PET combined with CT has >90% sensitivity and specificity for the detection of metastases of most epithelial cancers[80], however this imaging has not been helpful in the staging or detection of recurrent prostate cancer, likely due to a relatively low uptake of glucose. It has been shown that FDG accumulation does not correlate with increasing grade or stage of prostate cancer, and there is significant overlap in FDG uptake between benign prostate hyperplasia and prostate cancer[85,86]. As the rapid cellular proliferation associated with malignancy requires an increased energy supply, if glucose consumption is not elevated in prostate cancer, an alternative metabolic approach must dominate to provide this energy.

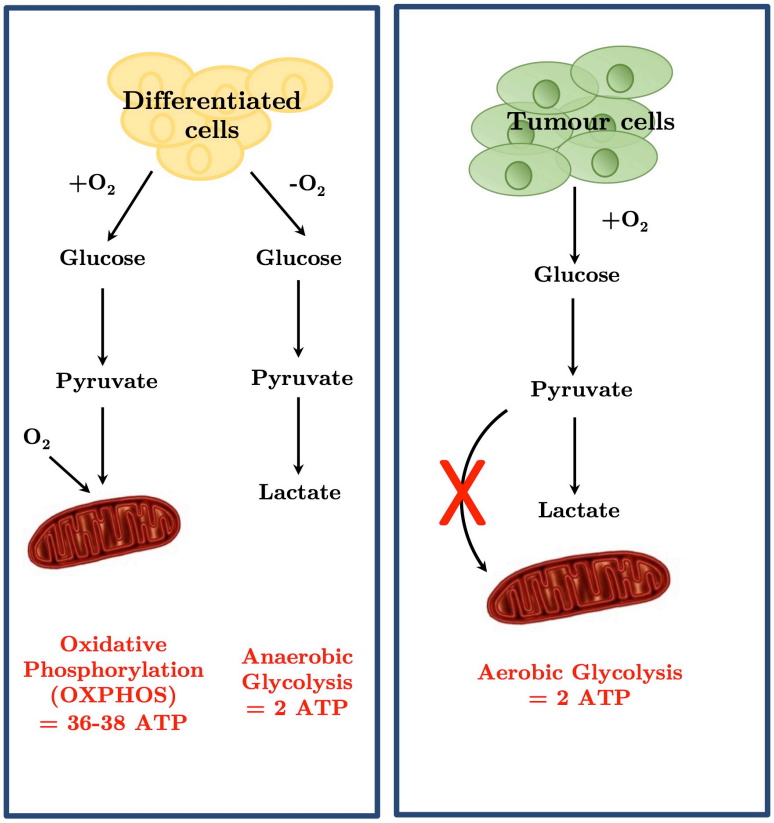


Figure 1.14: ***The Warburg effect***

1.5.2 Metabolic crosstalk in the tumour microenvironment and the "Reverse Warburg" effect

An emerging field in cancer metabolism involves examining the metabolic relationship between cancer cells and the cells of their surrounding environment. The tumour microenvironment, rather than being viewed as an innocent bystander, is increasingly being recognised as key player in cancer establishment and progression. In solid tumours it consists of cellular components (fibroblasts, mesenchymal stem cells, adipocytes, endothelial cells and immune cells), and non-cellular components, mainly the extracellular matrix (proteins, glycoproteins and proteoglycans). During primary tumour formation, cancer cells interact in cross talk with a range of cells from the local tumour microenvironment leading to the

secretion of large amounts of factors / cytokines that influence invasion and metastasis[87]. CAFs are the most prominent non-cancer cell type within the reactive stroma of many solid tumours[88], and are noted to play a fundamental role in tumour initiation, growth, invasion and dissemination (Figure 1.8). Unlike normal fibroblasts they are chronically activated leading to a secretory phenotype with increased proliferation and survival potential, augmented ECM remodelling ability, and metabolic reprogramming[89]. A symbiotic metabolic reprogramming occurs between cancer cells and their neighbouring CAFs, where the CAFs switch to aerobic glycolysis in the presence of cancer cells, secreting lactate and other energy rich intermediates that can be taken up preferentially by the cancer cells and used to fuel OXPHOS and the TCA cycle. This shift in cancer cell metabolism towards OXPHOS, allows more efficient energy production and higher proliferative capacity in the cancer cells. This effect is often referred to as the "Reverse Warburg effect"[87,90,91]. In prostate cancer CAFs have been shown to promote aggressiveness of PCa in terms of EMT induction[92], OXPHOS metabolic shift[87], microRNA (miRNA) deregulation[93], and they can induce androgen[94], and chemotherapy resistance[95] *in vitro*. However, to date only the effect of local CAFs have been published, while the effect of CAFs at prostate metastatic sites remain unexamined.

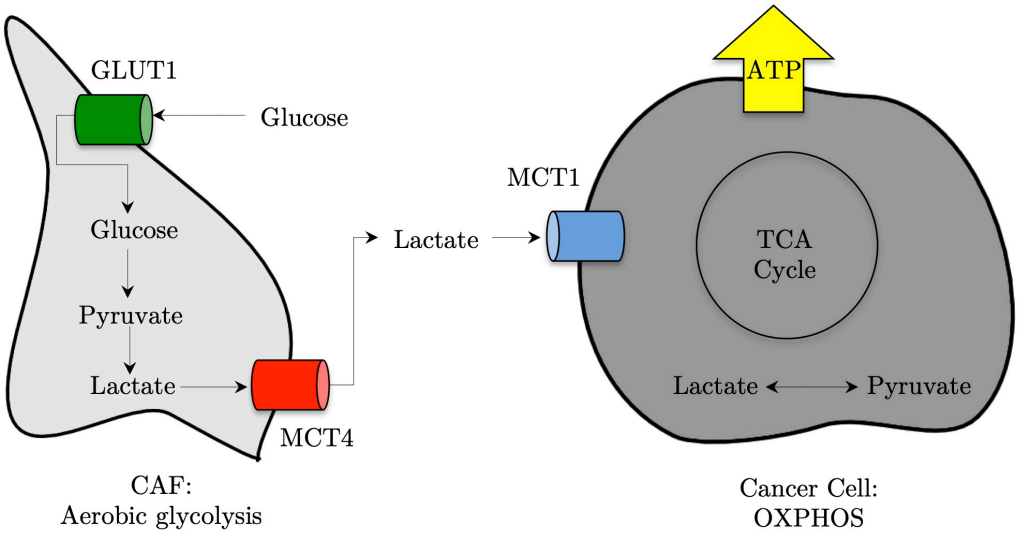


Figure 1.15 ***The Reverse Warburg effect between CAFs and cancer cells.*** *CAFs take up glucose via the GLUT1 glucose transporter and convert it to lactate via aerobic glycolysis. The lactate is extruded via the monocarboxylate transporter (MCT) MCT4 and taken up by cancer cells via the MCT1 transporter. The lactate is then used to fuel the TCA cycle, as well as anabolic processes and cell proliferation.*

Bone provides a unique metabolic microenvironment in that it is energy rich with an abundant source of lipids[96]. It has been shown that bone metastatic prostate cancer cells actively move towards adipocyte-rich regions of the bone marrow stroma, and are able to actively take up lipids[97,98]. Therefore it is likely that prostate cancer cells are able to benefit metabolically from utilising the cells of the bone microenvironment; however, these metabolic changes have yet to be characterised.

1.5.3 Prostate cancer metabolism

The normal human prostate has a unique metabolism compared to other tissues. Healthy prostate epithelial cells, notably the epithelial cells in the peripheral zone of the prostate, are able to accumulate and secrete extraordinarily high levels of citrate rather than oxidising it

in the TCA cycle. As a result seminal fluid citrate concentrations (4-150 mM) are considerably higher than in blood plasma (0.1-0.3 mM)[99]. The citrate is thought to act as a buffering agent and as a possible scavenger of ROS in prostatic fluid[100]. Citrate excretion is maintained by inhibition of the TCA enzyme aconitase by high levels of zinc accumulated in the prostate epithelial cells. This zinc accumulation is achieved by increased amounts of the zinc transporter ZIP1 in benign tissue[101]. A hallmark of malignant transformation of the prostate is the loss of ability to concentrate zinc and citrate, releasing inhibition of the TCA cycle (Figure 1.16).

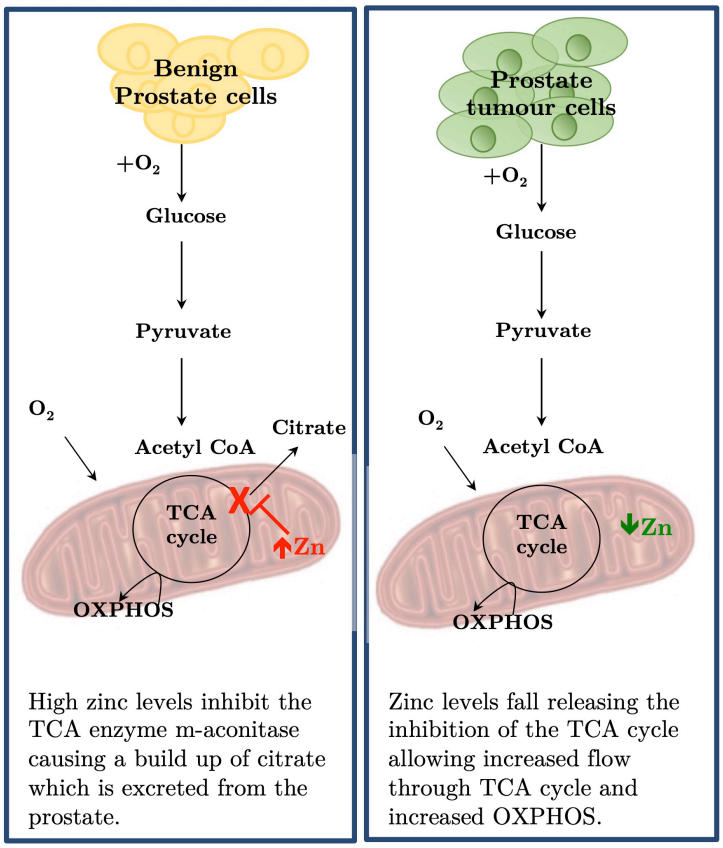


Figure 1.16: ***Alteration in prostate cell metabolism during malignant transformation.***

The majority of cells become less energy efficient as they transform to malignant cells[83,84], however prostate cancer cells become more energy efficient, transforming from citrate

producing cells to citrate oxidising cells, allowing increased flow through the TCA cycle and increased OXPHOS. It has been proposed that this metabolic transformation is an early event in preparation for the progression to malignancy[102]. Rather than rely on glycolysis as their energy supply to feed the rapid cellular proliferation associated with malignancy, PCa instead is thought to have an increased reliance on OXPHOS and the TCA cycle[82], with aberrations seen in nearly all major aspects of metabolism. These alterations may allow for novel targeted metabolic approaches to diagnosis, prognosis, monitoring and anti-cancer therapeutics.

The pentose phosphate pathway

The PPP provides cells with ribose 5-phophate and NADPH – necessary for cell division, and also buffers against ROS damage. It is therefore unsurprising that changes in PPP activity occur with cancer development. Indeed it has been proposed that deregulation of the entire PPP can be regarded as a hallmark of cell transformation[73], and several experiments have suggested that the PPP has a role in promoting invasion, angiogenesis and resistance to therapy.

Disrupting NADPH production in cancer cells can increase their sensitivity to ROS and thereby promote apoptosis. G6PD is generally considered the pace-setter for NADPH production in cells, and has been found to be overexpressed in multiple cancers including colorectal, prostate, breast, gastric, lung, oesophageal, renal cell carcinoma, and acute myeloid leukaemia[103–108]. It is negatively regulated by the tumour suppressor p53[109]. High expression of G6PD predicts poor prognosis and correlates with poor outcomes to

chemotherapy and radiotherapy in some cancer models[103,104,107,108,110]. G6PD was suggested as a biomarker for PCa over 30 years ago[111,112], with levels found to be 4 times higher in PCa compared with BPH, however subsequent research is limited. More recently androgen treatment has been shown to increase G6PD expression in hormone-sensitive prostate cancer cell lines through mTOR-mediated regulation[113]. In other cancer models targeting G6PD has been shown to enhance cell death caused by both chemotherapy and radiotherapy[114–117]. It therefore likely that the PPP represents an important pathway in prostate cancer metabolism.

Fatty acid metabolism

Alongside the increased glycolysis seen in cancer, there is often also an increase in fatty acid metabolism[118,119], and this is also noted in prostate cancer. Fatty acids are an essential constituent of all biological membrane lipids, and can also be an important substrate for energy metabolism. There are two potential sources of fatty acid (FA) – exogenously derived (dietary) FAs, and endogenously synthesized FAs. Most human tissues, even those with high cellular turnover, preferentially use circulating lipids for the synthesis of structural lipids, and the de novo pathway of FA synthesis is of minor importance with the exceptions of the liver, mammary gland, and to a lesser extent adipose tissue[120]. De novo FA synthesis is suppressed by circulating dietary fats. Cancer cells however are resistant to this inhibition and preferentially perform increased endogenous FA biosynthesis irrespective of the levels of extracellular lipids. This de novo synthesis may account for more than 93% or triacylglycerol FAs in tumour cells. De novo FA synthesis allows a constant supply of lipids and lipid precursors to fuel membrane production and lipid-based post-translational modification of

proteins in a malignant highly proliferating cell population[121]. This exaggerated lipogenesis in tumour cells is evident by the significantly increased activity and expression of many of the major lipogenic enzymes, including ATP citrate lyase (ACLY), acetyl-CoA Carboxylase (ACACA) and FASN, often as a result of stimulation by oncogenic signalling pathways such as PTEN, phosphatidylinositol-3-kinase (PI3K), protein kinase B (AKT) and sterol regulatory element binding protein-1c (SREBP1c) via androgen signalling[122]. Up-regulation of FASN is thought to be one of the earliest and most common events in prostate cancer development[123], and high expression often correlates with a poor prognosis and bone metastases[124–126]. *In vitro* studies have shown that inhibition of FASN results in reduced cell adhesion and migration, reduced growth and apoptosis, whilst addition of palmitate, the product of FASN, can reverse the cytotoxic effects[127–129]. Several FASN inhibitors have been studied to date including orlistat, cerulenin, C75 and C93. Orlistat has been shown to inhibit the proliferation and induce apoptosis in PCa cells; however, there are many limitations of this drug including lack of selectivity, poor oral availability and low cell permeability, limiting its potential use[130,131]. Newer and more potent FASN inhibitors are currently being investigated.

The development and progression of prostate cancer is also associated with abnormalities in cholesterol metabolism. There is an epidemiological correlation between hypercholesterolaemia and aggressive prostate cancer[132], and animal models have linked hypercholesterolaemia to increased PCa growth and metastasis[133,134]. Statins inhibit the enzyme 3-hydroxy-3-methylglutaryl –Co enzyme A (HMG-CoA) which catalyses the conversion of HMG-CoA to mevalonate, the rate limiting step of steroidogensis. Multiple

studies have shown statins *in vitro* and *in vivo* to have anti-cancer activity[135,136], and studies exploring this relationship further are still underway.

While much of the research into dysregulated lipid metabolism has focused on lipogenesis, it is clear that FA oxidation also plays a role in supporting the malignant phenotype. Overexpression of β-oxidation pathway enzymes such as AMACR (alpha-methylacyl-CoA racemase), and DBP (D-bifunctional protein), are frequently seen in PCa[137,138]. FA oxidation is reported to be higher in immortalised PCa cells (LNCaP, PC3) compared to benign prostate cell lines (BPH-1, WPMY-1)[139], and pharmacological blockage of either FA oxidation (Etomoxir, carnitine palmitoyltransferase 1 inhibitor) or intracellular triglyceride hydrolysis (Orlistat) can decrease the proliferation and viability of PCa cell lines, patient-derived PCa cells and mouse xenografts[140,141].

Glutamine metabolism

Glutamine uptake and utilisation has been shown to be elevated in multiple cancers, including PCa, where glutamine is used for de novo lipid synthesis and ATP production via glutaminolysis. Glutaminase-1 (GLS-1), the main enzyme used by prostate cells to perform glutaminolysis, has been shown to be up-regulated[142], and inhibiting glutamine uptake can limit the proliferation and invasiveness of PCa *in vitro*[143] suggesting GLS-1 may be a viable therapeutic target.

1.6 Bone cell metabolism

The fuel sources and pathways utilised by bone cells are currently under intense scrutiny as it is being increasingly recognised that changes in bone cell energy metabolism can modify their differentiation and function. Bone remodelling is a highly energy consuming process, and therefore the cells that make up the bone microenvironment need to generate substantial amounts of ATP through metabolic adaptions.

Recent studies have shown that undifferentiated proliferating BMSCs depend on glycolysis[144] for their energy production, whilst osteoblasts rely on OXPHOS and glutamine metabolism during their differentiation[55,144]. It is proposed this shift is it to meet the high ATP demands needed for the extensive biosynthesis of ECM proteins during osteogenesis.

Very few studies have been published on the metabolism of osteoclasts, however they are thought to rely on glycolysis, with increases in glycolytic enzymes seen during differentiation[145]. Glycolysis in the cytoplasm may provide a more readily available source of ATP for the differentiated osteoclasts to rapidly pump protons into the sealing zone, rather than relying on ATP generated through OXPHOS in the mitochondria being transported via ADP/ATP transporters[146].

It is clear the metabolism of bone cells is a complicated field, with dependence on pathways changing during the process of differentiation and bone remodelling. Further work is needed in this field to elucidate these changes more thoroughly.

1.7 Prostate cancer mouse models

Preclinical PCa mouse models represent an essential tool to improve the understanding of PCa development, progression and metastatic spread. The most commonly used animal models include transgenic mouse models and human PCa xenografts. Mice very rarely develop spontaneous PCa, and so it is only with the advent of genetically engineered mice (GEM), that mouse models of prostate tumourigenesis have been possible. GEM models involve the targeted disruption of tumour suppressor or oncogenic genes. The first reported GEM of PCa was the TRansgenic Adenocarcinoma Mouse Prostate (TRAMP) model, generated by overexpressing the SV40 large T antigen[147]. This model exhibits many of the features of human disease, developing high grade PIN within 12 weeks from birth that progresses to poorly differentiated adenocarcinoma within 24-30 weeks, with 100% lymph node metastasis and 67% pulmonary metastasis. However, the tumours have neuroendocrine features[148] which are rare in the clinical setting, and metastasis to bone is very rare. Newer models have involved targeting genetic lesions observed in human PCa patients with the aim of developing more relevant mouse models. These include Myc overexpression, and PTEN and homeobox protein NKx3.1 (Nkx3.1) knockout mice. However, there are limited GEM which develop distal metastases, and these metastatic lesions tend to occur in visceral organs such as lymph nodes and lungs with limited evidence of bone metastases. Also the tumours generated are largely neuroendocrine and sarcomatoid carcinomas, which do not represent what is seen in human disease[149]. These models also often require a considerable expenditure

of time, with a large number of animals needed to produce statistically meaningful data due to the heterogeneity of tumour incidence and progression.

In contrast, human PCa xenograft mouse models provide a useful alternative approach, particularly for studying the bone metastatic process of PCa *in vivo*. Human prostate cancer cells lines can be injected into immune-deficient mice leading to tumour formation. Various routes of tumour inoculation have been utilised including subcutaneous, sub-renal capsule, orthotopic, intra-cardiac and intra-tibial. The intra-cardiac model allows study of the later stages of the metastatic process, replicating the haematogenous spread of tumour cells, extravasation and colonisation in distant organs and tumour-stromal interactions. Prostate cancer cells (PC3, 22RV1, ARCaP M) are injected into the left ventricle of immune-deficient mice. The cells then enter the circulation and colonise distant sites (bone, liver, lungs, adrenals), developing metastatic lesions within 4-6 weeks[149]. The intra-tibial model can be used to specifically study PCa - bone microenvironment interactions, and involves injection of prostate cancer cells (e.g. PC3, C4-2B) directly into the tibia of immune-deficient mice, where they form tumours and osteolytic or osteoblastic bone lesions. PC3 cells have been most commonly used in xenograft studies due to their highly aggressive nature, and relatively quick tumour formation. However a weakness of this model is that the bone lesions are exclusively osteolytic, which is not what is seen in the human disease. C4-2B cells injected intra-tibially, or 22RV1/ARCaP M cells injected intra-cardiacally can produce bone tumours with mixed osteoblastic/osteolytic lesions. A drawback of the xenograft model is the necessity to use immune-deficient mice that lack host immunity; despite this, these models

have provided a wealth of information about the processes involved in prostate cancer bone metastasis.

1.8 Hypothesis and aims

Overall hypothesis

It is hypothesised that the bone microenvironment drives changes in prostate cancer metabolism that could increase proliferation and metastatic potential, and that by elucidating these changes novel metabolic targets might be found to ultimately treat PCa bone metastases.

Overall aim

The overall aim of this thesis was to identify the metabolic changes that occur when prostate cancer metastasises to the bone.

Specific Objectives

1) To identify metabolic changes that occur when PCa metastasises to the bone.

2) To determine the effect of the bone microenvironment on the PPP.

3) To investigate the function of the PPP in PCa bone metastases.

2

Materials and Methods

2.1 Cell Culture

MDA-PCa-2a (Cat. CRL-2421) human PCa cell line was purchased from American Type Culture collection (ATCC). C4-2B human PCa cell line was a gift from Prof. George Thalmann, University of Bern, Switzerland. PC3-EGFP cell line was a gift from Dr. Yolanda Calle, Kings College London. 22RV1 cells were a gift from Dr. Valentine Macaulay, University of Oxford. All other PCa cell lines were a gift from Dr. Richard Bryant, University of Oxford. PC3, PC3-EGFP, C4-2B, LNCaP, DU145 and 22RV1 cells were routinely maintained in RPMI 1640 medium (Sigma, Cat. R0883) supplemented with 10% fetal bovine serum (FBS) (Cat. FCS-SA, Labtech), 1% L-glutamine (Cat. G7513, Sigma),

1% penicillin/streptomycin (Cat. P0781, Sigma), 1% vitamins (Cat. 11120-037, Gibco), 1% sodium pyruvate (S8636, Sigma), 1% non-essential amino acids (Cat. M7145, Sigma) (complete RPMI medium). VCaP cells were cultured in DMEM medium (Cat. D5671, Sigma) supplemented with 10% FBS, 1% penicillin/streptomycin and 2% L-glutamine. MDA-PCa-2a cells were cultured in HPC1 media (Cat. 0403, Athena ES) supplemented with 20% FBS, 0.1% penicillin/streptomycin and 0.1% L-glutamine.

HS5 (Cat. CRL-11882) and HS27A (Cat. CRL-2496) human bone marrow stromal cells were purchased from ATCC. ST2 mouse bone marrow stromal cells and 2T3 mouse pre-osteoblast cells were a gift from the Mundy group, Vanderbilt University. All were routinely maintained in complete RPMI medium. MS-5 mouse bone marrow stromal cells were a gift from the Mead group, University of Oxford and were maintained in α-MEM medium (Cat. 22501-021, Gibco) supplemented with 10% FBS, 1% penicillin/streptomycin and 2% L-glutamine. HEK293T cells were a gift from the Oppermann group, University of Oxford, and were maintained in DMEM media supplemented with 10% FBS and 1% penicillin/streptomycin. Cells were routinely validated by genotyping

All cell lines were maintained at 37 $^{\circ}$C in a humidified 5% CO_2 atmosphere. Tissue Culture dishes and flasks were obtained from Corning Incorporated (NY, USA) or Greiner Bio-one (Kremsmünster, Austria).

Cell Line	Origin	Metastatic Potential	Nature of bone lesions	Androgen sensitivity
PNT1a	Benign prostate epithelium	N/A	N/A	+
22RV1	Prostate carcinoma	Moderate	Mixed lytic/blastic lesions (intra-tibial model)	Repressed
LNCaP	Supraclavicular lymph node metastasis	Very low	Poorly tumorigenic unless co-inoculated with MSCs	+
C4-2B	Serial passage of LNCaP in mice	High	Osteoblastic (intra-tibial model)	-
PC3	Vertebral metastasis	Very high	Osteolytic (intra-cardiac or intra-tibial model)	-
VCaP	Vertebral metastasis	Unknown	Osteoblastic lesions (intra-tibial model)	+
DU145	Brain Metastasis	High	Osteolytic (intra-cardiac or intra-tibial)	-
MDA-PCa-2a	Bone metastasis	Unknown	Unknown	+

Figure 2.1 ***Prostate cancer cell lines used***

2.1.1 Mycoplasma Testing

All cells were periodically tested to ensure the absence of mycoplasma contamination using MycoAlert detection kit (Cat. LT07-218, Lonza) according to manufacturers instructions. Briefly 1 ml of cell culture media was removed from the cell culture flask after a minimum of 48 hr culture. This was centrifuged at 1500 g for 5 min. MycoAlert reagent and substrate were reconstituted with assay buffer and allowed to equilibrate for 15 min. 100 µL of MycoAlert reagent was added to the 100 µL of cell culture supernatant in a 96 well plate. After 5 min luminescence was read on a plate reader (FLUOstar Omega, BMG labtech)(Reading A). 100 µL of MycoAlert substrate was then added to the well and after 10

min luminescence was read (Reading B). A ratio of Reading B/Reading A was then calculated. A Ratio < 0.9 was interpreted as negative for mycoplasma, a reading of 0.9-1.2 was considered borderline and cells were retested. A reading of > 1.2 was considered as positive for mycoplasma contamination.

2.1.2 Transwell Co-culture

PCa and BMSCs were seeded at a density of 5 x 10^5 in 6 well plates or transwell filters (0.4 µm pore size; Cat. 3412, Corning). After 24, 48 or 72 hr cells were washed in 1X phosphate buffered saline (PBS) and harvested for analysis.

2.1.3 Conditioned media (CM) Treatment

Cells were seeded at a density of 5 x 10^5 in 6 well plates or transwell filters. CM was obtained from 72 hr of single or PCa-BMSC cell co-culture, centrifuged at 1500 g for 5 min and the supernatant used fresh or stored at -20 ˚C for later use. Unless otherwise specified CM was used at a dilution of 1:1 in complete RPMI media.

2.1.4 Recombinant IL-6 and IL-6 neutralising antibody treatment

LNCaP cells were seeded at a density of 5 x 10^5 in a 6 well plate and left to settle overnight before treatment with 250 ng/ml and 1000 ng/ml recombinant IL-6, or 10 µg/ml neutralising antibody (206-IL; MAB2061; R&D Systems, Minnesota, USA) for 72 hr. 10 µg/ml IgG (MAB004, R&D Systems) was used as an isotype control for the neutralising antibody.

2.1.5 Drug treatments

Docetaxel (Cat. 01885, Sigma) and cabazitaxel (Cat. C046500, Toronto Research Chemicals,) were reconstituted in DMSO to a concentration of 0.5 M and stored in single use aliquots at -20 ˚ C until use. Cisplatin (Cat. 479306, Sigma) was reconstituted to a 1 M solution in 0.9% NaCl and stored at 4 ˚ C. 6-aminonicotinamide (Cat. A68203, Sigma) was reconstituted to 1 M in DMSO and stored at -20 ˚ C until use. Metformin (Cat. 317240, Calbiochem) was reconstituted to 1 M in ultrapure (MilliQ) water and stored at -20 ˚ C until use.

2.1.6 Hypoxic conditions

Cells were seeded at 5 x 10^5 in 6 well plates and left to settle overnight. Co-culture with transwells was commenced immediately prior to placement in a hypoxia chamber (New Brunswick, Galaxy 48R) set to 37°C 0.5% O_2. At the end of the time-point cells were rapidly washed with 1X PBS and lysed to limit normoxic exposure.

2.1.7 Glucose free conditions

Cells were seeded at 5 x 10^5 in 6 well plates and transwells and left to settle overnight. Media was then changes to RPMI with no glucose (Cat. R1383, Sigma) and co-culture commenced. At the end of the time-point cells were washed with 1X PBS and protein extracted.

2.1.8 Androgen deprivation conditions

Cells were seeded at a density of 5 x 10^5 in 6 well plates and left to settle overnight. Media was then removed and cells were washed with 1X PBS. RPMI with 10% Charcoal-stripped FBS (Cat. A3382101, Gibco) was added to the wells and incubated at 37°C for 72 hr to allow purging of androgens from the cells. Cells were then treated with androgen free RPMI, or 50% HS-5 conditioned androgen free RPMI for a further 72 hr. Protein or CM was extracted.

2.2 Cell proliferation

Cells were seeded at 2 x 10^4 in a black walled 96 well plate (Cat. 353219, Corning) and allowed to settle for 30 min. Bright-field or GFP fluorescent images were then taken on an IncuCyte camera every 4 hr. For green fluorescent protein (GFP) tagged cells fluorescent cells were counted using the IncuCyte analysis software. For non-GFP tagged cells bright-field images were used to calculate percentage confluency using the IncuCyte analysis software. Experiments were done with 3 technical replicates.

2.3 Cell viability

2.3.1 Alamar blue assay

Viability of cultured cells *in vitro* was determined using the Alamar Blue assay. Briefly a 1 mg/ml working solution of resazurin (Cat. R7017, Sigma) was added to cultured cells at a

ratio of 1:10 to the volume of growth medium (20 µl in each well of a 96 well plate containing 200 µl of growth medium). The cells were then incubated at 37°C in a humidified incubator for approximately 3 hr before being read using a fluorometer (FLUOstar Omega, BMG labtech; excitation: 544 nm, emission 590 nm). Readings from three blank wells (growth medium with resazurin but without cells) were averaged and subtracted from the raw fluorescent values to eliminate background fluorescence. Experiments were done with 3 technical replicates.

2.3.2 Trypan blue

Cells were seeded at 5 x 10^5 in a 6 well plate, trypsinised and counted by Trypan dye exclusion using an automated cell counter (TC20, BioRad) giving a live and dead cell count.

2.4 Colony formation assay

Cell were seeded at 1 x 10^4 in a 6 well plate and left for 7 (PC3-EGFP) or 10 (DU145, LNCaP) days. Media was then removed and cell stained with crystal violet fixing/staining solution (0.05% crystal violet, 1% formaldehyde, 1x PBS, 1% methanol) for 20 min at room temperature. Wells were then washed with 2 ml of water 4 times, and left to air dry. Colonies were quantified using a Celigo imaging system (Nexcelom, MA, USA).

2.5 Cell cycle by propidium iodide staining

Cells were washed with 1X PBS and trypsinised with 500 µL of trypsin/EDTA. 1 ml of complete media was then added to neutralise the trypsin and cells were counted. An equal number of cells were collected and centrifuged at 1500 g for 5 min. Cells were then re-suspended in 300 µl of 1X PBS and gently vortexed while 700 µl of 100% ice-cold ethanol was added drop-wise to fix the cells. Samples were the incubated on ice for 15 min before being pelleted at 1500 g for 5mins. The pellet was then re-suspended in 500 µL propidium iodide (PI) staining solution (50 µg/ml; ThermoFisher), 0.1 mg/ml RNase A (ThermoFisher), 0.05% Triton x-100 (Sigma)) for 40 min at 37 $^{\circ}$C. 500 µl of 1X PBS was added to the samples before they were spun down at 1500 g for 5 min. The supernatant was discarded and the pellet was re-suspended in 300 µL of 1X PBS for Flow Cytometric analysis on LSR Fortessa (BD Biosciences, USA). Cell cycle was analysed on FACSDiva software (BD Biosciences, USA) giving the percentage of cells in each phase of the cell cycle after appropriate gating.

2.6 Migration Assay

2.6.1 IncuCyte WoundMaker Assay

Cells were seeded at a density of 3 x 10^4 in a 96 well plate and allowed to adhere overnight. Cells were scratched at a confluency of >90% using an IncuCyte WoundMaker 96-pin woundmaking tool (Essen Bioscience, UK). Images were taken every 2 hr on the IncuCyte

and analysed using the IncuCyte software. Experiments were done with three technical replicates.

2.6.2 Transwell migration assay

Cells were seeded at a density of 1 x 10^4 in reduced serum RPMI (5% FBS) into the upper chamber of a 24 well plate transwell insert containing polycarbonate membranes with 8-µm pore size (Cat. 3422, Corning) with 1 ml of complete RPMI medium in the well below to act as the attractant. After 24 hr the media was removed and cells fixed using 10% formalin for 10 min. The transwells were then washed using 1X PBS. Cells were permeabilised with 100% methanol for 20 min before a further PBS wash. Cells were then stained with 1% toluidine blue for 20 min, and the cells in the upper chamber were removed using a cotton swab. Membranes were dissected off the transwell insert using a scalpel, wet with xylene/clearene, and mounted onto a microscope slide with coverslip using DPX mountant (Cat. 06522, Sigma). Images were taken using a BX40 Olympus microscope and cell counted. Experiments were done with three technical replicates. Migrated cells were quantified from the central field of view and statistically analysed.

2.7 Oxygen consumption assays

Cell seeding density was optimised with LNCaP cells in black-walled clear-bottomed 96-well plates. A seeding density of 2 x 10^5 was initially found to give the best signal curve, and so was used for further experiments (Figure 2.2). Oxygen consumption was assessed using MitoXpress-Xtra Oxygen Consumption Assay (Cat. MX-200-4, Agilent) according to manufacturer's instructions. Briefly 10 µl of reconstituted MitoXpress reagent was added to the 150 µl of media on the cells. The wells were then sealed with two drops of pre-warmed HS mineral oil and the fluorescence (excitation filter TRExL; emission filter 655-50 nm) was measured immediately on a FLUOstar Omega microplate reader using a TR-F Optical attachment (BMG labtech) at a z-height of 5mm for 90 minutes (Figure 2.3).

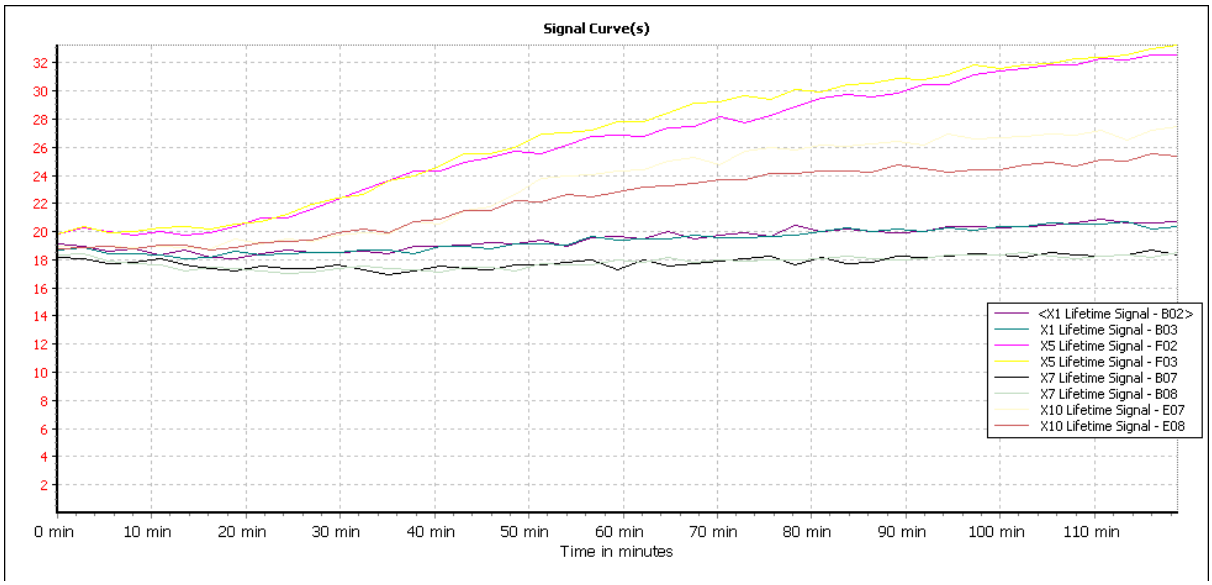


Figure 2.2 ***Cell seeding density optimisation MitoXpress kit.*** *LNCaP cells were seeded at 7.5 x 10^4 (X7), 15 x 10^4(X1), 20 x 10^4(X10), 25 x 10^4(X5) and signal read over 120 minutes.*

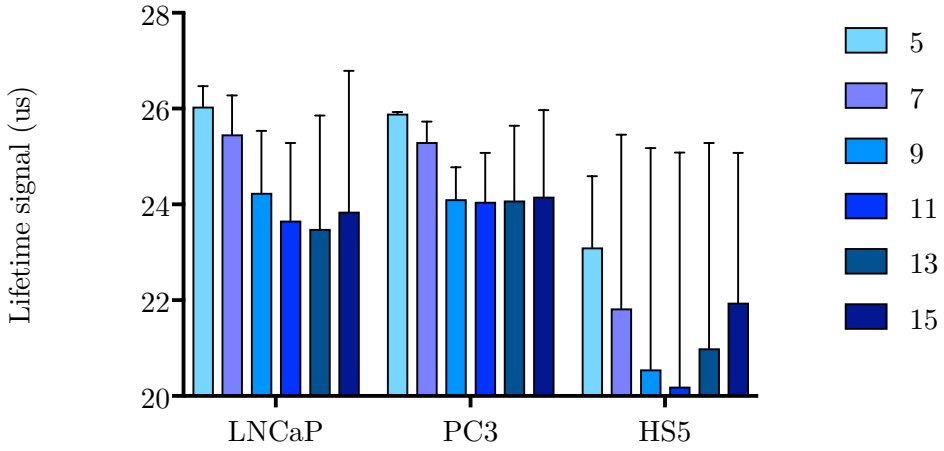


Figure 2.3 ***Z-depth on TRF Optic head optimisation.*** *Readings were taken at a range of z-depths (5-15 mm) in LNCaP, PC3 and HS5 cells. A depth of 5 mm consistently gave the strongest signal and so was used for further experiments.*

2.8 Extracellular acidification assay

Cells were seeded at 2 x 10^5 in black-walled clear-bottomed 96-well plates. Extracellular acidification rate (ECAR) was assessed using pH-Xtra Glycolysis Assay (Cat. PH-200-4, Agilent) according to manufacturer's instructions. Media and plastic ware was purged of CO_2 in a CO_2 free incubator for 2 hr prior to performing the assay. Briefly culture medium was removed from the cells and they were washed twice using 100 µl of Respiration Buffer. After the second wash, 90 µl of fresh Respiration Buffer was added to the cells with 10 µl of reconstituted pH-Xtra reagent. The fluorescence (excitation filter TRExL; emission filter 655-50 nm) was measured immediately on a FLUOstar Omega microplate reader using a TR-F Optical attachment (BMG labtech) at a z-height of 5mm for 90 minutes.

2.9 Capillary Electrophoresis Mass Spectrometry (CE-MS) analysis

CE-MS was performed at the Institute for Advanced Biosciences, Keio University, Tsuruoka, Japan under the supervision of Prof Soga. Cells were washed twice with 5% mannitol solution and covered with 700 µl of methanol containing 25 µM internal standards [20 µM each of methionine sulphone, 2-(N-morpholino)-ethanesulphonic acid (MES) and D-Camphor-10-sulphonic acid (CSA)] for 10 min. The resulting extracts were mixed with 200 µL of Milli-Q water and 400 µL of chloroform and centrifuged at 4600 g for 15 min at 4°C. Then 400 µL of the aqueous phase of the sample solution was subjected to ultrafiltration

through a 5 kDa cut-off filter (Human metabolome Technologies) to remove proteins. The filtrate was centrifugally concentrated and dissolved in 25 μL Milli-Q water that contained reference compounds (200 μM each of 3-aminopyrrolidine and trimesate) immediately prior to metabolome analysis. The concentrations of all the charged metabolites were measured by capillary electrophoresis time-of-flight mass spectrometry (Agilent Technologies) using the methods described previously[150]. Briefly, to analyse cationic compounds, a fused silica capillary (50 μm i.d. x 100cm) was used with 1 M formin acid as the electrolyte. Methanol/water (50% v/v) containing 0.1 μM hexakis (2,2-difluoroethoxy) phosphazene was delivered as the sheath liquid at 10μl/min. ESI-TOFMS was performed in positive ion mode, and the capillary voltage was set at 4 kV. Automatic recalibration of each acquired spectrum was achieved using the masses of the reference standards ([13C isotopic ion of a protonated methanol dimer (2MeOH+H)]+, m/z 66.0632) and ([hexakis(2,2-difluoroethoxy)phosphazene +H]+, m/z 622.0290). To identify metabolites relative migration times of al peaks were calculated by normalisation to the reference compound 3-aminopyrrolidine. The metabolites were identified by comparing their m/z values and relative migration times to the metabolite standards. Quantification was performed by comparing their peak areas to calibration curves generated using internal standardisation techniques with methionine sulphone. The other conditions were identical to those described previously[151].

To analyse anionic metabolites, a commercially available COSMO(+) (chemically coated with cationic polymer) capillary (50 μm i.d. x 105cm) (Nacalai Tesque, Kyoto, Japan) was used with 50 mM ammonium acetate solution (pH 8.5) as the electrolyte. Methanol/5 mM ammonium acetate (50% v/v) containing 0.1μM hexakis(2,2-difluoroethoxy)phosphazene was

delivered as the sheath liquid at 10 µl/min. ESI-TOFMS was performed in negative ion mode, and the capillary voltage was set at 3.5 kV. For anion analysis, trimesate and CAS were used as the reference and internal standards respectively. The other conditions were identical to those described previously[150]. Analyses were performed by Futaba Shoji using MasterHands Software (v2.13.0.8h, Keio University).

2.10 Protein isolation and western blotting

Cultured cells were gently washed with 1X PBS to remove residual growth medium and then lysed using 40-100 µl of radioimmunoprecipitation assay buffer (Cat. R0278, RIPA; Sigma) with 4% protease inhibitor (Cat. 11873580001, Roche) and 1% phosphatase inhibitor cocktail 2 (Cat. P5726, Sigma). After incubation for 40 min on ice with periodic vortexing, the sample was centrifuged at 12,000 g for 15 min to pellet the cell debris. The supernatant was transferred to a new eppendorf and the lysates were stored at -20°C until further use.

Protein concentration was quantified used a Pierce bicinchoninic acid (BCA) assay kit (Cat. 23225, ThermoFisher Scientific) according to the manufacturer's instructions. This involves a colourimetric reaction when protein samples are mixed with the working solution. Plates were incubated at 37°C for 30 min and read on a plate reader at absorbance wavelength 562 nm. The concentration of the lysate was then calculated using a standard curve obtained from serial dilutions of bovine serum albumin (BSA) provided in the kit. Known concentrations of protein were mixed with appropriate volumes of 4X LDS Sample buffer and 10X Sample Reducing Agent (Invitrogen, Carlsbad, USA) and denatured at 95°C for 5

min. An equal amount of protein (40-60 µg) was loaded into lanes of a 4-20% gradient sodium dodecyl sulphate-polyacrylamide gel (SDS-PAGE; Biorad). Gels were run at 120 V for approximately 1 hr in 1X TGS Running Buffer (Biorad) for protein separation. Precision Plus Protein Kaleidoscope pre-stained protein ladder (Biorad) was used as a size standard. Once the SDS-PAGE running process was complete, the gel was transferred to a polyvinylidene difluoride membrane (PVDF; Biorad) using a semi-dry transfer system (Trans-Blot Turbo, Biorad). The membranes were blocked in 1X Tris-buffered saline (TBS), 5% BSA and 0.1% TWEEN (TBST) for 1 hr against non-specific binding. Primary antibodies were used at the manufacturers recommended concentration diluted in TBST (Table 2.1) and incubated with the membrane overnight with gentle rocking at 4 ˚C. Following this the membrane was washed in TBST 4 times for 5 min duration each, followed by incubation with secondary antibody (anti-rabbit or anti-mouse respectively) diluted 1:5000 in TBST for 2 hr at room temperature with gentle shaking. The membrane was washed a further 4 times as above. Antigen-antibody complexes were visualised by enhanced chemiluminescent detection using Clarity Western ECL Substrate (Biorad) and imaged on a gel doc system (Alliance 6.7,Uvitech, Cambridge, UK). The intensity of protein bands was measured using ImageJ software. Between different primary antibody incubations membranes were stripped with stripping buffer (Sigma) before blocking and antibody incubations as above.

Target	Host	Type	Manufacturer	Product No.	Concentration used
G6PD	Rabbit	Polyclonal	Cell Signalling Technology	8866	1:1000
G6PD	Rabbit	Polyclonal	Abcam	ab76598	1:1000
RPE	Rabbit	Polyclonal	Abcam	ab98354	1:1000
Citrate Synthase	Mouse	Monoclonal	Santa Cruz	sc-390693	1:1000
Fumarase	Rabbit	Monoclonal	Cell Signalling Technology	4567	1:1000
SDHA	Rabbit	Monoclonal	Cell Signalling Technology	11998	1:1000
Anti-OXPHOS Complex kit	Mouse	Monoclonal	Life technologies	457999	1:250
IL-6	Rabbit	Polyclonal	Abcam	ab6672	1:1000
STAT3	Rabbit	Monoclonal	Cell Signalling Technology	12640	1:1000
p-STAT3 (Tyr705)	Rabbit	Monoclonal	Cell Signalling Technology	9145	1:2000
PSA	Rabbit	Polyclonal	Abcam	ab53774	1:1000
β-actin	Mouse	Monoclonal	Sigma	A2228	1:20000
GAPDH	Rabbit	Monoclonal	Cell Signalling Technology	5174	1:1000
Anti-mouse IgG	Horse	-	Cell Signalling Technology	7076	1:5000
Anti-rabbit IgG	Goat	-	Cell Signalling Technology	7074	1:5000

Table 2.1 ***Antibodies used***

2.11 Ribonucleic acid (RNA) isolation

Total RNA was isolated from cultured cells using a RNeasy kit (Cat. 74106, Qiagen) according to the manufacturer's instructions. Briefly cells were collected into 350 µl RLT lysis buffer. One volume of 70% ethanol was added to homogenise the lysate. The sample was centrifuged in an RNeasy spin column for 30 sec at 8000 g. The flow through was discarded and 700 µl of buffer RW1 was added to the top of the column. The sample was centrifuged for 30 sec at 8000 g and flow through was discarded. 500 µl of buffer RPE was added to the top of the column and the sample was centrifuged for 30 sec at 8000 g and flow through was discarded. 500 µl of buffer RPE was added to the column and the sample was centrifuged for 2 min at 8000 g. The column was then moved to a new RNase/DNase free 1.5 ml eppendorf and 30 µl of RNase/DNase free water was added to the top of the collection tube and centrifuged for 1 min at 8000 g to elute the RNA. RNA was quantified using a NanoDrop 100 spectrophotometer (ThermoFisher). Quality of the RNA was assessed by measuring the ratios of absorbance (A260/A280 and A260/A230); ratios greater than 1.8 were considered suitable for further analysis.

2.12 cDNA synthesis

1 µg of RNA was DNase treated using a DNase kit (Cat. DNASE-50, Primer Design) to eliminate any contaminating genomic DNA. This was then reverse transcribed into complementary DNA (cDNA) using 20 µl of Nanoscript 2 (Cat. RT-premix-48, Primer

Design) and cycled in a Veriti thermocycler (Applied Biosystems) according to the manufacturers instructions.

2.13 Quantitative real-time polymerase chain reaction (qPCR)

cDNA was appropriately diluted with RNase/DNase free water and used for qRT-PCR with either Taqman or Fast SYBR Green reagents.

Taqman q-PCR was performed using Taqman primers (Life Technologies, Table 2.2) and Taqman Universal Mastermix (Cat. 4440041, Life Technologies). Briefly, a 20 µl total volume reaction comprised of 10 µl Taqman Universal Mastermix, 1 µl of each primer (if multiplexing), 7 µl of RNase/DNase free water and 1 µl of cDNA. SYBR Green qPCR was performed using Qiagen (Table 2.3) or SYBR green (Table 2.4) primers and Fast SYBR Green Mastermix (Life Technologies). Briefly, a 20 µl total volume reaction comprised of 10 µl SYBR Green Mastermix, 0.4 µl of SYBR green primers, or alternatively 2 µl of Qiagen primer mix, 2 µl cDNA, and made up to 20 µl with RNase/DNase free water.

The expression of genes was normalised against that of a housekeeping gene, Polr2a (RNA polymerase II subunit A) when comparing different conditions in the same cell line, and GAPDH (glyceraldehyde 3-phosphate dehydrogenase) when comparing between different cell lines. Plates were cycled on a Viia7 (Applied Biosystems) real-time thermal cycler according

to the manufacturer's instructions. Samples were plated with 3 technical repeats. Gene expression was analysed by the ΔΔCT method in Excel (Microsoft Office):

$$\Delta Ct = Ct_{target} - Ct_{housekeeping}$$

$$\Delta\Delta Ct = \Delta Ct_{(treated)} - \Delta Ct_{(untreated)}$$

$$\text{Relative expression level} = 2^{-\Delta\Delta Ct}$$

Gene Name	Species	Reporter Dye	Assay ID
POLR2A	Human	VIC	Hs00172187_m1
GAPDH	Human	VIC	Hs99999905_m1
G6PD	Human	FAM	Hs00166169_m1
IL6	Human	FAM	Hs00985639_m1
TKT	Human	FAM	Hs01115545_m1
PGD	Human	FAM	Hs00427230_m1
PGLS	Human	FAM	Hs00359986_m1

Table 2.2 ***Taqman primer list.*** *All Taqman primer mixes were purchased from Thermo Scientific.*

Gene Name	Species	Catalogue number
CDH1	Human	QT00080143
STAT3	Human	QT00068754

Table 2.3 ***Qiagen Primer list.*** *All Qiagen primer mixes were purchased from Qiagen.*

Gene	Species	Sequence
Vimentin F	Human	CCTTGAACGCAAAGTGGAATC
Vimentin R	Human	GACATGCTGTTCCTGAATCTGAG
ZEB2 F	Human	AACACCCCTGGCACAACAA
ZEB2 R	Human	AATTGCGGTCTGGATCGTGG
TWIST F	Human	AGCTGAGCAAGCTTCAGACCC
TWIST R	Human	GCAGCTTGCCATCTTGGAGT

Table 2.4 ***SYBR primer list.*** *All SYBR green primers were designed using NCBI primer blast and purchased from Eurofins.*

2.14 *In silico* analysis

Hutchinson 2016 data set[152] was obtained via CBioPortal (Center for Molecular Oncology, Memorial Sloan Kettering Cancer Center, USA). MSKCC[153], Michigan 2005[154] and Michigan 2012[155] data sets were obtained via Geo (National Center for Biotechnology Information, USA). Analysis was performed using Prism 8 (Graphpad) and GSEA (Broad Institute, USA). Gene set enrichment analysis was done using GSEA cancer hallmark gene set, or a metabolic specific gene set curated from Gaude & Frezza[156]. Pathways were considered to be significantly altered in the GSEA analysis if they had a nominal p value <0.05 and false discover rate (FDR) q-value <0.25 (Appendix A.1).

2.15 Glucose-6-phosphate dehydrogenase (G6PD) activity quantification

G6PD activity was measured by a G6PD activity assay kit (Cat. ab102529, Abcam) according to the manufacturer's instructions. Briefly cells were washed with cold 1X PBS and then lysed in 100 µL G6PD Assay Buffer and homogenized by pipetting up and down. Samples were kept on ice for 10 min before being centrifuged for 5 min at 12,000 g at 4°C to remove insoluble material. The supernatant was then transferred to a new tube and kept on ice. Samples were diluted 1:10 for the assay. 50 µL of G6PD Reaction Mixture was added to each diluted sample and the standard curve, and mixed thoroughly. Absorbance was then

measured on a microplate reader in kinetic mode for 30 min at 37 °C protected from light. G6PD activity was then calculated from the linear phase of the reaction:

$$G6PD\ Activity = \left(\frac{B}{\Delta T \times V}\right) \times D$$

Where:

B = amount of NADH in sample well calculated from standard curve (nmol)

ΔT = linear phase reaction time T2-T1 (minutes)

V = original sample volume added into the reaction well (mL)

D = sample dilution factor

1 Unit G6PD activity is defined as the amount of G6PD that will generate 1.0 µmol of NADH per minute at 37 °C.

2.16 Mitochondrial superoxide (MitoSox) quantification

MitoSOX Red (Cat. M36008, Thermofisher) was used to measure mitochondrial superoxide according to the manufacturer's instructions. Briefly a 5 mM stock solution was made by dissolving 50 µg of MitoSOX in 13 µL of dimethylsulfoxide (DMSO), and then a working solution was made by diluting the 5 mM stock solution in RPMI media. Cells were treated with 2.5 µM MitoSOX and 200 µg/ml Hoechst (bisBenzimide H 33342 trihydrochloride,

Sigma) in complete RPMI media and incubated for 30 min at 37°C protected from light. Fluorescence was then measured for MitoSOX (excitation 485 nm; emission 590 nm) and Hoechst (excitation 346 nm, emission 460 nm).

2.17 Reactive oxygen species (ROS) quantification

Total ROS levels were measured using a ROS-Glo Kit (Cat. G8820, Promega) according to the manufacturer's instructions. Briefly 20 µL of H_2O_2 substrate solution was added to 80 µL of media on adherent cells giving a final well volume of 100 µL. Cells were then plated in an incubator for 6 hr. 100 µl of ROS-Glo Detection Solution was then added to each well and the plate incubated at room temperature for 20 min before luminescence was measured using a plate-reading luminometer. Luminescent signal is proportional to the H_2O_2 concentration.

2.18 Glutathione (GSH) quantification

Glutathione levels were measured using a GSH Glo Kit (Cat. V6911, Promega Wiconsin, USA) according to the manufacturer's instructions. Briefly cells were seeded at 1 x 10^4 in a 96 well plate and allowed to adhere. Medium was then removed from the cells and 100 µl of 1X GSH Glo reagent added (100 µL GSH Glo reaction buffer, 1 µL Luciferin NT, 1 µL Glutathione S-transferase). Samples were incubated for 30 min at room temperature with gently shaking on an orbital shaker. 100 µL of luciferin detection reagent was then added,

and the plate incubated for a further 15 min with gentle shaking. Luminescence was then read using a plate reader.

2.19 Transfection

2.19.1 Short hairpin RNA (shRNA) and Open Reading Frame (ORF) Transfection

G6PD MISSION shRNA (TRCN0000281204, TRCN0000281206, TRCN0000281207) (Figure 2.4), G6PD MISSION TRC3 ORF (TRCN000046117) (Figure 2.5), and scrambled control (Cat. SHC002) bacterial glycerol stocks and MISSION BFP TRC3 ORF (ORFBFPV) lentivirus were purchased from Sigma.

Colonies were grown on agar with ampicillin (0.1 mg/ml). After 24 hr at 37°C a single colony was picked and grown in LB broth with ampicillin (0.1 mg/ml) overnight on a shaker at 200 RPM. The plasmid was then purified using Qiagen Endofree plasmid purification kit according to the manufacturer's instructions. Plasmid DNA was eluted in water and purity and concentration were checked using a Nanodrop 100 spectrophotometer.

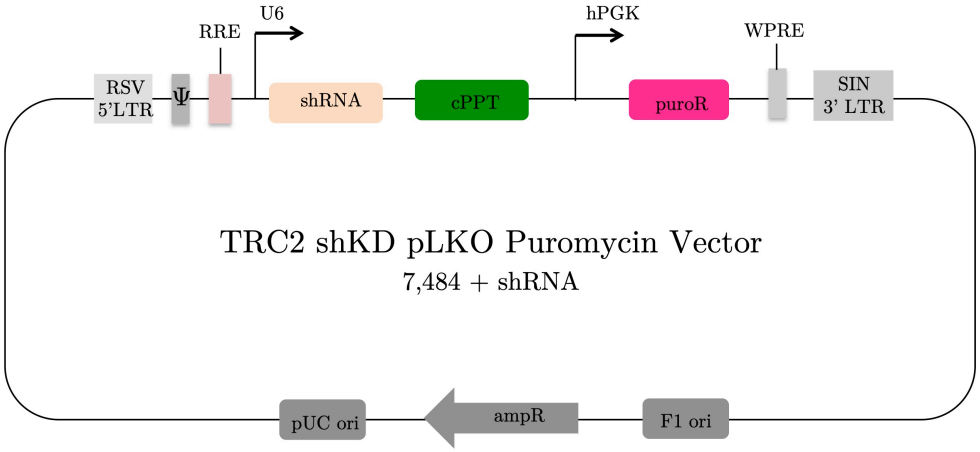


Figure 2.4 ***TRC2 Puromycin shKD Vector map and features.*** *5' LTR: 5' long terminal repeat, Ψ: Psi viral genome packaging signal, RRE: Rev response element – increases full length viral packaging, U6: U6 promoter, cPPT: Central polypurine tract, hPGK: Human phosphoglycerate kinase eukaryotic promoter, puroR: Puromycin resistance gene for selection, WPRE: Woodchuck Hepatitis Post-Transciptional Regulatory Element, SIN 3'LT: 3' self inactivating long terminal repeat, F1 ori: f1 origin of replication, ampR: Ampicillin resistance gene for bacterial selection, pUC ori: pUC origin of replication. SCR control: same construct except no WPRE.*

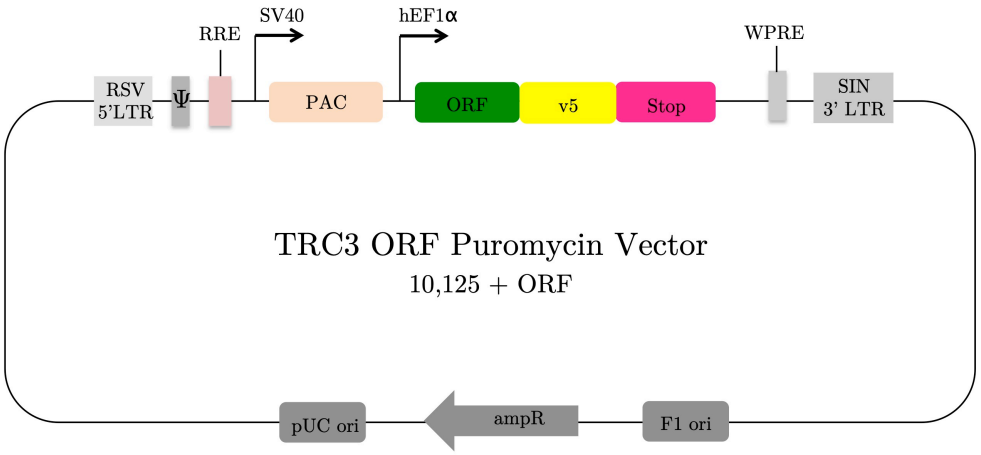


Figure 2.5 ***TRC3 Puromycin ORF Vector map and features.*** *SV40: Simian virus 40 promoter, PAC; Puromycin N-acetyl-transferase gene confers puromycin resistance, hEF1α: RNA Polymerase II Promoter Human Elongation Factor-1 alpha, ORF: open reading frame, v5: V5 epitope tage, Stop: Termination codon.*

2.19.2 Lentiviral packaging and transduction

Lentiviral packaging was performed in HEK 293T cells using a 2nd generation packaging system. Briefly, HEK 293T cells were seeded in 100 mm tissue culture dishes (Corning) and incubated at 37°C at 5% CO_2 in a humidified incubator until they were ~90% confluent. 10 µg of transfer vector was added to 5 µg psPAX2, 5 µg pMD2.G and 500 µl OptiMEM (Cat. 31985062, Life Technologies). Separately 30 µl Lipofectamine 2000 (Cat. 11668019, Life Technologies,) was added to 500 µl OptiMEM. These were then mixed and incubated at room temperature for 20 min with regular inversion. The transfection solution (1 ml) was then added to the HEK 293T cells in 10 ml of antibiotic-free DMEM media. Plates were incubated at 37°C for 72 hr and culture supernatant containing the lentivirus was collected. Transfection was confirmed at this point by expression of fluorescent protein in the HEK 293T cells transfected with a control fluorescent construct. The supernatant was centrifuged at 4000 g for 10 min at 4°C and then filtered through a 0.45 mm polyethersulfone (PES) filter. The lentivirus was made into a 10 times concentrated stock using the Lenti-X Concentrator Solution (Cat. 631232, Clontech) added at a dilution of 1:10 to the cell suspension for transduction. The solution was incubated at 4°C overnight before being centrifuged at 1500 g for 45 min at 4°C. The supernatant was then removed and the pellet re-suspended, flash frozen in liquid nitrogen and stored at -80°C.

Prostate cancer cells were seeded at 5 x 10^5 in 6 well plates and treated with 200 µl of virus and 8 µg/ml Polybrene (Cat. H9268, Sigma) to enhance transduction efficiency, and incubated for 72 hr at 37°C. Transduced cells were selected using Puromycin (Sigma, Cat

P7130) for 6 weeks (2 µg/ml for LNCaP; 4 µg/ml for PC3-EGFP and DU145). A puromycin kill curve of non-transfected LNCaP, C42B and DU145 cells was previously performed over 14 days to confirm the appropriate dose of puromycin (Figure 2.6). Knockdown was confirmed by qPCR.

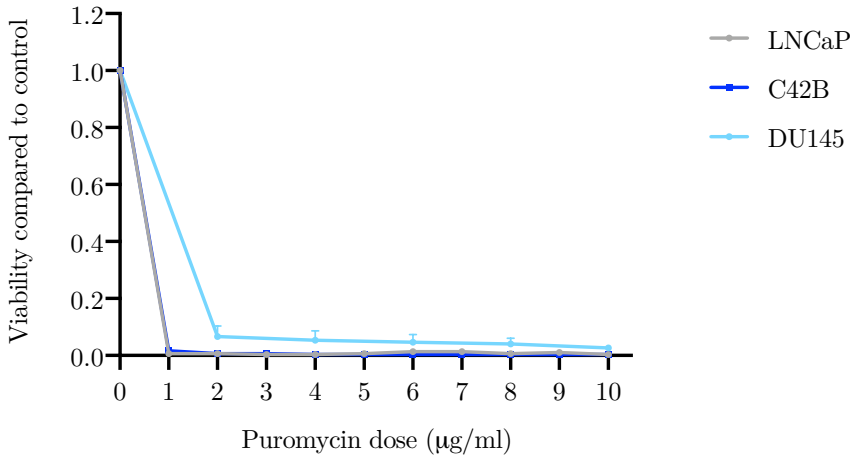


Figure 2.6 ***Puromycin kill curve.*** *Cells were seeded at 1x10⁴ in a 96 well plate and treated for 14 days. Treatment was changed every 72 hours. Viability was determined by Alamar blue assay.*

2.20 RNA Sequencing (RNA Seq)

2.20.1 NEBNext Ultra II RNA library prep for Illumina

RNA was DNase I treated, cleaned and concentrated according to the manufacturer's instructions using Zymo RNA Clean and Concentrator -5 (R1013, Zymo). mRNA was enriched from total RNA according to the manufacturer's instructions using a NEBnext poly(A) mRNA magnetic isolation module. Firstly mRNA was isolated and fragmented from total RNA using oligo dT beads and a magnetic rack. Beads were mixed with 1µg RNA and then washed twice. Samples were then heated to 65 ˚C for 5mins before being washed. Tris buffer was added and samples were heated once again to 80 ˚C and held at 25 ˚C to perform the first elution of the mRNA from the beads. Beads were subsequently washed and mRNA was eluted and fragmented with the addition of first strand synthesis reaction buffer and random primer mix. Samples were heated to 94 ˚C for 15 min and held at 4 ˚C Sequencing libraries were prepared according to the manufacturer's recommendations using the NEBNext Ultra II RNA Library Prep kit (E7770S, NEB). Briefly, first and second strand cDNA synthesis was performed using mRNA isolated as above. Double strand cDNA was purified using NEBNext sample purification beads, and DNA was eluted in 0.1X TE buffer. End prep reaction and adaptor ligation was performed and purification was done using sample purification beads. RNA and DNA quantification was performed using HS RNA and HS DNA assay kits (Q32852, Q32851, Invitrogen) Qubit fluorometer (Life Tech) according to the manufacturer's instructions. RNA and DNA quality was determined using High

Sensitivity RNA Screentape and D1000 High Sensitivity DNA Screentape respectively on Agilent 4200 tapestation system according to the manufacturer's instructions.

2.20.2 Illumina Sequencing

Single-indexed and multiplexed samples were run on an Illumina Next Seq 500 sequencer using a NextSeq 500 v2 kit (150 cycles) (FC-404-2005) for paired-end sequencing (75 bases x 2). Results from RNA-Seq were aligned to the human genome assembly version 38 (hg38 or GRCh38). At least 14 million aligned reads were obtained per sample.

2.20.3 Bioinformatics

Bioinformatic analysis for the RNA-Seq was performed by Dr. Srinivasa Rao, University of Oxford. Briefly, sequencing reads were de-multiplexed based on the sample index and aligned to the human genome (hg38) using the STAR (Spliced Transcipts Alignment to a Reference) aligner[157]. Differential expression analysis was performed using DESeq2[158] between two groups designated as SCR (scrambled) and shG6PD (G6PD knockdown).

2.21 *In vivo* model

Mice were acquired from Charles River (Wilmington, Massachusetts, US). All animals were maintained in conditions in accordance with the Animal (Scientific Procedures) Act 1986, and the guidelines of the University of Oxford. All procedures were approved by the Home Office under project licence PCCCC8952. Animals were maintained in individually ventilated cages under controlled temperature (19-23°C) and light (12 hr light/dark cycles) with food and water ad libitum. Schedule 1 procedures were used to sacrifice and confirm death in all animals.

2.21.1 C4-2B Intra-tibial model

Four-week old male CB17 SCID mice were purchased from Charles Rivers and allowed to acclimatise to their new environment for one week prior to experimentation. Mice were anaesthetised using 3% isoflurane for induction, and maintained on a heated pad at 2-2.5% using a nose cone for the procedure. A 21G sterile needle was used to pierce through the patella tendon into the tibia. 1 x 10^6 cells suspended in 40 µL PBS, or 40 µL of PBS control, was then injected into this space using a sterile 23G needle. Alternatively, 2 x 10^6 cells suspended in 80 µL PBS were inoculated subcutaneously. After inoculation, animals were placed in a preheated recovery chamber and carefully monitored until the animal had fully regained consciousness and was mobilising.

Mice were weighed weekly and bled at specified time points via tail scratch into a microvette 500 z-Gel tube (Sarstedt) and serum separated by spinning at 10,000 g for 5 min at 20°C. Serum was used fresh or stored at -80°C until use.

2.21.2 Human PSA (KLK3) enzyme-linked immunosorbent assay (ELISA)

For the C4-2B mouse model tumour burden was calculated using a PSA ELISA kit (ab113327, Abcam) according to the manufacturer's instructions. Serum was diluted 1:10 or 1:20 for the PSA ELISA depending on serum availability. 100 µl of diluted serum sample or standard was incubated on the ELISA plate overnight at 4°C with gentle shaking on an orbital shaker. The following day the sample was then discarded and the well washed 4x with wash solution. 100 µL of Biotinylated PSA detection antibody was then added to each well and incubated for 1 hr at room temperature with gentle shaking. This was then discarded and the well washed 4 times. 100 µl of HRP Streptavidin solution was added to each well and incubated at room temperature for 45 min with gentle shaking. This was then discarded and the well washed 4 times. 100 µl of TMB One-Step Substrate Reagent was added to each well and incubated for 30 min at room temperature in the dark with gentle shaking before 50 µL of Stop Solution was added. Absorbance was then measured at 450 nm using a FLUOstar Omega microplate reader (BMG labtech).

2.21.3 PC3-EGFP Intra-tibial model

Five-week old male CB17 severe combined immune deficient (SCID) mice were purchased from Charles Rivers and allowed to acclimatise to their new environment for one week prior to the start of the experiment. Mice were anaesthetised using 3% isoflurane for induction, and maintained on a heated pad at 2-2.5% using a nose cone for the procedure. A 21G sterile needle was used to pierce through the patella tendon into the tibia. 2 x 10^5 cells suspended in 40 µL PBS, or 40 µL of PBS control, was then injected into this space using a sterile 23G needle. After inoculation, animals were placed in a preheated recovery chamber and carefully monitored until the animal had fully regained consciousness and was mobilising.

Mice were weighed weekly, and bled at pre-tumour inoculation via tail scratch into a microvette 500 z-Gel tube (Sarstedt), and on cull day by cardiac puncture. Serum was separated by spinning at 10,000 g for 5 min at 20°C. Serum was used fresh or stored at -80 °C until use.

2.21.4 IVIS imaging

For the PC3-EGFP model, tumour burden was measured using fluorescent imaging on day 7, 14, 21 and 28. Animals were anaesthetised using 3% isoflurane for induction, and maintained at 2-2.5 % using a nose cone during the imaging. Animals were placed inside an IVIS Lumina LT Series III *in vivo* imaging system (PerkinElmer) and imaged for green fluorescence (excitation 465nm). Fluorescence units were measured from a 1 cm diameter

circular region of interest at the proximal tibia measuring in Living Image 4.5.5 software (PerkinElmer).

2.21.5 *Ex-vivo* µCT of bones

Bones were scanned using a Skyscan 1172 (Bruker) machine, performed at 37kV/228 µA, with an isometric resolution of 8.79 µm/pixel using a 0.5 mm aluminium filter, rotation of 0.1˚ with 4 frame averaging. Reconstruction of images was done using NRecon software (SkyScan).

2.21.6 Extraction of *ex-vivo* tumour RNA

Tibias were dissected immediately post-mortem, stripped of muscle, and snap frozen in liquid nitrogen. Bones were homogenised using a bone crusher and the powder placed into buffer RLT. RNA was then extracted (protocol as previously described). Extracted RNA was concentrated using Zymo Clean and Concentrator -5 kit (Cat. D4013). RNA was quantified and made into cDNA (protocol as above). cDNA was run on a custom designed metabolism specific TLDA card (ThermoFisher) (Table 2.5).

ALDOA	HK2	FBP2	DLST	PDHB	PRPS1L1	CPT2	UQCRFS1
ENO1	HK3	PCK1	FH	SDHD	PRPS2	ACADL	CYC1
ALDOC	PFKL	G6PC3	IDH1	SDHB	RBKS	LIPE	NDUFB5
BPGM	PGAM2	PC	IDH2	SDHC	RPE	GPAM	NDUFB7
ENO1	PGK1	PCK1	IDH3A	SDHD	RPIA	ACADL	ATP5A1
ENO2	PGK2	PCK2	IDH3B	SUCLA2	TALDO1	PNPLA2	UQCRC2
ENO3	PGM1	ACLY	IDH3G	SUCLG1	TKT	ACAT1	NDUFA4L2
GALM	PGM2	ACO1	MDH1	SUCLG2	POLR2A	CPT1B	ATP6V0D2
GCK	PGM3	ACO2	MDH1B	G6PD	PGD	COX7A1	NDUFS2
GPI	PKLR	CS	MDH2	H6PD	FASN	ATP5C1	ATP5I
GAPDH	TPI1	DLAT	OGDH	PGLS	ACACA	NDUFA11	UQCR10
ATP6V1E1	FBP1	DLD	PDHA1	PRPS1	ACADS	COX4I2	NDUFB8

Table 2.5 ***Genes included on custom metabolism TLDA gene card.***

2.21.7 Histopathology

After bone specimens were fixed in 10% formalin for a minimum of 72 hr, decalcification was performed using 10% EDTA for 10 – 14 days. The specimens were then paraffin embedded for histopathology. Bones were cut into 5-µm sections on a microtome and mounted onto adhesive microscope slides using warm water (40 ˚C). Sections were de-paraffinized using xylene and re-hydrated in a series of decreasing concentrations of alcohol. They were then stained with hematoxylin and eosin (H&E) to assess histology.

2.22 Statistical Analysis

Statistical analysis was performed using GraphPad Prism 8 (GraphPad Software, California, USA). Experiments were performed in triplicate unless otherwise stated. Statistical significance was determined using Student's T-test or for three or more groups ANOVA was used with post hoc Dunnett's test unless otherwise specified. Results were considered significant if * $p<0.05$; ** $p<0.01$; *** $p<0.001$; **** $p<0.0001$. Data is represented as mean ± standard error of mean (SEM).

3

Bone marrow stromal cells alter the metabolic profile of prostate cancer

3.1 Introduction

It is known that stromal cells, and in particular CAFS, play a role in altering the metabolism of cancer cells[87,159], however the effects of stromal cells of the bone metastatic niche remain poorly examined. The bone microenvironment is a rich source of energy and is composed of a large number of stromal components that secrete an abundant amount of growth factors and cytokines that all may impact on cancer cell metabolism[52]. Therefore this

chapter will explore whether the bone microenvironment can alter the metabolism of prostate cancer cells.

3.2 Aims

The aims of the work described in this chapter are:

1. To investigate whether the bone microenvironment alters prostate cancer metabolism *in vivo*, *in vitro* and in patient samples.

2. To establish which metabolic pathways in prostate cancer are most altered by the bone microenvironment.

3.3 The bone microenvironment creates a permissive environment for prostate cancer cells to grow

C4-2B prostate cancer cells are derived from the cell line LNCaP, passaged several times through nude mice. They are able to reliably form tumours *in vivo* in immuno-compromised mice when injected intra-tibially or subcutaneously unlike their parental cell line[160,161]. They form mixed lytic/blastic lesions when injected intra-tibially, and therefore more accurately represent the human disease compared to the faster lytic PC3 xenograft model. To investigate whether the bone microenvironment promotes prostate cancer growth *in vivo* C4-2B prostate cancer cells were injected intra-tibially (1×10^6) and subcutaneously (2×10^6) into male SCID mice. Disease progression was monitored with serial serum PSA measurements (Figure 3.1A).

C4-2B cells were able to grow intra-tibially however they were unable to form tumours subcutaneously, suggesting there may be bone specific factors that promote the survival and growth of prostate cancer in this metastatic site (Figure 3.1A-B). As expected, on radiograph mixed lytic/blastic tumours were visible in the tumour inoculated legs, but not in the control legs from the same animals (Figure 3.1C). H&E staining confirmed the bone marrow was filled with tumour cells compared to the normal bone architecture seen in the control legs from the same animals.

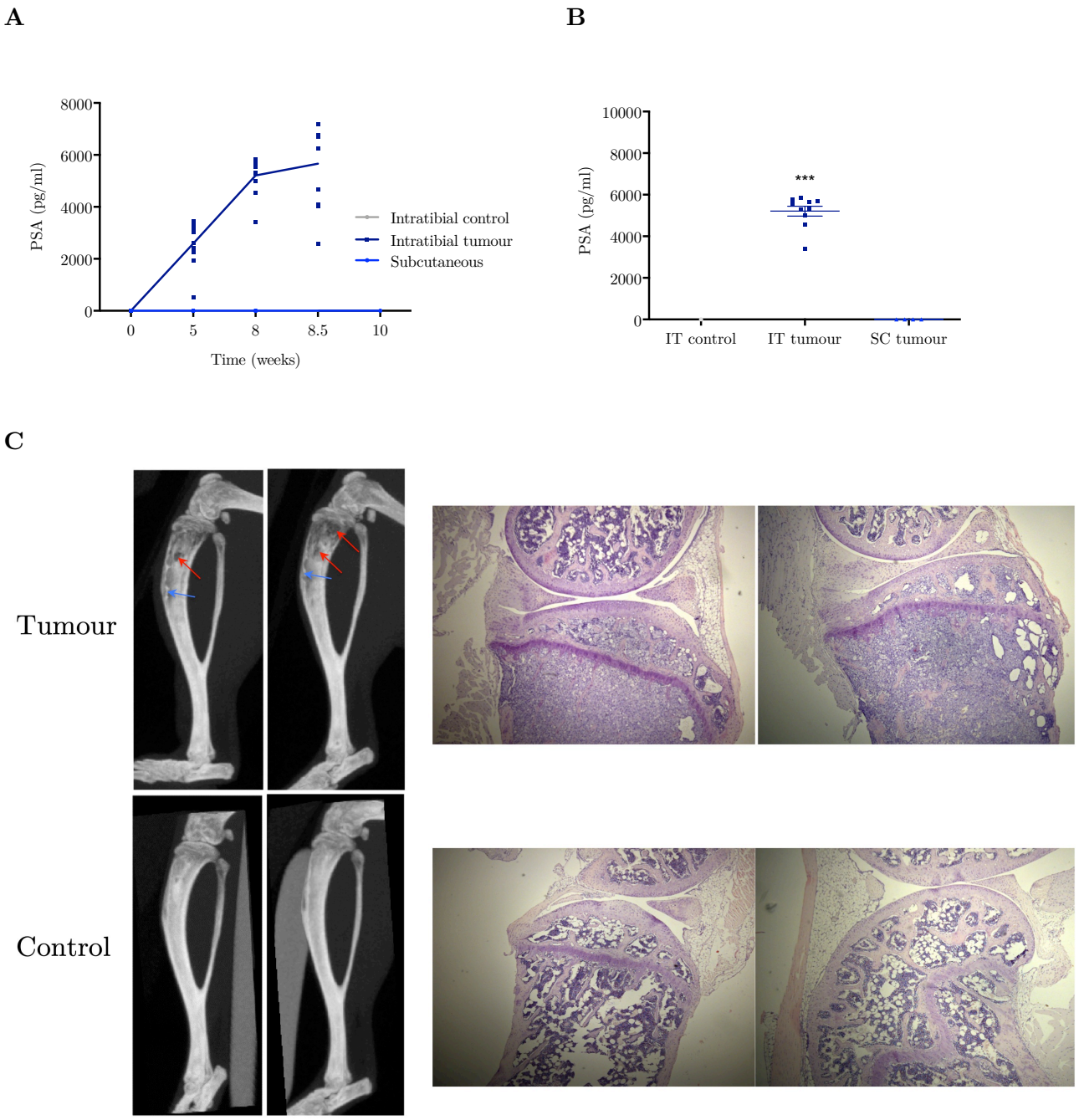
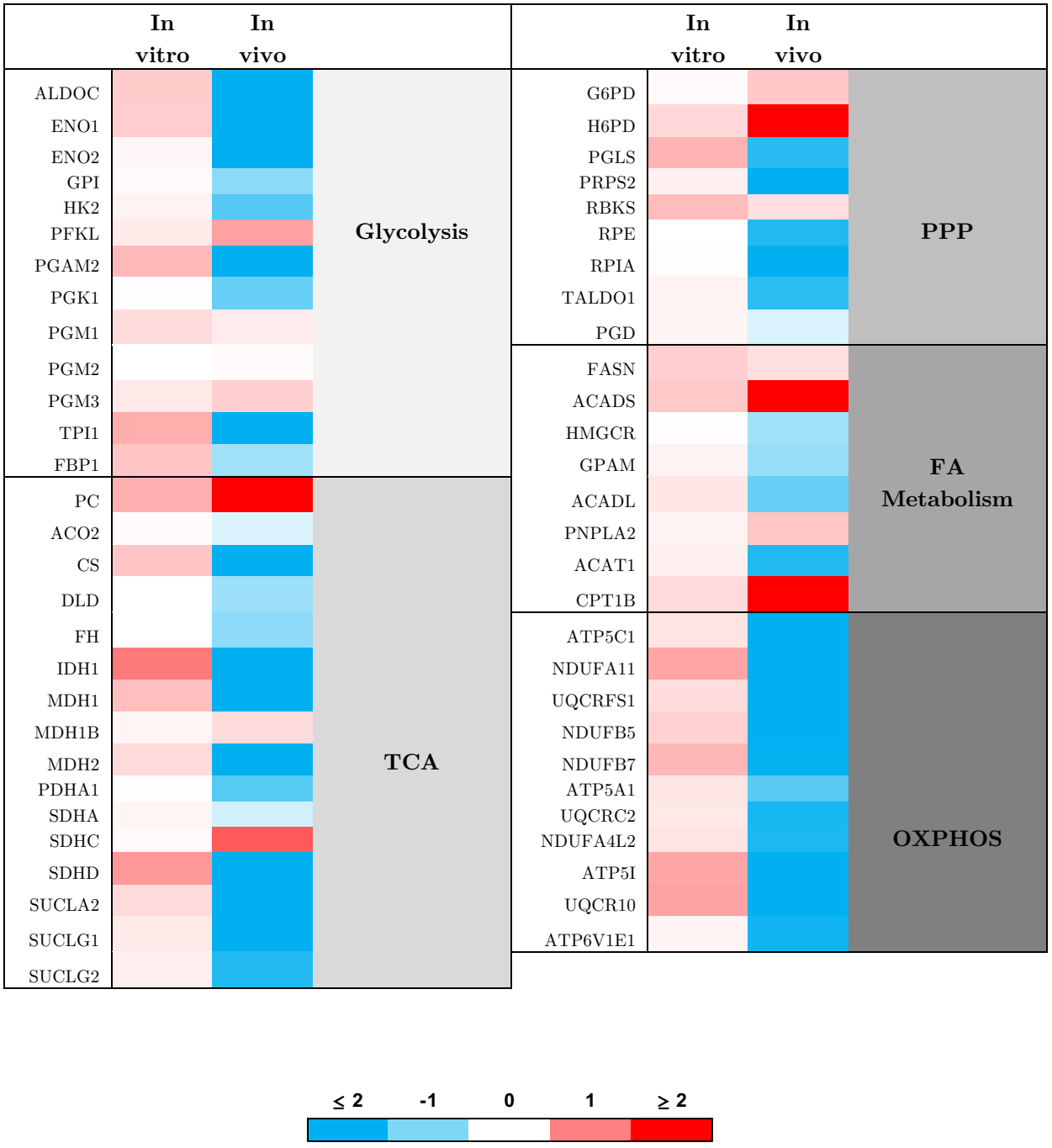


Figure 3.1 ***In vivo growth of C4-2B PCa cells.*** *(A) Serum PSA values over time. IT: intratibial; SC: subcutaneous. (B) Serum PSA values at 8 weeks. Statistical test used = one-way ANOVA with post hoc Dunnett's test. (C) Radiographs from in vivo CT of the tibias on the left. The top radiographs show evidence of bone disease (red arrows = lytic lesions, blue arrows= blastic lesions), while the bottom images show the non-tumour inoculated leg of the same animals. On the right is H&E staining of the proximal tibia. Top images show tumour within the bone, bottom images show the non-tumour inoculated tibias of the same mouse with normal bone marrow architecture.*

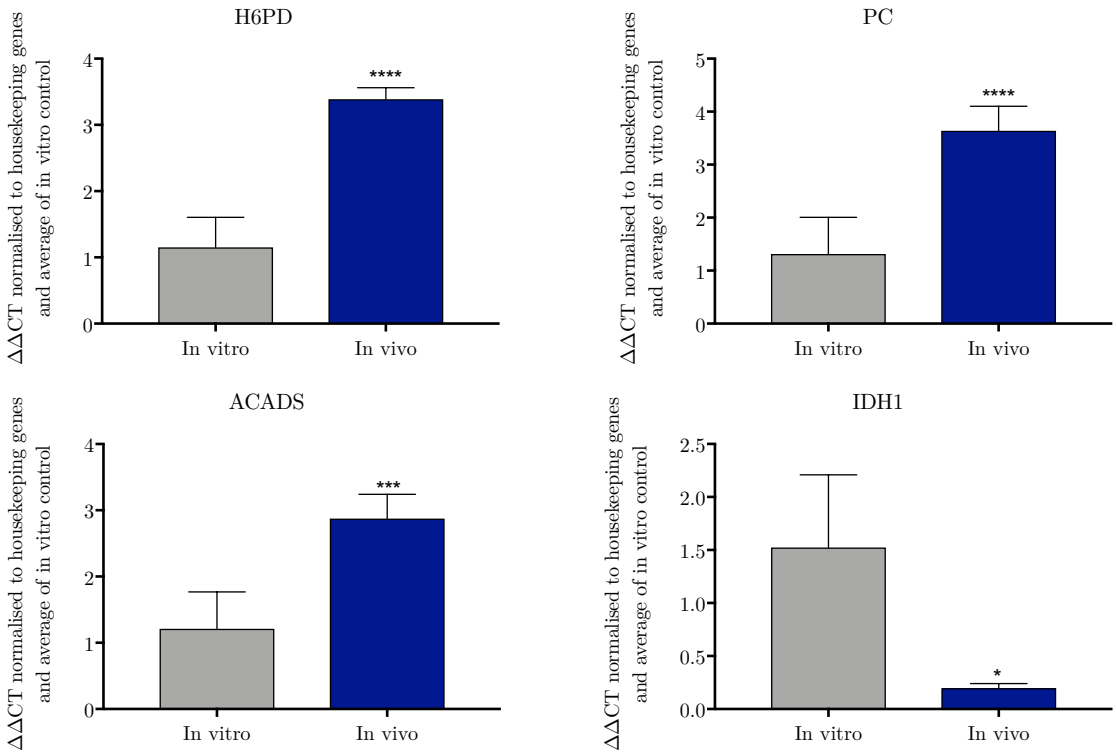
3.4 The bone microenvironment alters the expression of metabolic genes

RNA was extracted from the tumour inoculated tibias of the mice, made into cDNA, and run on a metabolism specific TLDA gene card (Table 2.5). Gene expression was compared to C4-2B cells that had been maintained *in vitro*. Of the 96 genes examine on the TLDA card, 2 genes were used as housekeeping controls (GAPDH, Polr2a), 14 were insufficiently expressed for analysis, and 23 were excluded due to amplification in the control non-tumour mouse tibia sample, suggesting the primers were not species specific. Therefore 57 genes were analysed. Multiple genes were differentially expressed in the *in vivo* bone conditioned cells compared to the cells maintained *in vitro* (Figure 3.2A), however only 4 genes were significantly altered when allowed for multiple testing (two-way ANOVA with Holm-Sidak correction for multiple comparisons), H6PD, PC, ACADS, and IDH1 (Figure 3.2B). The majority of genes were down regulated perhaps suggesting some dilution from mouse RNA. H6PD was up-regulated *in vivo* and encodes hexose-6-phosphate dehydrogenase, the autosomally linked formed of glucose-6-phosphate dehydrogenase – the rate-limiting enzyme of the PPP. PC was up-regulated and encodes pyruvate carboxylase which catalyses the conversion of pyruvate to oxaloacetate. ACADS was also up-regulated and encodes acyl-CoA dehydrogenase short chain, an enzyme that catalyses the initial step of the mitochondrial fatty acid beta-oxidation pathway. IDH1 was down-regulated and encodes isocitrate dehydrogenase 1 which catalyses the conversion of isocitrate to α-ketoglutarate in the TCA cycle with the concomitant reduction of $NADP^+$ to NADPH.

A


In vitro
In vivo
ALDOC
ENO1
ENO2
GPI
HK2
PFKL
PGAM2
PGK1
PGM1
PGM2
PGM3
TPI1
FBP1
Glycolysis
PC
ACO2
CS
DLD
FH
IDH1
MDH1
MDH1B
MDH2
PDHA1
SDHA
SDHC
SDHD
SUCLA2
SUCLG1
SUCLG2
TCA
In vitro
In vivo
G6PD
H6PD
PGLS
PRPS2
RBKS
RPE
RPIA
TALDO1
PGD
PPP
FASN
ACADS
HMGCR
GPAM
ACADL
PNPLA2
ACAT1
CPT1B
FA Metabolism
ATP5C1
NDUFA11
UQCRFS1
NDUFB5
NDUFB7
ATP5A1
UQCRC2
NDUFA4L2
ATP5I
UQCR10
ATP6V1E1
OXPHOS
≤ 2
-1
0
1
≥ 2

B



.

Figure 3.2 ***Gene expression changes in C4-2B intra-tibial tumours compared to C4-2B cells maintained in vitro.*** *(A) Heat map of TLDA gene expression analysis of RNA extracted from mouse tumour bones (in vivo) vs. C4-2B cells grown in vitro. (B) Differences in expression for the four genes that reached significance after adjustment for multiple testing. Statistical test used = two-way ANOVA with post-hoc Holm-Sidak test. * p=<0.05, *** p=<0.001, **** p=<0.0001. Error bars = SEM. In vivo group N=4, in vitro group N=3.*

3.5 Oxidative phosphorylation is increased in bone metastatic prostate cancer cells

It has been shown by others that prostate cancer becomes more energy efficient as it undergoes malignant transformation, transforming from citrate producing cells to citrate oxidising cells, leading to increased flow through the TCA cycle and increased OXPHOS[102]. However the changes that occur when prostate cancer metastasises to the bone remain unknown. To investigate whether the bone microenvironment affects the metabolic profile of prostate cell lines, the basal oxygen consumption rate (OCR) was measured as a marker of their rate of OXPHOS. Prostate cancer cell lines originating from bone metastases (PC3, MDA2a) had a higher OCR compared to a benign prostate cell line (PNT1a), however prostate cancer cell lines originating from other sites (LNCaP, 22RV1) did not (Figure 3.3A). When PC3 cells were treated with PC3-HS5 BMSC co-culture conditioned media their OCR increased significantly, suggesting factors in the PCa-BMSC co-cultured conditioned media can further drive increased OXPHOS (Figure 3.3B). To investigate whether there was a shift towards glycolysis in the BMSCs the extracellular acidification rate (ECAR) of HS5 BMSCs after treatment with PC3-HS5 CM was measured. As lactate production is the main contributor to extracellular acidification, ECAR provides a convenient measure of glycolytic flux. There was a non-significant trend towards increased ECAR when HS5 cells were treated with PC3-HS5 CM (Figure 3.3C). Metformin is an inhibitor of OXPHOS, and the C4-2B cell line was more sensitive to metformin than its

parental LNCaP cell line, or the benign PNT1a cell lines suggesting a greater reliance on OXPHOS in this modified bone metastatic cell line (Figure 3.3D).

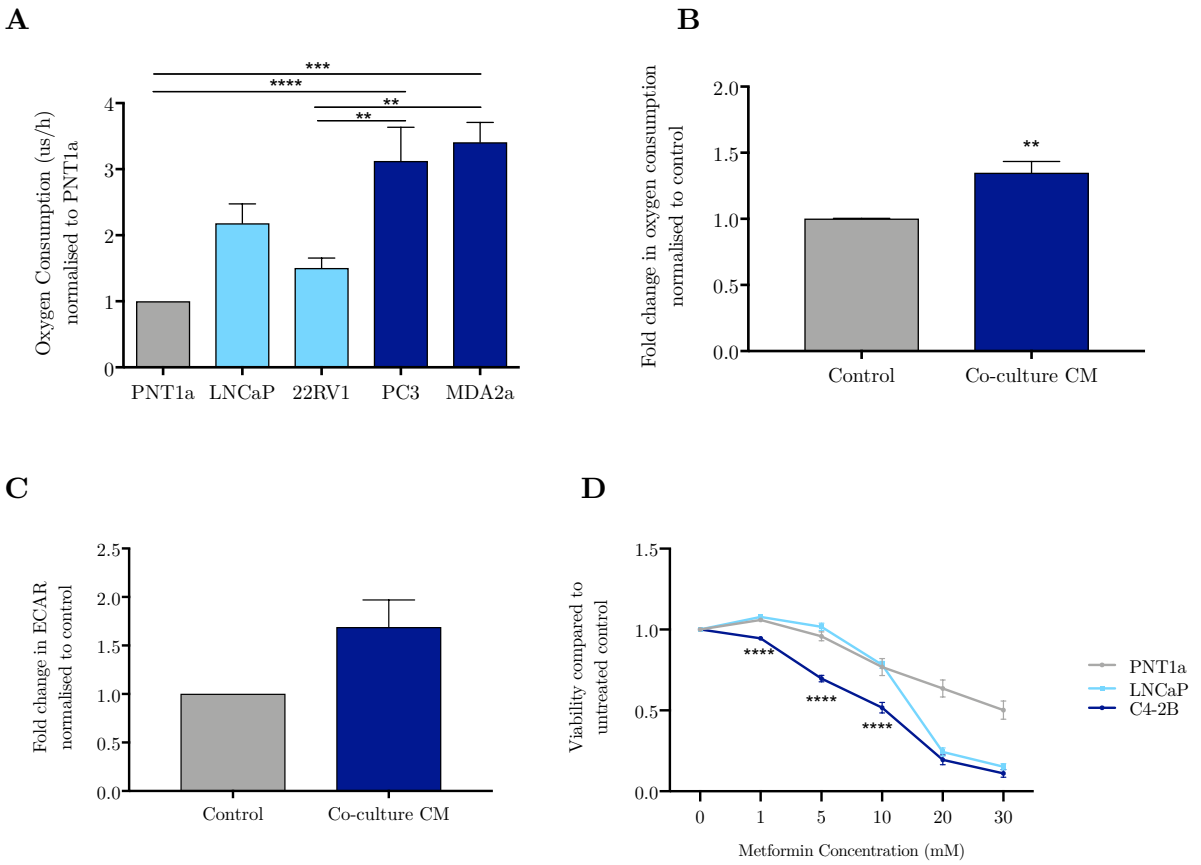


Figure 3.3 ***Metabolic profile of prostate cell lines.*** *(A) Baseline OCR measured in a benign cell line (PNT1a), non-bone metastatic cell lines (LNCaP, 22RV1) and bone metastatic cell lines (PC3, MDA2a). Statistical test used = one-way ANOVA with post-hoc Tukey's test. (B) Oxygen consumption was measured in PC3 cells after 6 hr treatment with fresh RPMI media or PC3-HS5 co-cultured conditioned media. Statistical test used = Student's t-test. (C) ECAR measured in HS5 cells after 6 hr treatment with fresh RPMI media or PC3-HS5 co-cultured conditioned media, N=2. Statistical test used – Student's t-test. (D) Viability of prostate cancer cells measured by Alamar blue after 48 hours treatment with metformin, an inhibitor of complex I of the electron transport chain, N=2 with 3 technical repeats. Statistical test used = Student's t-test. ** =p<0.01, **** = p<0.0001 analysed by student t-test comparing LNCaP to C4-2B. Error bars = SEM.*

3.6 Bone marrow stromal cells alter the metabolite profile of prostate cancer cells

To more thoroughly explore the metabolic changes induced by prostate cancer cells exposure to the bone microenvironment PC3 cells were co-cultured with human (HS5) and mouse (2T3, ST2) BMSCs for 24 hr, and then the metabolites were measured using capillary-electrophoresis time-of-flight mass spectrometry (CE-MS).

The bone microenvironment is comprised of a range of stromal cells, and therefore the effects of co-culture with three different types of BMSC were explored. HS5 cells are a human bone marrow stromal cell line that appear fibroblastoid and secrete significant levels of growth factors and cytokines including granulocyte-colony stimulating factor (G-CSF) and IL-6. They are able to support the proliferation of haematopoietic progenitor cells[162]. ST2 cells are a stromal cell line from mouse bone marrow and can function as haematopoietic supporting cells as well as being able to differentiate into osteoblast-like cells or adipocytes under the correct conditions[162]. 2T3 cells were derived from the calvaria of a transgenic mouse expressing T antigen driven by the BMP-2 promoter and are primarily specified to differentiated into mature osteoblasts[163].

CE-MS was used to analyse the metabolic changes as this technique is particularly well suited to metabolite analysis due to the charge these molecules possess, and it allows the simultaneous analysis of hundreds of metabolites from a single sample. It initially separates metabolites on the basis of their charge-to-size ratios and then on the basis of the mass-to-

charge ratios. It is thought to provide better separation efficiency than gas-chromatography (GC-MS) and liquid chromatography mass spectrometry (LC-MS)[164].

Alterations in the levels of many metabolites were identified in PC3 cells after transwell co-culture compared to single PC3 culture (Figure 3.4 - Figure 3.9). There were also differences in the metabolite alterations between the different BMSC lines suggesting different types of BMSC may have differing effects on cancer metabolism (Figure 3.4). Metabolites of the PPP were elevated in co-culture samples with an associated increased level of NADPH and decreased level of $NADP^+$, suggesting there is increased flux through the PPP (Figure 3.8). In the glycolytic pathway there was an increase in lactate, DHAP, 3PG and PEP (Figure 3.6) after co-culture. In the TCA cycles there were increases in fumarate, malate and α-ketoglutarate (Figure 3.7). Glutamine and Glutamate were decreased after co-culture with HS5 and 2T3 cells but not ST2 cells (Figure 3.9).

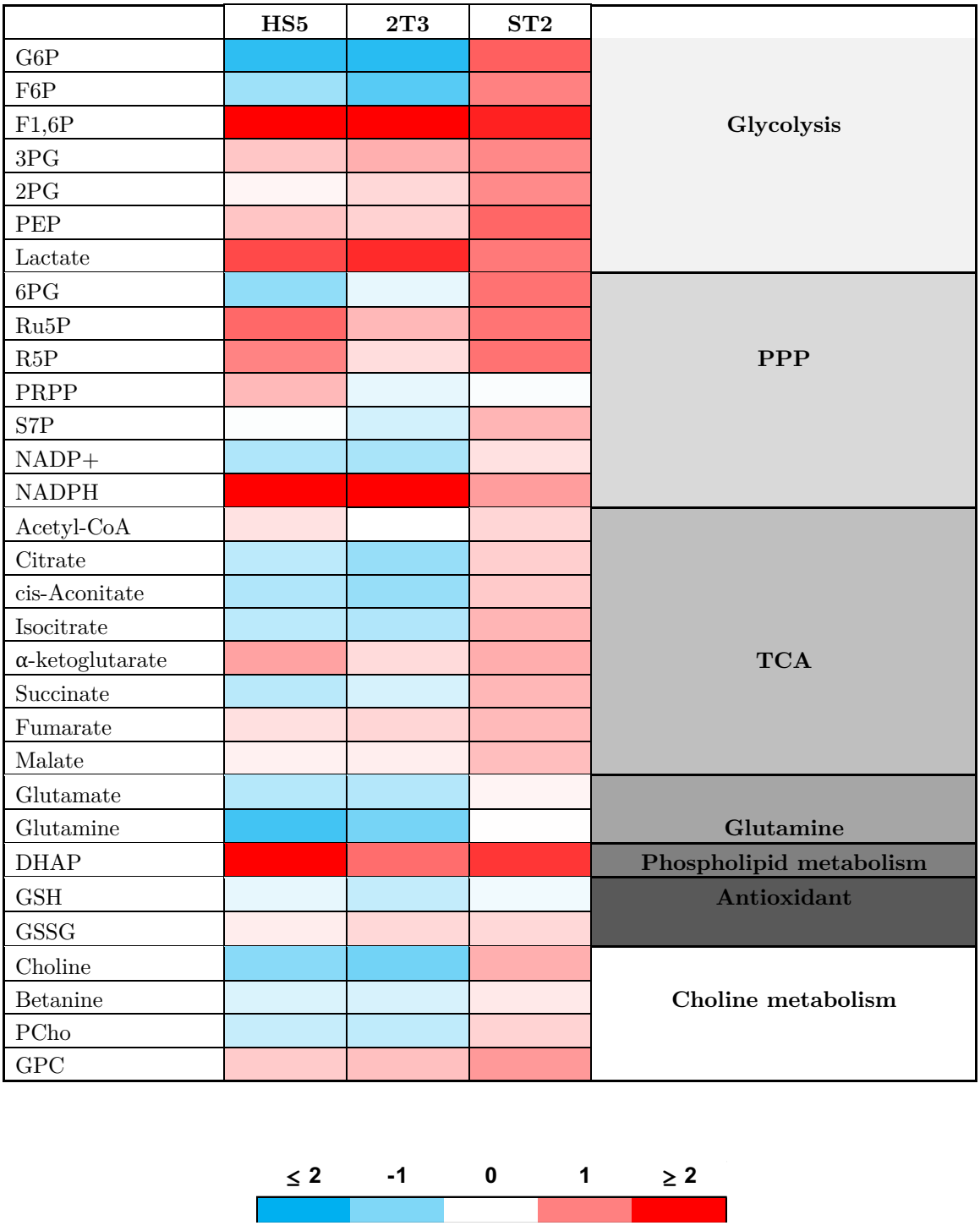


Figure 3.4 ***Heat map showing changes in intracellular metabolite levels.*** *PC3 cells were co-culture for 24 hr with HS5, ST2 or 2T3 bone stromal cells and metabolite levels measured with CE-MS. Heat map identifies metabolites with the highest fold change after co-culture.*

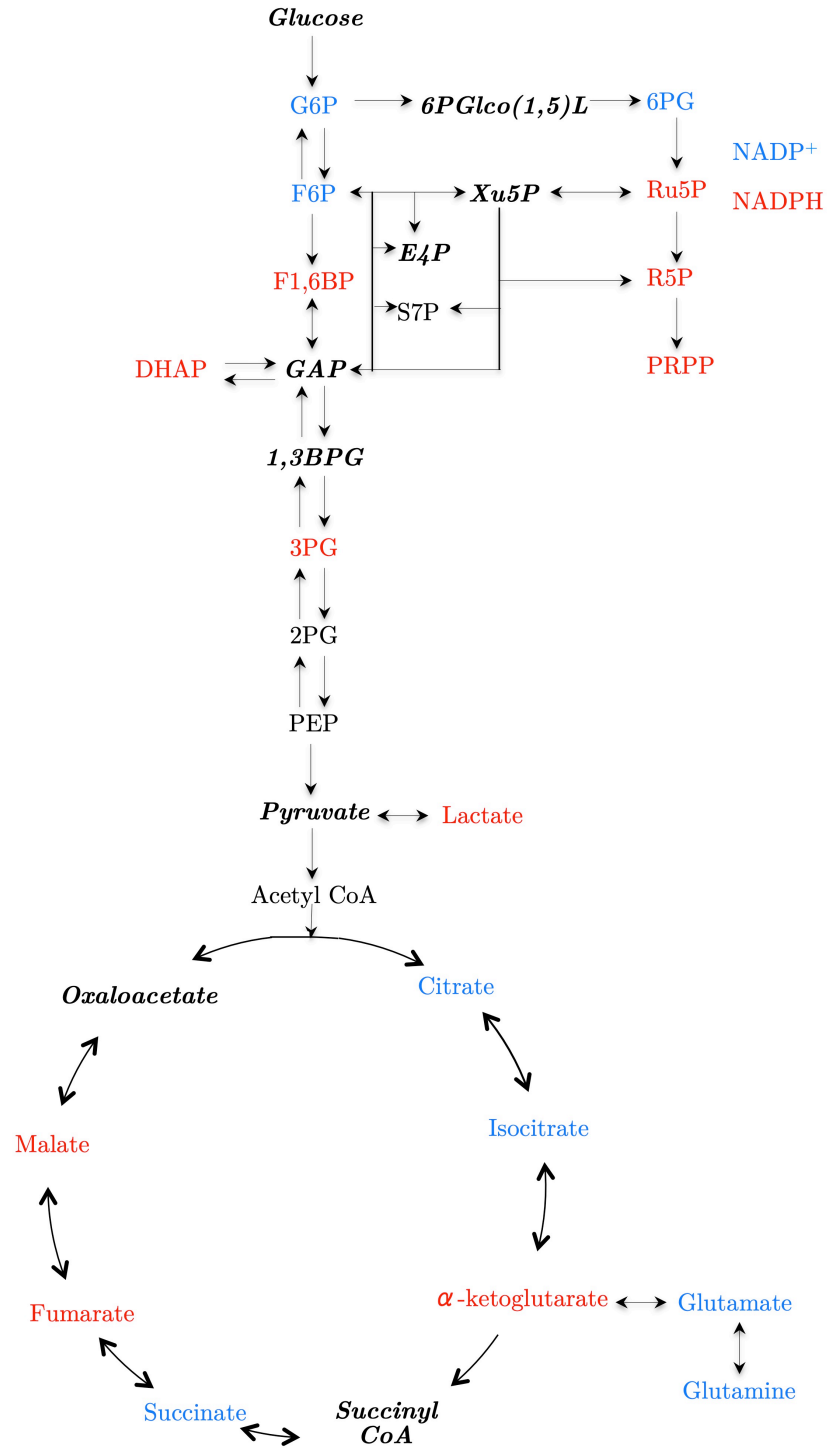


Figure 3.5 ***Pathway map demonstrating changes in intracellular metabolite levels in PC3 cells after co-culture with HS5 cells.*** *Red= significantly increased, Blue = significantly decreased, Black = not significantly changed, Italic bold black = not measured. Statistical test used – one-way ANOVA with post-hoc Dunnett's test. N=4*

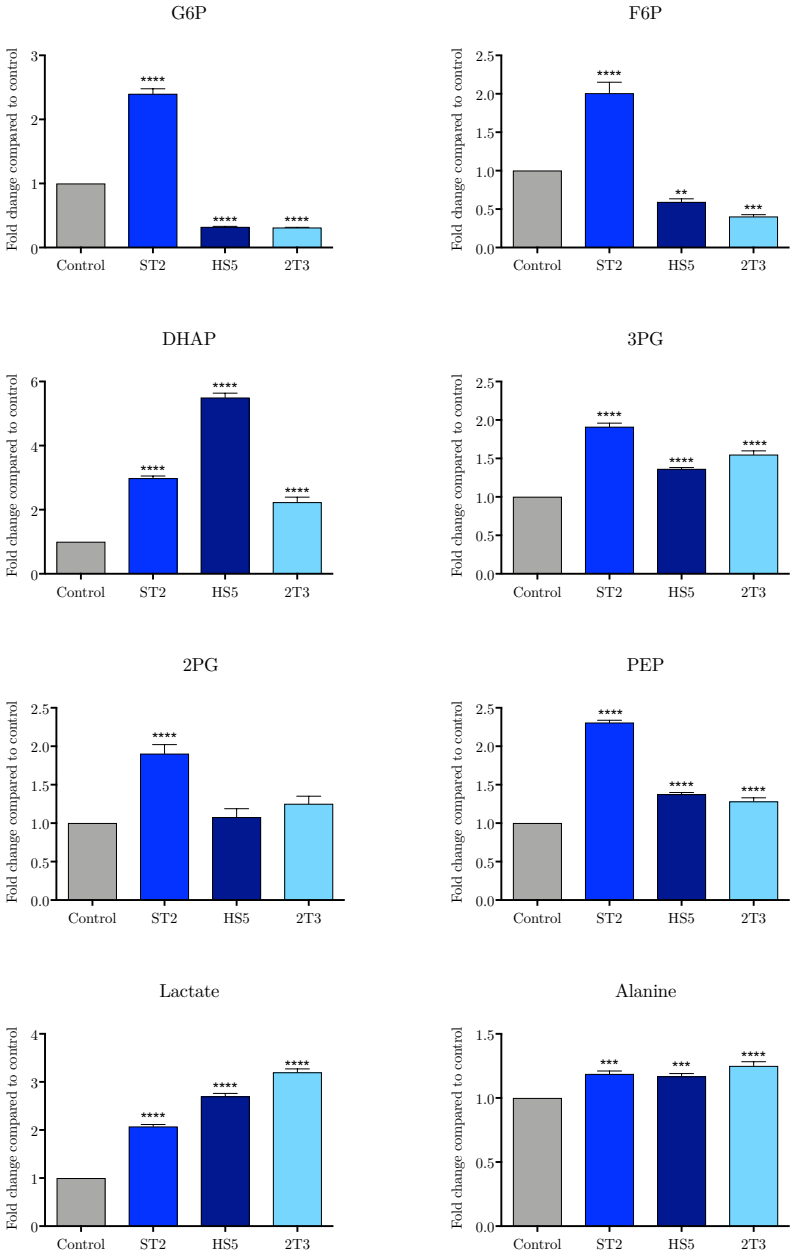


Figure 3.6 ***Changes in levels of intracellular metabolites of the glycolysis pathway*** *in PC3 cells after 24 hr co-culture with bone marrow stromal cells measured with CE-MS. Statistical test used= one-way ANOVA with post-hoc Dunnett's test. **=p<0.01, ***=p<0.001, ****=p<0.0001. N=4. Error bars = SEM.*

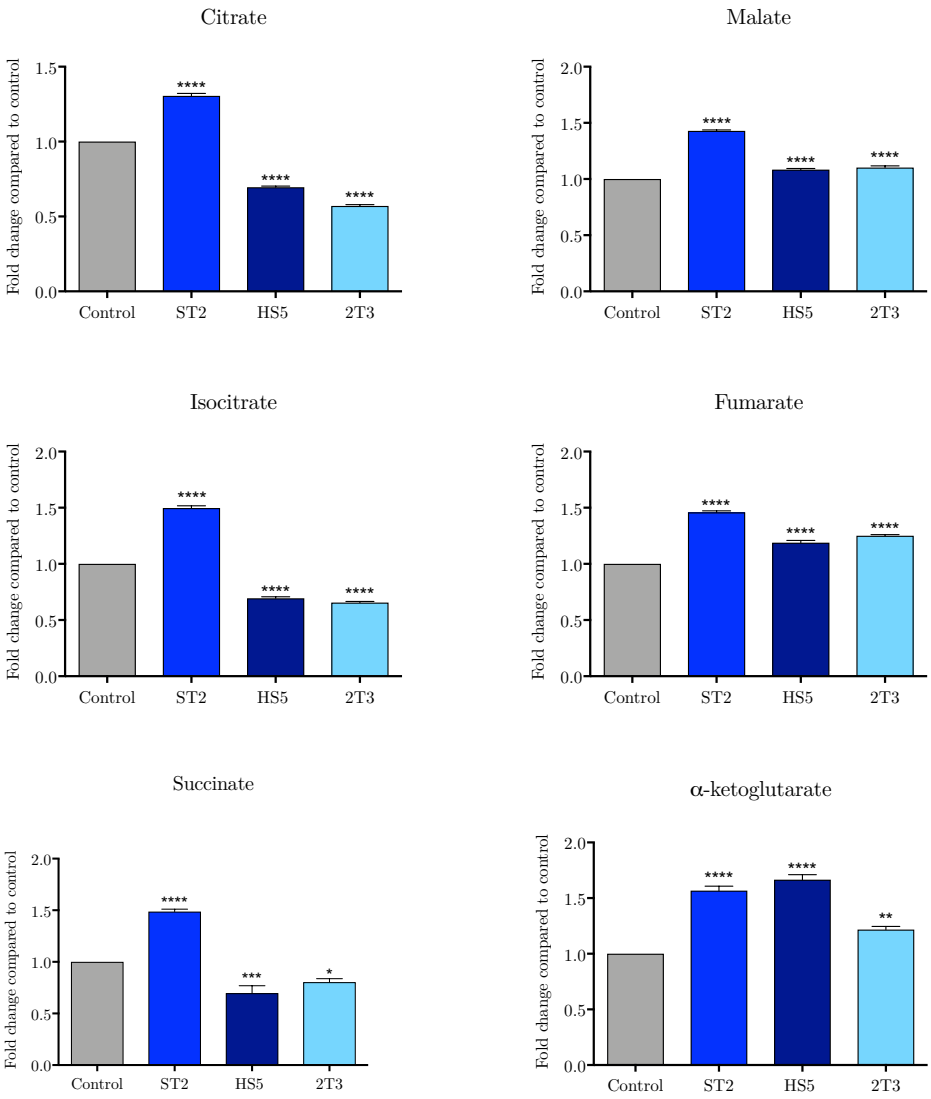


Figure 3.7 ***Changes in levels of intracellular metabolites of the TCA cycle*** *in PC3 cells after 24 hr co-culture with bone marrow stromal cells measured with CE-MS. Statistical test used= one-way ANOVA with post-hoc Dunnett's test. *=p<0.05, **=p<0.01, ***=p<0.001, ****=p<0.0001. N=4. Error bars = SEM.*

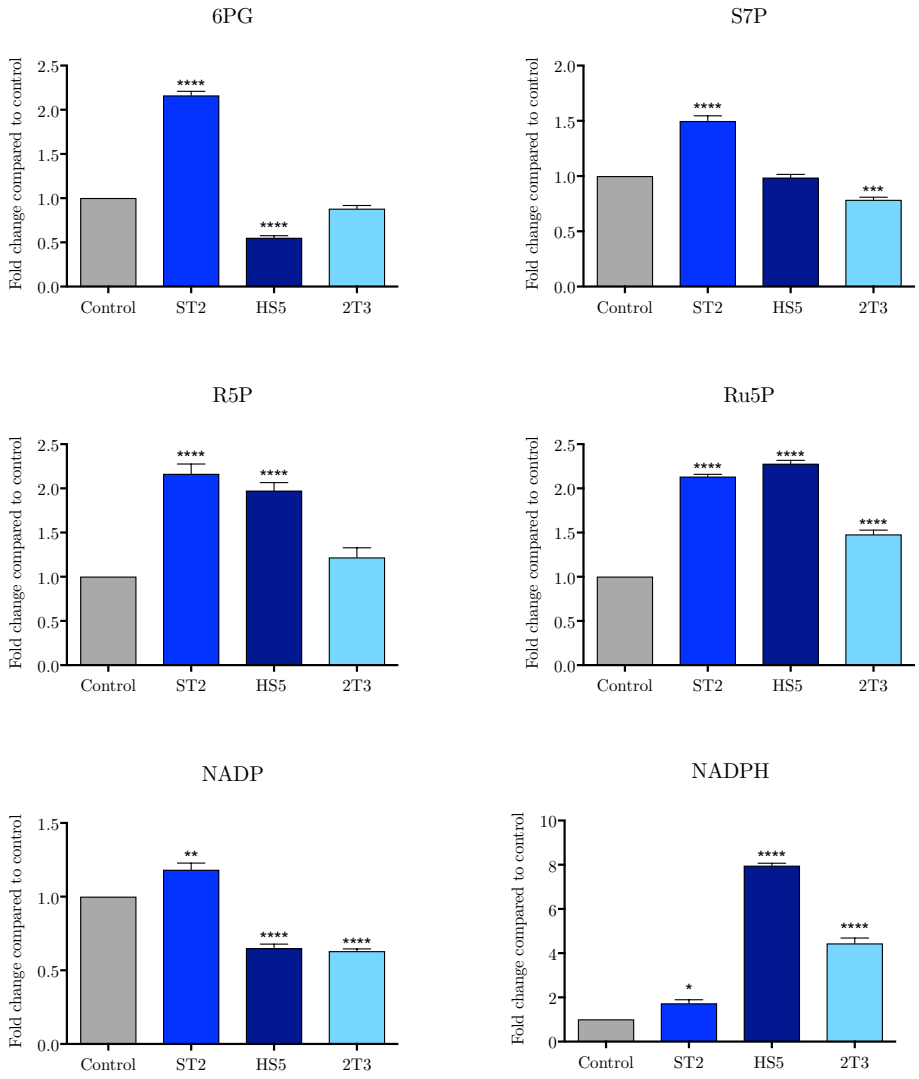


Figure 3.8 ***Changes in levels of intracellular metabolites of the PPP*** *in PC3 cells after 24 hr co-culture with bone marrow stromal cells measured with CE-MS. Statistical test used= one-way ANOVA with post-hoc Dunnett's test. *=p<0.05, **=p<0.01, ***=p<0.001, ****=p<0.0001. N=4. Error bars = SEM.*

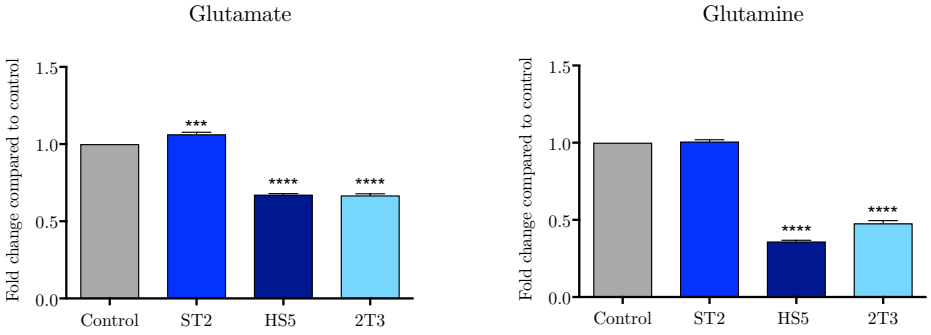


Figure 3.9 ***Changes in levels of intracellular metabolites of the glutamine pathway*** *in PC3 cells after 24 hr co-culture with bone marrow stromal cells measured with CE-MS. . Statistical test used= one-way ANOVA with post-hoc Dunnett's test. ***=p<0.001, ****=p<0.0001. N=4. Error bars = SEM.*

3.7 Metabolic pathways are significantly altered in prostate cancer cells isolated from metastases when compared to primary tumours

Whilst *in vitro* studies play an important role in defining metabolic changes, cell culture conditions have intrinsic limitations. The process of establishing cancer cell lines often selects for the fastest growing clones, negatively selecting characteristics which can be found *in vivo* cancer cell populations. Furthermore, cell culture media contains nutrients often in large excess, and in different ratios compared to that seen *in vivo*, with considerably less diversity of nutrients. Cell culture represents a useful but simplistic model within which there are limited cell types and therefore limited cellular interactions. Therefore, to determine whether the changes seen *in vitro* could also be seen in more complex patient samples an *in-silico* analysis was performed of publically available patient data sets that had analysed transcriptome data from primary tumours and metastases. This was used to explore metabolic gene pathways that might be altered in metastatic, and particularly bone metastatic, samples.

3.7.8 Hutchinson Data set (Kumar *et al.* 2016)

The Hutchinson data set consists of 176 primary or metastatic tumours from 63 men with metastatic castrate resistant PCa (mCRPC) taken at the time of rapid autopsy. The samples were used for whole-exome sequencing (n=141 tumours from 56 men), array

comparative genomic hybridization (n=149 from 60 men) and RNA transcript profiling (n=171 tumours from 63 men). RNA was extracted after laser-capture micro-dissection to confirm tumour content. The majority of tumours were confirmed adenocarcinoma on histology (n=156) while 20 tumours from two men were small-cell neuroendocrine tumours. All men were treated with ADT, and after disease progression most of them also received additional treatments, including at least one additional AR pathway-targeted agent and at least one systemic chemotherapy, most commonly docetaxel.

The transcriptome data is available publically via CBioPortal. Using GSEA analysis the expression of cancer hallmark genes in bone prostate cancer specimens was compared to primary prostate tumour specimens. It was found that metabolic pathway changes were among the most significantly altered cancer hallmark pathways along with ROS pathways (Table 3.1). Using a separate metabolism specific gene set, OXPHOS and the TCA cycle were the top two up-regulated metabolic gene sets in metastatic samples compared to primary tumours. The PPP was the sixth most up-regulated gene set, although this did not quite reach significance. There were also significant increases in ROS detoxification and glutathione metabolism genes (Table 3.2). When comparing expression of the genes making up the OXPHOS, TCA and PPP pathways in bone, prostate, lung and liver sites, changes in these pathways were much more prominent in bone metastases compared to other metastatic sites (Figure 3.10A-C). 57 genes were identified as being part of the TCA cycle of which 14/57 were significantly altered in bone metastases vs. primary tumours, while 2/57 were altered in liver and 1/57 in lung metastases. 81 genes were identified as being part of the electron transport chain of which 30/81 were significantly altered in bone metastases vs.

primary tumours, while 2/81 were altered in liver and 12/81 in lung metastases. 19 genes were identified as being part of the PPP of which 7/19 were significantly altered in bone metastases vs. primary tumours, while 0/19 were altered in liver or lung metastases. This suggests that many of these metabolic alterations are specific to the bone microenvironment.

NAME	SIZE	ES	NES	NOM p-val	FDR q-val	FWER p-val
OXIDATIVE PHOSPHORYLATION	197	0.516605	1.733235	0.010101	0.24645	0.102
ADIPOGENESIS	190	0.443361	1.530368	0.015595	0.71235	0.433
REACTIVE OXYGEN SPECIES PATHWAY	47	0.439149	1.430938	0.079208	0.91229	0.62
PI3K AKT MTOR SIGNALING	103	0.3368	1.39786	0.023576	0.82045	0.68
FATTY ACID METABOLISM	154	0.416375	1.32879	0.125984	0.94601	0.787

Table 3.1 ***In silico gene set enrichment analysis of metabolic changes in metastatic sites compared to primary tumours from the Hutchinson Data Set using GSEA cancer hallmark gene set****. The top 5 gene sets up-regulated in prostate bone cancer samples compared to primary prostate tumours are listed. All were significant with a nominal p value <0.05 and FDR q-value <0.25.*

NAME	SIZE	ES	NES	NOM p-val	FDR q-val	FWER p-val
OXIDATIVE PHOSPHORYLATION	81	0.615495	2.52739	0.0000000	0.00000	0
CITRIC ACID CYCLE	57	0.499756	1.93230	0.0000000	0.0088	0.014
GLUTATHIONE METABOLISM	23	0.562726	1.75203	0.0039841	0.04051	0.095
NUCLEOTIDE METABOLISM	26	0.520331	1.6768	0.0000000	0.06657	0.2
ROS DETOXIFICATION	31	0.478784	1.60680	0.0176471	0.09449	0.316
FATTY ACID BIOSYNTHESIS	22	0.507265	1.56125	0.0224033	0.11138	0.422
PENTOSE PHOSPHATE PATHWAY	19	0.463112	1.40880	0.0804598	0.26454	0.781

Table 3.2 ***In silico gene set enrichment analysis of metabolic changes in metastatic sites compared to primary tumours from the Hutchinson Data Set using a metabolic specific gene set****. The top 7 up-regulated genes in prostate bone cancer samples compared to primary prostate tumours are listed. The top 6 were significant with a nominal p value <0.05 and FDR q-value <0.25.*

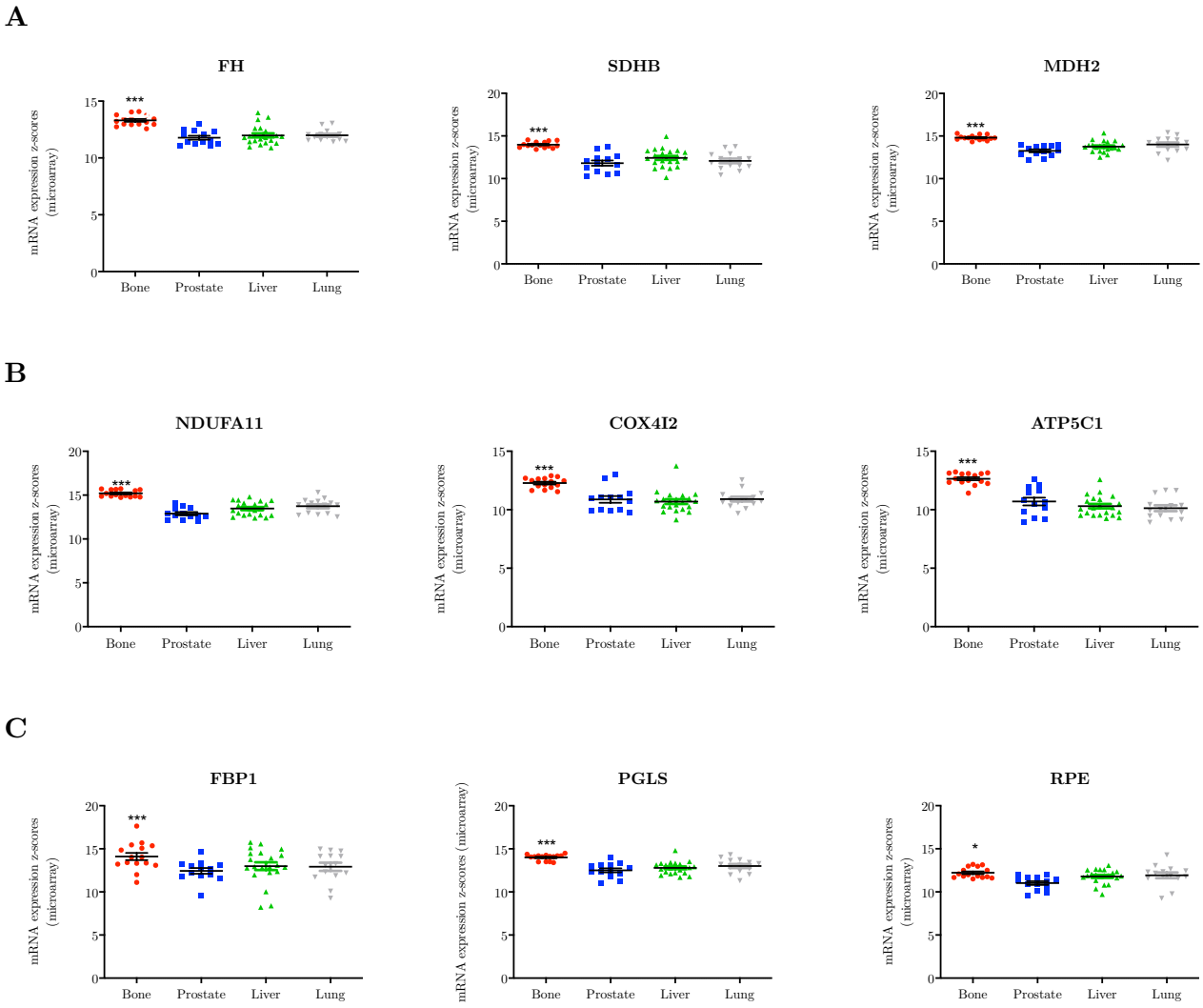


Figure 3.10 ***In-silico analysis of metabolic changes in the different metastatic sites compared to primary prostate tumours from the Hutchinson Data Set.*** *(A) Changes in 3 of the genes of the TCA cycle. FH=fumarate hydratase, SDHB=succinate dehydrogenase B, MDH2=malate dehydrogenase 2. (B) Changes in 3 of the genes involved in OXPHOS. NDUFA11= NADH:Ubiquinone Oxidoreductase subunit A11, COX4I2=cytochrome c oxidase subunit 4 isoform 2, ATP5C1=ATP synthase F1 subunit gamma. (C) Changes in 3 of the genes involved in the PPP. FBP1= fructose-bisphosphatase 1, PGLS= 6-phosphogluconolactonase, RPE= ribulose-5-phosphate-3-epimerase. Statistical test used = one-way ANOVA with post-hoc Tukey's test. *=p<0.05, ***=p<0.001. Error bars= SEM.*

3.7.9 MSKCC 2010 Data set (Taylor *et al.* 2010)

The MSKCC data set contains 181 primary and 37 metastatic tumour samples from patients treated with radical prostatectomy. Patients were followed up with clinical history, physical examination and serum PSA testing every 3 months for the first year, 6 months for the second year, and annually thereafter. Biochemical recurrence (BCR) was defined as PSA ≥0.2 ng/ml on 2 occasions. DNA and RNA was extracted from tissue collecting during surgery containing >70% tumour content based on histological examination. This was run on an Affymetrix human exon 1.0 ST array. The transcriptome data is available publically via Geo Datasets (NCBI; GSE21032).

When primary vs. metastatic tumours were analysed through GSEA using a metabolism specific gene set for pathways up-regulated in metastatic samples no pathways reached significance, however the PPP was the second most up-regulated, and OXPHOS the eighth (Table 3.3).

NAME	SIZE	ES	NES	NOM p-val	FDR q-val	FWER p-val
FOLATE METABOLISM	17	0.49103	1.48176	0.077253	0.440122	0.531
PENTOSE PHOSPHATE PATHWAY	19	0.39816	1.04909	0.436853	1	0.982
TRIACYLGLYCEROL SYNTHESIS	24	0.34133	1.02521	0.422833	1	0.99
PURINE METABOLISM	28	0.29541	1.01203	0.415948	0.92737	0.99
PORPHYRIN AND HEME METABOLISM	20	0.37469	0.99513	0.448276	0.776911	0.99
KERATAN SULFATE BIOSYNTHESIS	21	0.30023	0.91454	0.550388	0.812173	0.997
TRANSPORT, LYSOSOMAL	24	0.31311	0.85806	0.612245	0.808892	1
OXIDATIVE PHOSPHORYLATION	81	0.32302	0.82056	0.629482	0.769475	1

Table 3.3 ***In-Silico analysis of metabolic changes in metastatic sites compared to primary tumours from the MSKCC Data Set.*** *Gene set enrichment analysis using a metabolism specific gene set. The top 8 gene sets up-regulated in prostate cancer metastatic samples compared to primary prostate tumours are listed. No pathways reached significance defined as a nominal p value <0.05 and FDR q-value <0.25.*

3.8 Expression of pentose phosphate pathway enzymes, is increased in bone metastatic prostate cancer cells

Having identified that the bone microenvironment can induce changes in the PPP via CE-MS and via *in-silico* analysis this effect was investigated further *in vitro*. It was found that the enzymes of the PPP are more highly expressed in prostate cancer cell lines originating from bone metastases compared to prostate cancer cell lines originating from other sites. These differences can be seen at the protein (Figure 3.11A) and mRNA level (Figure 3.11B). In contrast, expression of TCA enzymes was increased in all prostate cancer cell lines compared to a benign prostate cell line (Figure 3.11C). Expression of OXPHOS enzymes appears higher in non-bone metastatic cell lines compared to bone metastatic cells lines (Figure 3.11D).

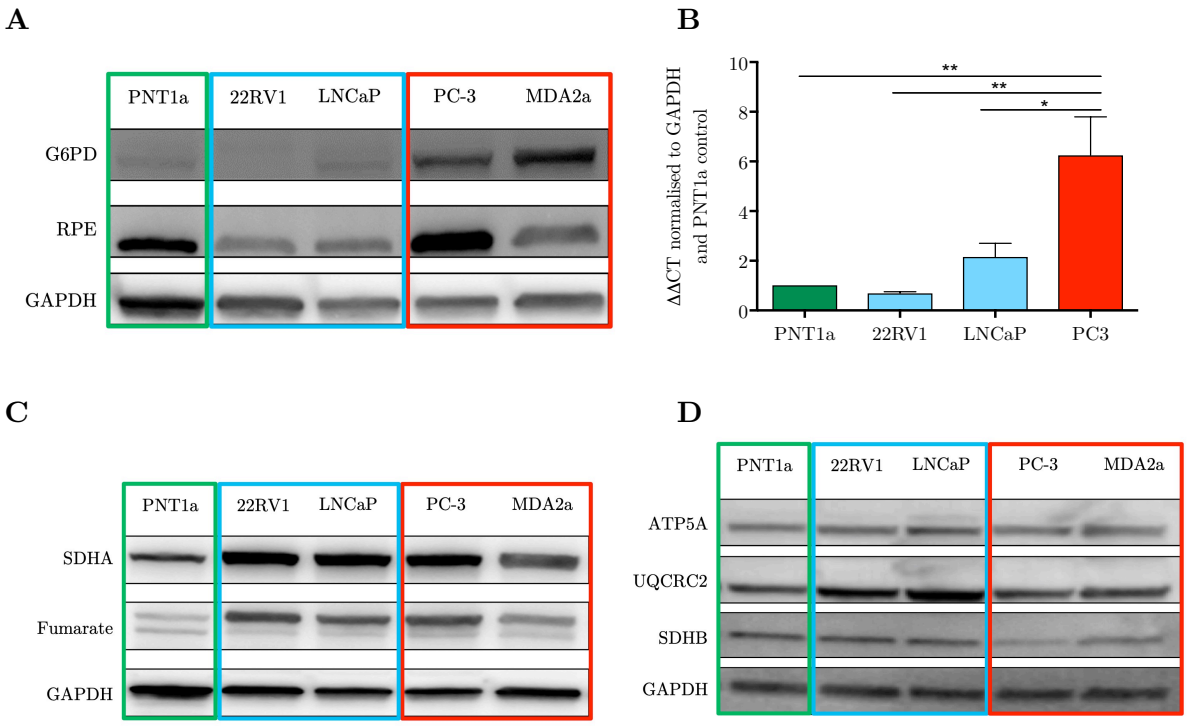


Figure 3.11 ***Baseline expression of metabolic proteins in a range of prostate cancer cell lines.*** *(A) Protein expression of PPP enzymes from benign (PNT1a), non-bone metastatic (22RV1, LNCaP) and bone metastatic prostate cancer cells lines (PC3, MDA2a). (B) mRNA expression of G6PD in different prostate cell lines. Statistical test used = one-way ANOVA with post-hoc Tukey's test. *=p<0.05, **=p<0.01. Error bars=SEM. (C) Protein expression of TCA enzymes. SDHA: succinate dehydrogenase complex flavoprotein subunit A. (D) Protein expression of OXPHOS complexes. ATP5A: ATP synthase F1 subunit alpha; UQCRC2: ubiquinol-cytochrome C reductase core protein 2; SDHB: succinate dehydrogenase B. Blots representative of 3 biological repeats.*

3.9 Discussion

The analyses performed in this chapter provide evidence that the bone microenvironment, and in particular BMSCs, can alter the metabolism of prostate cancer cells. To elucidate the effects of the bone microenvironment on PCa an *in vivo* model was utilised, inoculating C4-2B PCa cells intra-tibially and subcutaneously. C4-2B cells were unable to form tumours subcutaneously, but were able to proliferate intra-tibially, suggesting the bone creates a supportive environment for prostate cancer growth and proliferation. When the changes in metabolic genes were examined in these intra-tibial tumours, and compared to C4-2B cells grown *in vitro*, there were changes in the expression of multiple genes, but only 4 genes were found to be significantly altered when allowed for multiple testing – H6PD from the PPP, PC from the gluconeogenesis pathway, ACADS from the fatty acid beta-oxidation pathway, and IDH1 from the TCA cycle. However, this experiment was limited by the lack of growth of the subcutaneous tumours. This meant *in vitro* cultured C4-2B cells were used as the control for gene expression changes. It is not unexpected that there are differences between cancer cells grown *in vitro* and *in vivo*, and how much of this can be attributed specifically to the bone microenvironment is unclear. It is also important to note that the mouse has a metabolic rate 7-8 fold greater than humans, so xenografted cells will have greater competition for energy metabolites from mouse stromal cells than they would from human stromal cells, also potentially limiting their translation to the human disease[165].

Using *in vitro* cell line models changes in OXPHOS rates in PCa cells were investigated. Bone metastatic PCa cell lines had a higher OCR compared a benign cell line, whilst non-

bone metastatic PCa cell lines OCR was not significantly different. This is in contrast to the study by Higgins *et al.* which found that LNCaP cells have higher oxygen consumption compared to DU145 and PC3 PCa cells[166]. However they measured respiration in cell suspensions using Clarke-type electrodes fitted into water-jacketed vessels, and they maintained cells in high glucose DMEM media, both of which may attribute to the differences between the results. However, the results are in keeping with the more recent results of Pertega-Gomes *et al.* who also found PC3 cells have higher OCR compared to LNCaP when measured using Seahorse technology, an assay similar in design to the assay used in this study[167]. However it is important to note that these assays measure oxygen consumption as a proxy measure of OXPHOS, and do not account for oxygen that might be consumed to fuel other metabolic processes within the cell such as the beta-oxidation of fatty acids.

Treating PCa cells with PCa-BMSC co-cultured CM caused a significant increase in their OCR, suggesting the bone microenvironment might further drive a shift towards OXPHOS in PCa cells. The increase in oxygen consumption in PCa cells was accompanied by a trend towards increased glycolysis, measured by ECAR, in the BMSCs. This supports the work by Fiaschi *et al.* demonstrating that a reciprocal relationship develops between PCa cells and CAFs. They found that exposure of fibroblasts isolated from men with BPH (HPFs) to PCa-CM elicited a clear increase in their lactate secretion. The shift towards Warburg metabolism in the fibroblasts was characterised by increased expression of the GLUT1 glucose transporter and enhanced glucose uptake[87].

Significant differences in the sensitivity to metformin, an inhibitor of complex I of the ETC, was identified between C4-2B cells and its related parental cell line LNCaP, supporting the idea that PCa cells may become more dependent on OXPHOS as they become more bone metastatic. Previous studies on this have been conflicting, with some reporting PC3 bone metastatic cells are more sensitive to metformin than the non-bone metastatic LNCaP cell line[168], whilst others report they are less sensitive[169]. It is also clear cell culture conditions, and in particular glucose concentrations in the media, can have considerable impact on PCa sensitivity to metabolic inhibitors.

To enable a greater overview of the metabolic changes induced by BMSCs on PCa cells CE-MS was utilised to measure multiple metabolite pathways simultaneously. Co-culture of PC3 cells with distinct BMSC lines induced different metabolic changes, suggesting distinct stromal cell types may induce different metabolic pathway changes. This is not unexpected, as these stromal cells represent different bone cell populations and so are likely to behave in different manners. However, there were some changes that were consistent across the different stromal cells. Metabolites of the PPP were consistently elevated, with a significant increase in NADPH and decrease in $NADP^+$, supporting a role for increased PPP flux during co-culture. In the glycolysis pathway increases in lactate, DHAP, 3PG and PEP were identified, while in the TCA cycle there were increases in fumarate, malate and α-ketoglutarate. Glutamate and glutamine were consistently down in co-culture samples compared to single culture. While CE-MS is able to give a snap shot of metabolite levels at a particular moment, it does not provide information on metabolic flux. When levels of a metabolite are altered it is not possible to accurately say whether the changes are induced

by increased metabolite utilisation, or decreased metabolite production. To my knowledge this is the first study of metabolic changes in cancer cells co-cultured with stromal cells. A previous study of patient samples from normal and prostate cancer tissue found high lactate, but very little difference in glycolytic intermediates in PCa samples. Levels of TCA intermediates were higher in tumour than normal prostate tissue[170]. However, this study did not look at metastatic samples, only comparing tumour to non-tumour.

To explore whether these *in vitro* changes are relevant in human samples multiple *in silico* analyses of patient PCa samples were performed. The Hutchinson 2016 data set confirmed metabolic pathways were among the most altered of all the cancer hallmark pathways in metastases compared to primary tumours. OXPHOS was the most up-regulated cancer hallmark gene set in metastases compared to primary tumours. This is in keeping with the up-regulation of oxygen consumption seen *in vitro* when PCa cells were co-cultured with HS5 BMSC. Analysing changes in metabolism specific pathways in the Hutchinson 2016 data set identified up-regulation of OXPHOS, the TCA cycle, glutathione metabolism, nucleotide metabolism, ROS detoxification and fatty acid biosynthesis, with the PPP being the 6th most up-regulated gene set, but not quite reaching significance. These results are supportive of the CE-MS data where it was found co-culture with BMSCs induced increases in NADPH and ribose sugars, which are important in glutathione metabolism, nucleotide metabolism and ROS detoxification, as well as being metabolites of the PPP.

Further *in silico* analysis of the MSKCC 2010 dataset confirmed changes in the PPP and OXPHOS could be seen in metastatic prostate cancer samples compared to primary tumours, although these pathways didn't reach significance, perhaps because these samples

were not laser capture micro-dissected and therefore may be contaminated with non-tumour tissue.

Having found that patient sample data supported many of the *in vitro* findings of this study more *in vitro* work was performed to further characterise the metabolic changes. PPP enzymes were found to be more highly expressed in bone metastatic PCa cell lines compared to benign or non-bone metastatic cell lines, providing further support for a role of the PPP in PCa bone metastases. Whilst expression of PPP enzymes in relation to metastatic site has not been previously examined, others have shown that G6PD, the rate-limiting enzyme of this pathway, is more highly expressed in more advanced / aggressive tumours[111,112].

Expression of TCA and OXPHOS enzymes were increased in PCa cell lines compared to a benign cell line. This would be in keeping with these pathways having a role in the early development of malignancy, and is in keeping with increased reliance on these pathway in the transformation to malignancy demonstrated by others[102,170].

The analyses performed in this chapter have shown that bone microenvironment can drive alterations in the metabolism of prostate cancer cells, with up-regulation of OXPHOS, the TCA cycle and PPP. From this data the PPP was identified as a potential novel target for further investigation.

3.10 Future Direction

Using an *in vivo* C4-2B intra-tibial model I was able to explore some of the genes that were changed after PCa cells grew in the complex bone microenvironment of a mouse. However, many metabolic changes can occur without measurable differences in gene expression and therefore repeating this experiment, and extracting the tibias for CE-MS analysis would provide a valuable insight into the metabolite alterations. Combining this with stable isotope labelled substrates would allow the tracing of carbon, nitrogen and hydrogen atoms through metabolic pathways and would be invaluable for investigating dynamic metabolic changes occurring during prostate cancer metastases[171]. In order to optimise growth of subcutaneous tumours as a control for metabolic changes subcutaneous tumours could be inoculated together with matrigel, as has been performed by others[161], however whether this would artificially affect the metabolism of subcutaneous tumours is unclear.

Whilst obtaining fresh tissue from bone metastases and matched primary tumours in prostate cancer patients is difficult, performing CE-MS on such samples would provide a valuable insight into the metabolic changes that occur in patients. As imaging techniques improve it may be possible to better elucidate these changes in a less invasive manner, visualising metabolic changes rather than requiring tissue extraction[172,173]. Magnetic resonance spectroscopic imaging (MRSI) allows multiple metabolites to be spatially resolved in a single imaging protocol, however with current clinical systems usually only a limited number of metabolites are present at concentrations that allow useful spatial mapping, limiting the ability of this technique to metabolically characterise tumours. Currently in

PCa citrate, creatine, polyamine, and Cho-group resonances are detectable. Another currently used form of metabolic imaging is PET, commonly associated with a CT scan to combine metabolic and anatomical information. FDG is the most common tracer, but has not been useful in PCa due to its limited glucose consumption. However Cho radiotracers (11C-Cho and 18F-fluorocholine) and 11C-acetate have been used in PCa for diagnosis and staging[172]. More recently hyperpolarised ^{13}C MRI has been shown to enable the study of the metabolic and catabolic pathways in mammalian cells, and this technology is still in its infancy and so improvements are to be expected[173]. These novel imaging techniques are likely to provide a more accurate picture of metastatic metabolism as the tissues are live and perfused, and the information can be collected over time to monitor changes over the course of metastatic disease and treatment.

Many of the techniques to study metabolic changes are relatively novel, and this remains very much an emerging field. Therefore there is still a considerable amount of work to do, in particularly with regards to metastatic metabolism and the role of the bone microenvironment.

4

The bone microenvironment promotes up-regulation of G6PD

4.1 Introduction

The pentose phosphate pathway, and in particular its rate limiting enzyme, glucose-6-phosphate dehydrogenase (G6PD) has previously been shown to be up-regulated in several cancers including colorectal, prostate, breast, gastric, lung, oesophageal, renal cell carcinoma and acute myeloid leukaemia. High expression of G6PD predicts poor prognosis and correlates with poor outcomes to chemotherapy and radiotherapy[103,104,107,108,174]. In prostate

cancer G6PD has been shown to be correlated with Gleason grade[112], but its expression in metastatic cancers has not been previously investigated.

The PPP pathway plays an important role in the synthesis of nucleotide precursors and in the generation of NADPH, a reducing equivalent vital in cellular detoxification. In other cancers, suppressing G6PD can decrease NADPH production, lower GSH levels and impair cancer cells ability to scavenge ROS. Targeting G6PD has been shown to enhance cell death caused by both chemotherapy[114,115] and radiotherapy[116,117]. In view of this, it is not surprising that changes in PPP activity occur during cancer development and progression.

The results of the previous chapter suggested that the PPP is up-regulated in prostate cancer bone metastases. This chapter will examine whether BMSCs are involved in causing this up-regulation.

4.2 Aims

The specific aims of the work described in this chapter were:

1) To establish whether BMSCs play a role in driving G6PD up-regulation.

2) To explore the mechanisms by which BMSCs might be driving alterations in the PPP.

4.3 G6PD is up-regulated in prostate cancer isolated from the bone of patients with bone metastases

To determine the relationship between G6PD expression, tumour metastatic status and patient outcomes further *in silico* analysis of the MSKCC[153] data set was performed, along with analyses of two other PCa patient data sets, the Michigan 2005 and Michigan 2012 data sets.

Analysis of the MSKCC 2010 data set found that G6PD was significantly up-regulated in metastatic and specifically bone metastatic prostate cancer samples compared to primary tumours (Figure 4.1A). The MSKCC 2010 data set has a 5-year median clinical follow-up allowing us to assess the effect of G6PD expression on prognosis. Expression of G6PD in complete samples was stratified into high expression (>1 SD from mean) and low expression (<1 SD from mean) to establish if expression level correlated with time to biochemical recurrence (BCR), defined as PSA $\geq$ 0.2 ng/ml on two occasions. High G6PD gene expression was not found to be significantly associated with shorter time to BCR in a univariate analysis (p=0.0878) (Figure 4.1B), although the number of events in both groups was low (4/11 in high; 10/37 in low). Multivariate analysis of this data showed no significant correlation between BCR and high/low G6PD expression (HR 3.24, CI 0.92-11.43, p=0.067), or high/low pathological stage ($\geq$T3 = high) (HR 0.46, CI 0.15-1.43, p=0.182).

There was a correlation between BCR and high/low Gleason grade (≥ 7 = high) (HR 0.26, CI 0.08-0.88, p=0.03).

The Michigan 2005 dataset[154] is made up of 13 individual and 6 pooled samples from benign, primary and metastatic prostate cancer tissue. Transcriptome alterations were analysed using the Affymetrix human genome U133 Plus 2.0 Array platform. The raw data is publicly available via GEO (NCBI; GSE3325). In this dataset G6PD gene expression was significantly up-regulated in metastatic samples compared to both benign, and localised prostate cancer samples (Figure 4.1C).

The Michigan 2012 data set[155] is made up of matched benign (n=28), treatment-naive high grade localised (n=59) and heavily pre-treated metastatic castrate resistant (n=35) patient samples taken at rapid autopsy. Transcriptome alterations were analysed using the Agilent 014850 whole genome microarray platform. The raw data was accessed via Geo (NCBI; GSE35988). G6PD gene expression was significantly up-regulated as prostate cancer progressed from treatment naive to castrate resistant, suggesting G6PD may be up-regulated in response to prostate cancer treatments (Figure 4.1D).

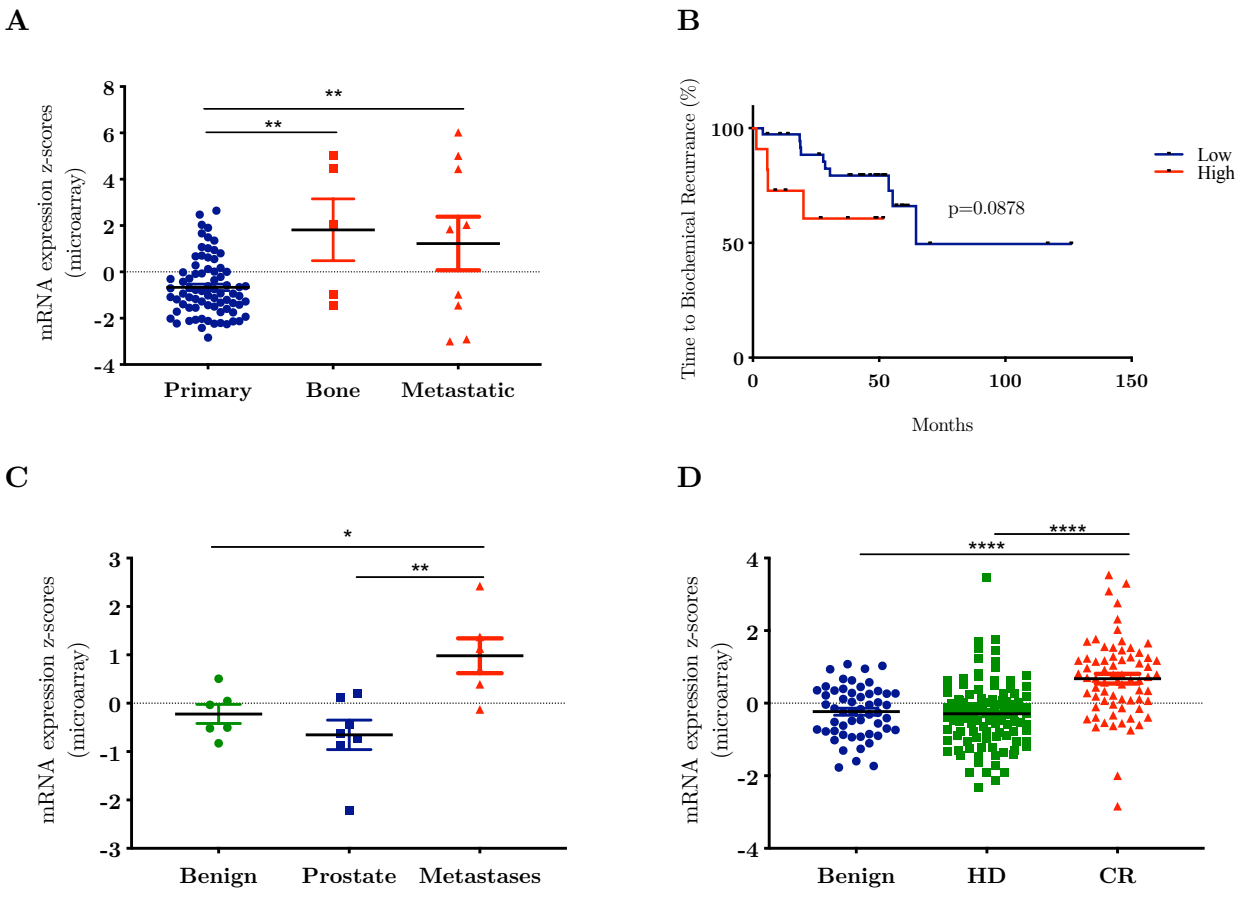
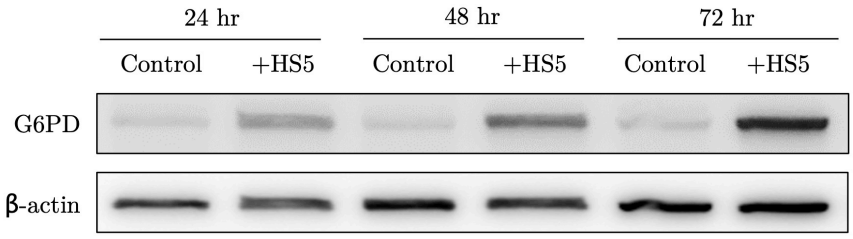


Figure 4.1 ***In Silico analysis of G6PD expression in publicly available advanced PCa patient sample data sets.*** *(A) mRNA expression z-scores of G6PD in patient samples from the MSKCC data set. Statistical test used= one-way ANOVA with Tukey's post-hoc test. (B) Survival curve of G6PD showing no significant correlation between high G6PD expression and progression free survival analysed by Log-rank (Mantel-Cox) test. (C) mRNA expression z-scores of G6PD in patient samples from Michigan 2005 data set. Statistical test used =one-way ANOVA with Tukey's post-hoc test. (D) mRNA expression z-scores of G6PD in patient samples from Michigan 2012 data set. HD = hormone dependent, CR = castrate resistant. Statistical test used= one-way ANOVA with Tukey's post-hoc test. *=p<0.05, **=p<0.01, ***=p<0.001, ****=p<0.0001. Error bars = SEM.*

4.4 Expression of G6PD can be induced in non-bone metastatic cell lines by co-culture with BMSCs

To investigate whether the bone microenvironment could be driving the up-regulation of G6PD seen in bone metastatic patient sample, a localised hormone sensitive prostate cancer cell line, LNCaP, with low baseline G6PD expression (Figure 3.7A) was cultured with HS5 BMSCs in transwell co-culture over a time course. HS5 cells were able to induce a time dependent increase in G6PD protein (Figure 4.2A) and an increase in G6PD mRNA (Figure 4.2B), indicating BMSCs can drive this up-regulation.

A



B

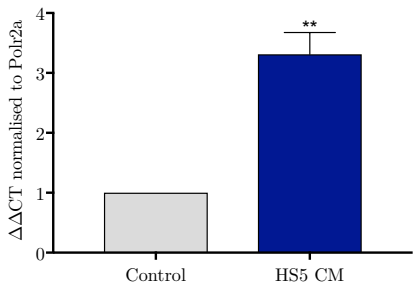


Figure 4.2 ***G6PD expression is induced by BMSCs.*** *(A) Protein expression of G6PD in LNCaP cells after transwell co-culture with HS5 BMSCs for 24, 48 or 72 hr. Blot representative of 3 biological repeats. (B) mRNA expression of G6PD in LNCaP cells after transwell co-culture with HS5 cells for 72 hr. Statistical test used = Student's t-test. *=p<0.01. Error bar=SEM.*

4.5 Expression of TCA and OXPHOS enzymes is not affected by bone stromal cells

It was investigated whether bone stromal cells can also affect the expression of OXPHOS and TCA enzymes over a time course. There was no significant difference in the expression of these proteins after co-culture of LNCaP cells with BMSCs (Figure 4.3) suggesting that these bone stromal cells do not directly drive changes in expression of these metabolic pathway proteins.

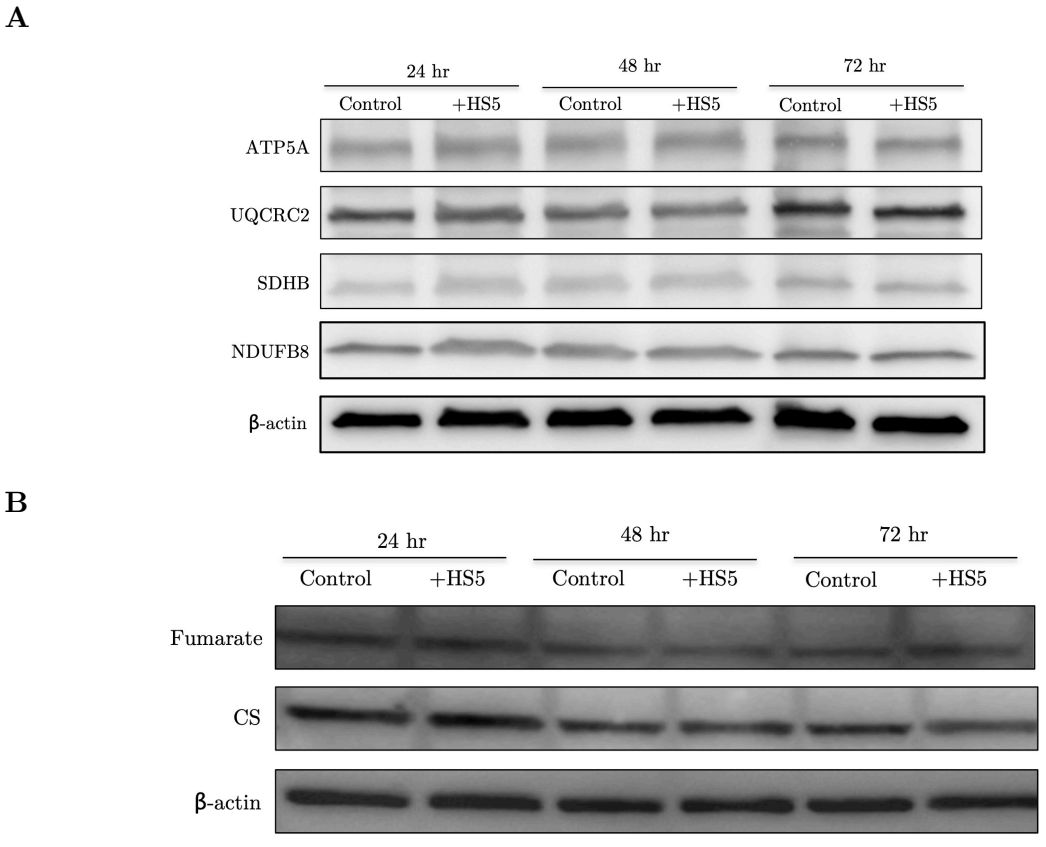


Figure 4.3 ***Expression of OXPHOS and TCA proteins after co-culture with HS5 BMSCs.*** *(A) Protein expression of OXPHOS complexes in LNCaP after transwell co-culture with HS5 cells for the specified time points. (B) Protein expression of TCA enzymes (CS= citrate synthase; βA = beta-actin) in LNCaP after transwell co-culture with HS5 cells for the specified time point. Blots representative of 3 biological repeats.*

4.6 The increase in G6PD expression is not dependent on extracellular glucose or oxygen levels

The conditions used in tissue cell culture are not necessarily representative of the conditions seen in patients. In particular the glucose concentration of standard RPMI (~11mM) is considered to be at pre-diabetic levels, while standard DMEM contains ~25mM glucose, considered to be at untreated diabetic levels[175]. The PPP is an offshoot of glycolysis, and therefore the high glucose levels in media could conceivably affects cancer cells in a way that might not be relevant in normoglycaemic patients. In view of this, LNCaP and C4-2B cells were treated with RPMI with no glucose in single culture or transwell co-culture with HS5 cells, and the levels of G6PD protein examined. Culturing these cells in no glucose conditions did not affect the up-regulation of G6PD seen with BMSC co-culture (Figure 4.4) suggesting that the effect is not dependent on the high glucose levels experienced in RPMI media. Therefore standard RPMI was used for all further experiments.

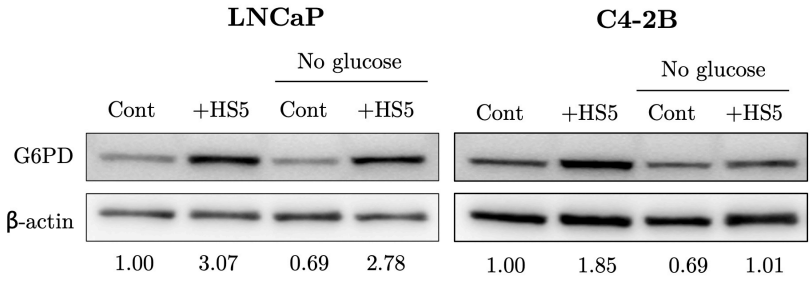


Figure 4.4 ***Glucose levels do not affect G6PD up-regulation.*** *Western blot showing G6PD protein expression in LNCaP and C4-2B cells after 72 hr single or co-culture with HS5 BMSC in normal or glucose free RPMI. Blot representative of 3 biological repeats. Densitometry quantification of G6PD band normalised to β-actin and control shown below blot.*

Despite being a highly vascularised tissue, the bone is a hypoxic environment. Oxygen tension in most normal tissues falls between 2-9% (14-65 mm Hg); however, it is widely accepted that in the bone oxygen levels range from < 1% - 6% (~7 mmHg – 43 mmHg)[176]. Many metabolic reactions require oxygen, and so in view of this it was investigated whether hypoxia would affect the up-regulation of G6PD seen. Whilst hypoxia did reduce the overall protein expression of G6PD, it did not inhibit the up-regulation seen with BMSC co-culture (Figure 4.5), suggesting that the effect could occur in the hypoxic bone microenvironment. In view of this all further experiments were done in normoxia.

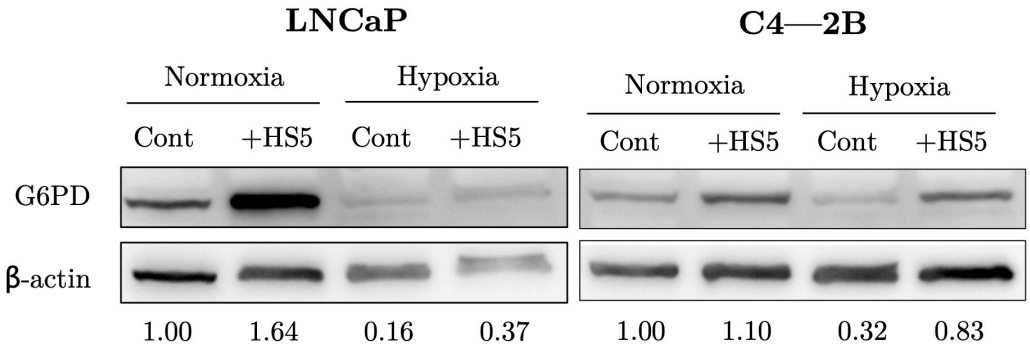


Figure 4.5 ***Hypoxic conditions lower G6PD expression but do not affect G6PD up-regulation.*** *Western blot analysis of G6PD protein expression in LNCaP and C4-2B cells after 72 hr single or co-culture with HS5 BMSCs in normoxic or hypoxic conditions. Blot representative of 3 biological repeats. Densitometry quantification of G6PD band normalised to β-actin and control shown below blot.*

4.7 The increase in G6PD expression is enhanced in androgen deprived conditions

Patients with advanced bone metastatic prostate cancer are typically treated with anti-androgen therapy. The role of androgens and AR signalling has been well characterised in metastatic prostate cancer and therefore it was important to establish if androgen manipulation had any effect on the expression of G6PD. The LNCaP prostate cancer cell line expresses the AR and hence has functional androgen signalling. Androgens are present in the FBS that is added to regular growth media. Therefore to investigate the effect of androgen deprivation, charcoal stripped FBS, which is free of androgens, was added to regular RPMI in place of FBS. Cells were purged of androgens for 72 hr in charcoal stripped FBS media before experiments were performed. PSA expression is dependent on the AR and therefore this was used as a readout of successful androgen depletion. The increase in G6PD with HS5 CM was greater in androgen deprived conditions (Figure 4.6), suggesting androgen deprivation may further drive this up-regulation, which would be highly significant in patients, and would be in keeping with the up-regulation seen in heavily treated patient samples (Michigan 2012 data set; Figure 4.1D).

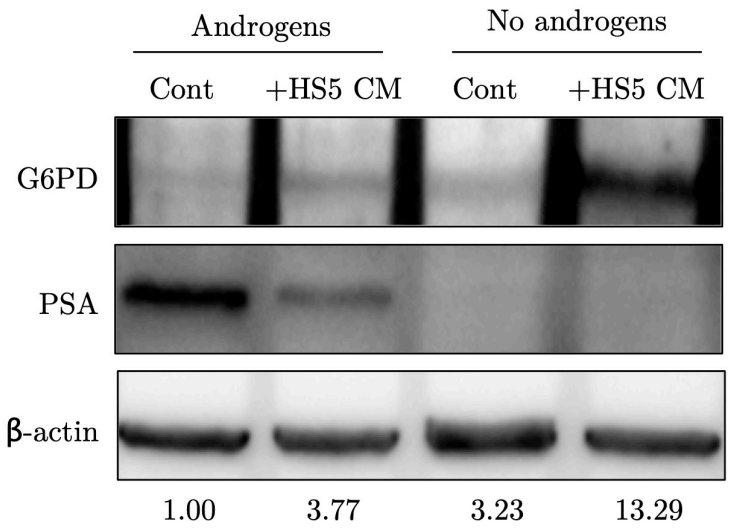


Figure 4.6 ***G6PD up-regulation is enhanced in androgen-deprived conditions.*** *Western blot showing G6PD and PSA protein expression in LNCaP cells after 72 hr treatment with androgen-free media +/- 50% HS5 androgen-free CM. Blot representative of 3 biological repeats. Densitometry quantification of G6PD band normalised to β-actin and control shown below blot.*

4.8 The increase in G6PD is via a factor secreted by BMSCs

To investigate whether the increase in G6PD expression was reliant on communication between prostate cancer and BMSCs, LNCaP cells were treated with 50% self (LNCaP CM) conditioned media, conditioned media from 72 hr transwell co-culture (Co-culture CM), and 50% conditioned media from HS5 BMSCs single culture (HS5 CM). Single culture HS5 CM was able to induce the same increase in G6PD protein levels as that seen with co-culture CM (Figure 4.7A). This suggests that communication between the PCa cells and the BMSCs is not necessary for the induction of G6PD expression, and that it is a factor secreted by HS5 BMSCs that is responsible for the effect. This was confirmed in a dose response to HS5 CM, with G6PD increased in a dose-dependent manner at both the protein (Figure 4.7B) and mRNA level (Figure 4.7C). However, whilst the effect can be seen in a non-bone metastatic cell lines with low basal G6PD expression (LNCaP), there is no significant effect in a bone metastatic cell line (PC3) (Figure 4.7C). This may be because PC3 cells have higher basal G6PD expression, at a level comparable to LNCaP cells after co-culture (Figure 4.7D; Figure 4.2B).

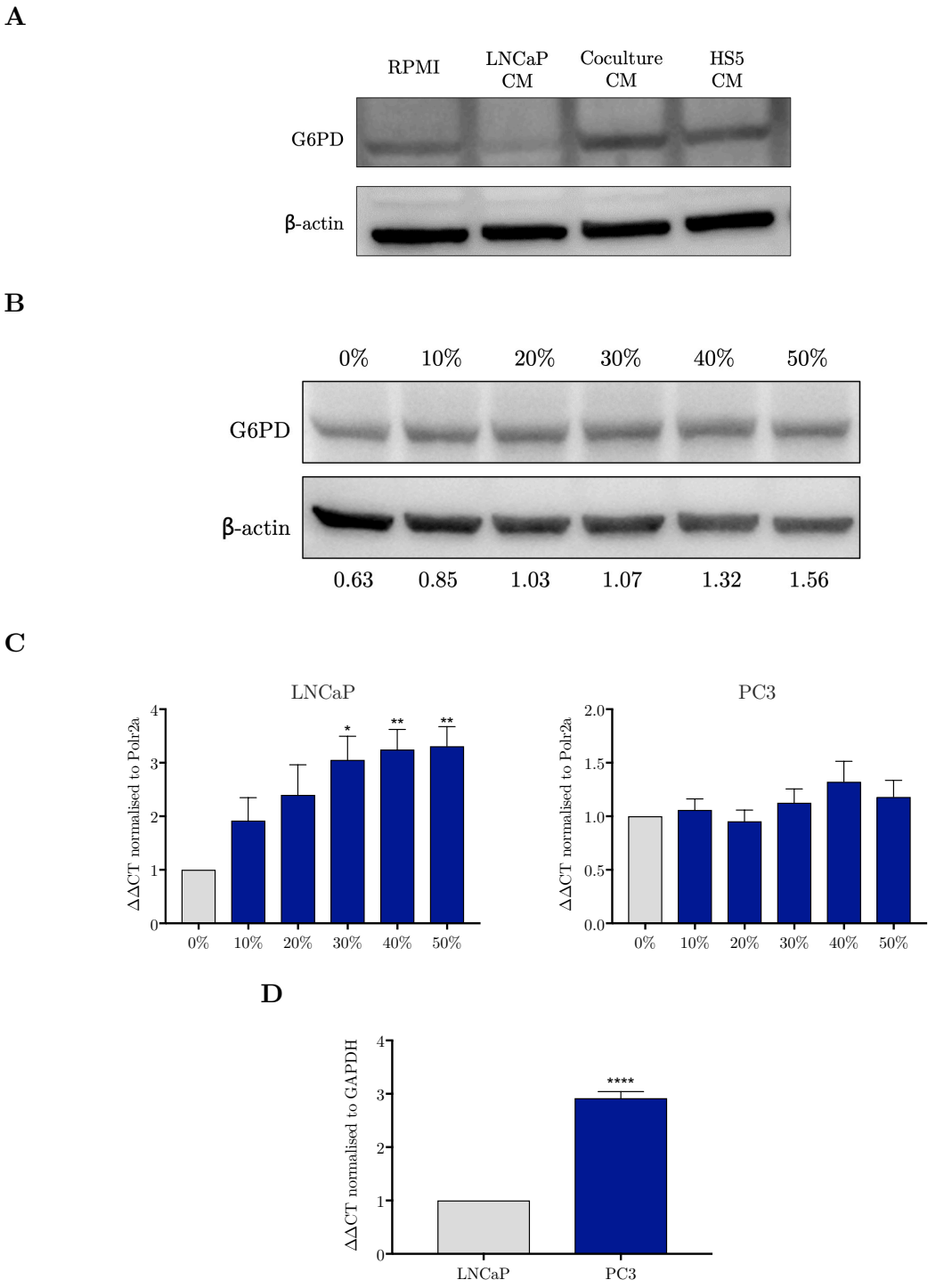


Figure 4.7 ***HS5 BMSCs CM promote expression of G6PD.*** *(A) Effect of RPMI, 50% LNCaP CM, 50% Co-culture CM or 50% HS5 CM on the protein expression of G6PD in LNCaP cells after 72 hr treatment. (B) Increasing dose of HS5 CM causes a dose related increase in G6PD protein expression in C4-2B cells at 72 hr. Densitometry quantification of G6PD band normalised to β-actin shown below blot. Blots representative of 3 biological repeats. (C) LNCaP and PC3 cells treated with an increasing dose of HS5 CM for 72 hr and G6PD mRNA levels examined by qPCR. Statistical test used= one-way ANOVA with post-hoc Dunnett's test. (D) qPCR of G6PD expression in LNCaP and PC3 cells. *=p<0.05, **=p<0.01, ****=p<0.0001. Error bars = SEM.*

4.9 The increase in G6PD expression induced by BMSCs is specific to HS5 BMSCs

Having found the HS5 cells are able to induce up-regulation of G6PD via a secreted factor, it was investigated whether other BMSCs can stimulate the same effect. HS5 cells are long term BMSCs taken from a 30 year old Caucasian male transformed with the amphotropic retrovirus vector LXSN16E6E7. Twenty-seven immortalized clones designated HS1 to HS27A were isolated. HS5 cells appear to be fibroblastoid and secrete significant levels of growth factors and cytokines. Another clone isolated is the HS27A cell line; they resemble "blanket" cells, with an epithelioid morphology, and are much larger, broader, and flatter when compared with HS5. They secrete low levels of growth factors and do not support proliferation of isolated progenitor cells in co-cultures. MS-5 cells are a murine stromal cell lines established by irradiation of the adherent cells in long-term bone marrow cultures derived from C3H/HeNSlc strain mice. They have the capacity to support the growth of haemopoietic stem cells.

The increase in G6PD protein and mRNA expression induced by BMSCs was found to be specific to HS5 BMSCs, and could not be reproduced by the related stromal cell line HS27A or the mouse stromal cell lines MS5, ST2 or 2T3 (Figure 4.8A-C). This suggests it is a factor secreted specifically by HS5 stromal cells, that is either not secreted, or not secreted at the same levels by these other stromal cell lines, that drives G6PD up-regulation.

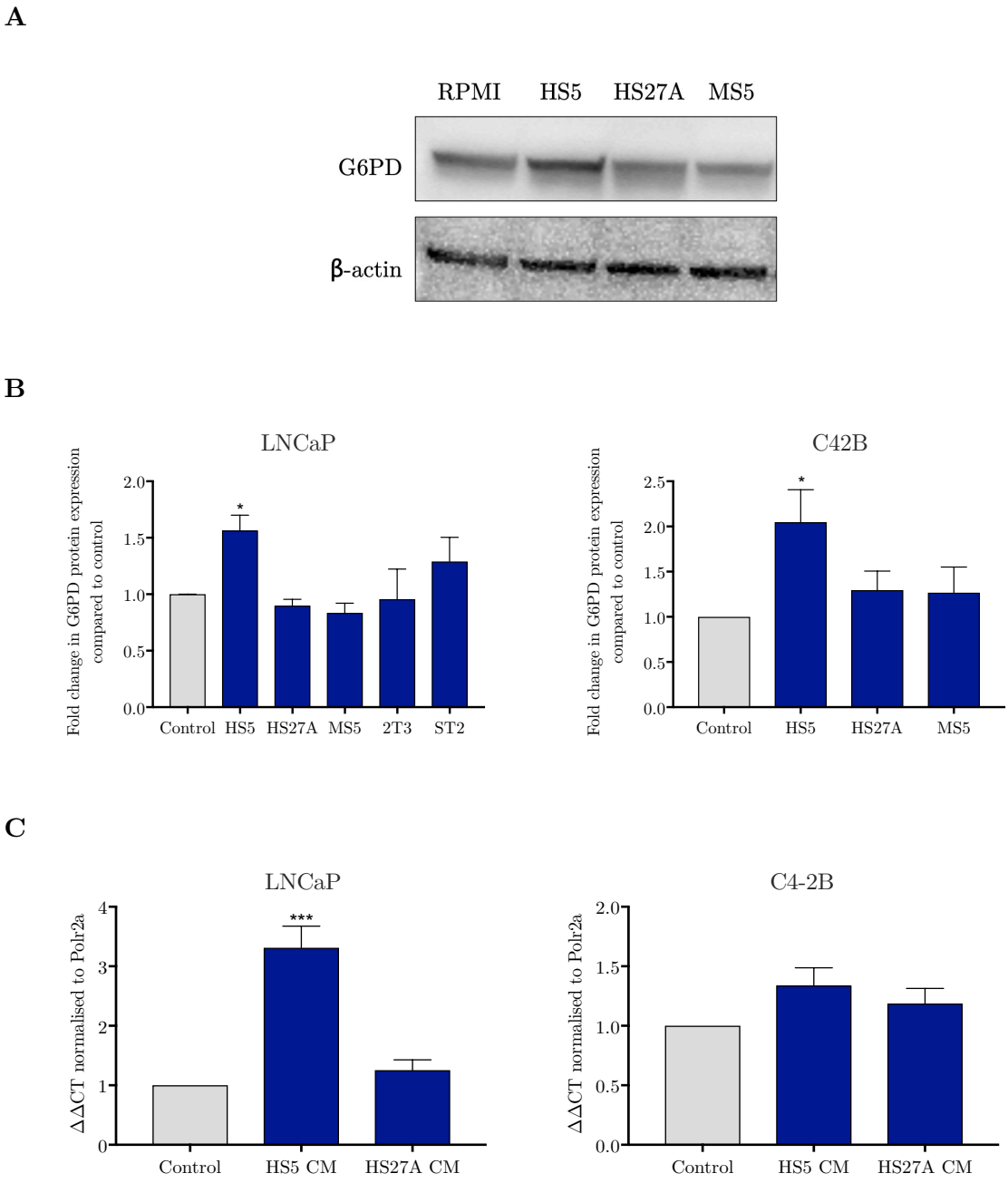


Figure 4.8 ***The increase in G6PD protein expression is specific to HS5 BMSCs.*** *(A) LNCaP cells treated with fresh RPMI or 50% CM from HS5, HS27A or MS5 BMSCs for 72 hr. Blot representative of 4 biological repeats. (B) Densitometry of G6PD western blot band normalised to β-actin and control in LNCaP and C4-2B cells after treatment with 50% CM (HS5, HS27A, MS5) or transwell co-culture (2T3, ST2) for 72 hr. N=4, except LNCaP 2T3 where N=3. (C) mRNA expression of G6PD normalised to Polr2a after 72 hr treatment with 50% HS5 or 50% HS27A CM. Statistical test used= one-way ANOVA with post-hoc Dunnett's test. *=p<0.05, ***=p<0.001. Error bars=SEM.*

4.10 HS5 cells secrete high levels of IL-6 which activates STAT3 signalling in PCa cells

Having identified that CM from HS5 BMSCs is able to induce up-regulation of G6PD, but CM from the HS27A BMSCs is not, the literature was explored to establish the differences between these related cell lines. A study by Graf *et al.*[177] performed transcriptome profiling on these two cell lines and identified which genes had greater than 10-fold difference in expression. IL-6 was the 2nd most significantly lowered gene transcript in HS27A compared to HS5 cells. It has been shown by Zhang *et al.* that IL-6 may play a role in regulating expression of G6PD in renal cell carcinoma, but this has not been examined in prostate cancer[174].

In the cells used in these experiments IL-6 mRNA levels were more than 100 times greater in HS5 compared to HS27A cells (Figure 4.9A). Western blot confirmed that human IL-6 protein level is high in HS5 CM, and not detectable in the CM of other prostate cancer and BMSC cell lines tested (Figure 4.9B). Treatment of LNCaP and C4-2B prostate cancer cells with HS5 CM caused a dose-dependent increase in phosphorylation of signal transducer and activator of transcription 3 (STAT3), a downstream signalling pathway of IL-6, and increased total STAT3 (Figure 4.9C,D).

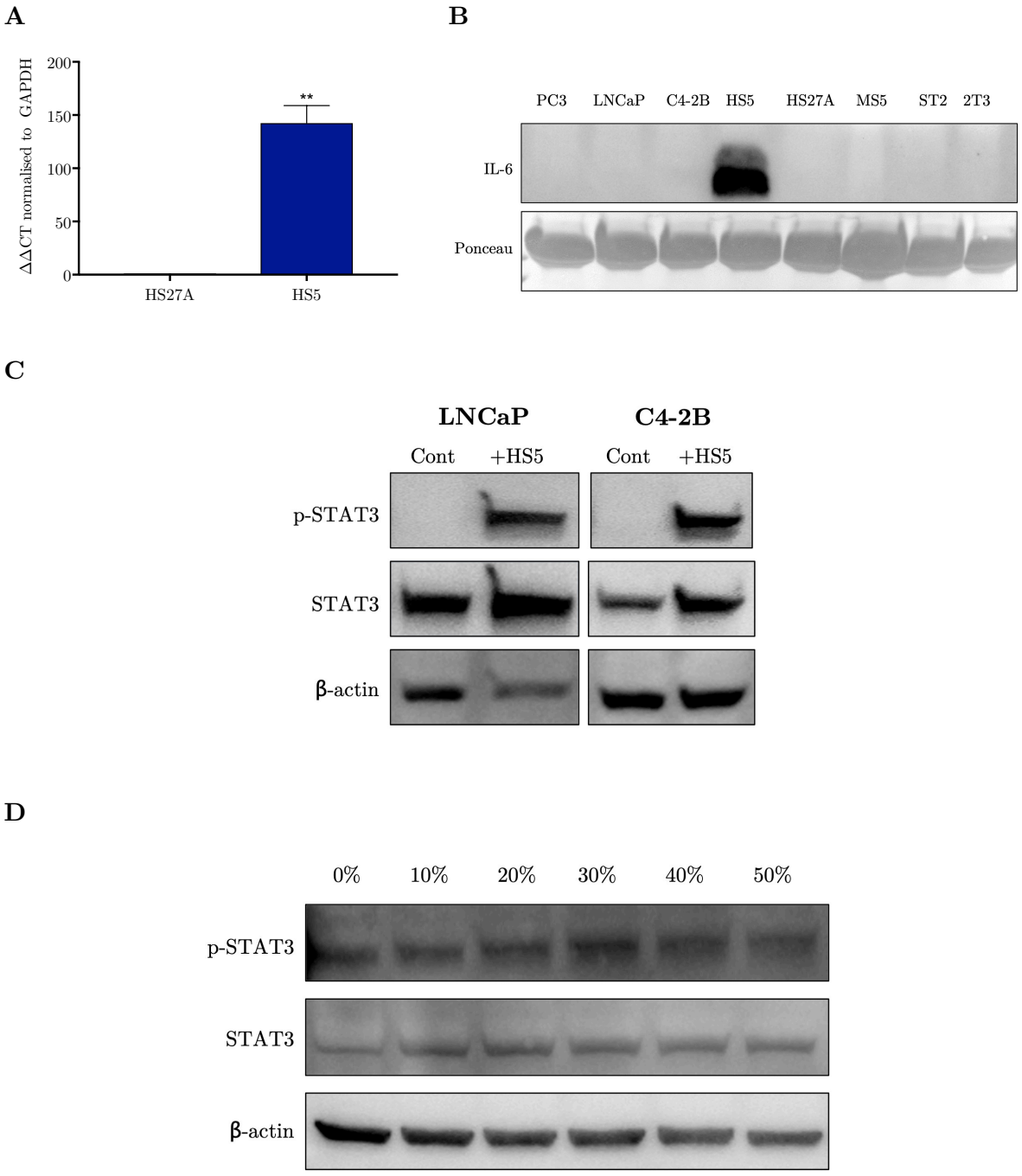


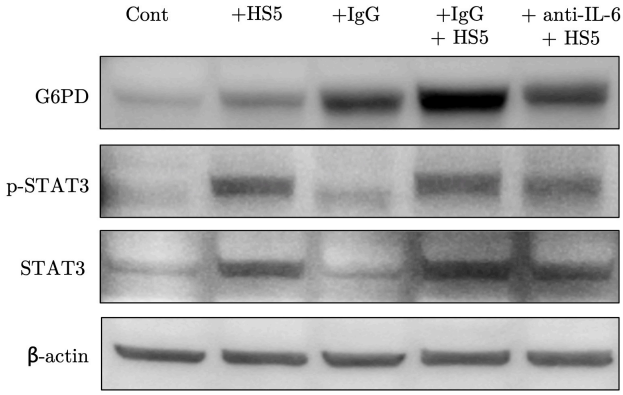
Figure 4.9 ***HS5 cells secrete IL-6 and cause phosphorylation of STAT3****. (A) qPCR of human IL-6 levels in HS5 and HS27A cells normalised to GAPDH, Statistical test used = Student's t-test. **=p<0.01. Error bars=SEM. (B) Western blot of CM from a range of prostate cancer cells (PC3, LNCaP, C4-2B), human stromal cell lines (HS5, HS27A) and mouse stromal cell lines (MS5, ST2, 2T3) showing high expression of human IL-6 in HS5 cells, but no detectable expression in other cell lines CM. (C) Western blot confirming 50% HS5 CM activates p-STAT3 signalling in LNCaP and C4-2B cells. (D) Western blot showing dose dependent increase in p-STAT3 signalling in C4-2B cells after treatment with HS5 CM. Western blots shown representative of 3 biological repeats.*

4.11 Neutralising IL-6 in HS5 CM inhibits the up-regulation of G6PD protein in LNCaP cells

Having identified that HS5 CM contains high amounts of IL-6, and that the CM was able to activate the STAT3 pathway, it was investigated whether this effect was specific to IL-6 by using an IL-6 neutralising antibody (anti-IL-6). 72 hr HS5 CM or complete RPMI was treated with 10µg/ml IgG or 10µg/ml anti-IL-6 and left on a plate shaker for 30 min to allow binding of the antibody to any free IL-6. LNCaP cells were then treated for 72 hr with complete RPMI, 50% HS5 CM, complete RPMI + 10µg/ml IgG, 50% HS5 CM + 10µg/ml IgG, or 50% HS5 CM + 10µg/ml anti-IL-6.

Anti-IL-6 was able to inhibit the increase in G6PD protein seen in LNCaP cells treated with HS5 CM for 72 hr (Figure 4.10A-B), suggesting that IL-6 secreted by HS5 cells is driving the increase in G6PD expression seen.

A



B

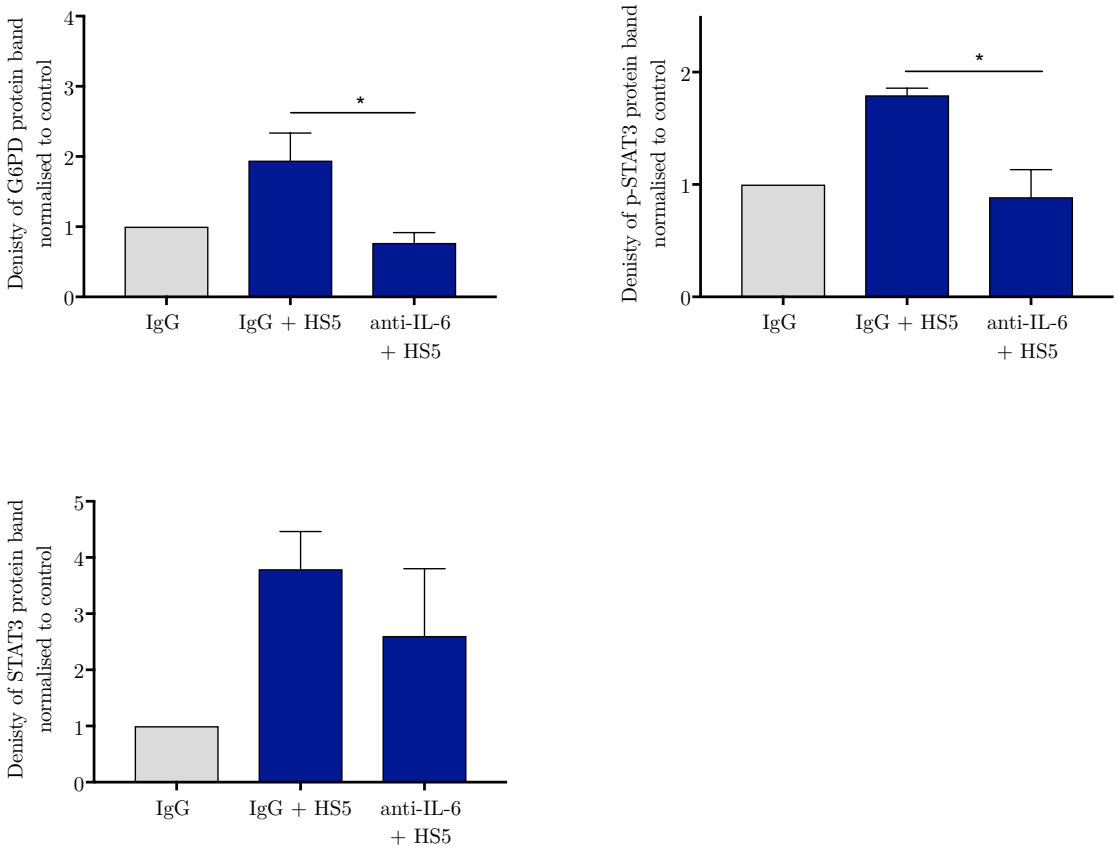


Figure 4.10 ***Neutralising IL-6 inhibits the up-regulation of G6PD protein*** *(A) LNCaP cells treated with 50% HS5 CM +/- 10µg/ml IgG +/- 10µg/ml IL-6 anti-IL-6 for 72 hr. Blot representative of 3 biological repeats. (B) Densitometry from the 3 biological repeats confirming anti-IL-6 significantly inhibits the up-regulation in G6PD protein expression caused by 50% HS5 CM, and also inhibits the up-regulation of p-STAT3 expression. Statistical test used= Student's t-test between IgG + HS5 and anti-IL-6 + HS5. *=p<0.05. Error bars=SEM.*

4.12 Recombinant IL-6 causes up-regulation of G6PD in LNCaP cells

To further evaluate whether IL-6 secreted by HS5 cells is sufficient to drive G6PD up-regulation LNCaP cells were treated with recombinant IL-6 for 72 hr. High dose recombinant IL-6 was able to increase G6PD mRNA levels, although not to the same extent as 50% HS5 CM (Figure 4.11).

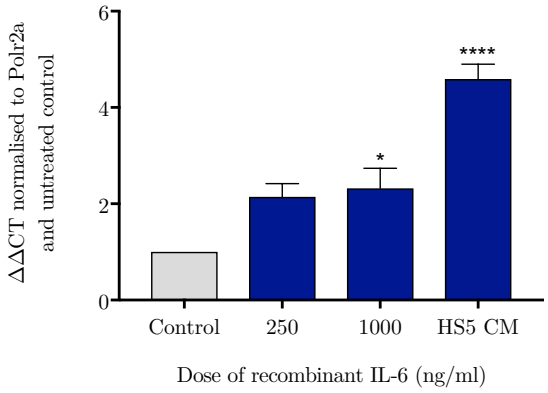


Figure 4.11 ***Recombinant Il-6 causes increased G6PD mRNA expression.*** *LNCaP cells were treated for 72 hr with complete RPMI (Control), 250 ng/ml IL-6, 1000 ng/ml IL-6 or 50% HS5 CM (HS5 CM). Statistical test used= one-way ANOVA with Dunnett's post-hoc test. *=p<0.05, ****=p<0.0001. Error bars=SEM.*

4.13 Mammalian target of rapamycin (mTOR) signalling is not stimulated by HS5 BMSCs

mTOR is known to be one of the master regulators of cellular metabolism, and previous studies have implicated mTOR signalling in regulating the PPP in part by regulating levels of G6PD[113,178]. It was therefore investigated if HS5 BMSCs might also be activating mTOR signalling to up-regulate G6PD.

LNCaP cells were co-cultured with HS5 cells for 48 hr and mTOR signalling was examined by protein expression of phosphorylated mTOR (pmTOR) and its downstream effector p70S6K (Figure 4.12). Co-culture of LNCaP cells with HS5 cells did not cause any increase in pmTOR or p70S6K.

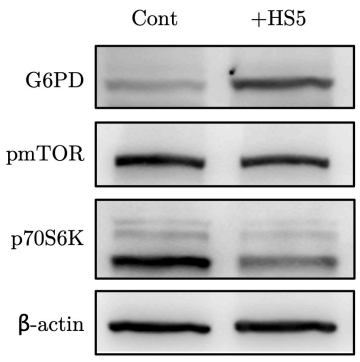


Figure 4.12 ***HS5 BMSC do not activate the mTOR pathway in prostate cancer cells.*** *LNCaP cells were co-cultured with HS5 cells for 48 hr. Blot representative of 2 biological repeats.*

4.14 Discussion

The analyses carried out in this chapter provide evidence that the PPP, and in particular, its rate limiting enzyme G6PD, are up-regulated in bone metastatic prostate cancer patient samples, and expression correlates with disease severity characterised by hormone sensitivity, but not time to BCR. This relationship was seen in multiple data sets with large and small patient numbers strengthening the evidence for this effect. This is in keeping with what has been shown by others in different cancer models. Nagashio *et al.* examined G6PD expression in 124 lung cancer patient specimens and found that high G6PD expression in the tumour correlated with high pathological TNM stage, poorer differentiation, increased tissue invasion and poorer survival[104]. Wang *et al.* examined G6PD expression in 167 patients with gastric cancer and found overexpression was associated with the size of tumour, depth of invasion, lymph node (LN) metastasis, distant metastasis, TNM stage and survival rate, and was an independent prognostic factor for patients after radical resection[105]. Zhang *et al.* analysed G6PD expression levels in 149 renal cell carcinoma patients and found that high expression was significantly correlated with tumour extent, lymph node metastasis, TNM stage and poorer overall survival[110]. Pu *et al.* analysed G6PD protein levels in 20 patients treated with surgery for primary breast carcinoma and found that overexpression of G6PD protein predicted a high risk of recurrent metastasis and shorter progression free survival (71.36 +/- 6.53 months in G6PD-negative patients compared to 32.23 +/- 5.67 months in G6PD positive patients (p=0.002))[107]. In prostate cancer Pretlow II *et al.* in 1985 found that increased G6PD enzyme activity correlated with Gleason grade[112], but no studies have

explored this further. Therefore, this data has shown for the first time that G6PD expression is elevated in hormone refractory disease in PCa. The data did not show a significant relationship between G6PD expression and time to BCR, however the number of events in both groups was very low limiting the significance. In a multivariate analysis it was not possible to identify a significant correlation between time to BCR and pathological stage, which is a known prognostic markers of BCR[179,180], suggesting this data set may not have enough events to detect a correlation.

Up-regulation of G6PD could be recreated in an *in vitro* model by co-culturing LNCaP cells with HS5 BMSCs, supporting a role for the bone microenvironment driving this effect. The role of stromal cells in driving G6PD up-regulation has not been shown before in any disease model. Up-regulation of G6PD protein was not affected by altering the glucose concentration of the media, or by performing co-culture in hypoxic conditions, suggesting that this effect is likely to be seen in more physiological conditions. However, there was overall down-regulation of G6PD in hypoxic conditions, which contrasts with what has been shown by others in different cell types. Chettimada *et al.* showed G6PD expression was increased by hypoxia in pulmonary artery smooth muscle cells[181], while Gao *et al.* showed that hypoxia caused an increase in G6PD expression in PC12 rat pheochromocytoma cells, a classic O_2-sensitive excitable cell, but not in non-excitable Buffalo rat liver cells[182]. It has been suggested that it is the ROS generated under hypoxic conditions that promote G6PD expression via an oxidative stress-sensitive transcription factor, rather than hypoxia itself[73]. Therefore, how G6PD expression is regulated by low oxygen tension is still not clear and remains controversial.

Up-regulation of G6PD protein was enhanced in androgen-deprived conditions. Most men with metastatic prostate cancer are treated with ADT as first line therapy, and therefore this data indicates that current treatments may in fact be enhancing the G6PD up-regulation seen. This would be in keeping with the data showing that G6PD mRNA levels increase as patients progress from treatment naive hormone sensitive disease to heavily treated castrate resistant disease (Figure 4.1D). However this is in contrast with one previous study by Tsouko *et al.* that showed G6PD protein levels are increased with androgen treatment[113]. They found that knockdown of the androgen receptor led to decreased G6PD protein levels but did note a moderate increase in G6PD mRNA. The endogenous steroid hormone dehydroepiandrosterone (DHEA), is produced by the adrenal glands as a metabolic precursor of androgen and oestrogen and is a known uncompetitive inhibitor of G6PD[183]. DHEA is the most abundant steroid in humans, and an important source of androgens. When metabolised by prostate cells DHEA can contribute up to 1/6 of dihydrotestosterone (DHT) present in the prostate[184]. In prostate cancer rat models DHEA has been shown to confer significant protection against prostate cancer[185]. Whereas in patients low serum levels of DHEA has been shown to correlate with high Gleason score, advanced clinical stage and poor prognosis[186] in hormone-naïve PCa[187], and worse cancer-specific survival among metastatic CRPC patients[188]. These studies, however, have not correlated DHEA levels with G6PD expression or PPP activity. The role of DHEA in prostate cancer progression remains controversial as DHEA has also been shown to stimulate PCa proliferation and PSA expression in PCa models *in vitro* and *in vivo*[189,190] via PI3K/Akt signalling. The role of androgens in modulating G6PD expression and activity therefore

remains far from clear, and further work needs to be done to fully elucidate the feedback mechanisms that may be involved between the androgen signalling and the PPP pathway.

G6PD up-regulation could be caused by HS5 CM, as well as co-culture CM indicating that it is a factor secreted by the BMSCs driving this effect, and it does not require interaction with PCa cells. The effect was specific to HS5 BMSCs, and could not be recreated by other stromal cell lines, including the related cell line HS27A. A literature review revealed that IL-6 was one of the most differentially expressed genes between these two cell lines[177], and that IL-6 has previously been implicated in G6PD transcriptional control in renal cell carcinoma[174]. In the cells used for these experiments G6PD mRNA levels were over 100-fold higher in HS5 cells compared to HS27A cells, and IL-6 protein was highly expressed in HS5 CM, but could not be detected in the CM from prostate cancer cell lines, or other BMSC lines including HS27A. This supports the previously published data suggesting that IL-6 is highly differentially expressed between HS5 and HS27A cell lines[177].

Blocking IL-6 in HS5 CM with neutralising antibody resulted in inhibition of the up-regulation of G6PD in LNCaP cells, supporting the hypothesis that IL-6 secreted by HS5 cells is driving the up-regulation of G6PD seen. Treatment with high dose recombinant IL-6 stimulated mRNA expression of G6PD, although not to quite the same extent as HS5 CM. This suggests that either the dose of IL-6 in 50% 72 hr HS5 CM is higher than 1000 ng/ml, or that other factors may also play a role in driving G6PD up-regulation in the bone microenvironment. A previous study suggested that 72 hr HS5 CM contained roughly 200 ng/ml IL-6[191], however in this study HS5 cells were maintained in T-medium with 5% FBS rather than complete RPMI. The concentration of IL-6 in the CM for these experiments

remains unknown. This data provides evidence for a role for IL-6 in driving G6PD overexpression in prostate cancer in the bone microenvironment, but suggests other pathways may also play a role. It has been reported by others that the mTOR pathway may play a role in G6PD modulation[113,178], but that was not seen in this model.

IL-6 is a potent inflammatory cytokine that mediates several important physiological functions, including inflammation, cell growth and survival[192]. There are two types of receptor for IL-6, a cell membrane IL-6 receptor with low affinity that forms a complex with the signal-transducing component gp130 (CD130) after binding with IL-6, and a soluble IL-6 receptor (sIL-6R) which binds with IL-6 and then with the membrane receptor β chain, gp130, leading to the intracellular signal. Binding of IL-6 to the IL-6 receptor complex activates the janus tyrosine family kinase (JAK)-signal transducers leading to activation via tyrosine phosphorylation of STAT3. Following phosphorylation and acetylation, STAT3 forms a dimer in which the SH2 domain of one phospho-STAT3 (pSTAT3) molecule binds to the phosphorylated Tyr^{705} of the other and vice versa. The pSTAT3 dimer then translocates from the cytoplasm to the nucleus where it binds to an interferon-gamma activated sequence (GAS) element and initiates a change in the transcription of a number of genes[193]. A negative feedback loop exists through up-regulation of suppressor of cytokine signalling 3 (SOC3) gene transcription by STAT3, which inhibits JAK by direct binding to the kinase. STAT3 can also bind to p53 and inhibit its function as a regulator of apoptosis. STAT3 has been identified as the prime transcriptional regulator mediating IL-6 dependent cell growth, differentiation and survival signals, but IL-6 can also activate the extracellular signal-regulated kinase 1 and 2 (ERK1/2)-mitogen-activated protein kinase (MAPK)

pathway and the PI3K pathway[192]. These different pathways together contribute to the pro-tumorigenic and anti-apoptotic activities of IL-6 in cancer cells (Figure 4.13).

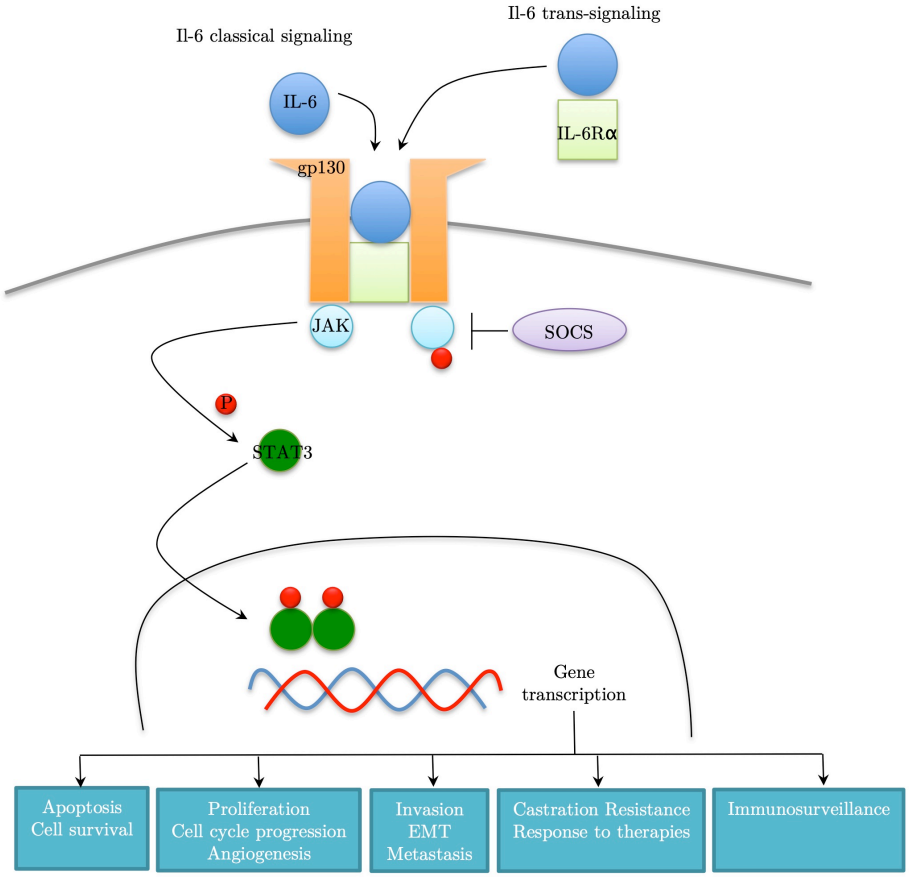


Figure 4.13 ***IL-6 signalling via STAT3 and its pro-tumourigenic effects.*** *IL-6: interleukin-6; gp130: glycoprotein 130; JAK: Janus tyrosine family kinase; STAT3: signal transducer and activator of transcription 3; SOCS: suppressor of cytokine signalling; EMT: epithelial-mesenchymal transition; p: phosphorylation.*

It has long been recognised that IL-6 serum levels are elevated in patients with untreated metastatic or CRPC compared to healthy men or patients with localised disease[194,195]. In a study of men with CRPC, IL-6 serum levels above the mean were associated with shorter survival time in a multivariate model[196]. It has been proposed that IL-6 secretion confers resistance to cytotoxic chemotherapeutics such as docetaxel in hormone independent prostate cancer cell lines[197], and pre-chemotherapy serum IL-6 levels can predict PSA and

clinical response to docetaxel in CRPC patients. In view of this several trials have taken place targeting IL-6. However, Siltuximab (CNTO 328), a chimeric monoclonal antibody targeting IL-6, has yielded mixed results[198,199], perhaps due to the multitude of effects IL-6 can have. Trials also found Siltuximab led to a range of toxicities including disseminated intravascular coagulation, central nervous system ischemia, blood cell abnormalities and neuropathy[200]. Targeting G6PD may therefore be a novel refined way to target some of the pro-tumourigenic effects IL-6 has on PCa growth and drug resistance.

4.15 Future Directions

G6PD protein expression has been correlated with higher pathological TMN stage, poorer differentiation, increased tissue invasion and poorer survival in other cancers but this has yet to be explored in PCa. It could prove to be a promising biomarker in predicting PCa patients that are at highest risk of progression, thereby better focusing treatments in these patients. It has also been shown in other cancer models that G6PD levels are correlated with patient's response to chemo- and radio-therapy. Hence this would be interesting to explore further in PCa, particularly in view of its links with IL-6 which has been shown by others to correlate with response to chemotherapy[197].

In view of the important role that androgens have in PCa, further work exploring the correlation between DHEA serum levels, G6PD expression and the effects of ADT in PCa patients appears to be an intriguing avenue. Improved understanding of the links between these pathways could lead to improvements in the efficacy of ADT.

5

Bone marrow stromal cells modulate the redox state and growth of prostate cancer

5.1 Introduction

The pentose phosphate pathway is viewed as a critical pathway in cell redox balance and proliferative fate. Its activity is strongly affected by the rate of cell proliferation due to the requirement for ribose-5-phosphate for nucleic acid synthesis, and the need for NADPH

which is required as a reducing agent in several synthetic and detoxification reactions. NADPH is the limiting substrate for glutathione reductase (GSR) the enzyme that regenerates reduced glutathione (GSH) from oxidised glutathione (GSSG). GSH converts H_2O_2 to water catalysed by glutathione peroxidase (GSH-Px)[73]. G6PD is often viewed as the pacesetter of NADPH production, and therefore plays a key role in handling oxidative stress. Each defect affecting the activity of G6PD, GSR and GSHPx makes cells more susceptible to oxidative stress, and therefore oxidative stress induced apoptosis.

Altered redox state is a key biochemical feature observed in tumour cells. In general ROS at moderate levels are important for cell survival and tumourigenesis[201], but above a certain threshold ROS may exert a cytotoxic effect typically leading to cell death[202]. ROS-mediated signalling pathways can activate pro-oncogenic signalling which aid cancer progression, angiogenesis and survival[203]. NADPH not only plays a role in maintaining anti-oxidants, but has also been proposed to play a role in sustaining ROS production via increased NADPH oxidases (NOX) activity. The NOX family includes five homologs, NOX1-5 and two related enzymes DUOX1 and DUOX2. Targeting NOX can cause cell cycle arrest and reduced prostate cancer migration, indicating increased ROS are necessary for the invasive phenotype of prostate cancer[204,205]. Under persistent intrinsic oxidative stress, many cancer cells become well adapted to ROS and develop an enhanced endogenous antioxidant capacity. Recent evidence suggests that such adaptation contributes to malignant transformation, metastasis and resistance to chemotherapy[73].

Mitochondria are still viewed as the main contributor to cellular ROS generation consuming approximately 80% of molecular oxygen during OXPHOS[203]. Superoxide radicals generated

in the mitochondria can pass into the cytoplasm where they are dismuted to hydrogen peroxide catalysed by superoxide dismutase located in the mitochondrial matrix (MnSOD) or in the cytosol (by Cu/ZnSOD). Therefore alterations in OXPHOS can impact the redox state of the cell.

The previous chapter identified that BMSCs are able to induce expression of G6PD, therefore this chapter will examine the impact of BMSCs on PCa's cellular proliferation and oxidative state.

5.2 Aims

The specific aims of this chapter are to:

1) Establish the effect of BMSCs on ROS levels and the anti-oxidant state of PCa cells.

2) Establish the effect of BMSCs on PCa growth and viability *in vitro* and *in vivo.*

5.3 Bone marrow stromal cell conditioned media increases reactive oxygen species

Having previously found that HS5 CM stimulates an increase in G6PD levels, and due to G6PD's role as the pacesetter of NADPH production, it was investigated whether BMSC CM has any effect on the redox state of prostate cancer cells. HS5 CM causes an increase in total ROS (Figure 5.1A), and specifically in the amount of mitochondrial ROS in PCa cells (Figure 5.1B-C). The increase in mitochondrial ROS suggests that HS5 CM may be driving an increase in OXPHOS leading to increased ROS generation. This would be in keeping with the previous *in vitro* work (Figure 3.3B) that showed HS5 CM caused an increase in oxygen consumption in PCa cells, and the *in silico* analysis which showed OXPHOS genes were significantly up-regulated in prostate cancer metastatic samples compared to primary tumours (Figure 3.5A-B).

Although knockdown of G6PD has a limited effect on ROS (Figure 5.1D), there is a trend for the amount of ROS to be further increased by 6-aminonicotinamide (6AN), a pharmacological inhibitor of G6PD (Figure 5.1A), however these differences did not reach significance. This suggests that G6PD is not responsible for the increased ROS produced after CM treatment, as if NOX were responsible ROS levels should decrease after G6PD inhibition. Instead this suggests that BMSCs may drive increased PPP flux to subsequently reduce the extra mitochondrial ROS produced by the cell.

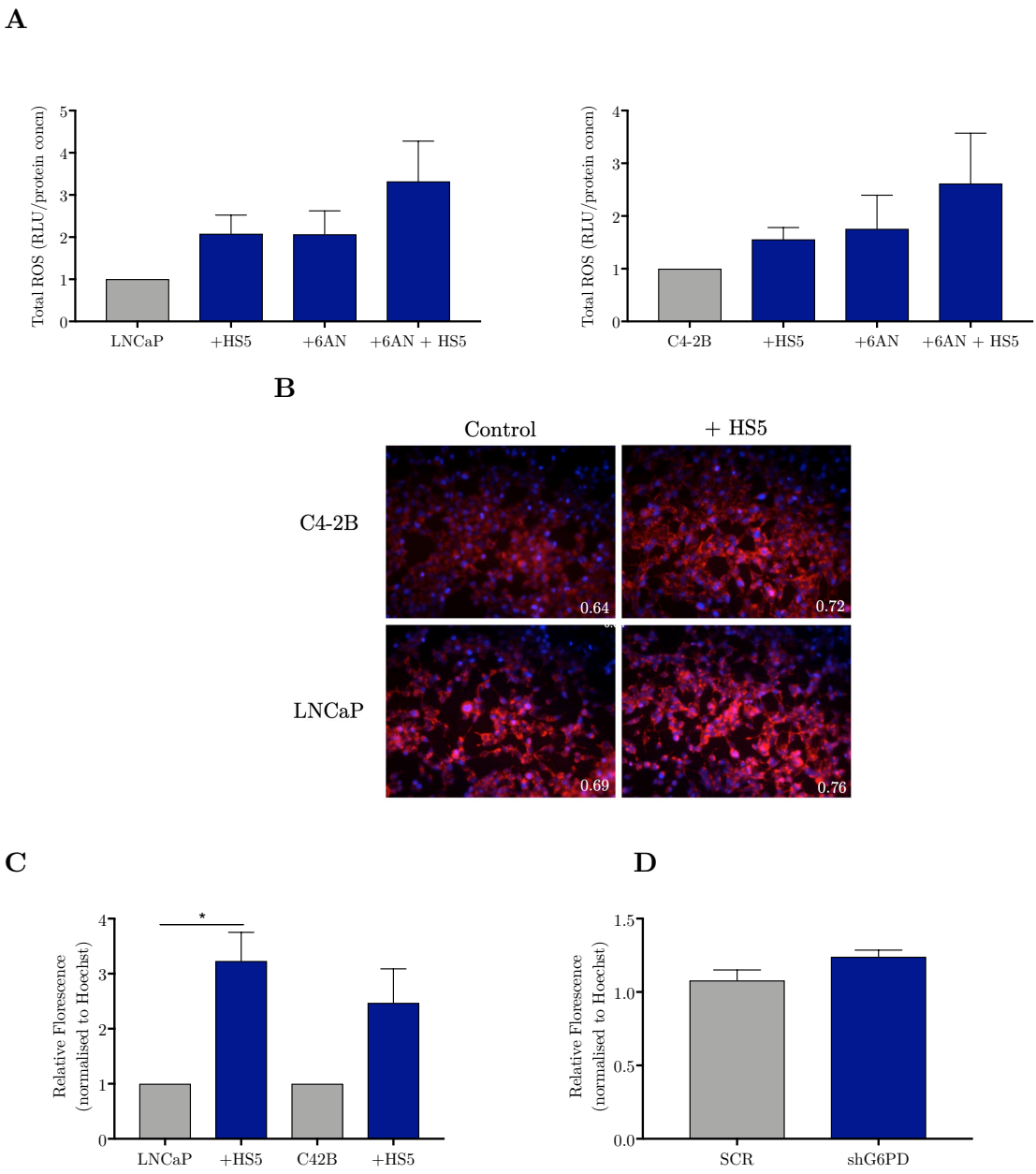


Figure 5.1 ***BMSC CM and G6PD inhibition increases cellular ROS.*** *(A) LNCaP or C4-2B cells treated with 6AN +/- HS5 co-culture for 72 hr. ROS levels were measured, and normalised to total protein concentration measured using a BCA assay. (B) Mitochondrial ROS after 72 hours co-culture of C4-2B or LNCaP cells with HS5 cells. Blue = Hoechst nuclear staining. Red = MitoSox mitochondrial ROS staining. Merged images taken on a Nikon Eclipse TE300 inverted microscope at 4X magnification. Images and values representative of 3 biological repeats. (C) Mitochondrial ROS after 72 hours co-culture with HS5 cells quantified by MitoSox fluorescence reading and normalised to Hoechst fluorescence. Statistical test used = Student t-test, * p=<0.05. (D) Mitochondrial ROS in LNCaP-SCR cells or LNCaP G6PD shKD cells. Error bars = SEM.*

5.4 Bone metastatic PCa cells have increased GSH

In the previous chapters it was shown that PC3 PCa cells have higher baseline G6PD expression compared to LNCaP cells (Figure 3.11A-B; Figure 4.7D). It was therefore investigated if this corresponded to a higher basal antioxidant ability as measured by the quantity of GSH. PC3 cells have a significantly higher amount of GSH compared to LNCaP (

Figure 5.2), suggesting that cells with higher G6PD protein also may have higher GSH levels and therefore better antioxidant capabilities.

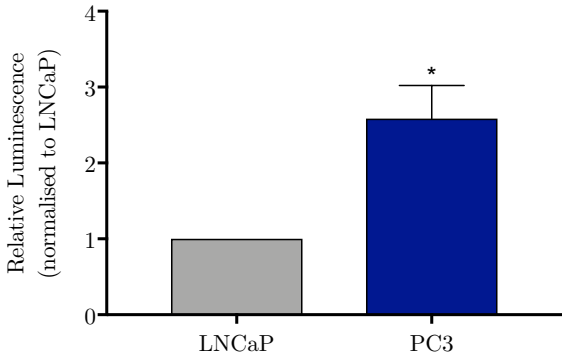


Figure 5.2 ***Metastatic PCa cells have higher GSH levels.*** *GSH levels measured by GSH-Glo assay in the non-bone metastatic LNCaP cell line and the bone metastatic PC3 cell line. Statistical test used= Student t-test. * p=<0.05. Error bars = SEM.*

5.5 BMSCs increase the anti-oxidant ability of prostate cancer cells

In the previous chapter co-culture of PCa cells with HS5 BMSCs caused an increase in G6PD expression (Figure 4.2A-B). It was therefore investigated whether BMSCs similarly elevated PCa's antioxidant abilities. When PC3 cells were co-cultured with HS5 BMSCs there was a significant increase in NADPH/$NADP^+$ levels as measured by CE-MS (Figure 5.3A). 72 hr treatment of LNCaP cells with HS5 CM caused a significant increase in GSH levels (Figure 5.3B). This indicates that HS5 BMSCs are able to increase the antioxidant level of PCa cells.

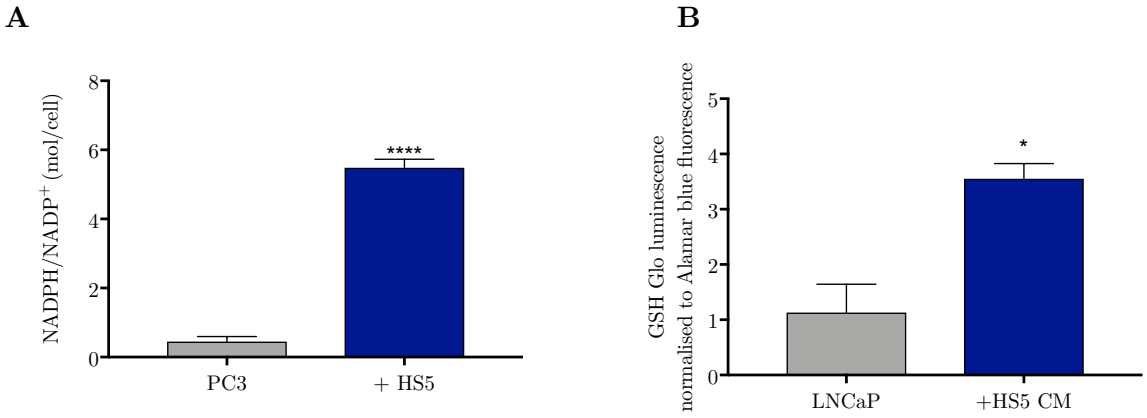


Figure 5.3 ***BMSCs increase the antioxidant level in PCa cells.*** *(A) NADPH/$NADP^+$ ratio in PC3 cells after 24 hr co-culture with HS5 cells measured by CE-MS. (B) GSH levels in LNCaP cells after 72 hr treatment with HS5 CM, normalised to Alamar blue fluorescence. Statistical test used= Student t-test. * p=<0.05, ***p=<0.0001. Error bars = SEM.*

5.6 Antioxidants can inhibit the increase in G6PD protein induced by HS5 CM

Give the important role of G6PD in redox balance it was investigated whether the increase in ROS seen with HS5 CM treatment could be driving the increase in G6PD protein expression. Treating cells with N-acetylcysteine (NAC), an anti-oxidant, partially blocks the increase in G6PD protein seen with HS5 CM (Figure 5.4A), however no increase in G6PD protein expression was observed in LNCaP cells following ROS induction by hydrogen peroxide (H_2O_2) treatment (Figure 5.4B).

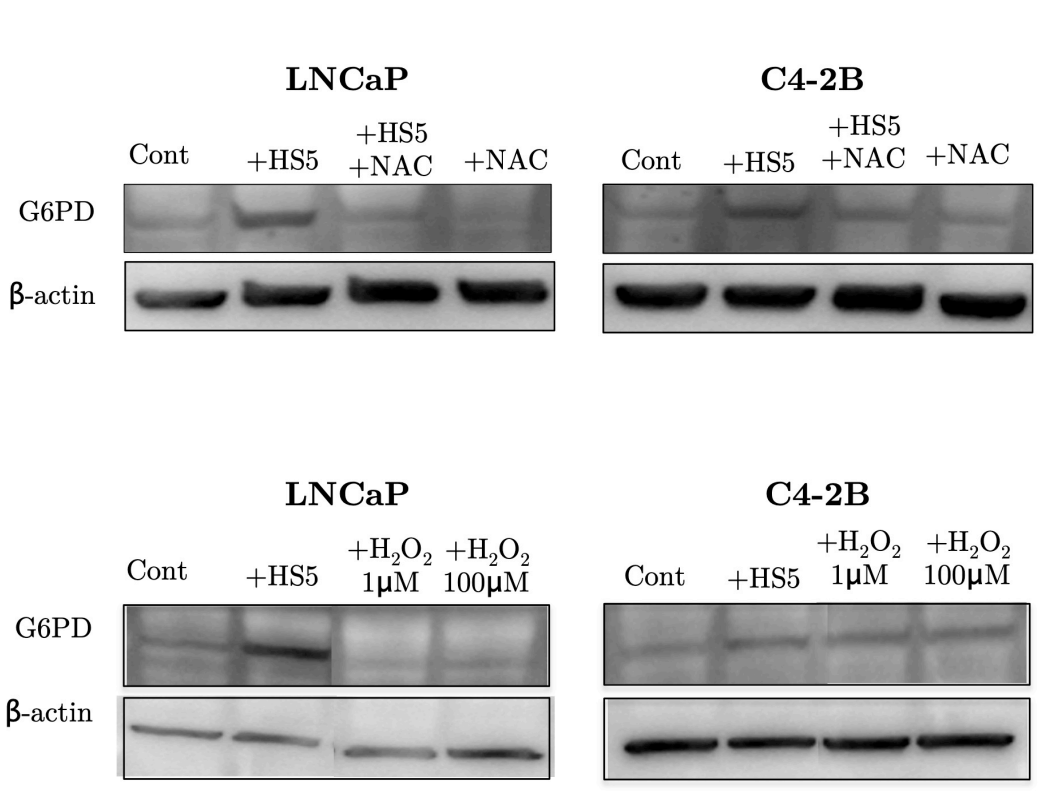


Figure 5.4 ***NAC inhibits the up-regulation of G6PD protein*** *(A) G6PD protein expression after 48 hr treatment with 50% HS5 CM +/- 10mM NAC. (B) G6PD protein expression after 48 hr treatment with 1μM H_2O_2 or 100μM H_2O_2. Blots representative of 3 biological repeats.*

5.7 HS5 CM causes cell cycle arrest and inhibits growth of non-bone metastatic prostate cancer cells

Having shown that HS5 CM increases ROS generation which could potentially increase apoptosis (Figure 5.1), but also increases ribose-5-phosphate (Figure 3.5, Figure 3.8) necessary for nucleic acid synthesis it was investigated whether BMSCs caused a change in cell cycle progression in PCa cells. Cells were stained with PI, a fluorogenic compound that binds stoichiometrically to nucleic acids. Florescence emission is proportional to the nucleic acid content of the cells, and has been shown to provide a quick and simple flow cytometry method to measure cell cycle and apoptosis. By measuring cellular DNA content it allows quantification of sub G1/G0 (apoptotic cells), G1 phase (haploid), G2 (diploid) and S phase (replication DNA) cells. It was found that 50% HS5 CM caused an increase in G1 phase compared to 50% HS27A CM or fresh RPMI (Figure 5.5A-B). This suggests that HS5 CM causes cells to be held in G1 phase slowing their progression through the cell cycle and impairing their proliferation. HS5 CM did not however have an effect on the cell cycle of PC3 cells (Figure 5.5C), suggesting this effect may be specific to less malignant non-bone metastatic cell lines.

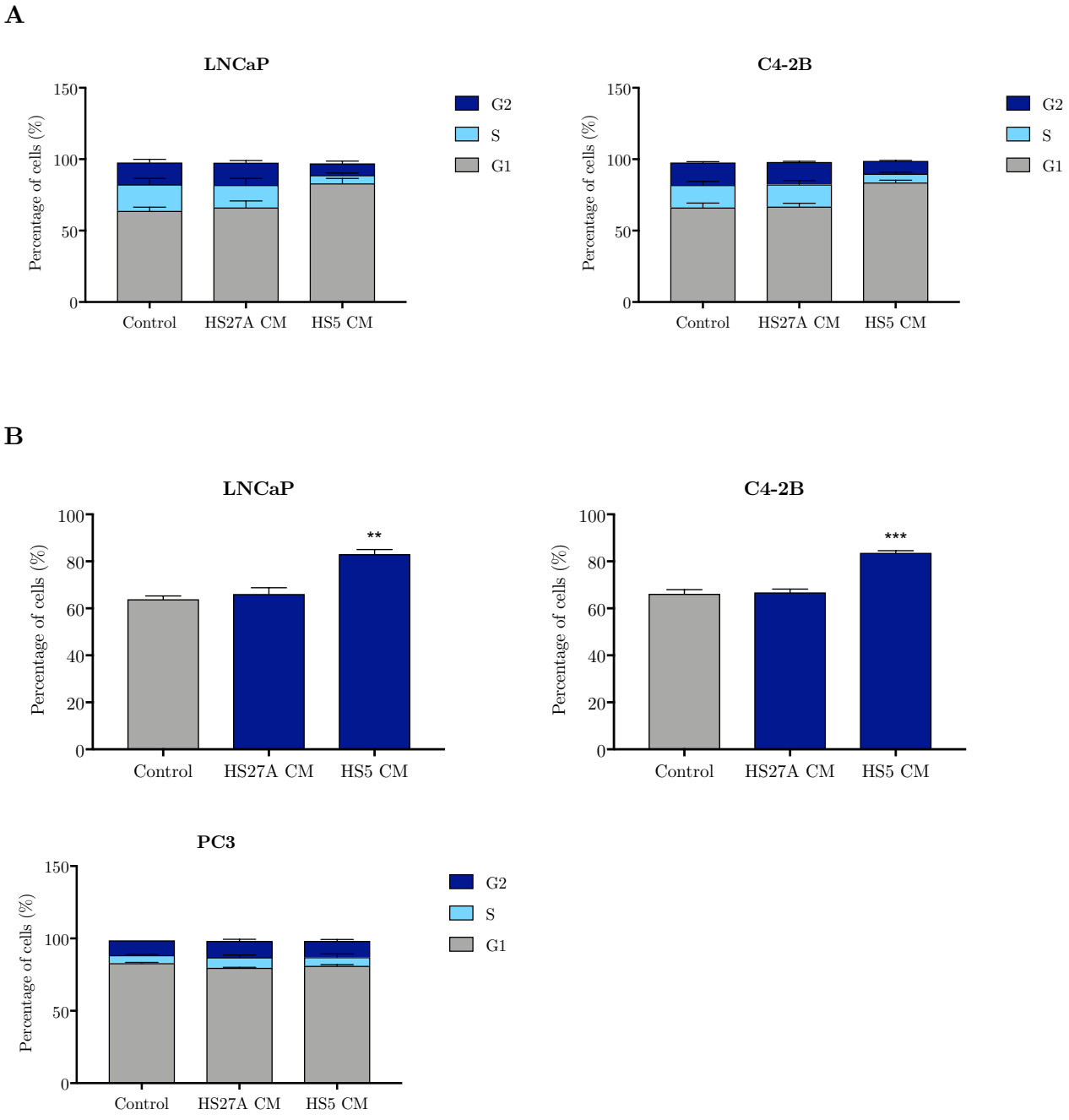


Figure 5.5 ***HS5 CM causes cell cycle arrest in G1 in non-bone metastatic PCa cell lines.*** *Cells were seeded at 0.5 x 10^6 and treated with 50% HS5 CM, 50% HS27A CM or fresh RPMI media for 48 hours. (A) Graph showing % of total cells in each phase of the cell cyle. (B) Graph showing % of cells in G1 phase of the cell cycle. N=3 for all except PC3 N=2. Statistical test used= one-way ANOVA with Dunnett's post-hoc test. ** p=<0.01, *** p=<0.001. Error bars = SEM.*

Having identified that HS5 CM can cause cell cycle arrest in non-bone metastatic PCa cell lines the effect of HS5 CM on PCa proliferation and viability was investigated. 72 hr culture with 50% HS5 CM caused reduced viability of LNCaP non-bone metastatic prostate cancer cells (Figure 5.6A), whilst it did not affect the viability of PC3 cells, a bone-metastatic cell line (Figure 5.6A). Indeed there appears to be a correlation between the cell lines ability to grow *in vivo* in mouse intra-tibial models and their sensitivity to the toxic effects of HS5 CM (LNCaP > C4-2B > PC3), perhaps suggesting that PCa might build tolerance to the toxic factor to enable propagation in the bone microenvironment.

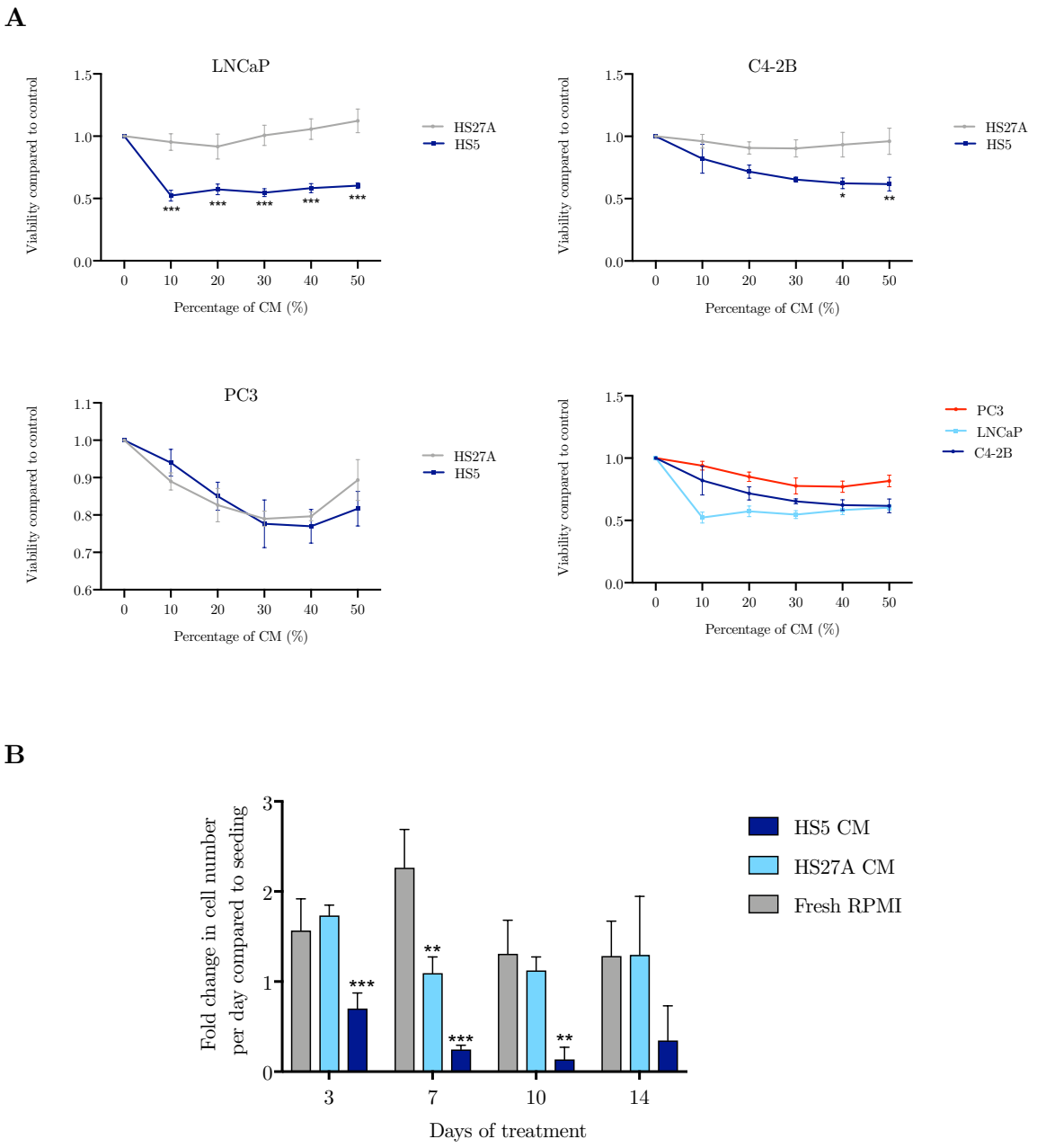


Figure 5.6 ***HS-5 CM reduces the viability of non-bone metastatic cell lines.*** *(A) Alamar blue viability assay of LNCaP, C4-2B and PC3 cells after 72 hr treatment with an increasing percentage of HS5 or HS27A CM. Statistical test used = Student t-tests with correction for multiple comparisons using the Holm-Sidak method. (B) Trypan blue cell counts of C4-2B cells at stated time points after treatment with fresh RPMI media, 50% HS27A CM or 50% HS5 CM represented as fold change in cell number per day compared to seeding. Statistical test used= one-way ANOVA with Dunnett's post-hoc test. * p=<0.05, ** p=<0.01, *** p=<0.001. Error bars = SEM.*

5.8 HS5 cells inhibit the growth of prostate cancer *in vivo*

Having identified that HS5 CM inhibited the growth of non-bone metastatic prostate cancer cells *in vitro,* the effect was investigated in a more complex and physiologically relevant *in vivo* model.

Four weeks old male CB17 SCID mice were injected intra-tibially with 1 x 10^6 C4-2B (N=5), or 1 x 10^6 C4-2B cells mixed with 1 x 10^6 HS5 cells (N=7) , 1 x 10^6 C4-2B cells mixed with 1 x 10^6 HS27A cells (N=6), or PBS as a control (N=5). Mice were weighed weekly and bled on weeks 4, 6, 8, and 10 and serum run on a PSA ELISA to monitor tumour burden. Mice were culled at week 14, or when they had lost 15% of their starting body weight.

Co-inoculation of C4-2B with HS5 bone stromal cells inhibited the growth of prostate cancer in the tibia of mice compared to co-inoculation with the related HS27A cell line, as measured by PSA (Figure 5.7A-B). The survival curve between the C4-2B+HS5 mice and the C4-2B+HS27A mice was significantly different (p=0.0076) suggesting a slower disease progression in the C4-2B+HS5 group. Interestingly when looking at the fold change in PSA between week 4 to 6 (Figure 5.7C) and week 6 to 8 (Figure 5.7D) there was a trend towards a larger fold increase in PSA in the HS5 group compared to the HS27A group, suggesting perhaps after an initial lag in tumour growth in the HS5 group, there was then a faster PCa cell growth towards the end of the experiment, however this did not reach significance. All tumour groups had a similar appearance to their bones on ex-vivo micro-CT (Figure 5.7E),

suggesting that despite a significant difference in tumour burden, the bone disease was comparable between the groups.

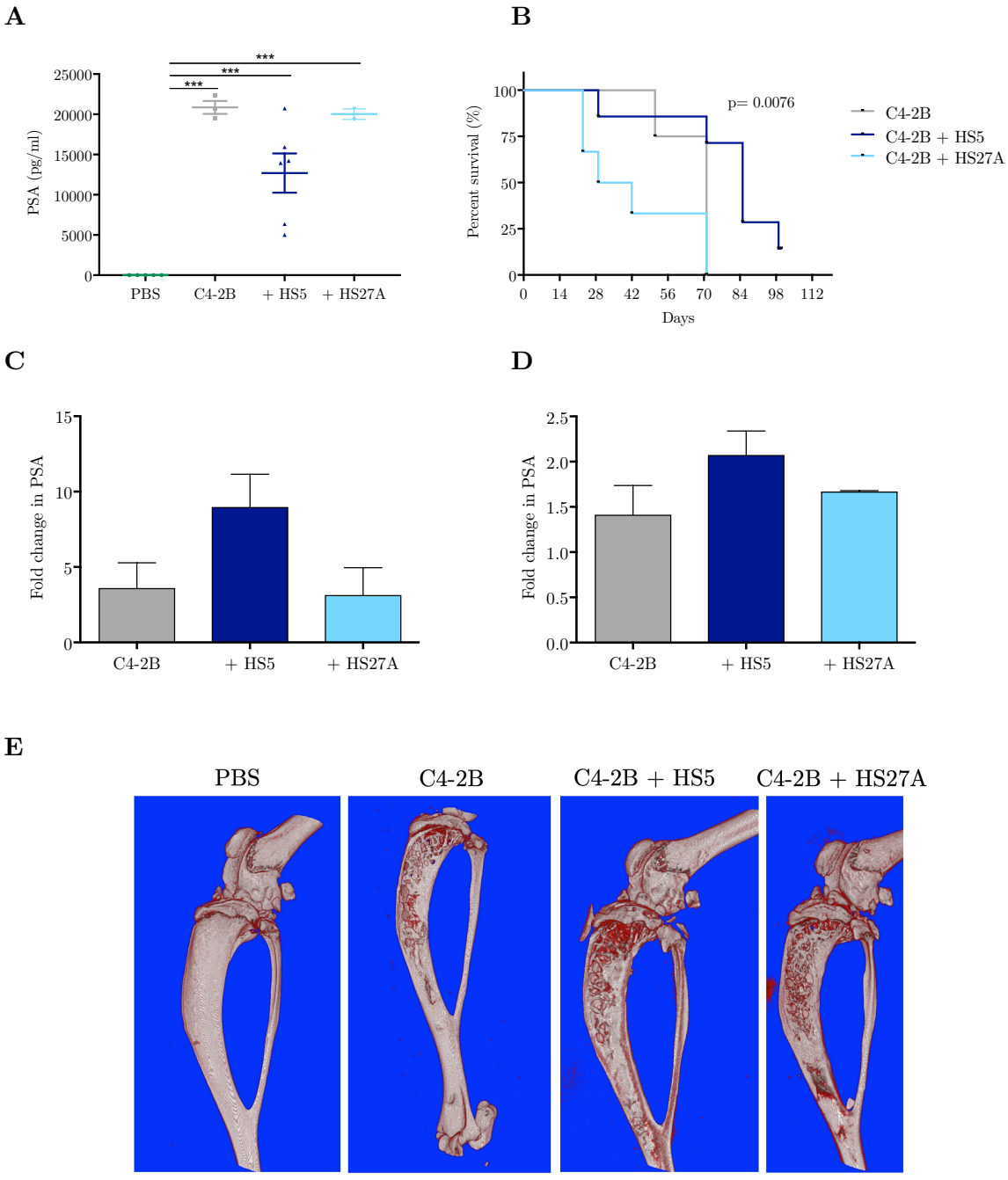


Figure 5.7 ***HS5 cells inhibit the growth of PCa cells in vivo.*** *(A) PSA levels in the mice alive at week 10 measured from the serum using a PSA ELISA. Statistical test used = one-way ANOVA with post-hoc Dunnett's test. ***=p<0.001. Error bars = SEM. (B) Survival curve. Significance represents differeces in suvival between the C4-2B+HS5 group and the C4-2B+HS27A group. Statistical test used = Log-rank (Mantel-Cox) test. (C) Fold change in PSA level between week 4 and week 6 measured using a PSA ELISA. (D) Fold change in PSA level between week 6 and week 8 measured using a PSA ELISA. (E) 3-D reconstruction of the ex-vivo micro-CT images a PSA innoculated mouse, a C4-2B innoculated mouse, a C4-2B+HS5 inncoulated mouse and a C4-2B+HS27A innoculated mouse. Images representative of the mice within each group.*

5.9 Discussion

The results of this chapter have shown that HS5 BMSC cause an increase in intracellular ROS, and more specifically mitochondrial ROS (Figure 5.1). I hypothesise that this increase in mitochondrial ROS may be a result of increased OXPHOS in these cells in keeping with the results of Chapter 3 that demonstrate the bone microenvironment can stimulate an increase in oxygen consumption and OXPHOS gene expression (Figure 3.3, Figure 3.5).

The increase in ROS stimulated by BMSCs is likely alleviated in part by up-regulation of G6PD, as inhibition of this enzyme trended to a further increase in ROS, although this did not reach significance. This would be in keeping with results in other disease models. Tian *et al.* showed that inhibition of G6PD with DHEA or 6AN can potentiate H_2O_2 induced cell death in cell lines, while overexpression of G6PD increased cell resistance to H_2O_2 induced cell death[206]. Ju *et al.* showed that knock down of G6PD in a colorectal cell line reduced the $NADPH/NADP^+$ and GSH/GSSG ratios and caused a substantial increase in ROS levels[103], while Mele *et al.* found that another G6PD pharmacological inhibitor, Polydatin, caused an accumulation of ROS leading to cell cycle arrest and apoptosis[207].

I found that neutralising ROS with an antioxidant such as NAC can inhibit G6PD protein up-regulation caused by HS5 BMSC CM. It has previously been shown that NAC can inhibit the G6PD up-regulation induced by hypoxia in PC12 rat pheochromocytoma cells[182], and that ROS can drive G6PD up-regulation. It was therefore hypothesised that increased ROS can further drive the up-regulation of G6PD expression, along with IL-6 released from the BMSCs.

The bone metastatic cell line PC3, with a higher basal G6PD level, has higher levels of the antioxidant GSH. This is in keeping with work performed by others[208]. Freitas *et al.* demonstrated that metastatic PCa cell lines are more resistant to ROS via this increase in GSH content when compared to the non malignant RWPE1 prostate cell lines, or the localised HPV10 prostate cancer cell line[209]. They hypothesise that this may contribute to the more aggressive phenotype. Treating PCa cell lines with HS5 BMSCs causes an increase in their levels of antioxidants, suggesting the bone microenvironment drives a pro-antioxidant phenotype in the PCa cells. This is supported by a study performed by Cheteh *et al.* that demonstrated that LNCaP cells grown in CM from localised prostate tumour CAF have a 30% increase in intracellular glutathione levels compared to LNCaPs cultured in fresh media[210]. However, this effect has not previously been shown with stromal cells of the bone microenvironment.

Overall HS5 BMSCs have a toxic effect on non-bone metastatic cell lines both *in vitro* and *in vivo* leading to cell cycle arrest and growth inhibition. Freitas *et al.* showed that RWPE1 and HPV10 prostate cancer cell lines are more susceptible to cell death from ROS than the bone metastatic PC3 cell line, so the differences between cell lines may be due to differences in ROS sensitivity[209]. I propose that this toxic environment may allow Darwinian selection of a prostate cancer cell population that is able to withstand high ROS levels through up-regulation of their anti-oxidant pathways, and this may in part drive drug resistance.

The altered redox state caused by BMSCs and their management by PCa cells with increased G6PD is of particular relevance in bone metastases as ROS are implicated in bone remodelling. ROS-producing stimuli have been shown to promote osteoclast activity whilst

inhibiting osteoblast activity[211–213]. If PCa cells improve the antioxidant levels in bone metastases it is possible that this could contribute to increased osteoblast activity and decreased osteoclast activity leading to osteoblastic metastases.

5.10 Future Directions

It is clear from these results that HS5 BMSC CM is toxic to non-bone metastatic PCa cells lines *in vitro*, and appears to be at least initially growth inhibitory *in vivo*. Therefore I hypothesise that the bone microenvironment may initially be a harsh 'soil' for the PCa cells to survive in with increased ROS leading to some PCa cell death, however this allows selection for a population that has raised G6PD expression, enabling them to not only survive and proliferate in the bone micro-environment, but also giving them enhanced ability to deal with oxidative stress. To test this in the future I would like to perform long term conditioning of non-bone metastatic PCa cells *in vitro* with HS5 CM to see if after the initial cytotoxic effect there was a selection of a more aggressive cell population. It could then be investigated if these long-term conditioned cells are more resistant to ROS, chemotherapy and radiotherapy, and if they have stable up-regulation of G6PD and increased anti-oxidants as a result.

Having found that IL-6 is driving, at least in part, the up-regulation of G6PD in PCa cells I would like to further investigate whether IL-6 is also driving the toxicity and increased ROS seen with HS5 CM. ROS have previously been shown to stimulate IL-6 production[214–216] but it is less clear whether IL-6 itself can drive ROS production, or increased OXPHOS. Whilst

it is known that IL-6 levels are increased in patients with prostate cancer the effects of IL-6 on prostate cancer *in vitro* remain unclear with some reporting that IL-6 is growth stimulatory whilst others report that it increases prostate cancer cell death[217]. A study by Lee *et al.*[218] found that when LNCaP were cultured in media supplemented with IL-6 lower passages (less than 28 passages) had severely retarded cell growth, while higher passages (greater than 42 passages) had accelerated growth. This suggests that long-term conditioning may be needed to overcome the initial toxicity seen with HS5 CM. This would be in keeping with the *in vivo* results where tumours were initially slower to grow intra-tibially, but then mice had a non-significant higher fold increase in PSA over weeks 4 to 6 and weeks 6 to 8.

Finally it would be interesting to see if the altered redox balance in the PCa cells has any impact on the ROS levels in surrounding cells in the bone microenvironment, and if this has any functional effects on the activity of osteoclasts and osteoblasts.

6

The effects of manipulating G6PD expression on prostate cancer

6.1 Introduction

In the previous chapters it has been shown that the bone microenvironment causes up-regulation of the PPP, and in particular G6PD. However, the PCa/bone *in vitro* model is complicated by other signalling pathways that might be activated, and by other cytokines and growth factors that may also be secreted by the stromal cells. It also doesn't allow exploration of the direct effects of targeting G6PD. Whilst there are some known pharmacological inhibitors of G6PD, they have limitations including their lack of specificity,

and so are likely to also have many off target effects. Therefore this chapter will examine the effects of genetically manipulating G6PD expression to further evaluate what functional effects G6PD may have in PCa cells.

6.2 Aims

The aims of this chapter are to:

1) Investigate the effects of G6PD knockdown in prostate cancer cells *in vitro.*

2) Examine the effect of G6PD knockdown in PCa cells *in vivo.*

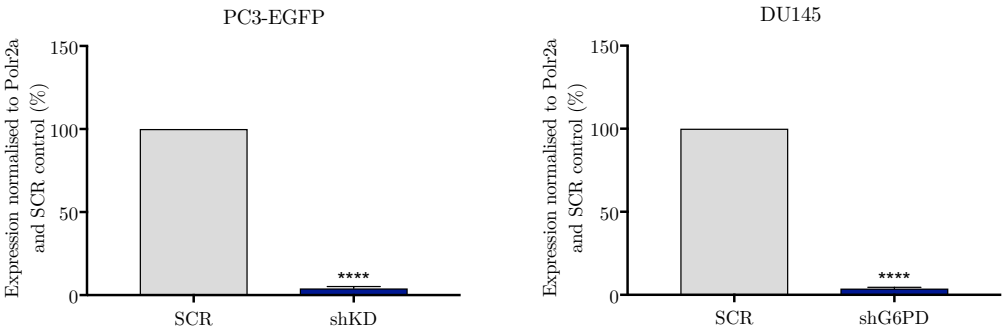
3) Explore the effects of G6PD overexpression *in vitro.*

6.3 Generation of stable G6PD knockdown cell lines

In order to investigate the functional effects of G6PD expression in prostate cancer, PC3-EGFP and DU145 cells which have high baseline expression of G6PD, were used to create stable G6PD knockdown (shG6PD) cell lines. Whilst the introduction of small interfering RNAs (siRNAs) into cultured cells provides a fast and efficient means of knocking down gene expression, short hairpin RNA constructs (shRNA) allow stable silencing of gene expression so that long-term effects can be studied and *in vivo* experiments performed.

The cell lines were created using a pLKO.1 plasmid with shRNA construct or scrambled control construct (SCR), which was transfected with packaging and envelope vectors (psPAX2 and pCMV-VSV-G) into HEK293T cells. After 48 hr the virus was collected, filtered and used to transduce the target prostate cancer cells, with the addition of Polybrene. Stable shG6PD cells were selected out using 4 μg/ml puromycin over 6 weeks. G6PD knockdown was confirmed at the mRNA (Figure 6.1A) protein level (Figure 6.1B).

A



B

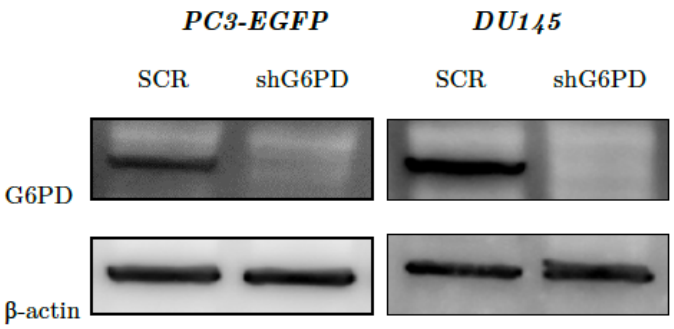


Figure 6.1 ***shKD of G6PD.*** *Stable knockdown was performed in PC3-EGFP and DU145 cells and confirmed at the mRNA (A), and at the protein level (B). Western blot representative of 3 biological repeats. Statistical test used = Student's t-test. **** p=<0.0001. Error bars = SEM.*

6.4 G6PD knockdown reduces the proliferation and colony forming ability of prostate cancer cells

Given the importance of the PPP in the proliferation of cells due to its role in the production of nucleotide precursors, the proliferation rate of shG6PD and SCR control prostate cancer cell lines was analysed. As might be expected, knockdown of G6PD reduced cell proliferation (Figure 6.2A), colony forming ability and colony size in PC3-EGFP and DU145 cells (Figure 6.2B); however, it did not have a significant effect on cell cycle in PC3-EGFP cells (Figure 6.2C).

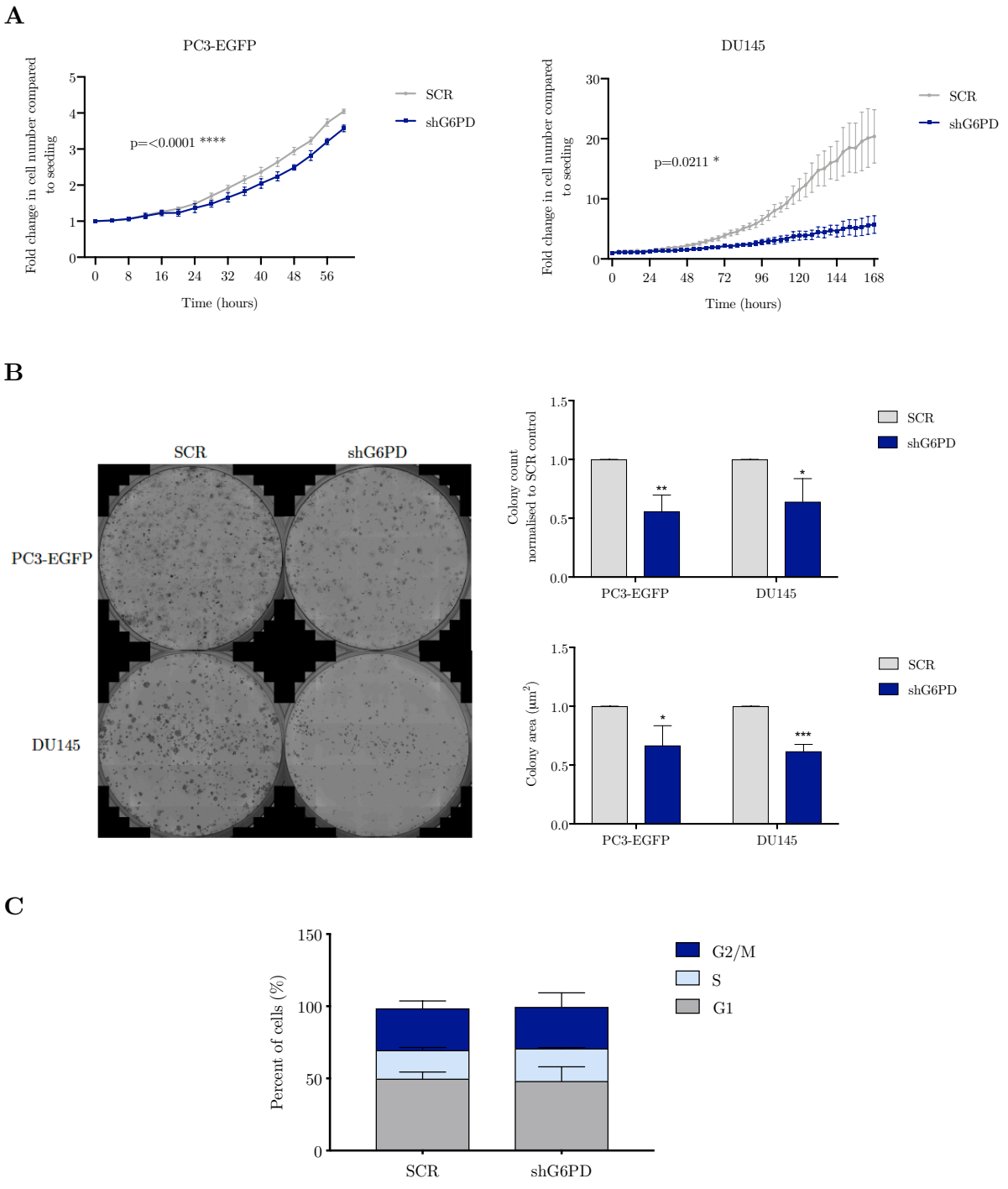
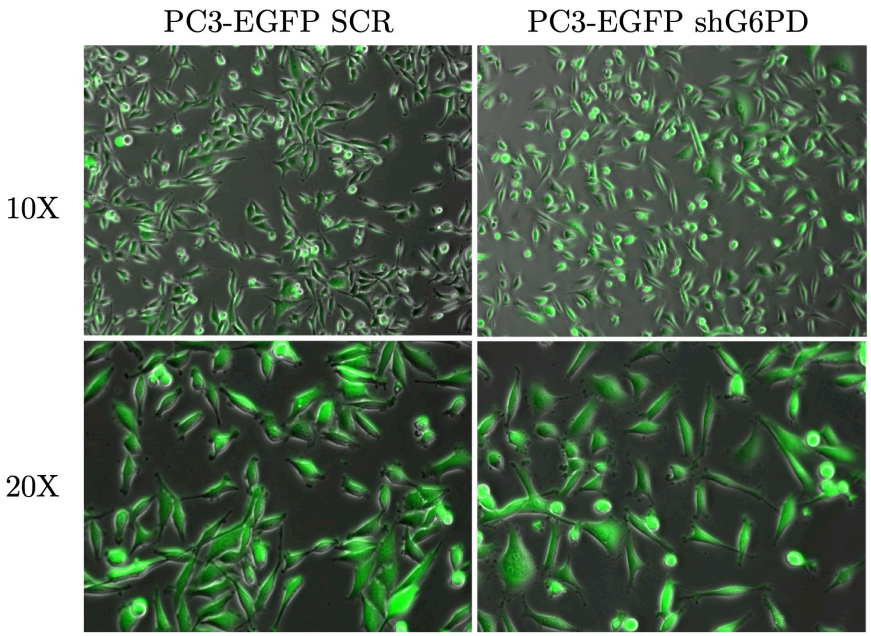


Figure 6.2 ***G6PD KD inhibits PC3-EGFP proliferation and colony formation but not cell cycle.*** *(A) Cell proliferation measured using an IncuCyte live cell imaging system. Statistical test used = two way ANOVA, column factor p-value shown. (B) Colony formation assay quantified using a Celigo imaging system. Statistical test used = Student's t-test. * p=<0.05, ** p=<0.01, ***p=<0.001. (C) PC3-EGFP SCR and shG6PD cell cycle stages analysed using flow cytometry. Error bars = SEM.*

6.5 G6PD knockdown alters the morphology of PCa cells

Cell morphology changes can dramatically alter cellular behaviours such as glucose uptake and metabolism, cell proliferation, differentiation and apoptosis[219]. After shKD of G6PD was performed, a subtle difference in the morphology of the PCa cell lines was noted. PC3-EGFP shG6PD cells became variable in morphology with an increase in the number of cells with a rounded appearance (Figure 6.3A). DU145 shG6PD cells also became more rounded in appearance, smaller, and appeared to lose their ability to form large stretched out cell clusters (Figure 6.3B).

A



B

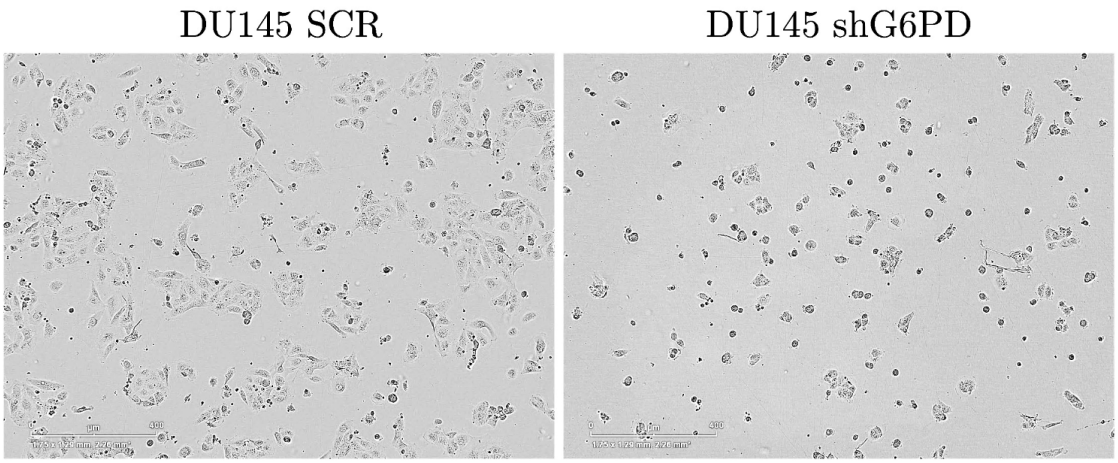


Figure 6.3 ***Morphology of G6PD shKD cells.*** *(A) PC3-EGFP SCR and shG6PD cells. Merged images of bright field and GFP. Images taken on a Nikon Eclipse TE300 inverted microscope. (B) DU145 SCR and shG6PD cells; 10X images taken on an IncuCyte live cell analysis imaging system.*

6.6 G6PD knockdown affects the expression of EMT markers

Epithelial-to-mesenchymal transition (EMT) was first defined as morphological reshaping of the epithelium that precedes mesenchymal invasion[220]. Having identified that shG6PD altered the morphology of PCa cells, it was postulated that this might reflect changes in the expression of epithelial and mesenchymal markers.

EMT plays an important role in prostate cancer invasion and metastases, and more recently has been shown to play a role in treatment resistance[221]. During EMT the cellular properties (cell-cell adhesion and cell polarity) of polarised epithelial cells are lost while an invasive mesenchymal phenotype is acquired. It is a complex and highly regulated process that can be characterised by the expression of certain transcription factors and cell-cell interaction markers by the cell. Epithelial markers include E-cadherin (CDH1) and β-catenin, whilst mesenchymal markers include Vimentin, N-cadherin and the transcription factors Slug, Snail, Twist, and Zinc finger E-box binding homeobox 2 (ZEB2), that are able to cause the transcriptional repression of CDH1, a defining event in EMT[17]. Expression of Twist and Vimentin have been shown to be prognostic of biochemical reoccurrence in prostate cancer patients undergoing radical prostatectomy for localised disease[222].

shG6PD caused down-regulation of ZEB2 in both PC3-EGFP and DU145 cells. In PC3-EGFP cells it also caused down-regulation of Vimentin and Twist, and CDH1 (Figure 6.4A). In DU145 cells shKD of G6PD caused up-regulation of CDH1 (Figure 6.4B). This suggests

shKD of G6PD might promote mesenchymal to epithelial transition (MET), repressing mesenchymal markers and promoting the expression of epithelial markers.

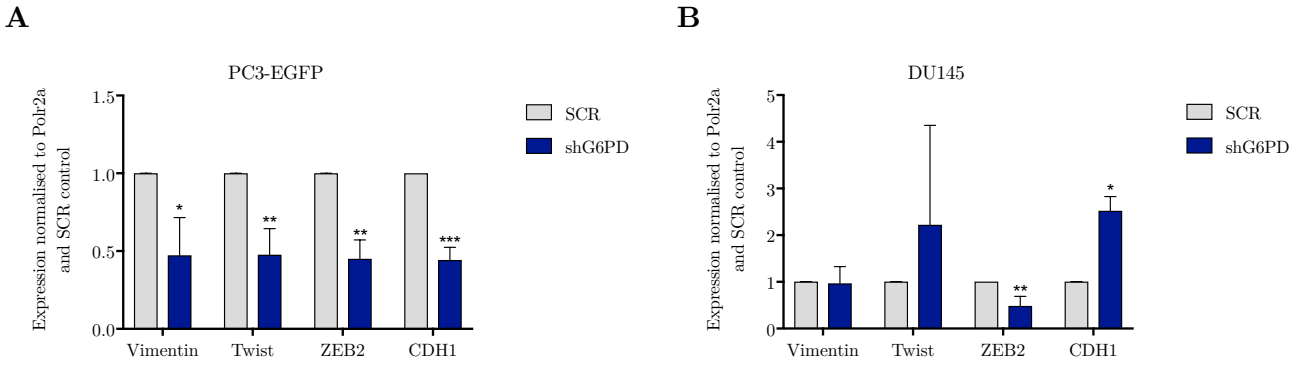
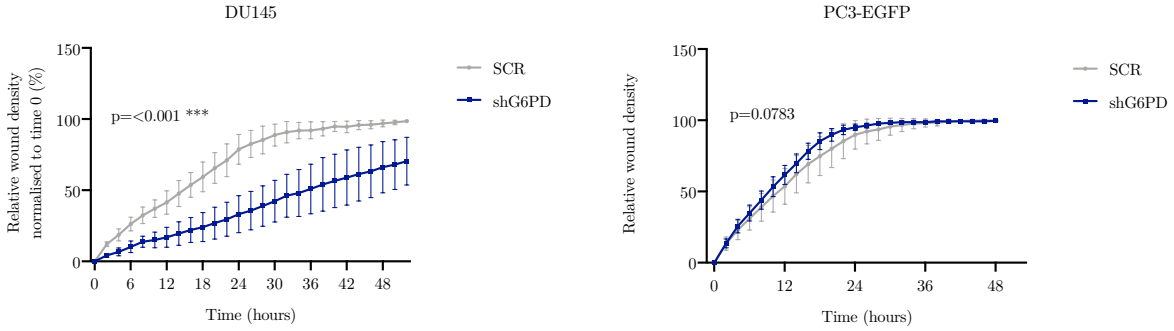


Figure 6.4 mRNA expression of EMT markers. *Sybr Green qPCR was performed to measure the expression of mesenchymal (Vimentin, Twist, ZEB2) and epithelial (CDH1) markers in PC3-EGFP (A) and DU145 (B) SCR and shG6PD KD cells. Expression normalised to the housekeeping gene Polr2a and the SCR control. Statistical test used = Student's t-test. * p=<0.05, ** p=<0.01, *** p=<0.001. Error bars = SEM.*

6.7 G6PD knockdown inhibits PCa cell migration

To investigate whether this alteration in expression of EMT markers had any functional effect on prostate cancer cells, the ability of shG6PD cells to migrate was examined using scratch wound assay and transwell migration assays. The scratch wound assay confirmed that shG6PD inhibited the migration of DU145 but not PC3-EGFP prostate cancer cells ($p<0.0001$)(Figure 6.5A). However, the migration of PC3-EGFP cells across a transwell was inhibited (Figure 6.5B) when compared to SCR control. This supports the finding of a reduced mesenchymal phenotype of shG6PD PCa cells.

A



B

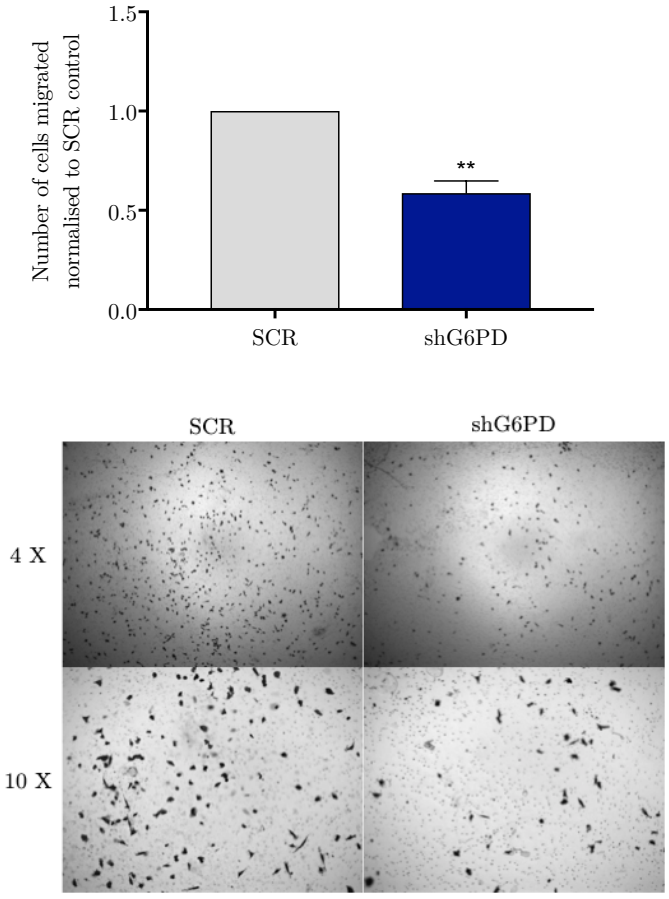
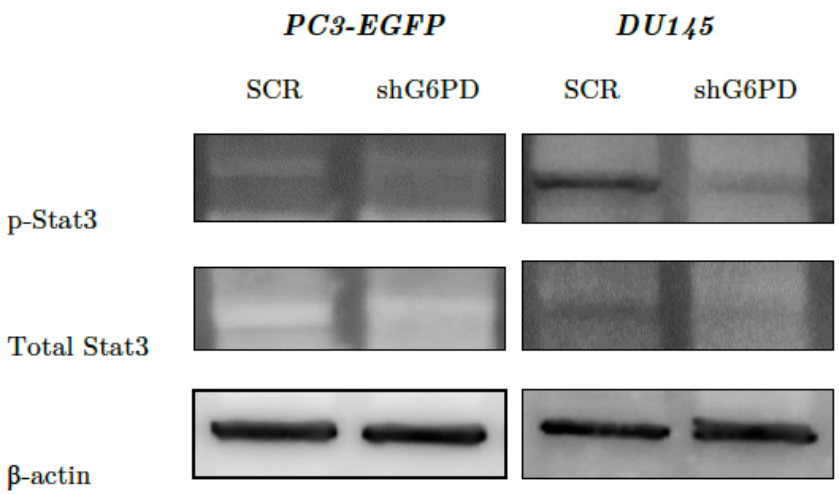


Figure 6.5 ***G6PD KD inhibits cancer cell migration.*** *(A) Scratch assay showing relative scratch wound confluency in DU145 and PC3-EGFP cells measured on an IncuCyte. Statistical test = two-way ANOVA. (B) Transwell migration assay showing PC3-EGFP migration through a transwell membrane at 24 hr and the number of cells migrated normalised to SCR control. Statistical test = Student's t-test, ** p=<0.01. Error bars = SEM.*

6.8 G6PD knockdown inhibits phosphorylation of STAT3

It has been reported by Lu *et al.* [223] that G6PD contributes to EMT via activation of the STAT3 pathway in hepatocellular carcinoma cells, and depletion of G6PD has been shown to reduce p-STAT3 protein levels in other cancer models[174]. Constitutive STAT3 activation is commonly seen in prostate tumours, and higher levels of STAT3 activation correlate with more malignant tumours exhibiting higher Gleason scores[224]. The effect of shG6PD on STAT3 phosphorylation was examined using western blotting. shG6PD reduced both p-STAT3 and total STAT3 protein in both PC3-EGFP and DU145 cells (Figure 6.6A), supporting a role for G6PD in modulating STAT3 signalling. It did not, however, have a significant effect on STAT3 mRNA levels (Figure 6.6B).

A



B

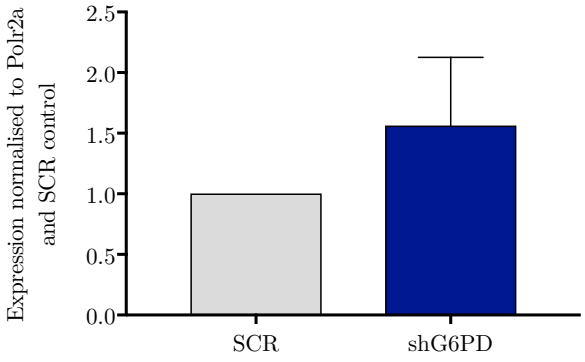


Figure 6.6 ***STAT3 inhibition by shG6PD KD.*** *(A) Protein expression of p-STAT3 and total STAT3 in PC3-EGFP and DU145 cells showed both p-STAT3 and total STAT3 are reduced in G6PD KD cells. (B) mRNA expression of total STAT3 in DU145. Statistical test= Student's t-test. Error bars = SEM.*

6.9 G6PD knockdown increases ROS levels and reduces levels of GSH

As previously described G6PD plays a vital role in ROS detoxification through its role in producing NADPH and regenerating GSH. The effect of G6PD knockdown on ROS and GSH levels was examined using specific luminescent assays. shG6PD significantly increased ROS levels in PC3-EGFP cells (Figure 6.7A), and significantly reduced GSH levels in DU145 cells (Figure 6.7B). This suggests that knockdown of G6PD can significantly alter the redox balance of PCa cells.

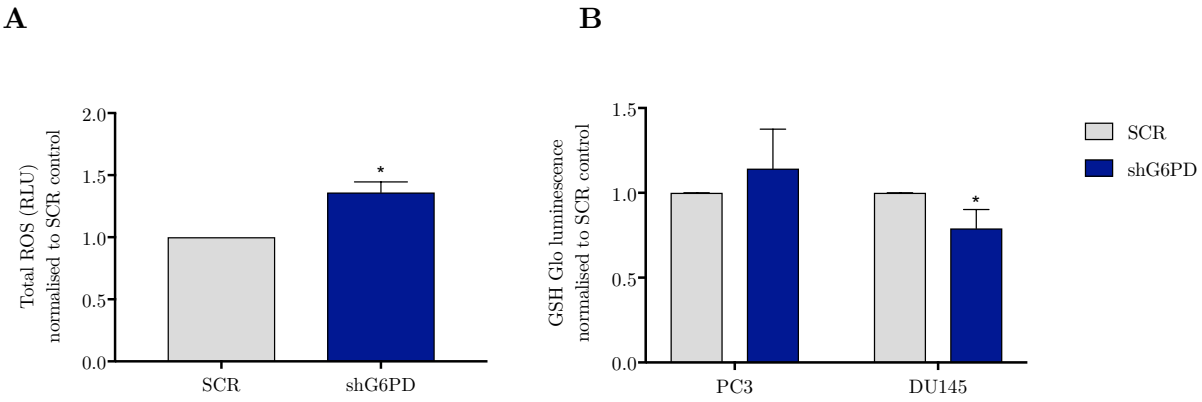


Figure 6.7 ***G6PD KD increases ROS levels and reduces GSH levels in prostate cancer cell lines.*** *(A) Total ROS levels measured by ROS-Glo in PC3-EGFP SCR and shG6PD KD cells. (B) GSH levels measure by GSH-Glo assay in PC3-EGFP and DU145 SCR and shG6PD KD cells. Statistical test = Student's t-test, * p=<0.05. Error bars = SEM.*

6.10 G6PD knockdown sensitises metastatic prostate cancer cell lines to chemotherapy

Chemotherapeutic agents are known to generate ROS, leading to oxidative stress and apoptosis induction. This increase in oxidative stress can interfere with cellular processes necessary for the anti-neoplastic activity (e.g. cell cycle progression), or can lead to increased apoptosis. Altering ROS levels has been shown by others to modulate sensitivity to chemotherapy. Docetaxel resistant PC3 cells have lower basal ROS compared to control PC3 cells, and NAC is able to reduce the sensitivity of PC3 cells to docetaxel[95]. In view of this, ROS levels and the effect of shG6PD on cell viability after chemotherapy treatment were investigated.

Docetaxel, cabazitaxel and cisplatin all caused a significant increase in mitochondrial ROS (Figure 6.8). shG6PD enhanced the reduced cellular viability caused by cisplatin and docetaxel in PC3-EGFP and DU145 cells (Figure 6.9), indicating that shG6PD can sensitise PCa to chemotherapy.

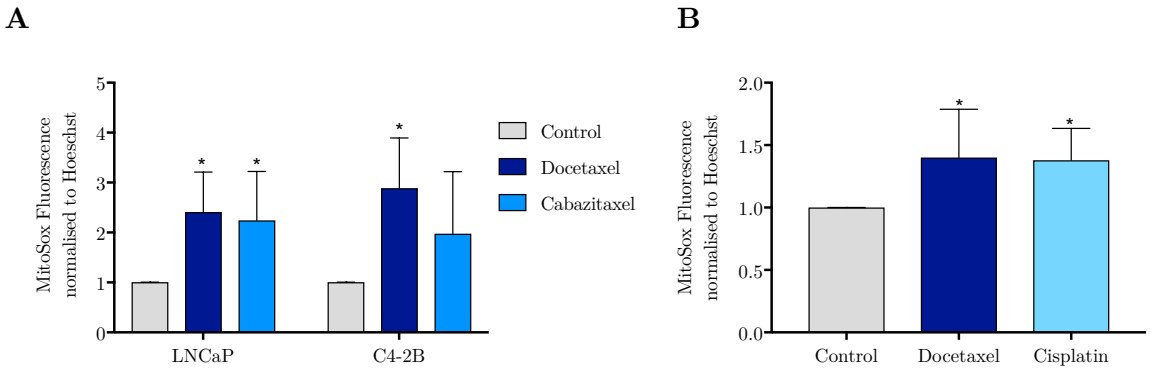


Figure 6.8 ***Chemotherapy increases mitochondrial ROS.*** *(A) MitoSox fluorescence measured after 72 hr treatment with 10nM docetaxel or 10μM cabazitaxel in LNCaP or C4-2B cells. (B) MitoSox fluorescence measured after 72 hr treatment with 10nM docetaxel or 10μM cisplatin in PC3 cells. Statistical test used = Student's t-test compared to untreated control. * p=<0.05. Error bars = SEM.*

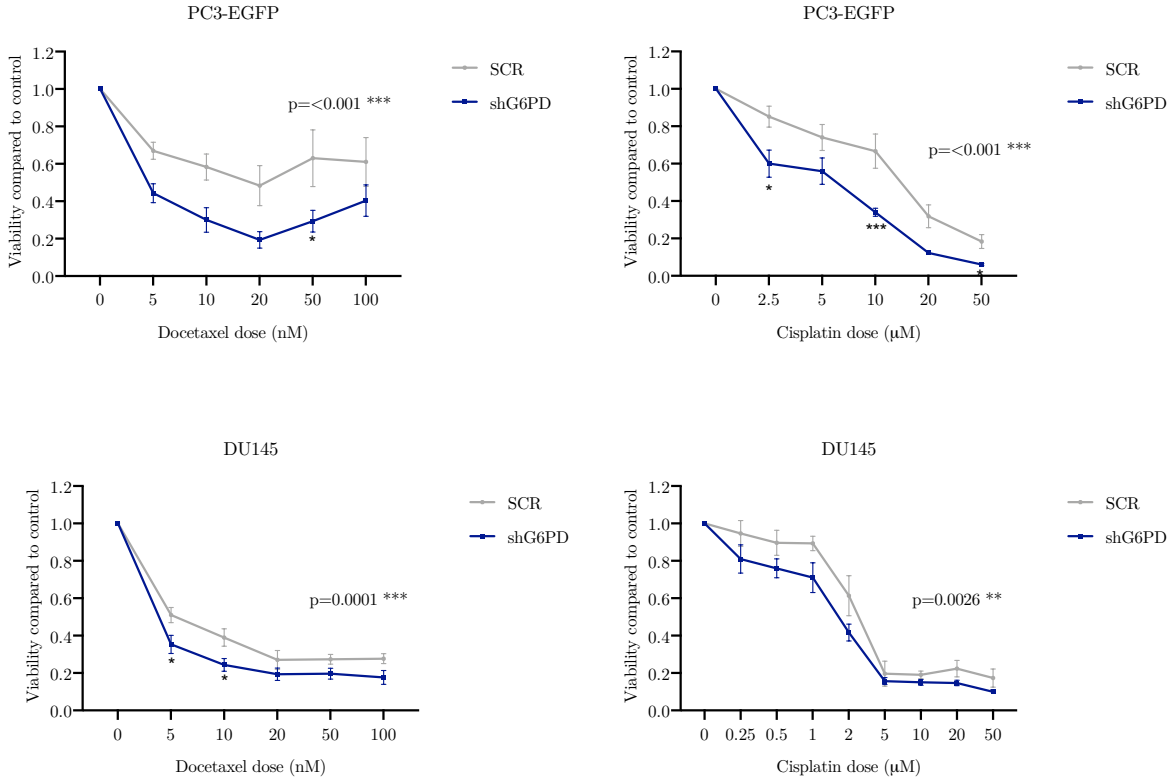


Figure 6.9 ***G6PD KD sensitises metastatic PCa cell lines to chemotherapy.*** *(A) Increase in mitochondrial ROS after 72 hr treatment with 10nM docetaxel or 10μM cabazitaxel. (B) Cell viability measured by Alamar blue in PC3-EGFP and DU145 scrambled (SCR) and shG6PD KD (shG6PD) cells. Statistical test used for all graphs = two way ANOVA with Sidak's multiple comparisons post hoc test. Error bars = SEM.*

6.11 Knockdown of G6PD causes alterations in the expression of several cancer hallmark gene sets

As shG6PD was observed to have a significant effect on the phenotype of PCa cells, it was investigated what other molecular pathways may be effected by performing RNA Seq of PC3-EGFP SCR and shG6PD cells.

A principal component analysis (PCA) plot confirmed good separation between SCR and shG6PD samples (Figure 6.10). A heat map was produced to show the top 30 differentially expressed genes after p-value adjustment (Figure 6.11A), and a volcano plot giving a graphical visualisation of the most altered genes (Figure 6.11B). As might be expected G6PD was one of the most differentially expressed genes between SCR and shG6PD ($p<0.0001$). However other genes that were noted to have a significantly lowered expression in shG6PD cells included LDHA, MT2A and REG4. LDHA encodes lactate dehydrogenase which catalyses the inter-conversion of pyruvate and L-lactate and has been shown to play a role in invasion and metastasis, and has been shown to be overexpressed in prostate cancer compared to benign tissue[225]. Inhibition of LDHA can inhibit PC3 proliferation, migration, invasion, and promote apoptosis. MT2A encodes metallothionein class 2A and is an antioxidant that is known to be overexpressed in prostate cancer and can promote PCa cell proliferation[226,227]. REG4 encodes regenerating islet-derived protein 4, a secretory protein involved in cell proliferation and differentiation that is known to be overexpressed in

hormone refractory prostate cancer[228]. Genes that were noted to be up-regulated in shG6PD included the structural genes EPB41L3, SDC1 and DAP. EPB41L3 plays a role in cytoskeletal rearrangement, cellular adhesion and motility and has been shown to be down-regulated in prostate cancer compared to benign tissue[229]. SDC1 encodes Syndecan 1, a cell surface heparin sulphate proteoglycan expressed by epithelial cells that is generally down-regulated in human cancers[230], and has been shown to be decreased in high Gleason grade PCa samples[231]; however, others have shown the opposite[232], so its role remains unclear. DAP encodes death-associated protein kinase 1, which plays a role in programmed cell death and can inhibit the migration of prostate cancer cells[233]. Overall, these findings would be in keeping with shG6PD causing a shift to a more epithelial, less invasive, less proliferative phenotype.

Pathway analysis was then performed using GSEA cancer hallmark gene set. 18/50 gene sets were found to be down-regulated in shG6PD compared to SCR PC3-EGFP cells, with 12 of these having an FDR <0.25, and 8 of these were significant with a nominal p-value <0.05 (Table 6.1A). Many of the down-regulated pathways are known to play a role in cell proliferation including "E2F targets", "G2M checkpoint", "Myc targets" and "TFG-β signalling", supporting the data showing differences in proliferative rate. There was also down-regulation of "hypoxia", "glycolysis" and "reactive oxygen species pathway". 32/50 genes sets were found to be up-regulated in shG6PD compared to SCR, but 21 of these had an FDR <0.25, and 13 had a nominal p-value <0.05 (Table 6.1B). Included in these gene sets were "epithelial mesenchymal transition" and two interleukin/STAT signalling pathways although these were not significant. This would be in keeping with the finding of

altered expression of EMT markers in shG6PD cells, and a non-significant increase in STAT3 which was noted at the mRNA level. Interestingly, immune / inflammatory response pathway ("interferon-α response", "inflammatory response", "complement") gene sets were noted to be up-regulated; however these were not investigated further.

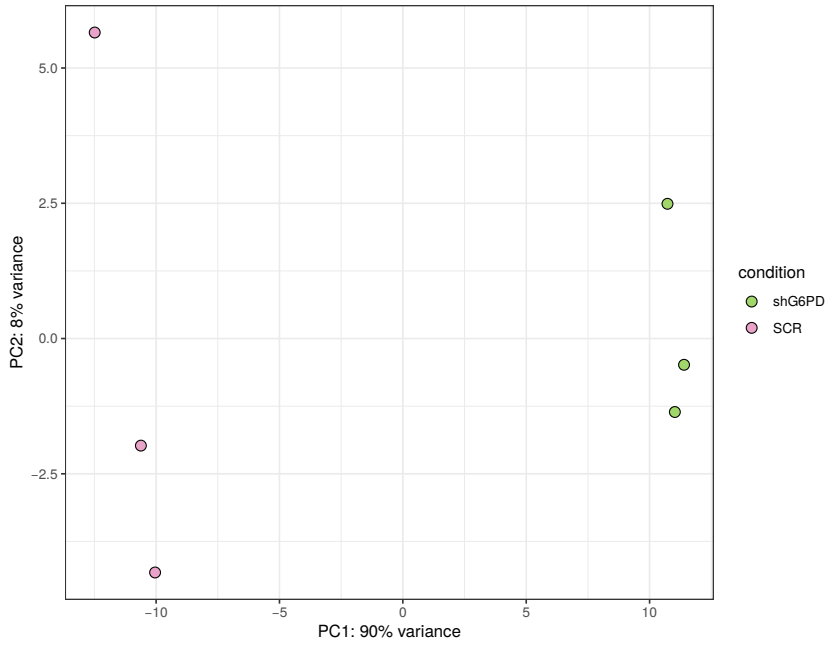
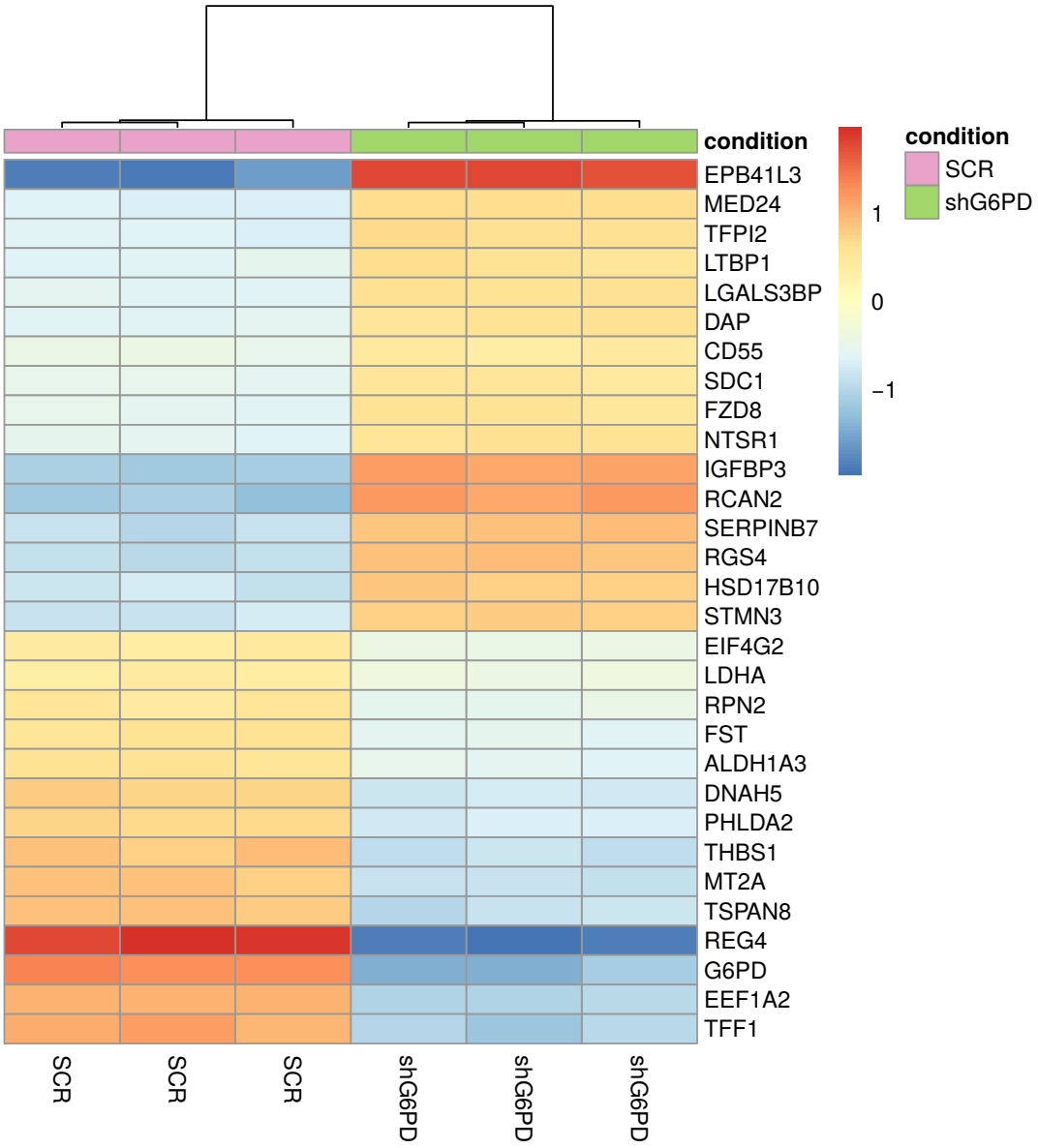


Figure 6.10 ***PCA plot from RNA Seq of PC3-EGFP SCR and shG6PD cells.***

A


condition
EPB41L3
MED24
TFPI2
LTBP1
LGALS3BP
DAP
CD55
SDC1
FZD8
NTSR1
IGFBP3
RCAN2
SERPINB7
RGS4
HSD17B10
STMN3
EIF4G2
LDHA
RPN2
FST
ALDH1A3
DNAH5
PHLDA2
THBS1
MT2A
TSPAN8
REG4
G6PD
EEF1A2
TFF1
SCR
SCR
SCR
shG6PD
shG6PD
shG6PD
1
0
−1
condition
SCR
shG6PD

B

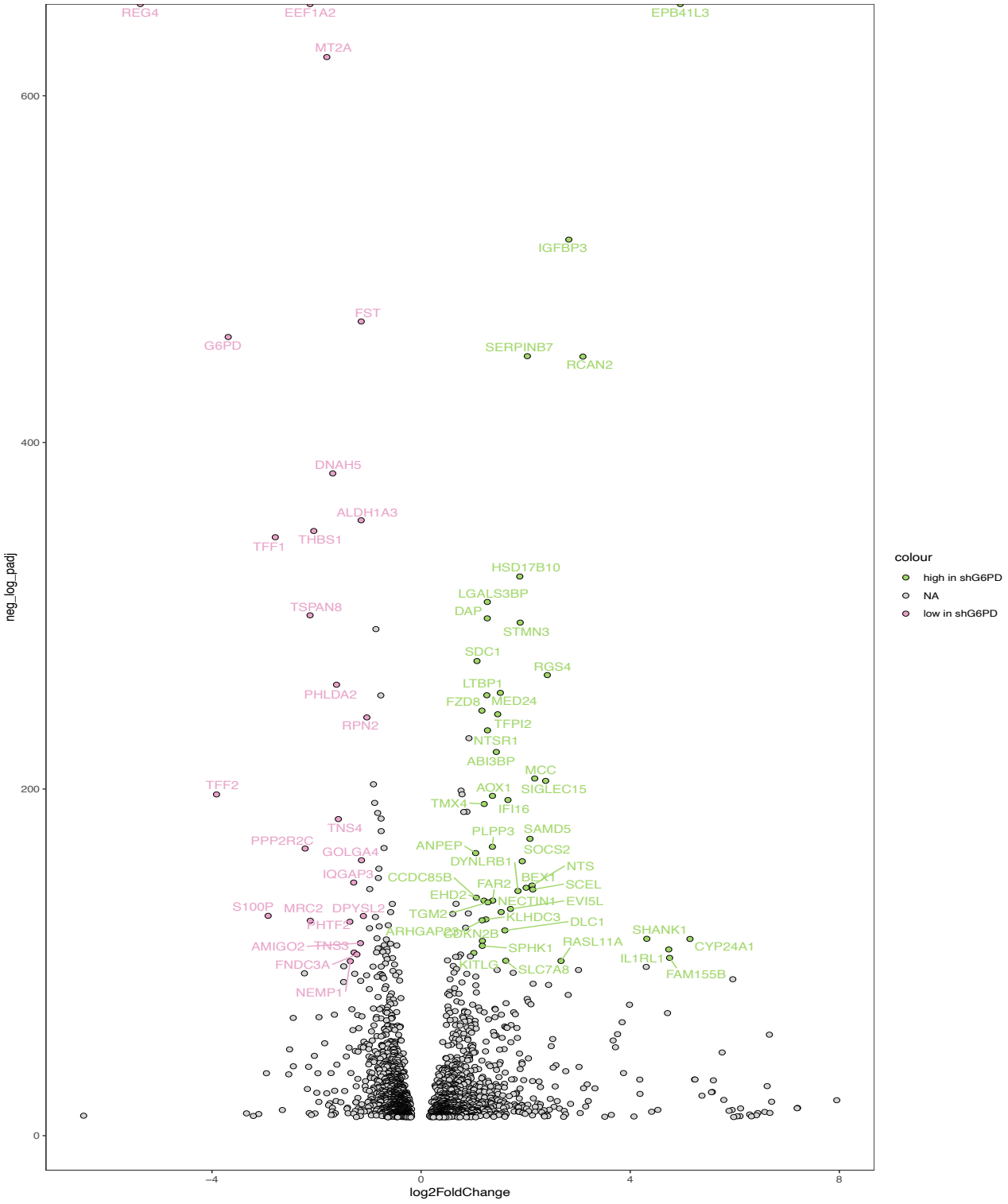


Figure 6.11 ***RNA Seq showing differentially expressed genes between PC3-EGFP SCR and shG6PD cells.*** *(A) Heat map of 30 most differentially expressed genes. (B) Volcano plot showing most differentially expressed genes (|log2FC|>1, -log10padj>100). N=3. Images and analysis performed by S.Rao.*

A

NAME	SIZE	ES	NES	NOM p-val	FDR q-val	FWER p-val
E2F TARGETS	196	-0.572	-2.589	0.000	0.000	0.000
G2M CHECKPOINT	195	-0.539	-2.489	0.000	0.000	0.000
MYC TARGETS V1	197	-0.396	-1.837	0.000	0.004	0.008
TGF BETA SIGNALING	53	-0.489	-1.820	0.000	0.004	0.010
MITOTIC SPINDLE	196	-0.337	-1.552	0.000	0.029	0.098
ESTROGEN RESPONSE LATE	174	-0.343	-1.545	0.000	0.026	0.103
GLYCOLYSIS	187	-0.319	-1.442	0.005	0.050	0.221
HYPOXIA	177	-0.280	-1.283	0.038	0.154	0.603
NOTCH SIGNALING	29	-0.396	-1.269	0.129	0.152	0.643
DNA REPAIR	140	-0.271	-1.212	0.102	0.208	0.789
ANGIOGENESIS	26	-0.381	-1.193	0.228	0.215	0.834
REACTIVE OXYGEN SPECIES	45	-0.319	-1.170	0.191	0.233	0.882

B

NAME	SIZE	ES	NES	NOM p-val	FDR q-val	FWER p-val
INTERFERON ALPHA RESPONSE	90	0.611	2.217	0.000	0.000	0.000
INFLAMMATORY RESPONSE	148	0.505	1.959	0.000	0.000	0.000
KRAS SIGNALING UP	154	0.486	1.905	0.000	0.001	0.002
INTERFERON GAMMA RESPONSE	162	0.474	1.857	0.000	0.001	0.005
PANCREAS BETA CELLS	22	0.631	1.740	0.002	0.005	0.031
APICAL SURFACE	35	0.529	1.657	0.017	0.012	0.081
COMPLEMENT	160	0.418	1.643	0.001	0.013	0.103
ALLOGRAFT REJECTION	126	0.425	1.614	0.003	0.017	0.143
TNFA SIGNALING VIA NFKA	186	0.393	1.581	0.001	0.020	0.185
EPITHELIAL MESENCHYMAL TRANSITION	176	0.393	1.571	0.001	0.019	0.200
UV RESPONSE DN	138	0.391	1.505	0.005	0.034	0.354
COAGULATION	99	0.397	1.445	0.023	0.056	0.548
P53 PATHWAY	187	0.345	1.376	0.015	0.097	0.785
CHOLESTEROL HOMEOSTASIS	70	0.372	1.315	0.084	0.150	0.925
IL2 STAT5 SIGNALING	165	0.326	1.283	0.057	0.181	0.964
APICAL JUNCTION	166	0.328	1.272	0.065	0.185	0.972
ESTORGEN RESPONSE EARLY	179	0.315	1.243	0.101	0.216	0.986
IL6 JAK STAT3 SIGNALING	67	0.356	1.236	0.166	0.215	0.989
MYOGENESIS	144	0.311	1.214	0.135	0.238	0.995
XENOBIOTIC METABOLISM	160	0.308	1.204	0.142	0.242	0.997
WNT BETA-CATENIN SIGNALING	35	0.392	1.202	0.216	0.233	0.997

Table 6.1 ***GSEA Cancer Hallmark gene sets analysis of PC3-EGFP shG6PD compared to SCR.*** *Gene sets with FDR q-val <0.25 shown. (A) Gene sets down-regulated in shG6PD compared to SCR. (B) Gene sets up-regulated in shG6PD compared to SCR.*

6.12 G6PD knockdown inhibits the proliferation of prostate cancer *in vivo*

To explore whether these effects were translatable to an *in vivo* mouse model the PC3 intra-tibial model was used. 1 x 10^5 PC3-EGFP SCR or shG6PD cells were inoculated into the tibias of 5 weeks old SCID mice and tumour burden was monitored by examining weight loss and fluorescence at the proximal tibia over time. Initial optimisation confirmed that GFP fluorescence of the cells as measured by the IVIS fluorescent imager correlated with cell number when PC3-EGFP cells were plated on tissue culture plastic (Figure 6.12A), while previous work confirmed mouse weight after tumour establishment correlated with PSA tumour burden in the C4-2B intra-tibial model (Figure 6.12B).

The mice inoculated with shG6PD PC3-EGFP cells had less weight loss when compared to the mice inoculated with SCR PC3-EGFP control cells (Figure 6.12C), and their weight loss was not significant compared to the PBS control group, while the SCR PC3-EGFP weight loss was significant. There was also less tumour fluorescence in the shG6PD PC3-EGFP inoculated mice compared to the SCR PC3-EGFP control mice, however this difference did not reach significance (Figure 6.12D-E). This suggests that shG6PD KD may inhibit the growth of prostate cancer cells *in vivo*.

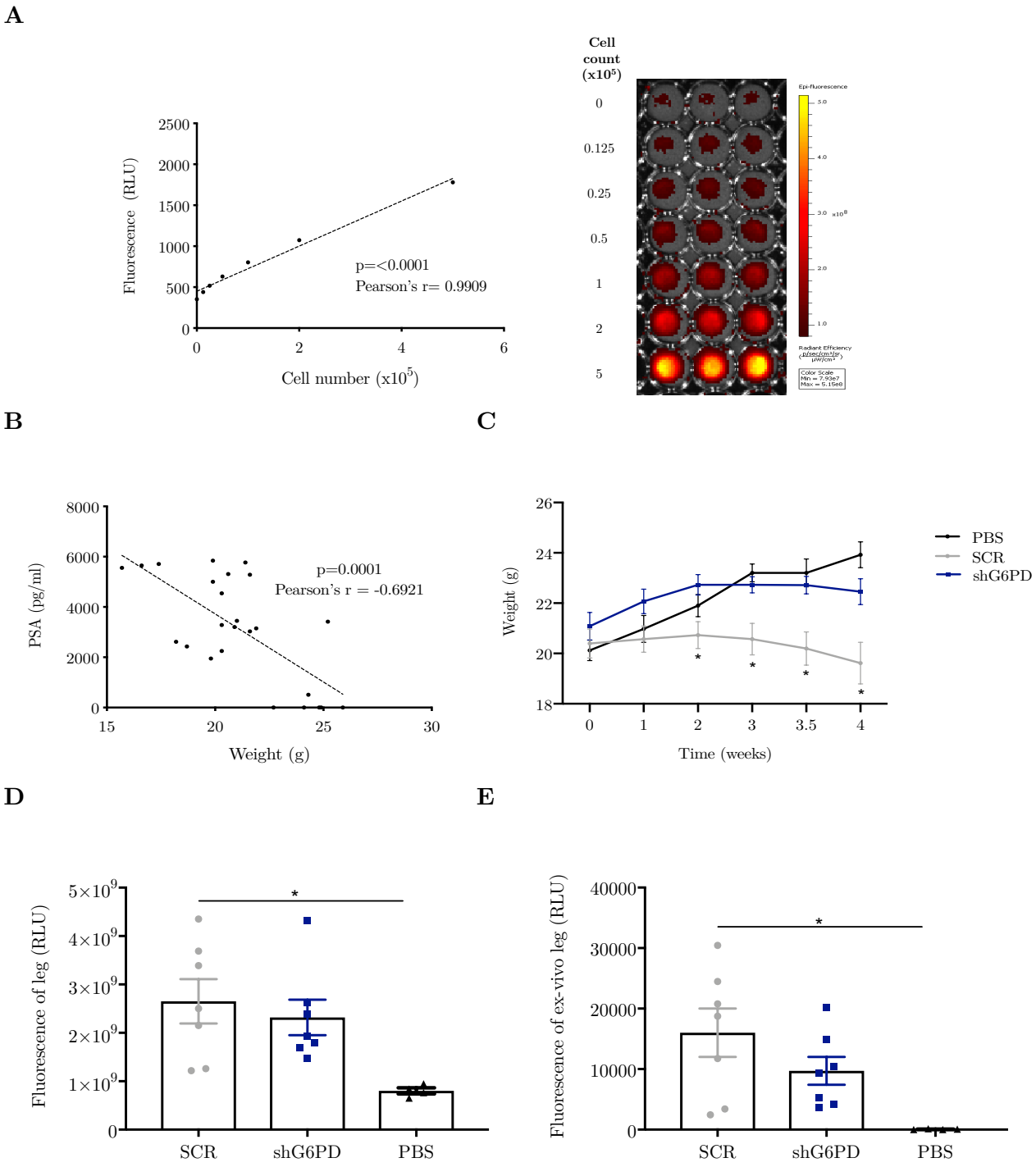


Figure 6.12 ***In vivo growth of PC3-EGFP SCR and shG6PD cells.*** *(A) Optimisation demonstrating fluorescence as measured by IVIS imager correlates with PC3-EGFP cell number. (B) Previous data showing that weight correlates with disease burden as measured by PSA in a C4-2B intra-tibial model. (C) Weight over time in the PC3-EGFP SCR and shG6PD mice. Statistical test = two-way ANOVA with Tukey post hoc test. Significance shown between SCR and shG6PD. (D) Fluorescence values as measured in vivo by the IVIS imager at week 4. (E) Fluorescence values as measured ex vivo by a Fluorostar Omega plate reader at week 4. Statistical test = one-way ANOVA with Tukey post hoc test. * p=<0.05. Error bars = SEM.*

6.13 Pharmacological inhibition of G6PD with 6-aminonicotinamide reduces viability and increases ROS in PCa cells

Having identified that shG6PD led to functional effects on prostate cancer cells, it was important to explore whether it is possible to target G6PD pharmacologically, and if this led to the same functional effects. 6-aminonicotinamide (6AN) has been reported by others to act as an inhibitor of G6PD[234], and it was able to significantly inhibit the activity of G6PD at a dose of 100 nM (Figure 6.13A). 6AN could reduce the viability of both LNCaP and PC3 cells, with a greater effect on the bone metastatic PC3 cells, suggesting that pharmacological inhibition of G6PD may have a greater effect in patients whose cancer has high baseline G6PD expression (Figure 6.13B). Cell death was increased in non-bone metastatic LNCaP and C4-2B cell lines after co-culture when compared to single culture (Figure 6.13C), again suggesting that G6PD inhibition may be most effective when cancer is in communication with the bone microenvironment or has higher G6PD expression. There was a trend for 6AN to increase ROS in prostate cancer cells, although it did not reach significance (Figure 6.13D).

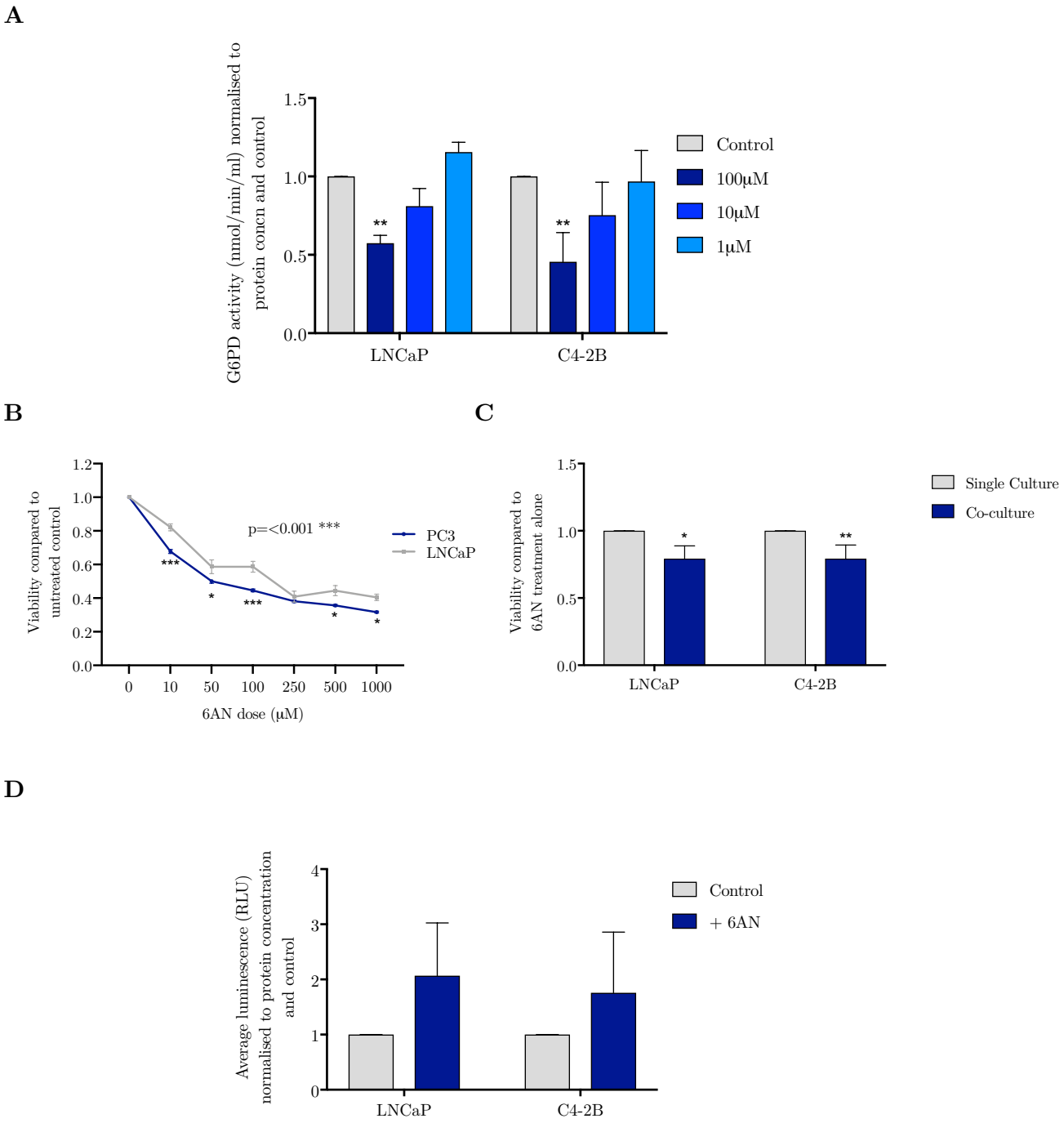


Figure 6.13 ***Pharmacological inhibition of G6PD with 6AN.*** *(A) G6PD activity in C4-2B (N=4) and LNCaP (N=2) cells after 24 hr treatment with varying doses of 6AN. Statistical test = one-way ANOVA with Dunnett's post hoc test. (B) Viability PC3 cells LNCaP cells measured by Alamar blue assay after 24 hr treatment with 6-AN. Statistical test = two-way ANOVA with Sidak's post hoc test. P-value shown = column factor. (C) Viability of LNCaP (N=3) and C4-2B (N=4) cells after treatment with 100nM 6AN for 72 hr in single culture or transwell co-culture measured by Alamar Blue assay after the removal of the transwell normalised to untreated control. Statistical test = Student's t-test. (D) Total ROS after 48 hr treatment with 100nM 6AN normalised to untreated control. Error bars = SEM. * p=<0.05, ** p=<0.01, *** p=<0.001. Error bars = SEM.*

6.14 Generation of G6PD overexpression cells

In order to investigate whether overexpression of G6PD as seen in the bone microenvironment has any functional effects on prostate cancer, LNCaP cells, which have low baseline expression of G6PD, were used to create a stable G6PD overexpressing (OE) cell line. The cell line was created using a TRC3 puromycin vector with an open reading frame (ORF) construct, which was transfected with packaging and envelope vectors (psPAX2 and pCMV-VSV-G) into HEK293T cells. After 48 hr the virus was collected, filtered and used to transduce, with the addition of Polybrene. Stable G6PD OE cells were selected out using 2 μg/ml puromycin over 6 weeks. G6PD OE was confirmed at the mRNA (Figure 6.14A) and protein level (Figure 6.14B). G6PD cells overexpressing blue fluorescent protein (BFP) under the same promoter were used as a control.

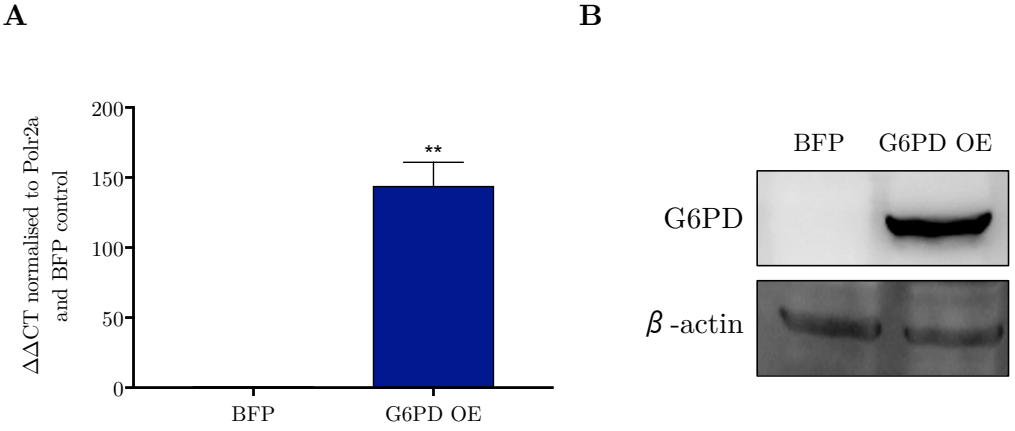


Figure 6.14 ***G6PD Overexpression in LNCaP cells.*** *(A) Taqman qPCR confirming G6PD overexpression. (B) Western blot confirming G6PD overexpression. Blot representative of 3 biological repeats. Statistical test = Student t-test. Error bars = SEM. ** p=<0.01. Error bars = SEM.*

6.15 Overexpression of G6PD increases the proliferation of PCa cells

The proliferation rate of G6PD OE LNCaP PCa cells was investigated using confluency measurements made by the IncuCyte plate reader, and a colony formation assay. In keeping with the shKD findings, overexpression of G6PD significantly increased the proliferation (Figure 6.15A) and colony forming ability (Figure 6.15B) of LNCaP cells.

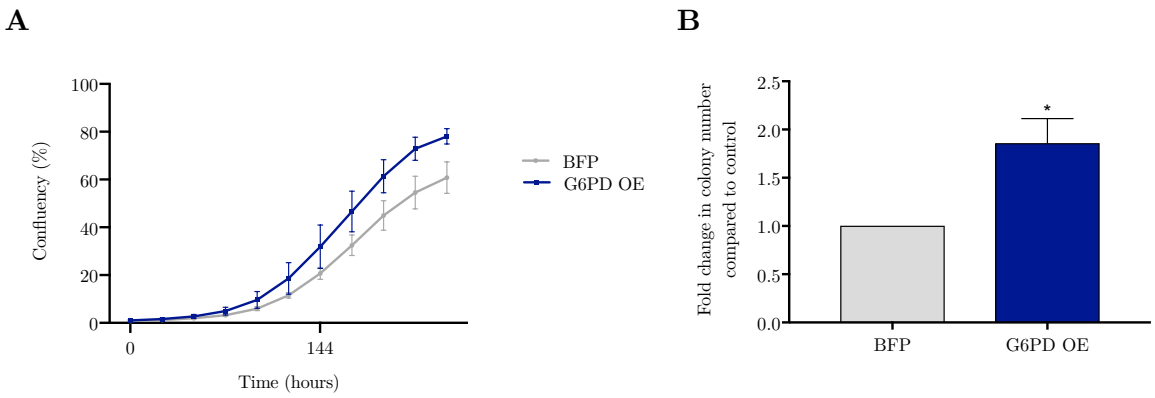
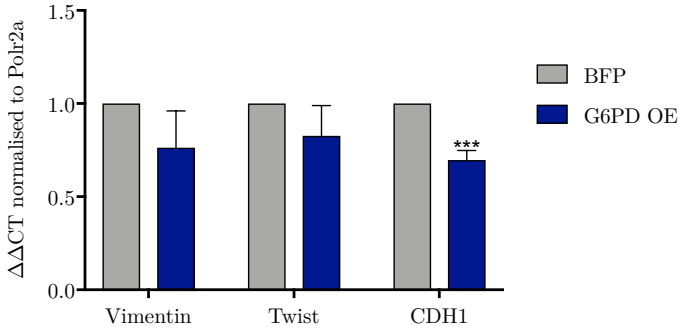


Figure 6.15 ***G6PD overexpression promotes proliferation and colony formation.*** *(A) LNCaP BFP or G6PD OE cells were seeded at 2 x 10^4 and percentage confluency measured by the IncuCyte every 24 hr. Statistical test = Student's t-test. p=<0.0001 ****. (B) LNCaP BFP or G6PD OE cells were seeded at 1 x 10^4 in a 6 well plate and left for 10 days before being fixed and stained with crystal violet and colonies counted by the Celigo imager. Statistical test used = Student's t-test. Error bars = SEM.*

6.16 Overexpression of G6PD down-regulates expression of an epithelial marker

Having demonstrated that shKD of G6PD might promote MET in PCa cells, the effect of G6PD overexpression on EMT markers was investigated. While G6PD OE did not significantly affect the expression of mesenchymal markers in PCa cells, it did decrease the expression of CDH1, a key epithelial marker, suggesting these cells might be less epithelial in phenotype (Figure 6.16A). No obvious change in morphology was noted between LNCaP BFP and LNCaP G6PD OE cells (Figure 6.16B).

A



B

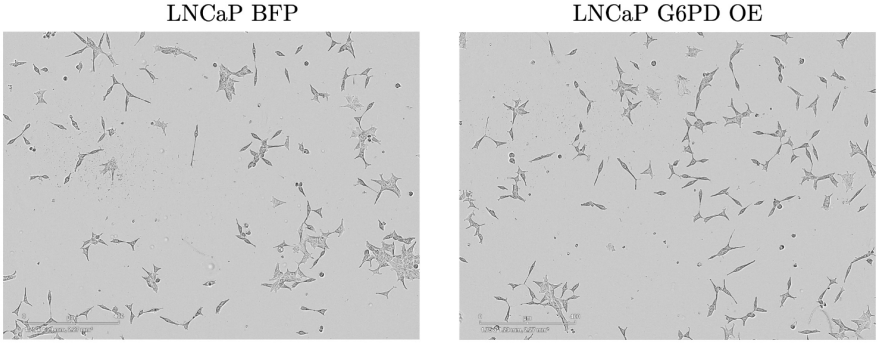


Figure 6.16 ***G6PD OE effect on EMT markers.*** *(A) Sybr Green qPCR examining the expression of EMT markers normalised to Polr2a. Statistical test = Student's t-test. Error bars = SEM. *** p=<0.001. (B) Morphology of LNCaP BFP and G6PD OE cells. 10X images taken on an IncuCyte live cell analysis imaging system.*

6.17 G6PD overexpression promotes STAT3 signalling

Having previously identified that shG6PD inhibited STAT3 phosphorylation it was hypothesised overexpression might also impact on this signalling pathway. G6PD OE led to increased phosphorylation of STAT3 protein (Figure 6.17A). In contrast however G6PD OE caused a significant decrease in total STAT3 mRNA levels (Figure 6.17B).

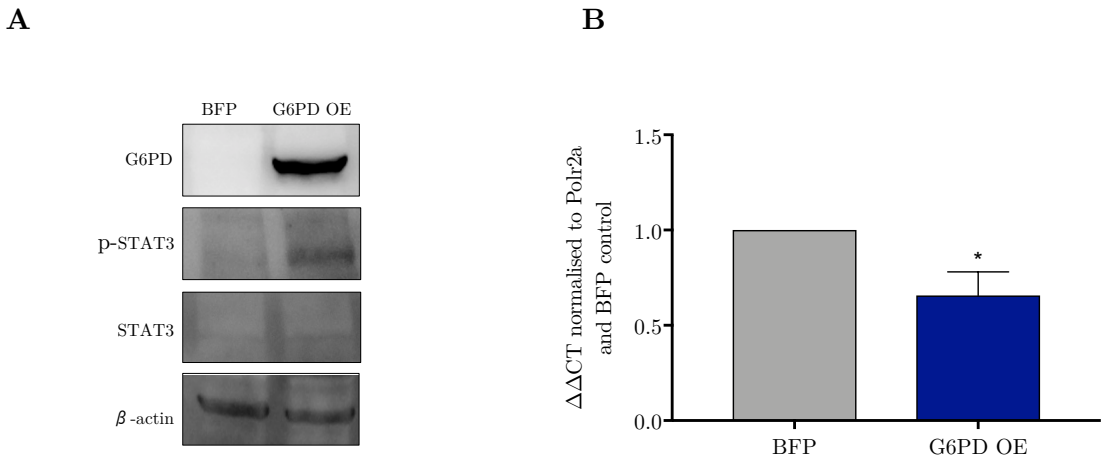


Figure 6.17 ***G6PD OE increases STAT3 phosphorylation.*** *(A) Western blot showing increased p-STAT3 in G6PD OE cells. (B) Sybr Green qPCR of STAT3 mRNA normalised to Polr2a and BFP control. Statistical test = Student's t-test. Error bars = SEM. * p=<0.05.*

6.18 Overexpression of G6PD in LNCaP cells decreases their baseline ROS level

In view of the finding that knockdown of G6PD increased basal ROS levels, it was investigated whether overexpression of G6PD might also impact on cellular ROS levels. In keeping with the shKD results G6PD OE significantly decreased LNCaP cells basal ROS levels (Figure 6.18).

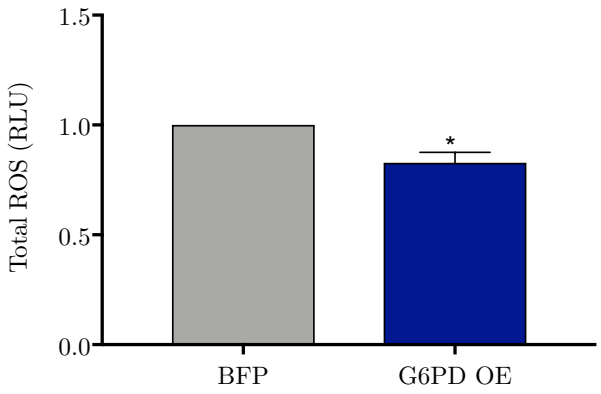


Figure 6.18 ***Total ROS in G6PD OE cells*** *normalised to BFP control. N=4. Statistical test = Student's t-test. Error bars = SEM. * p=<0.05.*

6.19 Overexpression of G6PD in LNCaP cells did not increase resistance to chemotherapy

Having noted that G6PD knockdown enhances sensitivity of PCa cells to chemotherapy, the chemosensitivity of G6PD OE cells was investigated. G6PD OE caused a trend towards increased resistance to docetaxel chemotherapy (Figure 6.19A) but did not appear to affect sensitivity to cisplatin chemotherapy (Figure 6.19B). These results did not reach statistical significance.

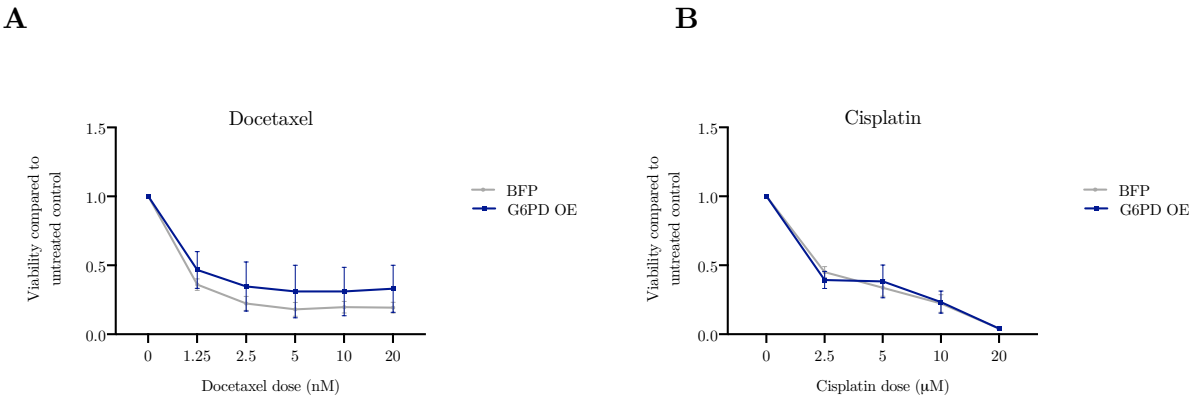


Figure 6.19 ***G6PD OE did not increase resistance to chemotherapy.*** *(A) LNCaP BFP and G6PD OE viability after docetaxel treatment as measured by Alamar Blue assay. (B) LNCaP BFP and G6PD OE viability after cisplatin treatment as measured by Alamar Blue assay. Statistical test = two-way ANOVA with post hoc Sidak's test. Error bars = SEM.*

6.20 Discussion

The results in this chapter have shown that targeting G6PD in metastatic prostate cancer cell lines can inhibit cancer cell proliferation and colony formation *in vitro*, and potentially also inhibit prostate cancer growth *in vivo*. In contrast, G6PD overexpression was found to increase PCa proliferation. RNA Seq identified that many of the genes altered in PC3-EGFP shG6PD cells are involved in cell proliferation, migration and invasiveness, in keeping with the *in vitro* findings. The *in vivo* model used was limited by the inability to sensitively monitor tumour burden with a serum marker such as PSA, as PC3-EGFP cells do not secrete this protein. Mice have a significant amount of auto-fluorescence that overlaps with the GFP spectrum making it difficult to accurately determine tumour burden in this model (Appendix A2). This likely limited the significance of the data achievable from this experiment. However, overall these results are in keeping with the finding of studies in other cancers. Zhang *et al.* have shown that subcutaneous growth of G6PD knockdown 786-O renal adenocarcinoma cells was slower and produced smaller tumours than control non-silenced cells, whilst G6PD overexpressing 786-O cells produced significantly faster and larger tumours in nude mice[174]. Kuo *et al.* have shown that G6PD overexpression in NIH 3T3 mouse fibroblast cells caused increased tumour size compared to the parental cell line[106]. Ju *et al.* have shown a trend towards smaller subcutaneous DLD-1 and HCT116 colorectal adenocarcinoma tumours in nude mice with G6PD knockdown cells compared to scrambled control, but like my study these differences did not reach statistical significance. However, the shG6PD tumours had significantly higher cleaved caspase 3 staining and percentage

apoptosis index quantified by terminal deoxynucleotidyl transferase dUTP nick end labelling (TUNEL) staining, suggesting that there is increased apoptosis in the shG6PD tumours[103]. Hu *et al.* have demonstrated that shG6PD significantly inhibited the growth of A375 human dermal melanoma cell subcutaneous xenografts in nude mice and significantly down-regulated the expression of the apoptosis inhibitory factors Bcl-2 and Bcl-xL[235]. My results are also in keeping with a previous study in prostate cancer where G6PD suppression inhibited the proliferation of LNCaP and C4-2 cells *in vitro*[113], however this thesis has explored this for the first time in bone metastatic prostate cancer cells *in vitro* and *in vivo*.

shG6PD inhibited expression of mesenchymal markers and promoted the expression of the epithelial marker CDH1 (E-cadherin) in DU145 cells, whilst G6PD OE caused significant down-regulation of CDH1. shG6PD also caused morphological alterations and inhibited the migration of PCa cells suggesting targeting G6PD causes a shift towards a more epithelial phenotype. In view of these results targeting G6PD may inhibit the spread of prostate cancer from its primary site, or potentially prevent the spread of further tumours from metastatic sites. Increasingly, it is being realised that EMT does not represent two distinct states but instead is a spectrum of epithelial and mesenchymal phenotypes with cancer cells undergoing partial EMT where both epithelial and mesenchymal markers may be co-expressed[236]. This might explain the down-regulation of both epithelial and mesenchymal markers seen in PC3-EGFP shG6PD cells. Overall these results are in contrast to a study performed by Wu *et al.* that found that knockdown of G6PD in A549 lung adenocarcinoma cells led to decreased CDH1 expression and increased migration[237]. However, the results are in keeping with work performed by others. Fang *et al.* found that G6PD inhibition or

silencing altered the morphology of HeLa cervical cancer cells with more variance in morphology and more rounded and less spindle like appearance to cells[238]. They also found that G6PD inhibition decreased cell motility in a dose-dependent manner. Kuo *et al.* found that overexpression of G6PD in NIH 3T3 mouse fibroblast cells led to the cells becoming smaller and loosing contact inhibition[106]. Nagashio *et al.* found that in patient lung cancer samples increased G6PD expression in the invasive front led to poorer survival, and that high G6PD expression correlated with greater pleural, vascular and lymphatic invasion suggesting that these results are translatable to patient samples[104]. Hu *et al.* found that G6PD silencing inhibited the migration and invasion of hepatocellular carcinoma cell lines *in vitro* and also inhibited STAT3 phosphorylation[239]. STAT3 has been shown by others to play a role in promoting EMT[240], with suppression of STAT3 phosphorylation leading to reduced expression of mesenchymal markers, increased expression of epithelial markers and decreased invasion and migration of PCa cells. shG6PD cells had reduced levels of phosphorylated STAT3, whilst G6PD OE cells had increased levels, and this may in part explain the altered expression of EMT markers seen. Zhang *et al.* also found that G6PD knockdown could attenuate the levels of p-STAT3 and STAT3 in renal cell carcinoma cells whilst G6PD overexpression increased their protein levels. However they did not examine EMT markers or the migratory phenotype of these cells. Overall there appears to be a greater body of evidence supporting G6PD inhibition leading to reduced migration and invasion and a more epithelial morphology, perhaps via alterations in STAT3 signalling. However, more work needs to be done to elucidate this further.

G6PD plays an important role in modulating the redox state of the cell, and it was found that shG6PD led to increased ROS levels and decreased GSH, whilst G6PD OE cells had decreased ROS. These results suggest that shG6PD leads to reduced NADPH levels, leading to increased sensitivity to oxidative stress, whilst G6PD OE leads to increased NADPH and greater protection against ROS. In keeping with this it was found shG6PD could sensitise prostate cancer cells to cisplatin and docetaxel chemotherapy; however, G6PD OE did not significantly increase chemotherapy resistance. These results are supported by work performed in other cancer models. Fang *et al.* found that G6PD inhibition led to increase ROS in HeLa cells[238]. Ju *et al.* found that G6PD inhibition led to decreased $NADPH/NADP^+$ ratio, decreased GSH/GSSG ratio, increased ROS, and increased sensitivity to H_2O_2 and chemotherapy in colorectal adenocarcinoma cell lines[103]. Hong *et al.* found that multidrug resistant A549 lung carcinoma cells had increased G6PD, increased GSH and increased $NADPH/NADP^+$ ratio compared to the parental non-drug resistant cell line, and that inhibiting G6PD could restore cisplatin sensitivity in this cell line via inducing oxidative stress[115]. Xu *et al.* found similar results in the ovarian cancer cell line SKOV3[241]. Collectively these data suggest that targeting G6PD in combination with currently used chemotherapies may improve their efficacy.

Targeting G6PD pharmacologically with 6AN was also able to inhibit proliferation and cause increased ROS, suggesting that it may be feasible to achieve results similar to the shG6PD model with pharmaceutical agents. The two most commonly studied G6PD inhibitors are 6AN[242] and DHEA[243]. Tsouko *et al.* also found 6AN could inhibit prostate cancer proliferation, reduce NADPH levels and increase intracellular ROS *in vitro*[113], further

supporting my data. 6AN is a competitive G6PD and 6PGD inhibitor however it causes severe side effects such as nerve damage and vitamin B deficiency. It is also rapidly excreted and so the doses required to sensitise tumour cells to chemotherapy *in vitro* are difficult to achieve *in vivo*[244]. DHEA acts as an uncompetitive G6PD inhibitor, but high oral doses are required and it can cause the generation of active androgens, the effects of which are unclear in prostate cancer[234]. Polydatin and other polyphenols have more recently been shown to inhibit G6PD and have been used in an *in vivo* study, inhibiting tumour growth and metastases and sensitizing tumours to chemotherapy[207]. However, they are also limited in their lack of specificity and therefore there is a need for novel pharmacological agents specifically targeting G6PD.

6.21 Future Direction

In view of the limitations of monitoring tumour burden in the PC3-EGFP shG6PD model, inoculating LNCaP OE cells intra-tibially, and monitoring disease burden via PSA levels in the serum might allow us to more accurately determine tumour growth *in vivo* and give more meaningful data. It would be particularly interesting to combine G6PD manipulation with chemotherapy or radiotherapy treatment, to see if G6PD OE increased resistance to these therapies *in vivo* although this has not yet been demonstrated *in vitro*. It would also be interesting to perform RNA Seq on G6PD OE cells to see which genes and pathway changes correlate with the shG6PD findings.

Whilst genetically manipulating G6PD expression has been vital in elucidating the exact effects of G6PD in prostate cancer cells, it is unlikely to represent a viable technique for the treatment of patients, and therefore it is important to identify new and specific inhibitors of G6PD. Further work exploring the effects of these inhibitors *in vitro* and *in vivo* will hopefully lead to future clinical trials targeting the PPP in patients.

Radiotherapy is a frequently used treatment modality in localised prostate cancer, and Radium-223 is the only bone metastatic targeted therapy that has been shown to improve survival as well as bone symptoms in mCRPC. Targeting G6PD has been shown to improve the efficacy of radiotherapy in other cancer cells[245,246], and therefore once a suitable pharmacological inhibitor has been identified it would be interesting to explore combining G6PD inhibition with radiotherapy to explore whether its efficacy could be improved.

7

Summary and Future Directions

7.1 Summary

Prostate cancer remains the most common malignancy in men in the Western world, and once it has metastasised, typically to the bone, management is currently palliative as the disease develops resistance to the treatments used. It has long been recognised that metabolic changes occur in cancer. However, for many years cancer metabolism has been a neglected field, and the importance of metabolic changes on the behaviour of cancer cells is only more recently being recognised. By better understanding the metabolic changes that

underpin malignant transformation and metastases, it may be possible to identify novel therapeutic targets to improve treatments for men with this currently incurable disease.

This project sought to identify the metabolic changes that occur in prostate cancer cells when they metastasise, specifically to the bone microenvironment, with the aim of identifying novel targets for advanced prostate cancer therapeutics.

Chapter 3 investigates the effect of the bone microenvironment, and more specifically BMSCs on the metabolism of PCa cells. Mass spectrometry screening of metabolite changes in PCa cells after co-culture with BMSCs found that BMSC induced metabolic changes in PCa cells, and that metabolites of the PPP and the later parts of the glycolysis and TCA pathways were consistently elevated in PCa cells across the different BMSCs. In particular a significant increase in NADPH, and decrease in $NADP^+$ supported a role for increased PPP flux during co-culture. To confirm that these findings were relevant to human disease, multiple *in silico* analyses of publicly available data sets were performed. This confirmed that metabolic pathways were among the most altered of all cancer hallmark pathways in metastases compared to primary tumours and identified up-regulation of OXPHOS, the TCA cycle, glutathione metabolism, ROS detoxification and fatty acid biosynthesis. The PPP was also noted to be up-regulated in metastases but did not quite reach significance in both data sets. Further, *in vitro* work confirmed that protein expression of TCA and OXPHOS enzymes is increased in prostate cancer compared to benign cell lines, but did not identify a difference between bone metastatic and non-bone metastatic cell lines. This supports work performed by others demonstrating that these pathways may have a role in the early development of malignancy. In contrast, PPP enzymes were found to be more

highly expressed in bone metastatic PCa cell lines compared to benign or non-bone metastatic cell lines, suggesting that this may be a metastatic / bone specific effect. This pathway was therefore selected for further studies.

Chapter 4 explored whether the bone microenvironment could drive this up-regulation of the PPP, and more specifically up-regulation of its rate-limiting enzyme G6PD, and the mechanisms by which this occurred. Further *in silico* analyses of multiple data sets revealed that G6PD was consistently up-regulated in metastatic, and specifically bone metastatic PCa samples. It also identified that treatment may drive up-regulation of G6PD as levels increased in castrate resistant disease. This is in keeping with previously published findings in other cancers including lung, gastric, breast and renal cell carcinoma[104,105,107,110], but is the first time this has been demonstrated in PCa. Up-regulation of G6PD could be recreated *in vitro* by co-culture with CM from HS5 BMSCs. This effect was enhanced in androgen-deprived conditions, supporting a role for PCa treatments in further driving this effect. It was identified that IL-6 secreted by the BMSCs was at least in part driving the up-regulation of G6PD in PCa cells, and the effect could be blocked by neutralising antibody or recreated by recombinant IL-6. IL-6 serum levels have long been recognised as being elevated in metastatic or CRPC patients compared to healthy men or men with localised disease[194,195] and high IL-6 has been correlated with poorer clinical outcomes and resistance to chemotherapies[196,197] however, the role of the PPP in modulating these IL-6 pro-tumourigenic effects has not been explored. Further, clinical trials targeting IL-6 have so far been disappointing, with a range of toxicities due to its impact on a multitude of pathways.

Targeting G6PD may therefore be a novel refined way to target some of the pro-tumourigenic effects IL-6 has on PCa growth and drug resistance.

In view of the PPP's known critical role in the cells redox balance and proliferative fate in other cellular systems, Chapter 5 investigated whether BMSCs modulate this in PCa cells. It was found that BMSCs caused an increase in mitochondrial and total ROS in PCa cells, but also caused an increase in their anti-oxidant ability. This is in keeping with what has been demonstrated in other cancer models[103,207]. Inhibition of G6PD caused a trend towards a further increase in ROS suggesting a feedback loop where G6PD may be up-regulated to manage the extra ROS produced after interactions with BMSCs. Neutralising ROS with an antioxidant could inhibit G6PD protein up-regulation caused by BMSC CM suggesting ROS might drive theses changes alongside IL-6. Finally, it was demonstrated *in vitro* and *in vivo* that BMSCs can have a toxic effect on non-bone metastatic cell lines leading to cell cycle arrest and growth inhibition. I hypothesise that this might be due to increased ROS produced by the BMSCs and secreted into the microenvironment, or the BMSCs causing a shift in PCa's metabolism towards greater OXPHOS leading to greater production of ROS, upsetting the redox balance in the prostate cancer cell. I hypothesise that this might cause selection of a PCa cell population that is able to withstand high ROS levels through up-regulation for their anti-oxidant pathways and in particular G6PD. This selection process could in part drive drug resistance. ROS are known to promote osteoclast activity and inhibit osteoblast activity[211–213] and therefore some of the features of PCa bone disease could also be explained by these changes in redox state. Initially high ROS in the bone microenvironment could drive increased osteoclast activity, but as the PCa cells become

more adept at managing ROS, the levels might fall promoting osteoblastic activity and contributing further to the osteoblastic metastases seen (Figure 7.1).

.

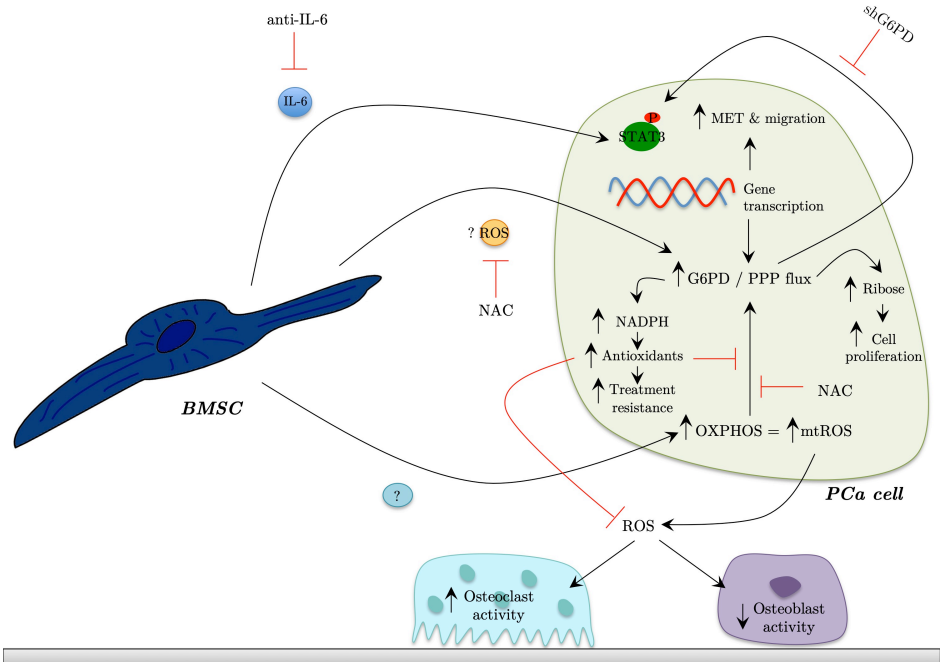


Figure 7.1 ***Summary of the main findings of this thesis*** *including the potential effects and control mechanisms.*

Chapter 6 examined the effects of targeting G6PD to better determine the effects this might have on PCa (Figure 7.2). Knocking down G6PD in metastatic PCa cell lines inhibited their proliferation and colony formation *in vitro*, and potentially also inhibited PCa growth *in vivo*, while G6PD OE could increase PCa proliferation. This is in keeping with the findings in several other cancer models[103,106,113,174,235]. shG6PD also caused in a shift in PCa cells towards a more epithelial phenotype with more rounded cell appearance, reduced migration, down-regulation of mesenchymal markers and up-regulation of an epithelial marker (CDH1),

while G6PD OE caused down-regulation of CDH1. RNA Seq confirmed that knockdown of G6PD reduced the expression of genes that promote a proliferative, invasiveness phenotype, and up-regulation of genes that inhibit this. This suggests that targeting this pathway could inhibit the spread of PCa from its primary site, or potentially prevent the spread of further tumours from metastatic sites. It is again in keeping with work performed in other cancer models *in vitro*[106,238,239] and in patient lung cancer samples[104] suggesting that these findings are also relevant in the clinical setting. I hypothesise that these effects on EMT might be regulated by alterations in the STAT3 signalling pathway as suppression of STAT3 signalling, as seen in the shG6PD cells, has been shown by others to lead to reduced expression of mesenchymal markers and increase expression of epithelial markers and decreased invasion and migration of PCa cells[240]. The effect of modulating G6PD expression on PCa cellular ROS levels and sensitivity to chemotherapy was examined. shG6PD led to increased ROS and decreased anti-oxidants (GSH), whilst G6PD OE lowered cellular ROS. Chemotherapy is known to induce its anti-cancer effects at least in part though ROS-induced cellular damage, and therefore in keeping with these results shG6PD sensitised PCa cells to cisplatin and docetaxel chemotherapy, whilst G6PD OE had a trend towards increased resistance to docetaxel that did not reach significance, potentially due to the doses used being too high for LNCaP cells that are relatively chemosensitive. These results are also supported by published findings in other cancer models[103,115,238,241] and have been shown to be translatable to *in vivo* mouse models.

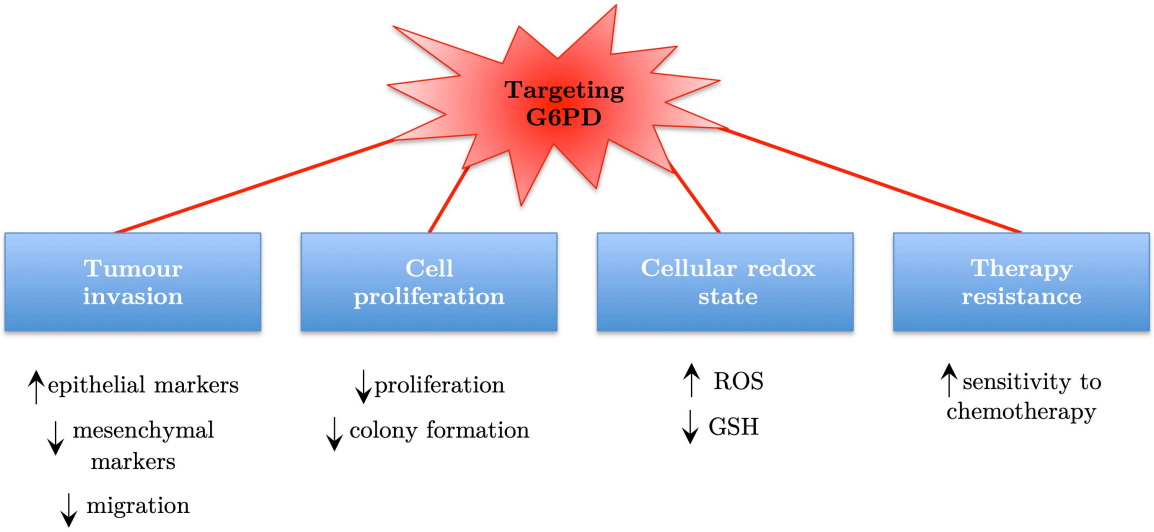


Figure 7.2 ***Summary of the effects of inhibiting G6PD in prostate cancer cells.***

Finally, the effects of targeting G6PD pharmacologically with 6AN were investigated. Whilst this inhibitor is not specific to G6PD, it was able to induce many of the effects seen in the shG6PD model, including inhibition of PCa proliferation and increased ROS. This suggests that G6PD may be a feasible pharmacological target, and as more G6PD inhibitors with greater specificity are identified it is hoped this will lead to further *in vivo* work confirming its efficacy as an anti-cancer strategy, and ultimately to clinical trials of these agents in advanced bone metastatic prostate cancer. These therapies have the potential not only to have direct anti-tumour effect on cancer proliferation and migration, but could also improve the efficacy of currently used therapies allowing them to be used at lower, less toxic doses.

7.2 Future Directions

7.2.10 Further exploration into the metabolic changes induced by the bone microenvironment

The impact of metastatic site stromal cells on cancer metabolism has been relatively unexamined to date. Whilst this thesis has demonstrated that BMSCs can impact PCa metabolism, there is much more work that needs to be done to further elucidate these changes, and to distinguish the effects of different BMSCs seen within the bone microenvironment. The CE-MS analysis was suitable for examining glycolysis, the TCA cycle and PPP, but was not suitable for the analysis of fatty acid pathways, and so this is an area that remains unexamined. The CE-MS analysis was only performed on *in vitro* samples, and it would be interesting to repeat the analysis on *in vivo* tumours or even patient samples to see if the changes are visible in these more relevant samples. Metabolomics remains a relatively novel field, and therefore the technologies and techniques to analyse metabolic changes is rapidly advancing. With this it is hoped that significant steps will be taken in elucidating the metabolic changes that underpin malignant change and metastatic progression. In particular advances in imaging techniques may enable us to visualise metabolic changes in a non-invasive manner allowing us an insight into the metabolic changes seen in patients and how these may change over the course of their treatment and disease[172].

7.2.11 The effect of androgens on G6PD expression

The thesis found that both in patient samples and *in vitro* cell culture ADT therapy increased G6PD expression. This is intriguing as DHEA, a testosterone precursor, is a recognised inhibitor of G6PD, and low serum DHEA is correlated with higher Gleason score, advanced clinical stage and poorer prognosis in PCa[186–188]. The correlation between DHEA levels and G6PD expression or PPP activity has not been previously reported, and therefore elucidating this in patient samples might provide information on the correlation between androgens and the PPP. Better understanding of this might enable us to enhance targeting of the androgen signalling pathway to improve the efficacy of ADT, which remains the mainstay of treatment in advanced bone metastatic PCa.

7.2.12 The correlation between G6PD expression and treatment resistance in PCa

The *in vitro* studies performed showed that knockdown of G6PD could increase sensitivity to chemotherapy. It has been shown in other cancers that G6PD expression in cancer cells correlates with patient chemosensitivity[103]; however, this has not been explored in PCa. By correlating G6PD expression via immunohistochemistry with patients' response to chemotherapy, it may be possible to better identify which patients will benefit most from this treatment, and potentially identify which patients might benefit most from combining chemotherapy with G6PD inhibition. This work could be complemented by further *in vivo* studies using shG6PD or G6PD OE cells combined with chemotherapy in an intra-tibial mouse model, to confirm whether the results achieved *in vitro* and achievable in the more

complex *in vivo* model. It would also be interesting to explore whether targeting G6PD could improve the efficacy of radiotherapy in PCa, in view of the fact this has been demonstrated in other cancers[245,246]. Radium-223 is the only PCa bone targeted therapy that has been shown to improve survival as well as bone symptoms, and combining it with G6PD inhibition could enhance its efficacy.

7.2.13 Does long term conditioning of PCa cells with BMSCs select a drug resistant population?

Whilst this thesis identified that BMSCs increased G6PD in PCa cells which could potentially increase their proliferation, it was also identified that HS5 BMSC CM was toxic to non-bone metastatic PCa cells both *in vitro* and *in vivo* models. I hypothesise that this might be due to high IL-6 causing increased ROS which are initially toxic to the PCa cells, but eventually select for a population with high G6PD and therefore higher antioxidants (NADPH) and proliferative potential (via increased ribose sugars). I hypothesise that IL-6 might drive this increase in ROS via inducing OXPHOS up-regulation, although this has yet to be investigated. To explore this, I would perform long-term conditioning over several months of non-bone metastatic PCa cells with HS5 CM to see if the surviving population was more resistant to chemotherapy, had stable up-regulation of G6PD, and had increased OXPHOS compared to non-conditioned or HS27A conditioned PCa cells. Combining this with anti-IL-6 or recombinant IL-6 could confirm whether it is IL-6 driving this effect.

7.2.14 Does manipulating G6PD in PCa cells impact on bone remodelling?

The work in this thesis has looked only at the effects of BMSCs on PCa, and not vice versa. Having identified that BMSCs induce increased antioxidant potential, but also increased ROS in PCa cells, it would be interesting to see if there is any diffusion of this altered redox state into BMSCs and if this impacts on bone remodelling (Figure 7.1). ROS-producing stimuli can promote osteoclast activity whilst inhibiting osteoblast activity[211–213] and so exploring this by co-culture of shG6PD or G6PD OE cells with osteoclasts or osteoblasts might provide further insight into this.

7.2.15 The identification of novel G6PD targeted therapies

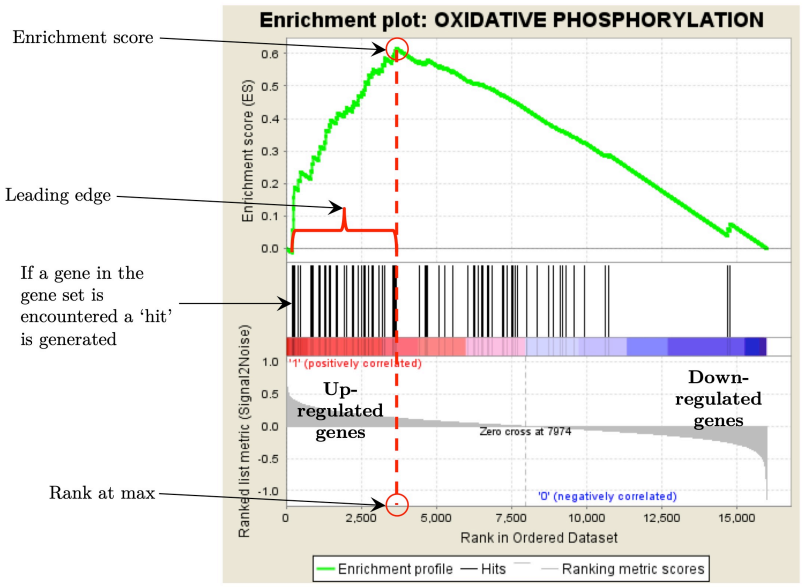
The identification of safe, specific G6PD inhibitors for use in patients will allow studies to translate the findings of this work into the clinic for patients' benefit. Work has already been performed by others to identify novel G6PD inhibitors, not only for use as an anti-cancer drug, but also as a drug for parasitic diseases[234,247–249]. As these drugs become more readily their efficacy in inhibiting cancer growth in models of prostate cancer bone metastases should be investigated.

7.3 Summary statement

In summary, the bone microenvironment, and in particular BMSCs, can induce changes in the metabolism of prostate cancer cells. In particular they induce up-regulation of the PPP and its rate-limiting enzyme G6PD. This occurs via IL-6 signalling, and by inducing high ROS levels. Targeting G6PD can inhibit PCa proliferation, migration, EMT, redox state and drug sensitivity, and therefore has the potential to be a novel therapeutic target in advanced bone metastatic PCa.

Appendix A

A.1 Metrics of GSEA analysis



Four key metrics of GSEA analysis:

1. Enrichment score (ES): reflects the degree to which a gene set is overrepresented at the top or bottom of a ranked list of genes.

2. Normalised enrichment score (NES): Corrects for the differences in ES between gene-sets due to differences in gene set sizes. It allows comparison between different gene sets.

3. False Discovery Rate (FDR): corrects for multiple hypothesis testing and is the estimated probability that the NES of a gene set is false. For this analysis a NES was judged to be significant if the FDR was <25% / 0.25 in view of the large sample size.

4. Nominal p-value (Nom p-value): estimates the statistical significance of the ES for a single gene set i.e. no correction for multiple hypothesis testing. For this analysis a Nom p-value of <0.05 was judged to be significant.

A.2 Autofluorescence of mice in the intra-tibial PC3-EGFP model

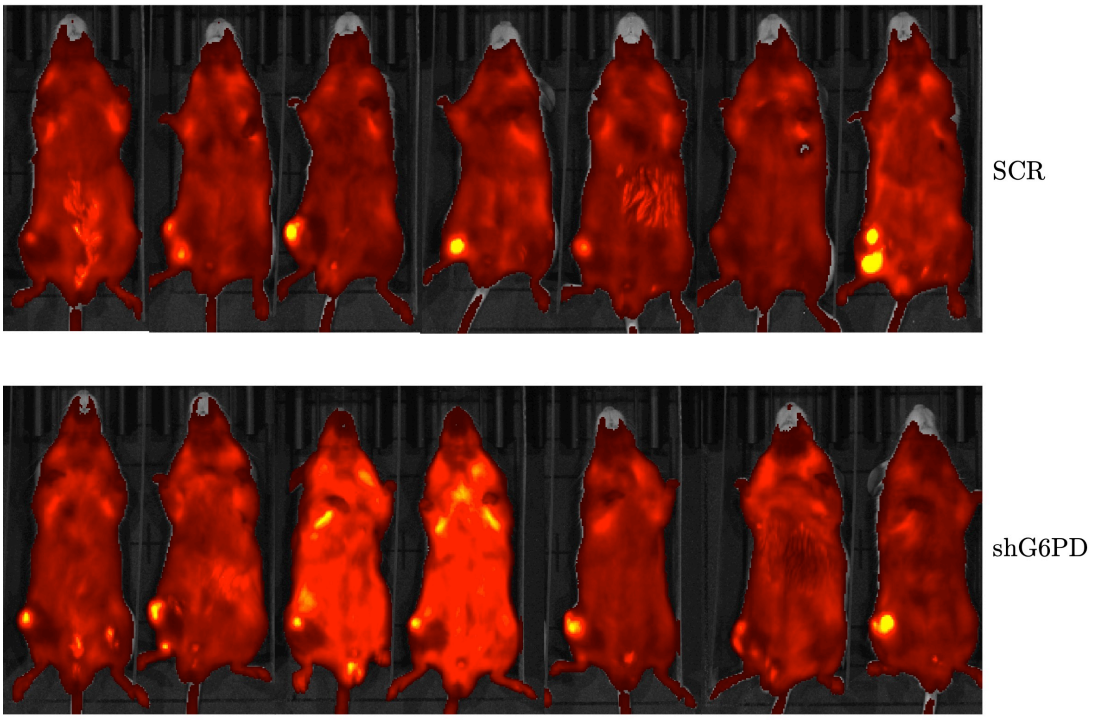


Figure A.2. ***Autofluorescence of CB17 SCID mice*** *inoculated with PC3-EGFP SCR (top) and shG6PD (bottom) cells demonstrating the difficultly of sensitively detecting tumour burden.*

Appendix B

Publications

Whitburn J, Edwards C, Sooriakumaran P. Metformin and prostate cancer: a new role for an old drug. Cur Urol Rep Jun 2017.

Prizes and Fellowships

British Association of Urological Surgeons Academic Research Prize (1st), London, 2019

European Association of Urology (EAU), Best Abstract by a Resident Prize (3rd), Barcelona, 2019

Merck Innovation Cup Finalist, Team Oncology, Frankfurt 2019.

International Society of Cancer Metabolism (ISCaM) Travel Prize, Bratislava, 2018

Japanese Society for the Promotion of Science (JSPS) Summer Fellowship, Japan, 2016.

Presentations

Whitburn J, Rao S, Tabata S, Hirayama A, Soga T, Hamdy F, Edwards C. The bone microenvironment drives upregulation of the pentose phosphate pathway in prostate cancer thereby promoting a pro-antioxidant environment. Presented at EAU Annual Meeting, Barcelona 2019, The Royal Society of Medicine Urology Section Malcolm Coptcoat spring short papers and BAUS academic research prize meeting, London 2019; and the Nuffield Department of Surgical Sciences Away Day, Oxford 2019.

Whitburn J, Rao S, Tabata S, Hirayama A, Soga T, Hamdy F, Edwards C. The prostate cancer-bone environment causes upregulation of the Pentose phosphate pathway. Presented at EAU Annual Meeting, London 2017.

Whitburn J, Rao S, Tabata S, Hirayama A, Soga T, Hamdy F, Edwards C. The prostate cancer-bone environment causes upregulation of the Pentose phosphate pathway. Presented at the Nuffield Department of Surgical Sciences Away Day, Oxford 2017.

Whitburn J, Edwards C, Hamdy F. Evaluating the metabolic relationship in the prostate cancer bone microenvironment. Presented at the JSPS Summer Fellowship Meeting, Tokyo 2016.

Posters

Whitburn J, Rao S, Tabata S, Hirayama A, Soga T, Hamdy F, Edwards C. Unravelling the metabolic relationship in the prostate cancer-bone microenvironment; a novel role for the pentose phosphate pathway. Presented at ISCaM Annual Meeting Bratislava 2018

Whitburn J, Rao S, Tabata S, Hirayama A, Soga T, Hamdy F, Edwards C. Unravelling the metabolic relationship in the prostate cancer-bone microenvironment; a novel role for the pentose phosphate pathway. Presented at Cancer and Bone Society (CABS) Annual Meeting Oxford 2018.

Whitburn J, Rao S, Tabata S, Hirayama A, Soga T, Hamdy F, Edwards C. Co-culture of prostate cancer cells with bone stromal cells causes up-regulation of the pentose phosphate pathway. Presented at the ISCaM Annual Meeting, Brussels 2016.

Whitburn J, Rao S, Tabata S, Hirayama A, Soga T, Hamdy F, Edwards C. Co-culture of prostate cancer cells with bone stromal cells causes up-regulation of the pentose phosphate pathway. MitOx Meeting, Oxford 2016.

Bibliography

1. Blandy JP, L. B. *The Prostate*. (London: Butterworths, 1986).
2. Kavanagh, J. P., Darby, C. & Costello, C. B. The response of seven prostatic fluid components to prostatic disease. *Int. J. Androl.* **5**, 487–496 (1982).
3. Gevaert, T. *et al.* Characterization of subepithelial interstitial cells in normal and pathological human prostate. *Histopathology* **65**, 418–428 (2014).
4. Packer, J. R. & Maitland, N. J. The molecular and cellular origin of human prostate cancer. *Biochim. Biophys. Acta - Mol. Cell Res.* **1863**, 1238–1260 (2016).
5. McNeal, J. Normal histology of the prostate. *Am J Surg Pathol* **12**, 619–33 (1988).
6. McNeal JE, Redwine EA, Freiha FS, S. T. Zonal distribution of prostatic adenocarcinoma. Correlation with histologic pattern and direction of spread. *Am J Surg Pathol* **12**, 897–906 (1988).
7. Cancer Research UK. Prostate Cancer Statistics. *Cancer Research UK* (2019).
8. Haas GP, Delongchamps N, Brawley OW, Wang CY, de la R. G. The worldwide epidemiology of prostate cancer: perspectives from autopsy studies. *Can J Urol* **15**, 3866–3871 (2008).
9. Perez-Cornago, A. *et al.* Prospective investigation of risk factors for prostate cancer in the UK Biobank cohort study. *Br. J. Cancer* **117**, 1562–1571 (2017).
10. Attard, G. *et al.* Prostate cancer. *Lancet* **387**, 70–82 (2016).
11. Kheirandish, P. & Chinegwundoh, F. Ethnic differences in prostate cancer. *Br. J. Cancer* **105**, 481–485 (2011).
12. Bruner, D. W., Moore, D., Parlanti, A., Dorgan, J. & Engstrom, P. Relative risk of prostate cancer for men with affected relatives: systematic review and meta-analysis. *Int. J. cancer* **107**, 797–803 (2003).
13. Leitzmann, M. . & Rohrmann, S. Risk factors for the onset of prostatic cancer: Age, location, and behavioral correlates. *Clin. Epidemiol.* **4**, 1–11 (2012).
14. Esposito, K. *et al.* Effect of metabolic syndrome and its components on prostate cancer risk: meta-analysis. *J. Endocrinol. Invest.* **36**, 132–9 (2013).
15. Vidal, A. C. *et al.* Obesity increases the risk for high-grade prostate cancer: Results from the REDUCE study. *Cancer Epidemiol. Biomarkers Prev.* **23**, 2936–2942 (2014).
16. Zhang, X. *et al.* Impact of obesity upon prostate cancer-associated mortality: A meta-analysis of 17 cohort studies. *Oncol. Lett.* **9**, 1307–1312 (2015).
17. Montanari, M. *et al.* Epithelial-mesenchymal transition in prostate cancer: an overview. *Oncotarget* **8**, 35376–35389 (2017).
18. Bubendorf, L. *et al.* Metastatic patterns of prostate cancer: an autopsy study of 1,589

patients. *Hum. Pathol.* **31**, 578–83 (2000).

19. Kuriyama, M. *et al.* Quantitation of prostate-specific antigen in serum by a sensitive enzyme immunoassay. *Cancer Res.* **40**, 4658–62 (1980).

20. Hayes, J. H. & Barry, M. J. Screening for prostate cancer with the prostate-specific antigen test: A review of current evidence. *JAMA - J. Am. Med. Assoc.* **311**, 1143–1149 (2014).

21. Gleason, D. F. & Mellinger, G. T. Prediction of prognosis for prostatic adenocarcinoma by combined histological grading and clinical staging (reprint). *J. Urol.* 58–64 (1974). doi:10.1016/S0022-5347(02)80309-3

22. Albertsen, P. C., Hanley, J. A., Gleason, D. F. & Barry, M. J. Competing risk analysis of men aged 55 to 74 years at diagnosis managed conservatively for clinically localized prostate cancer. *J. Am. Med. Assoc.* **280**, 975–980 (1998).

23. N. Mottet , J. Bellmunt, E. Briers , M. Bolla, L. Bourke, P. Cornford, M. De Santis, A.M. Henry, S. Joniau, T.B. Lam, M.D. Mason, H.G. van der Poel, T.H. van der Kwast, O. Rouvière, T. Wiegel, P. M. W. *EAU-ESTRO-ESUR-SIOG Guidelines on Prostate cancer*. (2017).

24. Brierley, A. TNM classification of malignant tumors. *UICC International Union Against Cancer* 8th edn (2016). Available at: http://www.uicc.org/resources/tnm/publications-resources.

25. Galsky, M. D. & Vogelzang, N. J. Docetaxel-based combination therapy for castration-resistant prostate cancer. *Ann. Oncol.* **21**, 2135–2144 (2010).

26. Sharifi, N. *et al.* A retrospective study of the time to clinical endpoints for advanced prostate cancer. *BJU Int.* **96**, 985–989 (2005).

27. Sternberg, C. N. Systemic chemotherapy and new experimental approaches in the treatment of metastatic prostate cancer. *Ann. Oncol.* **19**, vii91–vii95 (2008).

28. Sumanasuriya, S. & De Bono, J. Treatment of advanced prostate cancer—A review of current therapies and future promise. *Cold Spring Harb. Perspect. Med.* **8**, 1–14 (2018).

29. Ottewell, P. D. *et al.* Castration-induced bone loss triggers growth of disseminated prostate cancer cells in bone. *Endocr. Relat. Cancer* **21**, 769–781 (2014).

30. Ye, L., Kynaston, H. G. & Jiang, W. G. Bone metastasis in prostate cancer: molecular and cellular mechanisms (Review). *Int. J. Mol. Med.* **20**, 103–11 (2007).

31. James, N. D. *et al.* Addition of docetaxel, zoledronic acid, or both to first-line long-term hormone therapy in prostate cancer (STAMPEDE): Survival results from an adaptive, multiarm, multistage, platform randomised controlled trial. *Lancet* **387**, 1163–1177 (2016).

32. Eisenhauer, E. . & Vermorken, J. . The taxoids. Comparative clinical pharmacology and therapeutic potential. *Drugs* **55**, 5–30 (1998).

33. Haldar, S., Chintapalli, J. & Croce, C. M. Taxol induces bcl-2 phosphorylation and death of prostate cancer cells. *Cancer Res.* **56**, 1253–1255 (1996).

34. Marin-Aguilera, M. *et al.* Identification of Docetaxel Resistance Genes in Castration-Resistant Prostate Cancer. *Mol. Cancer Ther.* **11**, 329–339 (2012).

35. Hamberg, P., Verhagen, P. C. M. S. & de Wit, R. When to start cytotoxic therapy in asymptomatic patients with hormone refractory prostate cancer? *Eur. J. Cancer* **44**, 1193–1197 (2008).

36. Saad, F. *et al.* Long-term efficacy of zoledronic acid for the prevention of skeletal complications in patients with metastatic hormone-refractory prostate cancer (multiple letters) [2]. *J. Natl. Cancer Inst.* **96**, 1480–1481 (2004).

37. Fizazi, K. *et al.* A Randomized Phase III Trial of Denosumab versus Zoledronic Acid in Patients with Bone Metastases from Castration-resistant Prostate Cancer. *J. Clin. Oncol.* **28**, Suppl (2010).

38. Parker, C. *et al.* Alpha Emitter Radium-223 and Survival in Metastatic Prostate Cancer. *N. Engl. J. Med.* 213–223 (2013).

39. Valastyan, S. & Weinberg, R. A. Tumor metastasis: molecular insights and evolving paradigms. *Cell* **147**, 275–92 (2011).

40. Gunes Gundem *et al.* The evolutionary history of lethal metastatic prostate cancer. *Nature* **520**, 353–357 (2015).

41. Rubin, M. A. *et al.* E-cadherin expression in prostate cancer: a broad survey using high-density tissue microarray technology. *Hum. Pathol.* **32**, 690–7 (2001).

42. Yates, C. C., Shepard, C. R., Stolz, D. B. & Wells, A. Co-culturing human prostate carcinoma cells with hepatocytes leads to increased expression of E-cadherin. *Br. J. Cancer* **96**, 1246–1252 (2007).

43. Stylianou, N. *et al.* A molecular portrait of epithelial–mesenchymal plasticity in prostate cancer associated with clinical outcome. *Oncogene* **38**, 913–934 (2019).

44. Disibio, G. & French, S. W. Metastatic patterns of cancers: results from a large autopsy study. *Arch. Pathol. Lab. Med.* **132**, 931–9 (2008).

45. Stephen, P. The distribution of secondary growths in cancer of the breast. *Lancet* **133**, 571–573 (1889).

46. Autio, K. A. & Morris, M. J. Targeting bone physiology for the treatment of metastatic prostate cancer. *Clin. Adv. Hematol. Oncol.* **11**, 134–43 (2013).

47. Raggatt, L. J. & Partridge, N. C. Cellular and molecular mechanisms of bone remodeling. *J. Biol. Chem.* **285**, 25103–25108 (2010).

48. Macedo, F. *et al.* Bone metastases: An overview. *Oncol. Rev.* **11**, (2017).

49. Keller, E. T. & Brown, J. Prostate cancer bone metastases promote both osteolytic and osteoblastic activity. *J. Cell. Biochem.* **91**, 718–729 (2004).

50. Rosol, T. J. Pathogenesis of Bone Metastases: Role of Tumor-Related Proteins. *J.*

Bone Miner. Res. **15**, 844–850 (2010).

51. Boskey, A. L. Bone composition: relationship to bone fragility and anti-osteoporotic drug effects. *Bonekey Rep.* **4**, 1–11 (2015).

52. Zheng, Y., Zhou, H., Dunstan, C. R., Sutherland, R. L. & Seibel, M. J. The role of the bone microenvironment in skeletal metastasis. *J. Bone Oncol.* **2**, 47–57 (2013).

53. Aarden, E. M., Nijweide, P. J. & Burger, E. H. Function of osteocytes in bone. *J. Cell. Biochem.* **55**, 287–299 (1994).

54. Buenzli, P. R. & Sims, N. A. Quantifying the osteocyte network in the human skeleton. *Bone* **75**, 144–150 (2015).

55. Riddle, R. C. & Clemens, T. L. Bone Cell Bioenergetics and Skeletal Energy Homeostasis. *Physiol. Rev.* **97**, 667–698 (2017).

56. Logothetis, C. J. & Lin, S. H. Osteoblasts in prostate cancer metastasis to bone. *Nat. Rev. Cancer* **5**, 21–28 (2005).

57. Hall, C. L., Kang, S., MacDougald, O. A. & Keller, E. T. Role of Wnts in prostate cancer bone metastases. *J. Cell. Biochem.* **97**, 661–672 (2006).

58. Sottnik, J. L. & Keller, E. T. Understanding and targeting osteoclastic activity in prostate cancer bone metastases. *Curr. Mol. Med.* **13**, 626–39 (2013).

59. Garnero, P. *et al.* Markers of bone turnover for the management of patients with bone metastases from prostate cancer. *Br. J. Cancer* **82**, 858–864 (2000).

60. Cramer, S. D., Chen, Z. & Peehl, D. M. Prostate specific antigen cleaves parathyroid hormone-related protein in the PTH-like domain: inactivation of PTHrP-stimulated cAMP accumulation in mouse osteoblasts. *J. Urol.* **156**, 526–31 (1996).

61. Bar-Shavit, Z. The osteoclast: A multinucleated, hematopoietic-origin, bone-resorbing osteoimmune cell. *J. Cell. Biochem.* **102**, 1130–1139 (2007).

62. Boyle, W. J., Simonet, W. S. & Lacey, D. L. Osteoclast differentiation and activation. *Nature* **423**, 337–342 (2003).

63. Cuiffo, B. G. & Karnoub, A. E. Mesenchymal stem cells in tumor development: emerging roles and concepts. *Cell Adh. Migr.* **6**, 220–30 (2012).

64. Buenrostro, D., Park, S. I. & Sterling, J. A. Dissecting the Role of Bone Marrow Stromal Cells on Bone Metastases. *Biomed Res. Int.* **2014**, 1–11 (2014).

65. Gascard, P. & Tlsty, T. D. Carcinoma-associated fibroblasts: Orchestrating the composition of malignancy. *Genes Dev.* **30**, 1002–1019 (2016).

66. Lee, E. *et al.* Growth Arrest-Specific 6 (GAS6) Promotes Prostate Cancer Survival by G1Arrest/S Phase Delay and Inhibition of Apoptosis During Chemotherapy in Bone Marrow. *J. Cell. Biochem.* **2824**, 2815–2824 (2016).

67. Vazquez, A. *et al.* Cancer metabolism at a glance. *J. Cell Sci.* **129**, 3367–3373 (2016).

68. Berg, J. M., Tymoczko, J. L. & Stryer, L. *Biochemistry.* (W.H. Freeman and

Company, 2007).

69. Cooper, G. *The Cell: A Molecular Approach*. (2000).

70. Barcia-Vieitez, R. & Ramos-Martínez, J. I. The regulation of the oxidative phase of the pentose phosphate pathway: new answers to old problems. *IUBMB Life* **66**, 775–9 (2014).

71. Raïs, B. *et al.* Oxythiamine and dehydroepiandrosterone induce a G 1 phase cycle arrest in Ehrlich's tumor cells through inhibition of the pentose cycle. *FEBS Lett.* **456**, 113–118 (1999).

72. Stincone, A. *et al.* The return of metabolism: biochemistry and physiology of the pentose phosphate pathway. *Biol. Rev.* **90**, 927–963 (2015).

73. Riganti, C., Gazzano, E., Polimeni, M., Aldieri, E. & Ghigo, D. The pentose phosphate pathway: An antioxidant defense and a crossroad in tumor cell fate. *Free Radic. Biol. Med.* **53**, 421–436 (2012).

74. Cho, E. S., Cha, Y. H., Kim, H. S., Kim, N. H. & Yook, J. I. The pentose phosphate pathway as a potential target for cancer therapy. *Biomol. Ther.* **26**, 29–38 (2018).

75. Fico, A. *et al.* Glucose-6-phosphate dehydrogenase plays a crucial role in protection from redox-stress-induced apoptosis. *Cell Death Differ.* **11**, 823–831 (2004).

76. DeBerardinis, R. J., Sayed, N., Ditsworth, D. & Thompson, C. B. Brick by brick: metabolism and tumor cell growth. *Curr. Opin. Genet. Dev.* **18**, 54–61 (2008).

77. Altman, B. J., Stine, Z. E. & Dang, C. V. From Krebs to clinic: glutamine metabolism to cancer therapy. *Nat. Rev. Cancer* **16**, 619–634 (2016).

78. Labow, B. I. & Souba, W. W. Glutamine. *World J. Surg.* **24**, 1503–1513 (2000).

79. Hanahan D, W. R. Hallmarks of cancer: the next generation. *Cell* **144**, 646–74 (2011).

80. Kroemer, G. & Pouyssegur, J. Tumor Cell Metabolism: Cancer's Achilles' Heel. *Cancer Cell* **13**, 472–482 (2008).

81. Lewis, N. E. & Abdel-Haleem, A. M. The evolution of genome-scale models of cancer metabolism. *Front. Physiol.* **4 SEP**, 1–7 (2013).

82. Twum-Ampofo, J., Fu, D. X., Passaniti, A., Hussaind, A. & Siddiqui, M. M. Metabolic targets for potential prostate cancer therapeutics. *Curr. Opin. Oncol.* **28**, 241–247 (2016).

83. Warburg, O. The Metabolism of Carcinoma Cells. *J. Cancer Res.* **9**, 148–163 (1925).

84. Warburg, O., Wind, F. & Negelein, E. The Metabolism of tumors in the body. *J. Gen. Physiol.* **8**, 519–30 (1927).

85. Effert, P. J. *et al.* Metabolic Imaging of Untreated Prostate Cancer by Positron Emission Tomography with sup 18 Fluorine-Labeled Deoxyglucose. *J. Urol.* **155**, 994–998 (1996).

86. Hofer, C. *et al.* Fluorine-18-fluorodeoxyglucose positron emission tomography is

useless for the detection of local recurrence after radical prostatectomy. *Eur. Urol.* **36**, 31–35 (1999).

87. Fiaschi, T. *et al.* Reciprocal metabolic reprogramming through lactate shuttle coordinately influences tumor-stroma interplay. *Cancer Res.* **72**, 5130–5140 (2012).

88. Avagliano, A. *et al.* Metabolic Reprogramming of Cancer Associated Fibroblasts: The Slavery of Stromal Fibroblasts. *Biomed Res. Int.* **2018**, 1–12 (2018).

89. Reina-Campos, M., Moscat, J. & Diaz-Meco, M. Metabolism shapes the tumor microenvironment. *Curr. Opin. Cell Biol* 47–53 (2017). doi:10.1016/j.ceb.2017.05.006

90. Pavlides, S. *et al.* The reverse Warburg effect: Aerobic glycolysis in cancer associated fibroblasts and the tumor stroma. *Cell Cycle* **8**, 3984–4001 (2009).

91. Pértega-Gomes, N. *et al.* A lactate shuttle system between tumour and stromal cells is associated with poor prognosis in prostate cancer. *BMC Cancer* **14**, 1–8 (2014).

92. Giannoni, E. *et al.* Reciprocal activation of prostate cancer cells and cancer-associated fibroblasts stimulates epithelial-mesenchymal transition and cancer stemness. *Cancer Res.* **70**, 6945–6956 (2010).

93. Gandellini, P. *et al.* miR-205 Hinders the Malignant Interplay Between Prostate Cancer Cells and Associated Fibroblasts. *Antioxid. Redox Signal.* **20**, 1045–1059 (2014).

94. Eder, T. *et al.* Cancer-associated fibroblasts modify the response of prostate cancer cells to androgen and anti-androgens in three-dimensional spheroid culture. *Int. J. Mol. Sci.* **17**, 1–15 (2016).

95. Ippolito, L. *et al.* Metabolic shift toward oxidative phosphorylation in docetaxel resistant prostate cancer cells. *Oncotarget* **7**, (2016).

96. Compston, J. Bone marrow and bone: a functional unit. *J Endocrinol* **173**, 387–94 (2002).

97. Gazi, E. *et al.* Direct evidence of lipid translocation between adipocytes and prostate cancer cells with imaging FTIR microspectroscopy. *J. Lipid Res.* **48**, 1846–1856 (2007).

98. Brown, M. D., Hart, C. A., Gazi, E., Bagley, S. & Clarke, N. W. Promotion of prostatic metastatic migration towards human bone marrow stoma by Omega 6 and its inhibition by Omega 3 PUFAs. *Br. J. Cancer* **94**, 842–853 (2006).

99. Costello, L. C., Liu, Y., Franklin, R. B. & Kennedy, M. C. Zinc inhibition of mitochondrial aconitase and its importance in citrate metabolism of prostate epithelial cells. *J. Biol. Chem.* **272**, 28875–81 (1997).

100. Costello, L. . & Franklin, R. . Citrate metabolism of normal and malignant prostate epithelial cells. *Urology* **50**, 3–12 (1997).

101. Costello, L. C. *et al.* Human prostate cancer ZIP1/zinc/citrate genetic/metabolic relationship in the TRAMP prostate cancer animal model. *Cancer Biol. Ther.* **12**,

1078–1084 (2011).

102. Costello LC, F. R. The intermediary metabolism of the prostate: a key to understanding the pathogenesis and progression of prostate malignancy. *Oncology* **59**, 269–82 (2000).

103. Ju, H. Q. *et al.* Disrupting G6PD-mediated Redox homeostasis enhances chemosensitivity in colorectal cancer. *Oncogene* **36**, 6282–6292 (2017).

104. Nagashio, R. *et al.* Prognostic significance of G6PD expression and localization in lung adenocarcinoma. *Biochim. Biophys. Acta - Proteins Proteomics* **1867**, 38–46 (2019).

105. Wang, J. *et al.* Overexpression of G6PD is associated with poor clinical outcome in gastric cancer. *Tumor Biol.* **33**, 95–101 (2012).

106. Kuo, W. Y., Lin, J. Y. & Tang, T. K. Human glucose-6-phosphate dehydrogenase (G6PD) gene transforms NIH 3T3 cells and induces tumors in nude mice. *Int. J. Cancer* **85**, 857–864 (2000).

107. Pu, H. *et al.* Overexpression of G6PD is associated with high risks of recurrent metastasis and poor progression-free survival in primary breast carcinoma. *World J. Surg. Oncol.* **13**, 1–7 (2015).

108. Poulain, L. *et al.* High mTORC1 activity drives glycolysis addiction and sensitivity to G6PD inhibition in acute myeloid leukemia cells. *Leukemia* **31**, 2326–2335 (2017).

109. Jiang, P. *et al.* p53 regulates biosynthesis through direct inactivation of glucose-6-phosphate dehydrogenase. *Nat. Cell Biol.* **13**, 310–316 (2011).

110. Zhang, Q. *et al.* Overexpression of G6PD represents a potential prognostic factor in clear cell renal cell carcinoma. *J. Cancer* **8**, 665–673 (2017).

111. Zampella, E. J., Bradley Jr, E. L. & Pretlow II, T. Glucose-6-Phosphate Dehydrogenase : A Possible Clinical lndicator for Prostatic Carcinoma. *Cancer* **49**, 384–387 (1982).

112. Pretlow II, T. G. *et al.* Enzyme Activities in Prostatic Carcinoma Related to Gleason Grades. *Cancer Res.* **45**, 442–446 (1985).

113. Tsouko, E. *et al.* Regulation of the pentose phosphate pathway by an androgen receptor-mTOR-mediated mechanism and its role in prostate cancer cell growth. *Oncogenesis* **3**, e103-10 (2014).

114. Catanzaro, D. *et al.* Inhibition of glucose-6-phosphate dehydrogenase sensitizes cisplatin-resistant cells to death. *Oncotarget* (2015). doi:10.18632/oncotarget.4945

115. Hong, W. *et al.* Inhibition of Glucose-6-Phosphate Dehydrogenase Reverses Cisplatin Resistance in Lung Cancer Cells via the Redox System. *Front. Pharmacol.* **9**, 43 (2018).

116. Bhardwaj, R., Sharma, P. K., Jadon, S. P. S. & Varshney, R. A combination of 2-deoxy-D-glucose and 6-aminonicotinamide induces cell cycle arrest and apoptosis

selectively in irradiated human malignant cells. *Tumour Biol.* **33**, 1021–30 (2012).

117. Tuttle, S., Stamato, T., Perez, M. L. & Biaglow, J. Glucose-6-phosphate dehydrogenase and the oxidative pentose phosphate cycle protect cells against apoptosis induced by low doses of ionizing radiation. *Radiat. Res.* **153**, 781–7 (2000).

118. Hansell, D. T., Davies, J. W. L., Burns, H. J. G. & Shenkin, A. The oxidation of body fuel stores in cancer patients. *Ann. Surg.* **204**, 637–642 (1986).

119. Hyltander, A., Drott, C., Körner, U., Sandström, R. & Lundholm, K. Elevated energy expenditure in cancer patients with solid tumours. *Eur. J. Cancer* **27**, 9–15 (1991).

120. Menendez, J. A. & Lupu, R. Fatty acid synthase and the lipogenic phenotype in cancer pathogenesis. *Nat. Rev. Cancer* **7**, 763–777 (2007).

121. Costello, L. C. & Franklin, R. B. 'Why do tumour cells glycolyse?': From glycolysis through citrate to lipogenesis. *Mol. Cell. Biochem.* **280**, 1–8 (2005).

122. Swinnen, J V ; Esquenet, M ; Goossens, K ; Heyns, W ; Verhoeven, G. Androgens Stimulate Fatty Acid Synthase in the Human Prostate Cancer periods. *Cancer Res.* **57**, 1086–1090 (1997).

123. Swinnen, J. V *et al.* Overexpression of fatty acid synthase is an early and common event in the development of prostate cancer. *Int. J. cancer* **98**, 19–22 (2002).

124. Rossi, S. *et al.* Fatty Acid Synthase Expression Defines Distinct Molecular Signatures in Prostate Cancer. *Mol. Cancer Res.* **1**, 707–715 (2003).

125. Migita, T. *et al.* Fatty acid synthase: a metabolic enzyme and candidate oncogene in prostate cancer. *J. Natl. Cancer Inst.* **101**, 519–32 (2009).

126. Kuhajda, F. P. Fatty-acid synthase and human cancer: new perspectives on its role in tumor biology. *Nutrition* **16**, 202–208 (2000).

127. Yoshii, Y. *et al.* Fatty Acid Synthase Is a Key Target in Multiple Essential Tumor Functions of Prostate Cancer: Uptake of Radiolabeled Acetate as a Predictor of the Targeted Therapy Outcome. *PLoS One* **8**, (2013).

128. De Schrijver, E., Brusselmans, K., Heyns, W., Verhoeven, G. & Swinnen, J. V. RNA interference-mediated silencing of the fatty acid synthase gene attenuates growth and induces morphological changes and apoptosis of LNCaP prostate cancer cells. *Cancer Res.* **63**, 3799–3804 (2003).

129. Kuhajda, F. P. *et al.* Fatty acid synthesis: a potential selective target for antineoplastic therapy. *Proc. Natl. Acad. Sci.* **91**, 6379–6383 (2006).

130. Kridel, S. J., Axelrod, F., Rozenkrantz, N. & Smith, J. W. Orlistat Is a Novel Inhibitor of Fatty Acid Synthase with Antitumor Activity. *Cancer Res.* **64**, 2070–2075 (2004).

131. Flavin, R., Peluso, S., Nguyen, P. L. & Loda, M. Fatty acid synthase as a potential therapeutic target in cancer. *Futur. Oncol.* **6**, 551–562 (2010).

132. Pelton, K., Freeman, M. R. & Solomon, K. R. Cholesterol and prostate cancer. *Curr.*

Opin. Pharmacol. **12**, 751–759 (2012).

133. Zhuang, L., Kim, J., Adam, R. M., Solomon, K. R. & Freeman, M. R. Cholesterol targeting alters lipid raft composition and cell survival in prostate cancer cells and xenografts. *J. Clin. Invest.* **115**, 959–968 (2005).

134. Llaverias, G. *et al.* A western-type diet accelerates tumor progression in an autochthonous mouse model of prostate cancer. *Am. J. Pathol.* **177**, 3180–3191 (2010).

135. Kochuparambil, S. T., Al-Husein, B., Goc, A., Soliman, S. & Somanath, P. R. Anticancer Efficacy of Simvastatin on Prostate Cancer Cells and Tumor Xenografts Is Associated with Inhibition of Akt and Reduced Prostate-Specific Antigen Expression. *J. Pharmacol. Exp. Ther.* **336**, 496–505 (2011).

136. Graaf, M. R., Richel, D. J., van Noorden, C. J. F. & Guchelaar, H.-J. Effects of statins and farnesyltransferase inhibitors on the development and progression of cancer. *Cancer Treat. Rev.* **30**, 609–641 (2004).

137. Liu, Y. Fatty acid oxidation is a dominant bioenergetic pathway in prostate cancer. *Prostate Cancer Prostatic Dis.* **9**, 230–234 (2006).

138. Zha, S. *et al.* Peroxisomal branched chain fatty acid beta-oxidation pathway is upregulated in prostate cancer. *Prostate* **63**, 316–323 (2005).

139. Schlaepfer, I. R. *et al.* Inhibition of Lipid Oxidation Increases Glucose Metabolism and Enhances 2-Deoxy-2-[18F]Fluoro-d-Glucose Uptake in Prostate Cancer Mouse Xenografts. *Mol. Imaging Biol.* **17**, 529–538 (2015).

140. Carnell, A. J. *et al.* Inhibition of Human α-Methylacyl CoA Racemase (AMACR): a Target for Prostate Cancer. *ChemMedChem* **8**, 1643–7 (2013).

141. Schlaepfer, I. R. *et al.* Lipid catabolism via CPT1 as a therapeutic target for prostate cancer. *Mol. Cancer Ther.* **13**, 2361–71 (2014).

142. Pan, T. *et al.* Elevated expression of glutaminase confers glucose utilization via glutaminolysis in prostate cancer. *Biochem. Biophys. Res. Commun.* **456**, 452–458 (2015).

143. Wang, Q. *et al.* Targeting ASCT2-mediated glutamine uptake blocks prostate cancer growth and tumour development. *J. Pathol.* **236**, 278–289 (2015).

144. Shum, L. C., White, N. S., Mills, B. N., de Mesy Bentley, K. L. & Eliseev, R. A. Energy Metabolism in Mesenchymal Stem Cells During Osteogenic Differentiation. *Stem Cells Dev.* **25**, 114–122 (2016).

145. Indo, Y. *et al.* Metabolic regulation of osteoclast differentiation and function. *J. Bone Miner. Res.* **28**, 2392–2399 (2013).

146. Motyl, K. J., Guntur, A. R., Carvalho, A. L. & Rosen, C. J. Energy Metabolism of Bone. *Toxicol. Pathol.* **45**, 887–893 (2017).

147. Greenberg, N. M. *et al.* Prostate cancer in a transgenic mouse. *Proc. Natl. Acad. Sci.*

92, 3439–3443 (1995).

148. Kaplan-Lefko, P. J. *et al.* Pathobiology of autochthonous prostate cancer in a pre-clinical transgenic mouse model. *Prostate* **55**, 219–237 (2003).

149. Park, S. I., Kim, S. J., McCauley, L. K. & Gallick, G. E. Preclinical Mouse Models of Human Prostate Cancer and Their Utility in Drug Discovery. in *Current Protocols in Pharmacology* 1–35 (John Wiley & Sons, Inc., 2010). doi:10.1002/0471141755.ph1415s51

150. Soga, T. *et al.* Metabolomic profiling of anionic metabolites by capillary electrophoresis mass spectrometry. *Anal. Chem.* **81**, 6165–74 (2009).

151. Soga, T. *et al.* Differential metabolomics reveals ophthalmic acid as an oxidative stress biomarker indicating hepatic glutathione consumption. *J. Biol. Chem.* **281**, 16768–76 (2006).

152. Kumar, A. *et al.* Substantial interindividual and limited intraindividual genomic diversity among tumors from men with metastatic prostate cancer. *Nat. Med.* **22**, 369–378 (2016).

153. Taylor, B. S. *et al.* Integrative Genomic Profiling of Human Prostate Cancer. *Cancer Cell* **18**, 11–22 (2010).

154. Varambally, S. *et al.* Integrative genomic and proteomic analysis of prostate cancer reveals signatures of metastatic progression. *Cancer Cell* **8**, 393–406 (2005).

155. Grasso, C. S. *et al.* The mutational landscape of lethal castration-resistant prostate cancer. *Nature* **487**, 239–243 (2012).

156. Gaude, E. & Frezza, C. Tissue-specific and convergent metabolic transformation of cancer correlates with metastatic potential and patient survival. *Nat. Commun.* **7**, 1–9 (2016).

157. Dobin, A. *et al.* STAR: ultrafast universal RNA-seq aligner. *Bioinformatics* **29**, 15–21 (2013).

158. Love, M. I., Huber, W. & Anders, S. Moderated estimation of fold change and dispersion for RNA-seq data with DESeq2. *Genome Biol.* **15**, 550 (2014).

159. Diedrich, J. D. *et al.* Bone marrow adipocytes promote the Warburg phenotype in metastatic prostate tumors via HIF-1α activation. *Oncotarget* **7**, (2016).

160. Thalmann, G. N. *et al.* Androgen-independent cancer progression and bone metastasis in the LNCaP model of human prostate cancer. *Cancer Res.* **54**, 2577–81 (1994).

161. Zhang, J. *et al.* Osteoprotegerin inhibits prostate cancer–induced osteoclastogenesis and prevents prostate tumor growth in the bone. *J. Clin. Invest.* **107**, 1235–1244 (2001).

162. Ding, J., Nagai, K. & Woo, J.-T. Insulin-Dependent Adipogenesis in Stromal ST2 Cells Derived from Murine Bone Marrow. *Biosci. Biotechnol. Biochem.* **67**, 314–321 (2003).

163. Ghosh-Choudhury, N. *et al.* Immortalized murine osteoblasts derived from BMP 2-T-antigen expressing transgenic mice. *Endocrinology* **137**, 331–339 (1996).

164. Ren, J. L., Zhang, A. H., Kong, L. & Wang, X. J. Advances in mass spectrometry-based metabolomics for investigation of metabolites. *RSC Adv.* **8**, 22335–22350 (2018).

165. Seyfried, T. N., Flores, R. E., Poff, A. M. & D'Agostino, D. P. Cancer as a metabolic disease: Implications for novel therapeutics. *Carcinogenesis* **35**, 515–527 (2014).

166. Higgins, L. H. *et al.* Hypoxia and the metabolic phenotype of prostate cancer cells. *BBA - Bioenerg.* **1787**, 1433–1443 (2009).

167. Pertega-Gomes, N. *et al.* A glycolytic phenotype is associated with prostate cancer progression and aggressiveness: a role for monocarboxylate transporters as metabolic targets for therapy. *J. Pathol.* **236**, 517–30 (2015).

168. Adedeji, D., Hinton, B. & Payne, G. In - vitro Anti-Proliferative Analysis of Metformin Hydrochloride on Androgen-Sensitive (LNCaP) and Androgen-Insensitive (PC-3) Human Prostate Cancer Cell Lines. *FASEB* **31**, Ib525 (2017).

169. Biernacka, K. M. *et al.* Hyperglycaemia-induced resistance to Docetaxel is negated by metformin: a role for IGFBP-2. *Endocr. Relat. Cancer* **24**, 17–30 (2017).

170. Kami, K. *et al.* Metabolomic profiling of lung and prostate tumor tissues by capillary electrophoresis time-of-flight mass spectrometry. *Metabolomics* **9**, 444–453 (2013).

171. Reisz, J. A. & D'Alessandro, A. Measurement of metabolic fluxes using stable isotope tracers in whole animals and human patients. *Curr. Opin. Clin. Nutr. Metab. Care* **20**, 366–374 (2017).

172. Testa, C., Pultrone, C., Manners, D. N., Schiavina, R. & Lodi, R. Metabolic Imaging in Prostate Cancer: Where We Are. *Front. Oncol.* **6**, 1–8 (2016).

173. Golman, K. & Petersson, J. S. Metabolic Imaging and Other Applications of Hyperpolarized 13C1. *Acad. Radiol.* **13**, 932–942 (2006).

174. Zhang, Q. *et al.* G6PD promotes renal cell carcinoma proliferation through positive feedback regulation of p-STAT3. *Oncotarget* **8**, 109043–109060 (2017).

175. McKee, T. J. & Komarova, S. V. Is it time to reinvent basic cell culture medium? *Am. J. Physiol. Physiol.* **312**, C624–C626 (2017).

176. Johnson, R. W., Sowder, M. E. & Giaccia, A. J. Hypoxia and Bone Metastatic Disease. *Curr. Osteoporos. Rep.* **15**, 231–238 (2017).

177. Graf, L., Iwata, M., Torok-storb, B. & Mackinnon, S. Gene expression profiling of the functionally distinct human bone marrow stromal cell lines HS-5 and HS-27a. *Blood* **100**, 1509–1511 (2002).

178. Düvel, K. *et al.* Activation of a metabolic gene regulatory network downstream of mTOR complex 1. *Mol. Cell* **39**, 171–183 (2010).

179. Liesenfeld, L., Kron, M., Gschwend, J. E. & Herkommer, K. Prognostic Factors for Biochemical Recurrence More than 10 Years after Radical Prostatectomy. *J. Urol.*

197, 143–148 (2017).

180. Shahabi, A. *et al.* Predictors of time to biochemical recurrence in a radical prostatectomy cohort within the PSA-era. **10**, 1–4 (2016).

181. Chettimada, S. *et al.* Hypoxia-induced glucose-6-phosphate dehydrogenase overexpression and -activation in pulmonary artery smooth muscle cells: implication in pulmonary hypertension. *Am. J. Physiol. Cell. Mol. Physiol.* **308**, L287–L300 (2015).

182. Gao, L., Mejías, R., Echevarría, M. & López-Barneo, J. Induction of the glucose-6-phosphate dehydrogenase gene expression by chronic hypoxia in PC12 cells. *FEBS Lett.* **569**, 256–260 (2004).

183. Schwartz, A. G. & Pashko, L. L. Cancer prevention with dehydroepiandrosterone and non-androgenic structural analogs. *J. Cell. Biochem. Suppl.* **22**, 210–7 (1995).

184. Geller, J. Rationale for blockade of adrenal as well as testicular androgens in the treatment of advanced prostate cancer. *Semin. Oncol.* **12**, 28–35 (1985).

185. Rao, K. V. N. *et al.* Chemoprevention of rat prostate carcinogenesis by early and delayed administration of dehydroepiandrosterone. *Cancer Res.* **59**, 3084–3089 (1999).

186. Miyoshi, Y. *et al.* Low serum dehydroepiandrosterone examined by liquid chromatography-tandem mass spectrometry correlates with poor prognosis in hormone-naïve prostate cancer. *Prostate* **76**, 376–382 (2016).

187. Yano, A. *et al.* Baseline low serum dehydroepiandrosterone sulfate can predict poor responsiveness to hormone therapy in patients with hormone-naïve prostate cancer with skeletal metastases. *Int. J. Urol.* **24**, 861–862 (2017).

188. Ryan, C. J. *et al.* Serum androgens as prognostic biomarkers in castration-resistant prostate cancer: Results from an analysis of a randomized phase III trial. *J. Clin. Oncol.* **31**, 2791–2798 (2013).

189. Arnold, J. T., Le, H., McFann, K. K. & Blackman, M. R. Comparative effects of DHEA vs. testosterone, dihydrotestosterone, and estradiol on proliferation and gene expression in human LNCaP prostate cancer cells. *Am. J. Physiol. Metab.* **288**, E573–E584 (2004).

190. Sun, H. Z., Yang, T. W., Zang, W. J. & Wu, S. F. Dehydroepiandrosterone-induced proliferation of prostatic epithelial cell is mediated by NFKB via PI3K/AKT signaling pathway. *J. Endocrinol.* **204**, 311–318 (2010).

191. Delk N, F.-C. M. A bone marrow stromal cell paracrine signal that induces neuroendocrine differentiation and modulates autophagy in bone metastatic PCa cells. *Autophagy* **8(4)**, 650–63 (2012).

192. Nguyen, D. P., Li, J. & Tewari, A. K. Inflammation and prostate cancer: The role of interleukin 6 (IL-6). *BJU Int.* **113**, 986–992 (2014).

193. Guo, Y., Xu, F., Lu, T., Duan, Z. & Zhang, Z. Interleukin-6 signaling pathway in targeted therapy for cancer. *Cancer Treat. Rev.* **38**, 904–910 (2012).

194. Adler, H. L. *et al.* Elevated levels of circulating interleukin-6 and transforming growth factor-β1 in patients with metastatic prostatic carcinoma. *J. Urol.* **161**, 182–187 (1999).

195. Wise, G. J., Marella, V. K., Talluri, G. & Shirazian, D. Cytokine Variations in Patients With Hormone Treated Prostate Cancer. *J. Urol.* **164**, 722–725 (2003).

196. George, Daniel J ; Halabi, Susan ; Shepard, Timothy F ; Sanford, Ben ; Vogelzang, Nicholas J ; Small, Eric J ; Kantoff, P. W. The prognostic significance of plasma interleukin-6 levels in patients with metastatic hormone-refractory prostate cancer: results from cancer and leukemia group B 9480. *Clin. cancer Res.* **11**, 1815–20 (2005).

197. Domingo-Domenech, J. *et al.* Interleukin 6, a nuclear factor-κB target, predicts resistance to docetaxel in hormone-independent prostate cancer and nuclear factor-κB inhibition by PS-1145 enhances docetaxel antitumor activity. *Clin. Cancer Res.* **12**, 5578–5586 (2006).

198. Fizazi, K. *et al.* Randomised phase II study of siltuximab (CNTO 328), an anti-IL-6 monoclonal antibody, in combination with mitoxantrone/prednisone versus mitoxantrone/prednisone alone in metastatic castration-resistant prostate cancer. *Eur. J. Cancer* **48**, 85–93 (2012).

199. Karkera, J. *et al.* The anti-interleukin-6 antibody siltuximab down-regulates genes implicated in tumorigenesis in prostate cancer patients from a phase I study. *Prostate* **71**, 1455–1465 (2011).

200. Dorff, T. B. *et al.* Clinical and correlative results of SWOG S0354: A phase II trial of CNTO328 (siltuximab), a monoclonal antibody against interleukin-6, in chemotherapy-pretreated patients with castration-resistant prostate cancer. *Clin. Cancer Res.* **16**, 3028–3034 (2010).

201. Boonstra, J. & Post, J. A. Molecular events associated with reactive oxygen species and cell cycle progression in mammalian cells. *Gene* **337**, 1–13 (2004).

202. Trachootham, D., Alexandre, J. & Huang, P. Targeting cancer cells by ROS-mediated mechanisms: A radical therapeutic approach? *Nat. Rev. Drug Discov.* **8**, 579–591 (2009).

203. Kumari, S., Badana, A., Murali, M., Shailender, G. & RamaRao, M. Reactive Oxygen Species: A Key Constituent in Cancer Survival. *Biomark. Insights* **13**, 1177271918755391 (2018).

204. Kumar, B., Koul, S., Khandrika, L., Meacham, R. B. & Koul, H. K. Oxidative stress is inherent in prostate cancer cells and is required for aggressive phenotype. *Cancer Res.* **68**, 1777–1785 (2008).

205. Lim, S. D. *et al.* Increased Nox1 and hydrogen peroxide in prostate cancer. *Prostate* **62**, 200–207 (2005).

206. Tian, W.-N. *et al.* Importance of glucose-6-phosphate dehydrogenase activity in cell death. *Am. J. Physiol. Physiol.* **276**, C1121–C1131 (1999).

207. Mele, L. *et al.* A new inhibitor of glucose-6-phosphate dehydrogenase blocks pentose phosphate pathway and suppresses malignant proliferation and metastasis in vivo article. *Cell Death Dis.* **9**, (2018).

208. Canada, A. T. *et al.* Glutathione and glutathione S-transferase in benign and malignant prostate cell lines and prostate tissues. *Biochem. Pharmacol.* **51**, 87–90 (1996).

209. Freitas, M. *et al.* Oxidative stress adaptation in aggressive prostate cancer may be counteracted by the reduction of glutathione reductase. *FEBS Open Bio* **2**, 119–128 (2012).

210. Cheteh, E. H. *et al.* Human cancer-associated fibroblasts enhance glutathione levels and antagonize drug-induced prostate cancer cell death. *Cell Death Dis.* **8**, e2848 (2017).

211. Srinivasan, S. *et al.* Role of mitochondrial reactive oxygen species in osteoclast differentiation. *Ann. N. Y. Acad. Sci.* **1192**, 245–252 (2010).

212. Lee, N. K. *et al.* A crucial role for reactive oxygen species in RANKL-induced osteoclast differentiation. *Blood* **106**, 852–859 (2005).

213. Arai, M., Shibata, Y., Pugdee, K., Abiko, Y. & Ogata, Y. Effects of reactive oxygen species (ROS) on antioxidant system and osteoblastic differentiation in MC3T3-E1 cells. *IUBMB Life* **59**, 27–33 (2007).

214. Yoshida, Y. *et al.* Reactive oxygen intermediates stimulate interleukin-6 production in human bronchial epithelial cells. *Am. J. Physiol.* **276**, L900-8 (1999).

215. Kosmidou, I. *et al.* Production of interleukin-6 by skeletal myotubes: role of reactive oxygen species. *Am. J. Respir. Cell Mol. Biol.* **26**, 587–93 (2002).

216. Yoon, S. *et al.* STAT3 transcriptional factor activated by reactive oxygen species induces IL6 in starvation-induced autophagy of cancer cells. *Autophagy* **6**, 1125–1138 (2010).

217. Okamoto, M., Lee, C. & Oyasu, R. Interleukin-6 as a paracrine and autocrine growth factor in human prostatic carcinoma cells in vitro. *Cancer Res.* **57**, 141–6 (1997).

218. Lee, S. O., Chun, J. Y., Nadiminty, N., Lou, W. & Gao, A. C. Interleukin-6 undergoes transition from growth inhibitor associated with neuroendocrine differentiation to stimulator accompanied by androgen receptor activation during LNCaP prostate cancer cell progression. *Prostate* **67**, 764–773 (2007).

219. Nelson, C. M., Khauv, D., Bissell, M. J. & Radisky, D. C. Change in cell shape is required for MMP-induced EMT of mammary epithelial cells. *J Cell Biochem* **105**, 25–33 (2008).

220. Greenburg, G. & Hay, E. D. Epithelia suspended in collagen gels can lose polarity and express characteristics of migrating mesenchymal cells. *J. Cell Biol.* **95**, 333–9 (1982).

221. Bitting, R. L., Schaeffer, D., Somarelli, J. A., Garcia-Blanco, M. A. & Armstrong, A. J. The role of epithelial plasticity in prostate cancer dissemination and treatment

resistance. *Cancer Metastasis Rev.* **33**, 441–468 (2014).

222. Behnsawy, H. M., Miyake, H., Harada, K. I. & Fujisawa, M. Expression patterns of epithelial-mesenchymal transition markers in localized prostate cancer: Significance in clinicopathological outcomes following radical prostatectomy. *BJU Int.* **111**, 30–37 (2013).

223. Lu, M. *et al.* Elevated G6PD expression contributes to migration and invasion of hepatocellular carcinoma cells by inducing epithelial-mesenchymal transition. *Acta Biochim Biophys Sin (Shanghai).* **50**, 370–380 (2018).

224. Mora, L. B. *et al.* Constitutive activation of Stat3 in human prostate tumors and cell lines. *Cancer Res.* **62**, 6659–6666 (2002).

225. Xian, Z.-Y. *et al.* Inhibition of LDHA suppresses tumor progression in prostate cancer. *Tumour Biol.* **36**, 8093–100 (2015).

226. Yamasaki, M., Nomura, T., Sato, F. & Mimata, H. Metallothionein is up-regulated under hypoxia and promotes the survival of human prostate cancer cells. *Oncol. Rep.* **18**, 1145–1153 (2007).

227. Gumulec, J. *et al.* Evaluation of alpha-methylacyl-CoA racemase, metallothionein and prostate specific antigen as prostate cancer prognostic markers. *Neoplasma* **59**, 191–201 (2012).

228. Z., G. *et al.* Reg IV: A promising marker of hormone refractory metastatic prostate cancer. *Clin. Cancer Res.* **11**, 2237–2243 (2005).

229. Schulz, W. A. *et al.* Changes in cortical cytoskeletal and extracellular matrix gene expression in prostate cancer are related to oncogenic ERG deregulation. *BMC Cancer* **10**, 1–9 (2010).

230. Kiviniemi, J. *et al.* Altered expression of syndecan-1 in prostate cancer. *APMIS* **112**, 89–97 (2004).

231. Poblete, C. E. *et al.* Increased SNAIL expression and low syndecan levels are associated with high Gleason grade in prostate cancer. *Int. J. Oncol.* **44**, 647–654 (2014).

232. Brimo, F., Vollmer, R. T., Friszt, M., Corcos, J. & Bismar, T. A. Syndecan-1 expression in prostate cancer and its value as biomarker for disease progression. *BJU Int.* **106**, 418–23 (2010).

233. Dong, D. *et al.* UNC5D, suppressed by promoter hypermethylation, inhibits cell metastasis by activating death-associated protein kinase 1 in prostate cancer. *Cancer Sci.* **110**, 1244–1255 (2019).

234. Preuss, J. *et al.* Identification and characterization of novel human glucose-6-phosphate dehydrogenase inhibitors. *J. Biomol. Screen.* **18**, 286–297 (2013).

235. Hu, T. *et al.* Variant G6PD levels promote tumor cell proliferation or apoptosis via the STAT3/5 pathway in the human melanoma xenograft mouse model. *BMC Cancer* **13**, 251 (2013).

236. Aiello, N. M. & Kang, Y. Context-dependent EMT programs in cancer metastasis. *J. Exp. Med.* **216**, 1016–1026 (2019).

237. Wu, Y. H. *et al.* Glucose-6-phosphate dehydrogenase is indispensable in embryonic development by modulation of epithelial-mesenchymal transition via the NOX/Smad3/miR-200b axis. *Cell Death Dis.* **9**, (2018).

238. Fang, Z. *et al.* Effects of G6PD activity inhibition on the viability, ROS generation and mechanical properties of cervical cancer cells. *Biochim. Biophys. Acta - Mol. Cell Res.* **1863**, 2245–2254 (2016).

239. Hu, H. *et al.* Changes in glucose-6-phosphate dehydrogenase expression results in altered behavior of HBV-associated liver cancer cells. *Am. J. Physiol. Liver Physiol.* **307**, G611–G622 (2014).

240. Tong, D. *et al.* Metformin inhibits castration-induced EMT in prostate cancer by repressing COX2/PGE2/STAT3 axis. *Cancer Lett.* **389**, 23–32 (2017).

241. Xu, Y. *et al.* ABT737 reverses cisplatin resistance by targeting glucose metabolism of human ovarian cancer cells. *Int. J. Oncol.* **53**, 1055–1068 (2018).

242. Köhler, E., Barrach, H. & Neubert, D. Inhibition of NADP dependent oxidoreductases by the 6-aminonicotinamide analogue of NADP. *FEBS Lett.* **6**, 225–228 (1970).

243. Raineri, R. R. & Levy, H. R. Specificity of steroid interaction with mammary glucose 6-phosphate dehydrogenase. *Biochemistry* **9**, 2233–2243 (1970).

244. Walker, D. L. *et al.* Murine pharmacokinetics of 6-aminonicotinamide (NSC 21206), a novel biochemical modulating agent. *Biochem. Pharmacol.* **58**, 1057–66 (1999).

245. Varshney, R., Dwarakanath, B. S. & Jain, V. Radiosensitization by 6-aminonicotinamide and 2-deoxy-D-glucose in human cancer cells. *Int. J. Radiat. Biol.* **81**, 397–408 (2005).

246. Sharma, P. K., Bhardwaj, R., Dwarakanath, B. S. & Varshney, R. Metabolic oxidative stress induced by a combination of 2-DG and 6-AN enhances radiation damage selectively in malignant cells via non-coordinated expression of antioxidant enzymes. *Cancer Lett.* **295**, 154–166 (2010).

247. Zhang, Z. *et al.* The effect and mechanism of inhibiting glucose-6-phosphate dehydrogenase activity on the proliferation of Plasmodium falciparum. *Biochim. Biophys. Acta - Mol. Cell Res.* **1864**, 771–781 (2017).

248. Mercaldi, G. F., Ranzani, A. T. & Cordeiro, A. T. Discovery of new uncompetitive inhibitors of glucose-6-phosphate dehydrogenase. *J. Biomol. Screen.* **19**, 1362–1371 (2014).

249. Hamilton, N. M. *et al.* Novel Steroid Inhibitors of Glucose 6-Phosphate Dehydrogenase. *J. Med. Chem.* **55**, 4431–4445 (2012).